Modélisation hydrologique de l'infiltration des eaux pluviales dans les sols urbains en prenant en compte les chemins préférentiels

Asra Asry

To cite this version:

Asra Asry. Modélisation hydrologique de l'infiltration des eaux pluviales dans les sols urbains en prenant en compte les chemins préférentiels. Génie civil. INSA de Lyon, 2023. Français. NNT : 2023ISAL0095 . tel-04583706

HAL Id: tel-04583706
https://theses.hal.science/tel-04583706
Submitted on 22 May 2024

N°d'ordre NNT : 2023ISAL0095

THESE de DOCTORAT DE L'UNIVERSITE DE LYON

opérée au sein de
L'Institut National des Sciences Appliquées de Lyon

Ecole Doctorale N° 162
Mécanique, Energétique, Génie civil, Acoustique

Discipline de doctorat : Génie civil

Soutenue publiquement le 30/11/2023, par :
Asra Asry

Modélisation hydrologique de l'infiltration des eaux pluviales dans les sols urbains en prenant en compte les chemins préférentiels

---

Devant le jury composé de :

Dr. Pascal Molle	Directeur de recherche / INRAE-Lyon	Président du Jury
Dr. Fabrice Rodriguez	Chercheur IDTPE, HDR/ Université Gustave Eiffel	Rapporteur
Prof. Zahra Thomas	Professeur des universités / L'Institut Agro Rennes-Angers	Rapporteur
Dr. David Ramier	Chargé de recherche/ CEREMA	Examinateur
Prof. Gislain Lipeme Kouyi	Professeur des universités / INSA-LYON	Directeur
Prof. Laurent Lassabatère	Chercheur IDTPE-MTES, HDR / ENTPE	Co-Directeur
Prof. Tim D. Fletcher	Professeur des universités / Melbourne	Invité

Département FEDORA – INSA Lyon - Ecoles Doctorales

SIGLE	ECOLE DOCTORALE	NOM ET COORDONNEES DU RESPONSABLE
CHIMIE	**CHIMIE DE LYON** **https://www.edchimie-lyon.fr** Sec. : Renée EL MELHEM Bât. Blaise PASCAL, 3e étage secretariat@edchimie-lyon.fr	**M. Stéphane DANIELE** C2P2-CPE LYON-UMR 5265 Bâtiment F308, BP 2077 43 Boulevard du 11 novembre 1918 69616 Villeurbanne **directeur@edchimie-lyon.fr**
E.E.A.	**ÉLECTRONIQUE, ÉLECTROTECHNIQUE, AUTOMATIQUE** **https://edeea.universite-lyon.fr** Sec. : Stéphanie CAUVIN Bâtiment Direction INSA Lyon Tél : 04.72.43.71.70 secretariat.edeea@insa-lyon.fr	**M. Philippe DELACHARTRE** INSA LYON Laboratoire CREATIS Bâtiment Blaise Pascal, 7 avenue Jean Capelle 69621 Villeurbanne CEDEX Tél : 04.72.43.88.63 **philippe.delachartre@insa-lyon.fr**
E2M2	**ÉVOLUTION, ÉCOSYSTÈME, MICROBIOLOGIE, MODÉLISATION** **http://e2m2.universite-lyon.fr** Sec. : Bénédicte LANZA Bât. Atrium, UCB Lyon 1 Tél : 04.72.44.83.62 secretariat.e2m2@univ-lyon1.fr	**Mme Sandrine CHARLES** Université Claude Bernard Lyon 1 UFR Biosciences Bâtiment Mendel 43, boulevard du 11 Novembre 1918 69622 Villeurbanne CEDEX **sandrine.charles@univ-lyon1.fr**
EDISS	**INTERDISCIPLINAIRE SCIENCES-SANTÉ** **http://ediss.universite-lyon.fr** Sec. : Bénédicte LANZA Bât. Atrium, UCB Lyon 1 Tél : 04.72.44.83.62 secretariat.ediss@univ-lyon1.fr	**Mme Sylvie RICARD-BLUM** Institut de Chimie et Biochimie Moléculaires et Supramoléculaires (ICBMS) - UMR 5246 CNRS - Université Lyon 1 Bâtiment Raulin - 2ème étage Nord 43 Boulevard du 11 novembre 1918 69622 Villeurbanne Cedex Tél : +33(0)4 72 44 82 32 **sylvie.ricard-blum@univ-lyon1.fr**
INFOMATHS	**INFORMATIQUE ET MATHÉMATIQUES** **http://edinfomaths.universite-lyon.fr** Sec. : Renée EL MELHEM Bât. Blaise PASCAL, 3e étage Tél : 04.72.43.80.46 infomaths@univ-lyon1.fr	**M. Hamamache KHEDDOUCI** Université Claude Bernard Lyon 1 Bât. Nautibus 43, Boulevard du 11 novembre 1918 69 622 Villeurbanne Cedex France Tél : 04.72.44.83.69 **hamamache.kheddouci@univ-lyon1.fr**
Matériaux	**MATÉRIAUX DE LYON** **http://ed34.universite-lyon.fr** Sec. : Yann DE ORDENANA Tél : 04.72.18.62.44 yann.de-ordenana@ec-lyon.fr	**M. Stéphane BENAYOUN** Ecole Centrale de Lyon Laboratoire LTDS 36 avenue Guy de Collongue 69134 Ecully CEDEX Tél : 04.72.18.64.37 **stephane.benayoun@ec-lyon.fr**
MEGA	**MÉCANIQUE, ÉNERGÉTIQUE, GÉNIE CIVIL, ACOUSTIQUE** **http://edmega.universite-lyon.fr** Sec. : Stéphanie CAUVIN Tél : 04.72.43.71.70 Bâtiment Direction INSA Lyon mega@insa-lyon.fr	**M. Jocelyn BONJOUR** INSA Lyon Laboratoire CETHIL Bâtiment Sadi-Carnot 9, rue de la Physique 69621 Villeurbanne CEDEX **jocelyn.bonjour@insa-lyon.fr**
ScSo	**ScSo*** **https://edsciencessociales.universite-lyon.fr** Sec. : Mélina FAVETON INSA : J.Y. TOUSSAINT Tél : 04.78.69.77.79 melina.faveton@univ-lyon2.fr	**M. Bruno MILLY** Université Lumière Lyon 2 86 Rue Pasteur 69365 Lyon CEDEX 07 **bruno.milly@univ-lyon2.fr**

*ScSo : Histoire, Géographie, Aménagement, Urbanisme, Archéologie, Science politique, Sociologie, Anthropologie

Dedication

I dedicate this work to my father, my heroic father, who fueled my passion for this vital subject through his career. His profound expertise and unwavering commitment have left an indelible mark on my personal journey.

I also extend this dedication to my extraordinary mother. Her unwavering compassion and support have profoundly shaped my perspective on striving for better human beings. They have been my endless source of inspiration and I am eternally grateful for their unwavering love and constant support - moral, spiritual, emotional, and financial.

To my sisters and my brothers.

Words cannot express the depth of my gratitude.

Acknowledgments

I stand at the culmination of a long and challenging journey, and it is with immense joy and humility that I express my gratitude to all those who have contributed to the completion of this thesis.

First and foremost, I would like to thank my Ph.D. supervisors, Prof. Gislain Lipeme Kouyi, and Prof. Laurent Lassabatere for giving me the opportunity to carry out my PhD studies and for their continuous support, motivation, and academic guidance throughout this research. They always responded to my questions with patience and their door was always open for me for further discussions. I owe my profound gratitude to them for being a resourceful person with unfailing guidance and valuable suggestions for me to constantly fighting failures and disappointments. Their dedication to fostering an intellectually stimulating environment has been instrumental in my academic growth.

Gislain, your guidance has profoundly shaped me, and I am thankful for your assistance and consistent support whenever I sought your counsel. Your dynamic approach continues to inspire me.

Laurent, conveying the depth of my gratitude for your dedication to cultivating precision, especially in the domain of code development, is a challenge. Your consistent moral encouragement and the engaging dialogues we've shared have left a substantial imprint on my journey.

I should express my thanks to the members of the jury; Dr. Fabrice Rodriguez, Prof. Zahra Thomas, Dr. Pascal Molle, Dr. David Ramier, and Prof. Tim Fletcher for their time, valuable input, and constructive critiques that have enriched the quality of this thesis.

I should express my gratitude to Prof. Tim Fletcher, Dr. Damien Telodi, and Jérémie Bonneau for Their comments and fruitful discussions that helped me to increase the quality of my work.

I would also like to express my gratitude to the director of the DEEP laboratory, Pierre Buffiere, and Prof. Jean-Luc Bertrand-Krajewski for their invaluable assistance and unwavering support.

To my colleagues in the DEEP laboratory, your assistance and encouragement have been greatly appreciated. Our conversations in the coffee room have been a pleasure.

I can remember my first days in this laboratory when Nathalie was helping me to advance my administrative staff. Thanks, Nathalie, for helping me with administrative issues while always smiling.

I wish to express my profound gratitude to my family for their unwavering love and support throughout this journey. My parents, who have been my inspiration and pillar in every aspect of my life, including this thesis. My dear sisters, Asrin and Neda, and my brothers, Kia and Pouya, your unwavering faith in my abilities and constant encouragement have been my driving force. I am sincerely thankful for the sacrifices you have made and your understanding.

I would like to thank Enric for being a presence in my life and for his support during this period.

I would like to extend my heartfelt appreciation to the Institute Kurde de Paris for their invaluable assistance in helping me pursue a Campus France scholarship. I also extend my heartfelt appreciation to all the members of GRAIE for their support throughout this journey. I am grateful to H2O Lyon for their financial and scientific support.

I want to send a special note of gratitude to my colleagues at the office. To Violetta, whose lovely flowers brightened our workspace and whose stories about her chickens and their amusing history brought a touch of levity to our days. To my Brazilian colleagues, your support and the moments we shared were truly meaningful.

I want to express my deep appreciation to my dear friends, Sedighé, Fakheré and Maryam. Your encouragement, camaraderie, and moments of relief during challenging periods have made this academic pursuit more enjoyable and unforgettable. Your companionship has added a valuable dimension to this experience.

Lastly, I'd like to convey my thanks to all the unnamed participants and laboratory members. I'm also grateful for the insightful discussions with my Ph.D. colleagues, particularly Mathis, with whom I enjoyed conversations about Iranian cuisine. I extend my appreciation to the postdocs, Eloise, Amin and Jolie for their experiments, support, and engaging discussions.

In conclusion, I am aware that this thesis is the culmination of the collaborative efforts of numerous individuals, and I am profoundly thankful to each and every one of you for your contributions.

This journey has been transformative, and as I step into new horizons, I carry with me the lessons learned and experiences gained.

With heartfelt appreciation, Asra ASRY

Abstract

Infiltration plays a crucial role in the urban water cycle by acting as a threshold between runoff and flow or storage in soils. This study aims to address the challenge of modeling infiltration in a robust and practical way for Sustainable Urban Drainage Systems (SUDS), focusing on an easily adjustable physically-based approach that balances complexity and parsimony.

This involves minimizing the number of parameters, using physical parameters collected in the field, and examining the impact of macropores on infiltration rates through SUDS. Various methods have been introduced and evaluated to answer these questions. Firstly, this thesis proposes the development of a new module called INFILTRON-Mod, a physically-based infiltration model that can be easily calibrated, thus proving its potential for integration into hydrological models.

A large set of experimental data and synthetic results (Hydrus) are used for validation. This thesis then develops further the proposed model by incorporating a dual permeability concept to take into consideration the preferential flows in SUDS. Finally, this study leads to an analysis of the uncertainty and sensitivity of the proposed models.

In conclusion, this thesis has produced crucial information for optimizing the modeling of urban water management tools by coupling a 'soil science' component with a 'hydrological modeling of SUDS' component. Further research is recommended to improve and extend the scope of the proposed models, thus contributing to a more accurate representation of hydrological phenomena in their complexity within SUDS.

Keywords: SUDS, infiltration, hydrology, modeling, soil

Résumé

L'infiltration joue un rôle crucial dans le cycle urbain de l'eau en servant comme limite entre le ruissellement et l'écoulement ou le stockage dans les sols. Cette étude vise à relever le défi de modéliser de manière accessible et fiable l'infiltration au sein des Systèmes de Gestion Durable des Eaux Pluviales (SUDS en anglais), en mettant l'accent sur la prise en compte des processus physiques tout en cherchant un équilibre entre complexité et parcimonie.

Cela nécessite de réduire au maximum le nombre de paramètres, de s'appuyer sur des paramètres ayant un sens physique et obtenus à partir de mesures de terrain et de prendre en compte l'impact des macropores sur les taux d'infiltration à travers les SUDS. Diverses méthodes ont été mises en œuvre et évaluées pour répondre à ces questions. Dans un premier temps, cette thèse propose le développement d'un nouveau module appelé INFILTRON-Mod, fondé sur un modèle d'infiltration en appui sur des principes physiques et pouvant être calibré facilement, démontrant ainsi son potentiel d'intégration dans des modèles hydrologiques. Un ensemble important de données expérimentales ainsi que des résultats synthétiques (Hydrus) sont utilisés pour la validation. Ensuite, la thèse étend le modèle proposé en incorporant un concept de perméabilité duale pour prendre en compte les écoulements préférentiels dans les SUDS. Finalement, une analyse de l'incertitude et de la sensibilité des modèles proposés a également été réalisée.

Pour conclure, cette thèse a produit des informations cruciales pour l'optimisation de la modélisation des ouvrages de gestion des eaux urbaines en couplant un volet « physique du sol » et un volet « modélisation hydrologique des SUDS ». Il est recommandé de poursuivre les recherches pour améliorer et élargir le domaine d'application des modèles proposés, contribuant ainsi à une représentation plus en lien avec la complexité des phénomènes hydrologiques au sein des SUDS.

Mots clés : SUDS, infiltration, hydrologie, modélisation, sol

Table of contents

List of figures

List of tables

Nomenclature

SUDS	Sustainable urban drainage systems
CH	Canoe Hydrobox platform
CH1	Canoe Hydrobox model: initial version (first model)
CH2	Canoe Hydrobox model: first improvement (second model)
CH3	Canoe Hydrobox model: second improvement (third model)
SWMM	Storm water management model
LID	Low Impact development
BEST	Beerkan estimation of soil transfer parameters
$\boldsymbol{q}$ **(L T^{-1})**	Water flux
$\boldsymbol{h}$ **(L)**	Water pressure head
$\boldsymbol{\theta}$ **(L^{3} L^{-3})**	Water content
$\boldsymbol{K(\theta)}$ **(L T^{-1})**	Unsaturated hydraulic conductivity
$\boldsymbol{l\ (-)}$ **and** $\boldsymbol{n}$ **(-)**	Hydraulic shape factors of Mualem Van Genuchten eq.
$\boldsymbol{K_{\mathrm{s}}}$ **(L T^{-1})**	Saturated hydraulic conductivity
$\boldsymbol{I\ \ (L)}$	Cumulative infiltration
$\boldsymbol{\theta_{\mathrm{i}}}$ **(L^{3} L^{-3})**	Initial water content
$\boldsymbol{V_{\mathrm{w_{added}}}}$ **(L^{3})**	Volume of water added to the soil block
$\boldsymbol{\theta_{\mathrm{s}}}$ **(L^{3} L^{-3})**	Saturated water content
$\boldsymbol{\theta_{\mathrm{r}}}$ **(L^{3} L^{-3})**	Residual water content
$\boldsymbol{Z_{\mathrm{soil}}}$ **(L)**	Soil depth
$\boldsymbol{z_{\mathrm{f}}}$ **(L)**	Position of the wetting front
$\boldsymbol{h_{\mathrm{a}}}$ **(L)**	Water pressure head is fixed at surface
$\boldsymbol{h_{\mathrm{i}}}$ **(L)**	Initial isostatic water pressure head
$\boldsymbol{h_{w}}$ **(L)**	Water present in the saturated soil
IPCC	Intergovernmental Panel on Climate Change
IWS	Internal Water Storage
ET	Evapotranspiration
$\boldsymbol{Q_{overflow}}$ **(L T^{-1})**	Cumulative overflow from the ponding zone
$\boldsymbol{Q_{Infiltration}\ (L\,T-1)}$	Cumulative inflow volume from surface infiltration
$\boldsymbol{Q_{Inflow}\ L\,T-1)}$	Inflow discharge in the ponding zone
$\boldsymbol{\frac{dH}{dt}}$ **(L T^{-1})**	Water reserved at the ponding zone
$\boldsymbol{\frac{dF}{dt}}$ **(L T^{-1})**	Water stored in the filter media
$\boldsymbol{Q_{Out}}$	Signifies the outflow from the drainage pipe
$\boldsymbol{Q_{Exfiltration}}$	Infiltration to the subsoils or percolation
$\boldsymbol{\theta_{w}}$	Wilting point saturation
$\boldsymbol{\theta_{fc}}$	Field capacity saturation
$\boldsymbol{Q_{ETr}}$	Real evapotranspiration rate

$\boldsymbol{Q_{etp}}$	Potential evapotranspiration rate
FAWB	Facility for Advanced Water Biofiltration
$\boldsymbol{h_{pond}}$	Water level in the surface storage
$\boldsymbol{h_{weir}}$	Height of the overflow weir
$\boldsymbol{K_{s\,inf}}$	Saturated hydraulic conductivity of the surrounding soil
$\boldsymbol{S_{wet}}$	Wetted area of the filter storage
H	Difference between the water level in filter and the level of the underdrain orifice
F	Water level in filter
$\boldsymbol{C_{out}}$	Orifice coefficient to be calibrated
$\boldsymbol{g}$	Acceleration due to gravity
$\boldsymbol{\varphi}$	Matric suction at the wetting front
$\boldsymbol{K(S_e)}$	Mean unsaturated hydraulic conductivity
$\boldsymbol{S_e(\theta)}$	Soil moisture under residual, saturated, and actual conditions
$\boldsymbol{\alpha}$	Fitting parameter related to water pressure head
m	Shape parameters of infiltration equation
$\boldsymbol{\tau}$	Tortuosity shape parameters of infiltration equation
$\boldsymbol{\psi_g}$	Gravitational potential
$\boldsymbol{\psi_o}$	Osmotic potential
$\boldsymbol{\psi_c}$	Capillary potential
SWRC	Soil Water Retention Curve
PTF	Pedotransfer functions
SHPs	Specific soil hydraulic properties
$\boldsymbol{Z_{\mathrm{f}}}$	Position of the wetting front, the wetting front depth
$\boldsymbol{\theta_{\mathrm{m}}}$	Water contents of the matrix
$\boldsymbol{K_{\mathrm{m}}}$	Hydraulic conductivity
$\boldsymbol{K_{\mathrm{f}}}$	Hydraulic conductivity of the macropore (fracture)
$\boldsymbol{\theta_{\mathrm{f}}}$	Water contents of the macropore (fracture)
$\boldsymbol{\omega}$	Weighting factor of the macropore (fracture) volume
GLUE	The Generalized Likelihood Uncertainty estimate
SA	Sensitivity analysis
LSA	Local Sensitivity Analysis
OAT	The 'one-at-a-time'
GSA	Global SA
FAST	Fourier Amplitude Sensitivity Test
MCMC	Markov Chain Monte Carlo
PDF	Probability density function

Chapter 1

Introduction

Chapter 1. Introduction

Over the past decade, the hydrological cycle of the urban area has been altered by an associated shift in surface imperviousness or “soil artificialization,” which led to the decline and loss of natural and agricultural areas. Urbanization through soil artificialization leads to (i). a reduction in the rate of deep infiltration, which feeds the groundwater bodies, (ii). a reduction in surface infiltration into the unsaturated zone, (iii). a reduction in the rate of evapotranspiration, and (iv). an increased risk of runoff and flooding in urban areas (Federal Interagency Stream Restoration Working Group (US), 1998; Shuster et al., 2005).

Traditionally, stormwater management controls were designed to efficiently collect, convey, and discharge water as quickly and efficiently from cities. Hence the excess rainfall events that occur in the impervious urban area lead to combined sewer overflows, combining stormwater and wastewater, causing flooding, and then expensive water treatment. It also promotes flooding, erosion, and degradation of stream ecosystems and associated reduced biodiversity, as a direct consequence of stormwater discharged into freshwater bodies (Roy et al., 2008). This traditional approach has long been known not to be a sustainable way to manage urban stormwater (Marsalek et al., 1993).

Source and decentralized solutions for stormwater management emerged in the last decade as more viable and sustainable options. More studies were drawing attention to the benefits of controlling runoff at the source and increasing infiltration and evapotranspiration by using a Sustainable Urban Drainage System (SUDS) or Low-impact development (LID) (Schueler, 1987; Sieker, 1998).

The SUDS is the site design alternative strategy with attempts to minimize stormwater management costs by taking natural approaches like infiltration or soil water uptake (Flanagan et al., 2019; Fletcher et al., 2015a). Infiltration is the key principle of such systems, given that a high-performance stormwater drainage system is one that is designed to reduce the runoff volume, reduce the peak flow rate, and filter the pollution from the stormwater before it reaches the water table. Many experiments and research papers have been conducted on selecting the appropriate substrate or vegetation within SUDS, but modeling provides a practical approach to studying design performance.

In soil physics, hydraulic properties within soils including those in SUDS have been investigated using either mechanistic infiltration models such as Richards' equations, empirical models such as Philip's, Meyer and Warrick's, Brooks and Corey's, Gardner's, Brutsaert's, Haverkamp's, or physically-based conceptual models such as Green-Ampt's or van Genuchten's models.

The estimation of infiltration flow in SUDS can be achieved through numerical modeling, such as using HYDRUS. However, these models require information regarding the water retention curve and hydraulic conductivity of soils used in the filter media. This information can be obtained through specialized methods like ROSETA or BEST methods (Beerkan estimation of soil transfer parameters) developed by (Lassabatère et al., 2006). It is important to note that these models are typically used for site-specific conditions and specific boundary conditions. It may require additional measurements, extensive data collection, and a comprehensive understanding of the specific site characteristics. Overall, while numerical modeling techniques like HYDRUS offer powerful tools for estimating infiltration flow in SUDS, the complexity lies in acquiring the required soil information for accurate modeling. This highlights the need for careful consideration and evaluation of data availability and feasibility before implementing such models in practical applications of urban hydrological models.

Hydrologic modeling software packages like SWMM and MUSIC provide a comprehensive platform to simulate both the quantity and quality of urban runoff. These software packages incorporate various hydrological processes involved in the urban hydrological cycle, focusing on spatially modeling infiltration processes. Using a physically-based high parsimony module, they are designed to calculate the hydrological balance of a catchment from an operational point of view. Among the existing models for SUDS, the filter media is typically assumed to be homogeneous, and the flow is calculated using conceptual-physically-based infiltration models such as the Green-Ampt. However, Green-Ampt remains easy to use and to incorporate into the hydrological modeling of urban areas, but from an operational point of view, the calibration of the Green-Ampt equation can be complicated due to the challenge of determining the soil suction at the wetting front which defines one key parameter of the Green-Ampt model.

Furthermore, uncertainty can impact the computation of soil suction at the wetting front in the context of the PTF function, and variations in soil suction along the infiltrated depth can pose challenges to the calibration of the Green-Ampt model.

In addition, the heterogeneity of soil water storage such as the presence of coarse materials and plant root systems increases the sophistication required for application of the Green-Ampt model as it assumes a homogeneous soil medium. It is, therefore, necessary to use a physically-based infiltration model that takes into account non-equilibrium and preferential flow, while remaining parsimonious in its uses of easily measurable soil properties.

1.1. Problem statement, research questions, and objectives

Over recent years, there has been a significant focus on the development of physical water infiltration models to be applied in urban water management software tools. These models have proven to be useful tools for evaluating the performance of existing SUDS and for the design and implementation of new water management strategies in urban areas. Nevertheless, the complexity and data requirements associated with numerical water infiltration modeling can often limit its practical use by operational and SUDS managers.

Therefore, there is an increasing requirement for models that offer straightforward calibrations, high reliability, and ease of data use, specifically when it comes to the collection of soil properties data which are relatively easy to obtain. Such models would provide practical solutions for operational and SUDS managers who need to have a practical tool for evaluating and planning urban water management schemes. Therefore, through simplified calibration procedures and minimized data requirements, such models can effectively overcome the gap between complex numerical models and the practical needs of policymakers in urban water management. Despite the importance of preferential flow and the extensive research to understand the physical processes involved in preferential flow in soil, no well-documented, practical, simplified, physically-based urban infiltration models exist to predict preferential flow and water infiltration in heterogeneous soil. The well-known Green-Ampt infiltration model, which is widely used in SUDS modeling tools and implemented in many softwares, does not model all the times the physical processes within SUDS, in particular soil water content and its temporal and spatial variability, and soil heterogeneity.

In this context, the physically-based hydrological model that can be easily calibrated could be an interesting alternative for those responsible for urban water governance in both current and prospective cities in the context of global change (urban population growth, global warming).

The objective of this thesis is, therefore, to develop and test a simplified, physically-based model that requires little effort to calibrate in order to capture the hydraulic dynamics of soil infiltration within SUDS.

Three research questions were identified and answered in the following chapters:

- Can an infiltration model be developed that accurately reflects the movement of water through the filter media in SUDS? Ideally, the model should be simplified, physically-based, SUDS-specific, and easily calibrated using minimal parameters or readily available field data (Chapter 3)

- Can macroporosity and the impact of preferential flow be included in the infiltration modeling of SUDS? (Chapter 4)

- How various parameters can influence the model's behavior (Chapter 5)

1.2. Thesis outline

The primary objective of this study was to develop a comprehensive model that accurately represents water movement within the soil filter media of sustainable urban drainage systems, based on physically-based equations. Using readily available soil properties, the model sought to balance simplicity and accuracy. This thesis is divided into six chapters to achieve these objectives.

Chapter 1: The first chapter describes the presentation and introduces the work.

Chapter 2: The second chapter provides the general scientific context of this work by presenting a synthesis of urban hydrology and infiltration modeling in SUDS. This chapter is mainly bibliographical and allows us to situate the topic of our study and the methodology followed in this manuscript.

Chapter 3: Development of new global models and validation of all these models by comparison with reference numerically generated data models (Hydrus) and real experimental data (infiltrometry data obtained with a large infiltration ring prototype the co-called "INFILTRON-Exp" device developed within the framework of ANR, in direct and indirect modes (estimation of soil hydrodynamic parameters). This will allow us to review in detail all the models and to validate them properly, using the case of single-permeability porous media at first.

Chapter 4: Adaptation of the models for the dual-permeability porous media under both direct and indirect modes in the direct and indirect modeling to take into account the macroporosity of the soils (taking into account the preferential flow). The aim is to identify the dominant processes, such as the influence of preferential pathways, by comparing the fine infiltration model (Hydrus) with the global approaches (INFILTRON-Mod).

Chapter 5: Assessing the sensitivity of the model through various calibration approaches, this segment outlines uncertainty and sensitivity analyses for models discussed in Chapters 3 and 4. It gauges reliability via parameter shifts, enhancing comprehension and decision-making while applying it to inverse modeling for data fitting.

Chapter 6: The general conclusion will aim at the essential points of this research, and the perspectives envisaged following this thesis.

Chapter 3 represents the published journal article (Asry et al., 2023), while Chapter 4 is currently being revised for submission at the earliest opportunity.

Chapter 2

Literature review

Chapter 2. Literature review

Preface

This chapter aims to provide the scientific context and literature review to properly understand the hydrogeological processes in urban catchments that will be investigated in the remainder of this manuscript. The literature review has been organized into six main sections to achieve these objectives. We begin with a brief description of the hydrological cycle in urban areas, followed by a historical review of stormwater management, focusing on natural infiltration-based practices (Sustainable Urban Drainage Systems) and their modeling and performance evaluation. This is followed by a review of hydrological processes and infiltration into the unsaturated zone. Then, the impact of heterogeneity and preferential flow on modeling infiltration in unsaturated soils and related application to soils in SUDS is discussed. Finally, we provide an overview of model inversion methods for the parameterization of the infiltration modeling.

Contents

2.1. Introduction

The hydrological cycle serves as a comprehensive conceptual model that depicts the movement and storage of water components within a closed system, considering various physical processes like evapotranspiration, precipitation, infiltration, percolation, snowmelt, and runoff. In urban areas, the hydrological cycle becomes more complex and intricate due to multiple human-induced influences and interventions.

The artificialization of natural spaces has several consequences, including physical and chemical changes in soils, disruption of hydrological processes in watersheds, and the contamination of water resources (Bechet et al., 2017).

Contrary to natural and forested areas, urbanized areas are typically characterized by the establishment of impervious surfaces, disrupting the capacity to capture, retain, or infiltrate urban rainfall and runoff. (see Figure (2.1)) (Fletcher et al., 2013; Voter and Loheide, 2020). Moreover, impermeable surfaces such as asphalt, concrete, and roofs contribute to increased surface temperatures, amplifying the urban heat island (UHI) effect (Milelli, 2016; Masson et al., 2020).

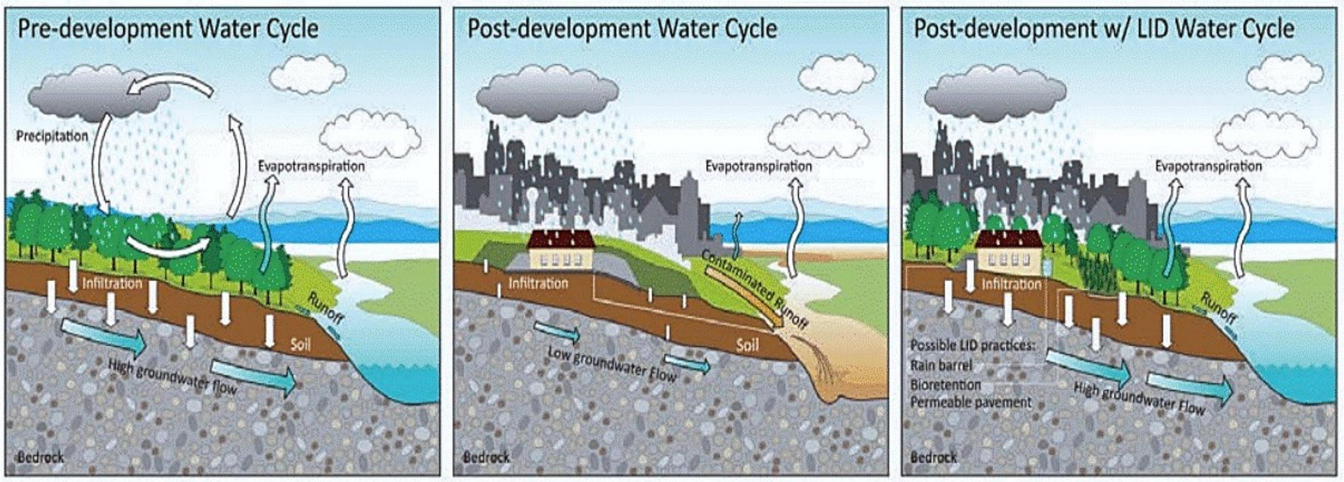

Figure (2.1): The left panel represents the rural water cycle: the natural water cycle encompasses processes such as infiltration, groundwater flow, and evapotranspiration, the center panel represents the urban water cycle (UWC): Urbanization's impermeabilization reduces water absorption, hindering infiltration and groundwater recharge, leading to increased flooding and pollutant transport and the right panel depicts the sustainable urban water cycle: Low-impact development by increase infiltration aim to restore the pre-development urban water cycle sustainably (University of Tennessee, 2014)

There has been a substantial increase in the global urban population, with the percentage rising from 25% in 1950 to approximately 50% in 2020 (Habitat, 2022). This combined influence of artificialization and population growth significantly impacts natural landscapes and watersheds' hydrological response (Grimm et al., 2008). Although the fundamental structure of the hydrological cycle remains intact in urban areas, it undergoes substantial modifications due to the impacts of urbanization on the environment and the requirements of providing water supply, drainage, and wastewater management.

The IPCC Sixth Assessment Report (GIEC, 2022) indicates that global warming will continue to rise until at least mid-century across all emissions scenarios, exceeding the critical 1.5°C and 2°C global warming thresholds within the 21st century. On the other hand, the urban population is expected to gradually increase to 58% over the next 50 years (Habitat, 2022). The entire urban water cycle (Marsalek et al., 2006; Mitchell et., 2001), including water supply, sewage treatment, and stormwater runoff systems, may face pressure due to climate hazards and anthropogenic impacts regarding the following issues:

- ➢ A rise in water demand can result from the addressed issues that can strain urban water supplies, contributing to water scarcity and compromising urban water security (Brears, 2017).
- ➢ Subsurface flow and groundwater recharge: Urbanization leads to a higher prevalence of impervious surfaces, significantly impacting the hydrological dynamics of a watershed. These impervious surfaces pose a significant barrier to the natural movement of water into the soil, causing a substantial decrease in both infiltration and the replenishment of groundwater resources. Modifying the structure and texture of the upper soil horizons (e.g., compaction, embankments) leads to uncertain hydrological behavior, even for permeable surfaces (Voter and Loheide II, 2020). The relationships between urbanization and subsurface flow processes are influenced by various factors, including natural catchment characteristics (such as geology, topography, and vegetation) and characteristics specific to urbanization (such as the arrangement of impervious areas and drainage systems) (Hamel et al., 2013). the influence of urbanization on baseflows exhibits a strong dependence on specific contexts and exhibits significant variability contingent upon local circumstances, land utilization trends, and the degree of urban expansion. To illustrate, impermeable surfaces hinder the infiltration of water in specific catchment regions, thereby diminishing baseflows. Conversely, the depletion of

vegetation in other more permeable zones can lead to a reduction in evapotranspiration, possibly resulting in heightened infiltration and consequently an augmentation of baseflows. In certain scenarios, the absence of vegetation in conjunction with soil compaction may yield substantially diminished rates of infiltration. This observation is consistent with studies that have examined the impact of urbanization and artificialization on the groundwater balance (Braud et al., 2013; Sanzana et al., 2019).

➢ Stormwater runoff: The artificialization of natural spaces primarily affects the surface components of the hydrological balance and the dynamics of flow transfer to the outlet of the basin. The covering of surfaces with impermeable objects (e.g., various buildings, road surfaces, parking lots) reduces the opportunities for infiltration and evapotranspiration of rainwater, consequently leading to an increase in runoff (Fletcher et al., 2013; Schueler et al., 2009). In addition, due to the low roughness characteristics of engineered surfaces, there is an accelerated transfer of runoff downstream in urban areas (Shuster et al., 2005). At the catchment scale, these changes in flow production and transfer directly translate into higher volumes and peak flows at the outlet (see Figure (2.2)) (Ferguson, 2017a). The extent of these effects is highly dependent on surface land uses (e.g., the proportion of urbanized area in the catchment, the proportion of impermeable surfaces attached to the drainage system, the spatial distribution of these surfaces within the catchment, and the nature of connections between surfaces) (Fletcher et al., 2013).

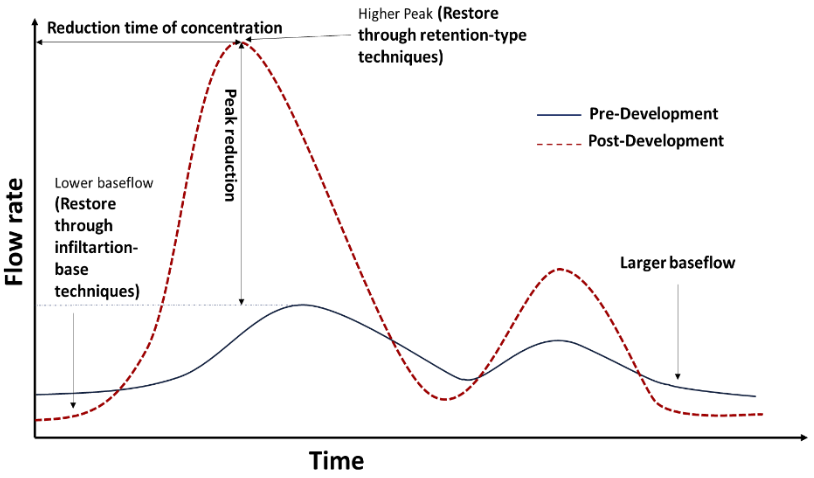

Figure (2.2): Schematic illustration of the significant impacts of urbanization on hydrology at the catchment scale (adopted from (Fletcher et al., 2013))

The heightened runoff exacerbates environmental stress and presents challenges for managing stormwater and wastewater systems. Nevertheless, stormwater management plays a crucial role in ensuring the sustainability of the urban water cycle in future cities.

Over time, stormwater management practices have evolved and been adapted to promote sustainable urban drainage systems. These systems aim to effectively manage stormwater runoff, minimize flooding risks, and mitigate the negative impacts of urbanization on the hydrological cycle. A look back at the history of stormwater management shows that before the 1950s, the main focus of urban wastewater management was on ensuring proper sanitation. The goal of sewerage systems at that time was to quickly remove rainwater and sewage from urban areas using a system of pipes known as a «united sewerage system, » which ensured the transportation of these effluents without distinction.

System overflows became more frequent due to postwar urban development's increased demand on the systems, especially the downstream segments (Chocat, 1997; Fletcher et al., 2013). In addition, the increase in impervious surfaces combined with the rapid discharge to the outlet implied an increase in response disruption at the basin outlet and an increase in the risk of flooding downstream of the urbanized area. In the 1960s, concerns about the environmental effects caused by sewage were addressed by installing central treatment systems downstream from the interceptor sewers. Weirs and storage basins for wastewater discharge were installed upstream of these treatment plants as a safety measure. This was done to ensure that the performance of these facilities was not compromised when rainfall occurred (Chocat et al., 2003; Chocat and Cabane, 1999; Fletcher al., 2013). “Separate” networks were also created to relieve the wastewater networks, based on an additional set of pipes used only to transport stormwater to the outlet.

As environmental concerns grew in the 1990s and scientific understanding of urban stormwater pollution advanced, initiatives were implemented to reduce the ecological impact of these stormwater discharges into the environment (Fletcher et al., 2015). With a system of more or less centralized structures that would temporarily hold a certain amount of water and then slowly restore it to the network, the first goal was to relieve the networks during periods of heavy rainfall and reduce the danger of flooding. Stormwater management strategies have gradually incorporated goals of reducing pollutant discharges and restoring basins' «natural» hydrologic functioning.

Considering these objectives from an operational point of view translates into managing current rainfall and associated pollution as far upstream as possible in structures that can result in a significant volume abatement. Impervious surface disconnection approaches are referred to as « source control » instead of strategies relying on traditional networks and centralized retention structures (Fletcher et al., 2013; Huber et al., 2004). The disconnection strategy or SUDS can be implemented at various locations within the urban catchment, depending on the objectives and desired flow regime control. Different approaches can be employed, such as stormwater infiltration-based and retention-based technologies (Yilmaz et al., 2016) or their combination can be applied near the source or at the end of the catchment.

Stormwater infiltration-based technologies include swales, infiltration trenches, basins, unlined bioretention systems (raingardens), and porous pavements. The defining characteristic of this group is that they help restore baseflows by recharging subsurface flows and groundwater. Stormwater retention-based technologies encompass wetlands, ponds, vegetated roofs, and rainwater/stormwater harvesting using tanks or storage basins.

The defining characteristic of this group is that they retain stormwater, either by attenuating outflow or through reductions caused by abstraction. Each approach has its own advantages and disadvantages, Centralized systems are often efficient for managing peak flows. However, there is a growing trend towards more decentralized at-source approaches that propose a more holistic approach to flow restoration. In fact, (Burns et al., 2012) demonstrated that achieving key elements of the natural flow regime requires a combination of retention techniques to address peaks and overall volume, along with infiltration-based techniques to compensate for the loss of infiltration caused by impervious areas distributed throughout the catchment (Shuster et al., 2005). A comprehensive analysis of 100 case studies reveals that achieving critical elements of the natural flow regime requires the installation of an adequate number of source control measures to address peak flows and overall volume and mitigate the loss of infiltration caused by impervious areas dispersed throughout the catchment (Jefferson et al., 2017).

The recent adaptation report from the IPCC (2022) strongly recommends the implementation of SUDS (Sustainable Urban Drainage Systems) and ecosystem-based solutions as effective measures to address global changes. This viewpoint was also supported by the study conducted by the French Water Agency (Feuillette, and Frédéric, 2016) in the suburban catchment of the Paris region.

Through the implementation of these approaches, green corridors are established, UHI (Urban Heat Island) effects are mitigated, and the sustainability of future food and water supply is ensured while simultaneously managing stormwater and wastewater to minimize urban flooding and enhance city resilience and sustainability by IPCC, 2022 (Chow et al., 2022). Figure (2.3) provides an overview of SUDSs in future cities as sustainable adaptation solutions to global change.

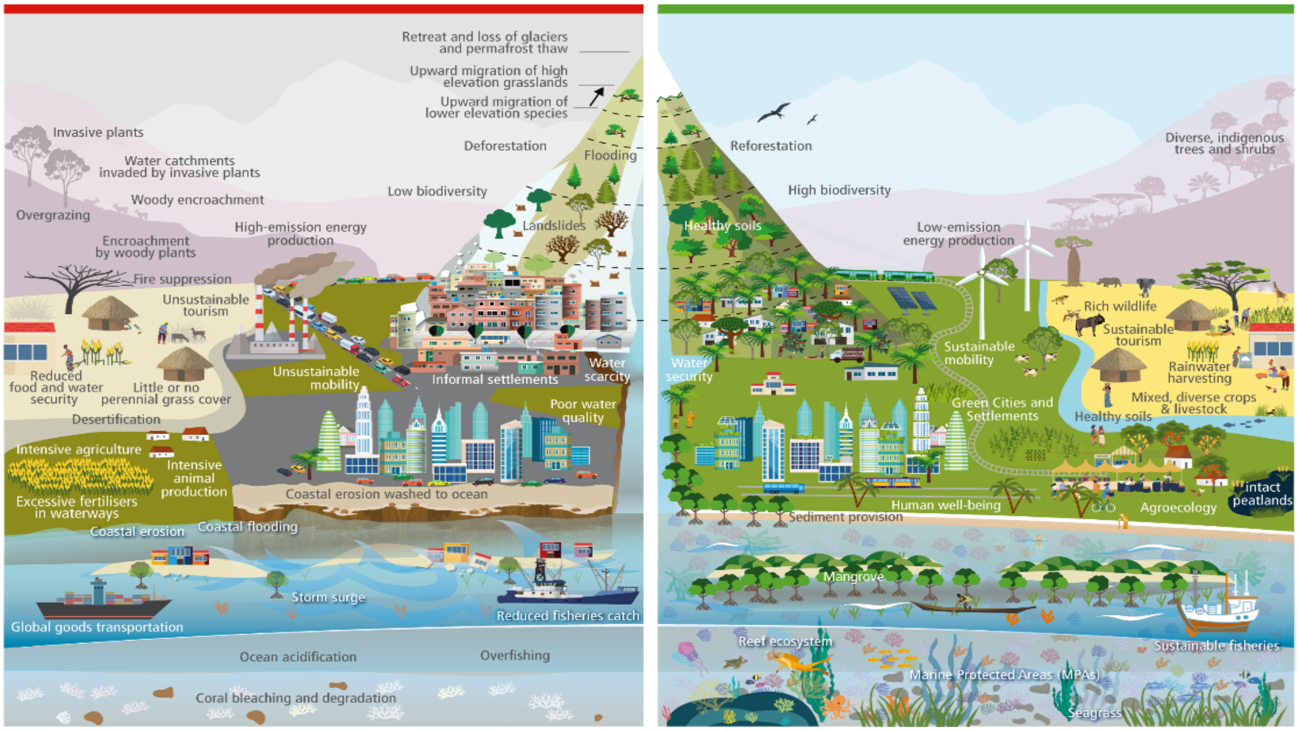

Figure (2.3): SUDS as sustainable adaptation solution to global change (Chow et al., 2022)

2.2. Urban soil Infiltration

Soil infiltration is critical in the urban hydrological cycle by serving as a boundary between runoff and absorption, influencing stormwater pathways and volumes in urban watersheds (Fletcher et al., 2013). It refers to the process through which water seeps through permeable soils, reaching the upper layers of the soil.

Urban soils receive significant disturbance during urbanization, including activities such as excavation, filling, and grading, which rapidly alter the soil and disrupt its formative processes and structure. Although less apparent, these changes represent another essential way urbanization impacts infiltration. Consequently, urban soil profiles typically lack well-developed intermediate soil horizons and do not align with published soil maps (Herrmann et al., 2018; Schifman and Shuster, 2019). The key characteristics of urban soils can be summarized in three points (Craul, 1985):

a- Considerable vertical and horizontal heterogeneousness.

b- An enveloping surface crust is present on top of the bare soil, usually water-repellent.

c- Modified soil structure, aeration, nutrients, temperature, and drainage properties.

The major effects of urbanization on essential soil hydrological and physical properties of soil (e.g., bulk density) (Wessolek, 2008) are summarized in Table (2.1). For example, urban development often leads to the removal of surface soil, exposing subsurface soil with low conductivity, resulting in soil compaction, reduced pore space, and decreased infiltration capacities (Wang, 2017, Craul, 1985, Millward et al., 2011).

Table (2.1): The responses of soil's physical and hydrologic properties to urbanization.

Soil property	The general trends to urbanization	Comments
Porosity	Decreased	Due to rising compaction and decreasing soil organic matter (Lal and Stewart, 2017)
Number of macropores	Decreased	Limited by the weakening of soil structure due to the loss of organic matter and compaction (Craul, 1985)
Saturated hydraulic conductivity	Decreased	Limited by the weakening of soil structure and compaction of subsurface soils (Craul, 1985)
Surface infiltration	Decreased	Limited by surface crusting and decreases in soil permeability (Pagliai et al., 2004)
Available water content	Decreased	Limited by increased stormwater runoff from low-infiltration, compacted soils (Rawls et al., 2003)
Bulk density	Increased	Results from the incorporation of construction debris, fill material, and compaction (Millward et al., 2011)

Soils, which cover a significant portion of urban areas (up to 60%), act as permeable surfaces (Pouyat et al., 2007). The impact of urbanization on the soil will vary depending on the geological characteristics, such as soil depth. In the case of confining layers, permeable urban soils may have such limited infiltration capacities that they may function similarly to impervious areas (Gregory et al., 2006; Voter and Loheide, 2020).

Additionally, deep-rooted plants play a role in creating macropores throughout the soil profile. These macropores allow for better water infiltration and drainage, mitigating the adverse effects of urbanization on soil hydrology (Price, 2011). A meta-analysis of 89 studies confirms that practices promoting surface vegetation and continuous roots, such as perennial grasses and agroforestry, effectively enhance infiltration rates by modifying and improving soil structure (Basche and DeLonge, 2019). In some studies, soil amendment is recommended, as thoroughly mixing in compost or another material with a high infiltration capacity (Voter and Loheide II, 2020). Infiltration-based drainage systems are commonly employed to disconnect impermeable surfaces from stormwater drainage, with the expectation that the subsoil native soil can naturally absorb a significant portion of the runoff for the non-linear and without underdrain type of SUDS (Voter and Loheide II, 2020). Modifications to the filtered soil, i.e., the use of engineered soils or geotextiles, or the installation of culvert pipe, etc., may be necessary depending on the project aims and the effectiveness of the SUDS, which is closely related to the subsoil infiltration rate (C. Li et al., 2017). In this literature review, we concentrate on infiltration and the mechanisms that impact infiltration capacity in the non-saturated zone in SUDS.

2.2.1. Infiltration and source control

Stormwater infiltration at the soil surface is a valuable means of regulating the volume of stormwater runoff, preventing excessive flows from reaching streams and allowing the flow to return to its natural place in the soil and contribute to long-term base flows. The source control stormwater infiltration approach, also known as LID (Low Impact Development) and referred to as SUDS (Sustainable Urban Drainage Systems), WSUD (Water Sensitive Urban Design), GI (Green Infrastructures), or BMPs (Best Management Practices), aims to reduce the costs associated with stormwater management by using natural methods such as retention and infiltration on-site (Fletcher et al., 2015).

There are a variety of infiltration facilities for source control measurements. Depending on the application, they might be installed on the surface or under the ground, compact or extensive, vegetated or unvegetated, etc. The most common structures are vegetated basins.

Examples of widely adopted LID practices include rain gardens, bio-swales, permeable pavement, subsurface retention facilities, tree box filters, rain barrels and cisterns, appropriate landscaping, green roofs, etc. Some examples are depicted in Figure (2.4).

The SUDS uses the natural properties of soils, vegetation, and landscape to rebalance the hydrological dynamics of urban environments. These systems restore water storage capacity, regulate flow patterns, enhance groundwater infiltration, and improve storage and recharge mechanisms. As a result, they effectively mitigate floods and droughts while promoting interconnected ecosystems that achieve a self-sustaining balance (Ferguson, 2017, Basche and DeLonge, 2019). Several factors influence stormwater infiltration into the soil, including:

a- Soil infiltration rate is a vital determinant of an infiltration SUDS's efficiency (Connor et al., 2003; Force et al., 2012). Although design rates vary by soil characteristics and properties such as the soil's grain size, bulk density, layering, and temperature can also affect its infiltration rate. "Engineered media" used in SUDS (custom-made materials designed to improve infiltration, plant growth, and pollution removal), varying from coarse aggregates under permeable pavements to organic-rich substances in bioretention systems. The choice of soil filter media for SUDS systems is essential to ensure adequate infiltration capacity and proper retention time for plant growth. Sandy loam media is preferred as it promotes effective infiltration, while high clay contents have adverse effects. On the other hand, fine fractions in the soil are typically highly reactive chemically and contribute to pollutant removal. Therefore, finding a balance optimizes infiltration capacity and pollutant removal efficiency (Guo et al., 2015). A thorough discussion of these topics can be found in section (2.3.1.) of the literature, which provides detailed insights and comprehensive analysis.

b- Evapotranspiration rate: The available literature on the impact of evapotranspiration flux in infiltration systems indicates that its contribution to runoff abatement is relatively minor, accounting for less than 5% of annual inflows (Bonneau et al., 2018; Fletcher et al., 2013; Hamel and Fletcher, 2014). This limited contribution is primarily attributed to the ratio between the area of the infiltration system and the contributing area, which is typically small, ranging from 2% to 10% in infiltration systems (Thom et al., 2020). Although the overall effect on the water balance is relatively modest, the proportion of evapotranspiration varies significantly over time due to changes in evaporative demand and seasonal variations. In addition to directly contributing to attenuation or increased evapotranspiration flux, vegetation transpiration reduces water content in the upper soil layers, thereby facilitating the infiltration process.

c- Storm Intensity: Runoff may occur when a storm exceeds the soil's infiltration rate, as intense rainfall quickly saturates surface and subsurface storage. The ability to control surface flows at the event scale is strongly influenced by the dynamics and magnitude of incoming flows (Eckart et al., 2017). The performance of infiltration systems significantly decreases with increasing precipitation accumulation or intensity. However, even at the same average precipitation accumulation and intensity, the performance can vary depending on the timing of the peak intensity during the event. The capacity to attenuate volumes varies significantly from one event to another, making it relevant to evaluate attenuation over long precipitation periods. The shape of the contributing surface, land use, and the nature of connections to the system can also influence inflows' dynamics and similarly affect infiltration systems' performance (Fanelli et al., 2017).

d- Antecedent Soil Moisture: The infiltration capacity directly depends on the degree of soil saturation. Soil saturation influences the available volume, hydraulic conductivity, and suction. These factors vary based on the soil's water content during and between events and are influenced by processes such as vegetation transpiration, which significantly redistributes the soil's moisture content. High pre-existing moisture reduces available pore space for infiltration, decreasing runoff water absorption (Sage et al., 2020).

Figure (2.4): Illustrates infiltration LID structures installed on the INSA-Lyon campus (adopted from Graie) above, and the bottom photo is the natural-based infiltration basins

2.3. Modeling infiltration-based practices

2.3.1. Key functional components

The concept of source control infiltration-based facilities is used to collect and filter runoff through the soil, drained to receiving waters (for subsurface drain systems), and absorbed by plants (i.e., Evapotranspiration) (Lisen bee et al., 2021). One of the widely implemented source control measures is bioretention systems. To gain a deeper understanding of the physical and chemical mechanisms involved in water and pollutant movement as well as retention within a bioretention system, each component of a bioretention system must be explained in terms of how it contributes to the system's function (Davis et al., 2009; Huber et al., 1975; Prince George’s County, 2007):

Inlet and Sediment forebay – This component serves as the entry point for stormwater into the rain garden, often through a pipe or kerb cut to prevent coarse litter from entering. An inlet may be equipped with a trash rack or sediment forebay.

Vegetation – in removing water through evapotranspiration and pollutant removal through nutrient cycling and is representative of a terrestrial forest ecosystem that uses native plant species. The root zone promotes soil permeability while the surface vegetation diverts and slows surface flow while filtering sediments. Pollutant removal depends on the area of the plant community created, the age of the plants, and continued maintenance (James, 1994).

Ponding zone – Prevents runoff from filtering through the soil bed, allowing particulates and water to settle and evaporate. Ponding depths are determined by ponding volume, infiltration rates, void space in soils/filter media, and maintenance practices.

Organic Mulch Layer on the surface of the soil – By acting as a filter, it traps pollutants in runoff, retains moisture in plant roots, decomposes leaves and organic material, degrades some pollutants, and protects the soil from drying out (Głąb et al., 2016).

Soil Media – The Bioretention system contains an area for storing stormwater and nutrient uptake by plants and providing water and nutrients to support plant life. Infiltration rates allow for periodic soil saturation, allowing it to maintain aerobic conditions while being well-drained. To assist in the adsorption of pollutants - hydrocarbons, heavy metals, and nutrients (total suspended solid, phosphorus, nitrogen) recommended planting soils composed of 50% sand, 30% topsoil, and 20% organic material (Prince George’s County, 2007).

Submerged zone or Internal Water Storage (IWS) – Some bioretention are designed with a submerged zone beneath the filter media, where water remains. This submerged zone enhances nitrogen removal and benefits bioretention plants during drier summer months.

Underdrain system – In bioretention with underdrain systems, a network of slotted pipes conveys treated stormwater from the base of the rain garden. However, bioretention in sandy soil may discharge infiltrated flows directly into the underlying soil, eliminating the need for underdrains.

Lining filter media – It is crucial to make a distinction between bioretention with permeable bottoms, which aid in water removal by infiltration and groundwater recharge, and those that are waterproofed with a geotextile, which aids in volume reduction through evapotranspiration, in this context (waterproofed rain gardens, vegetated roofs, etc.).

The effectiveness of infiltration-based stormwater control is influenced by three primary factors related to design parameters. Firstly, the type of filter used plays a significant role in rainwater retention and pollutant removal in bioretention (Liu et al., 2014). The filter's hydraulic conductivity, whether saturated or unsaturated, primarily affects the volume of retained rainwater, while the adsorption and interception capacity of the filter plays a crucial role in removing pollutants, such as heavy metals (Hsieh and Davis, 2005). The types of filters used in SUDS can be broadly categorized into three groups: natural materials, industrial by-products, and artificial materials. The filter type selection is often based on differences in hydraulic conductivity and pollutant absorption capacity (Davis et al., 2009). The hydraulic conductivity of a filter is crucial as low conductivity can lead to clogging of the bioretention system, reducing its rainwater retention capacity and overall effectiveness.

Conversely, excessively high hydraulic conductivity can compromise the system's ability to treat rainwater pollutants adequately. Therefore, most research on filter selection has focused on combining mixtures of sand, loam, and clay as additional filters for natural soils. This approach aims to balance infiltration range and pollutant removal efficiency since sandy loam enhances infiltration while a high clay content hampers, it (Hsieh and Davis, 2005). Commonly used natural soils include sand, loam, and clay. Both natural and artificial materials have shown promise for use in bioretention areas, as corroborated by several studies (Wang, 2017). These studies demonstrate that adding compost to the soil can increase water permeability and pollutant removal rates in bioretention areas.

Secondly, the selection of suitable plant species is also essential for the treatment performance of bioretention areas. For example, plants contribute to rainwater runoff reduction through evapotranspiration (ET), and their roots aid in pollutant removal through absorption (Upson et al., 2009; Wadzuk et al., 2015).

Finally, the design dimensions of the SUDS, such as surface ponding volume, filling depth, and IWS, play a significant role in the system's ability to retain runoff and remove pollutants effectively (Brown and Hunt, 2011; Thomas et al., 2011). A deeper filter allows for a longer contact time, enhancing the removal of pollutants. An IWS zone, located beneath the filter layer and formed by raising and bending the drainage pipe outlet, is a significant feature in SUDS, especially for bioretention areas. This zone exhibits vertical variations in moisture conditions, with the upper portion being unsaturated and aerobic while the lower portion is saturated and anaerobic, which can reduce nitrate leaching and increase total nitrogen removal rates. Incorporating an IWS zone should also be considered based on the operational requirements of the bioretention area. For example, in arid and semi-arid regions, the IWS zone can retain water for plant survival, whereas in tropical areas, its inclusion should depend on the need for pollutant removal (Guo et al., 2015). In addition, including the IWS zone can serve as a solution to meet groundwater recharge requirements (Brown and Hunt, 2011).

The volume of the water ponding significantly affects the hydraulic residence time of rainwater runoff. When the depth of the rainwater exceeds the depth of the ponding zone, overflow occurs. The rainwater retention capacity of the bioretention area is limited by the water storage capacity of the ponding zone when the soil infiltration rate reaches saturated hydraulic conductivity (Dussaillant et al., 2005). Moreover, the depth of the ponding zone also influences the soil's infiltration capacity to some extent.

Lining and bottom drainage systems are not essential components in the design of SUDS areas. If a bioretention area lacks a drainage system and lining, the rainwater infiltrates the surrounding soil and helps replenish overexploited groundwater resources. However, it is essential to note that a drainage system is recommended when subsoil has low water permeability (Lucas, 2010).

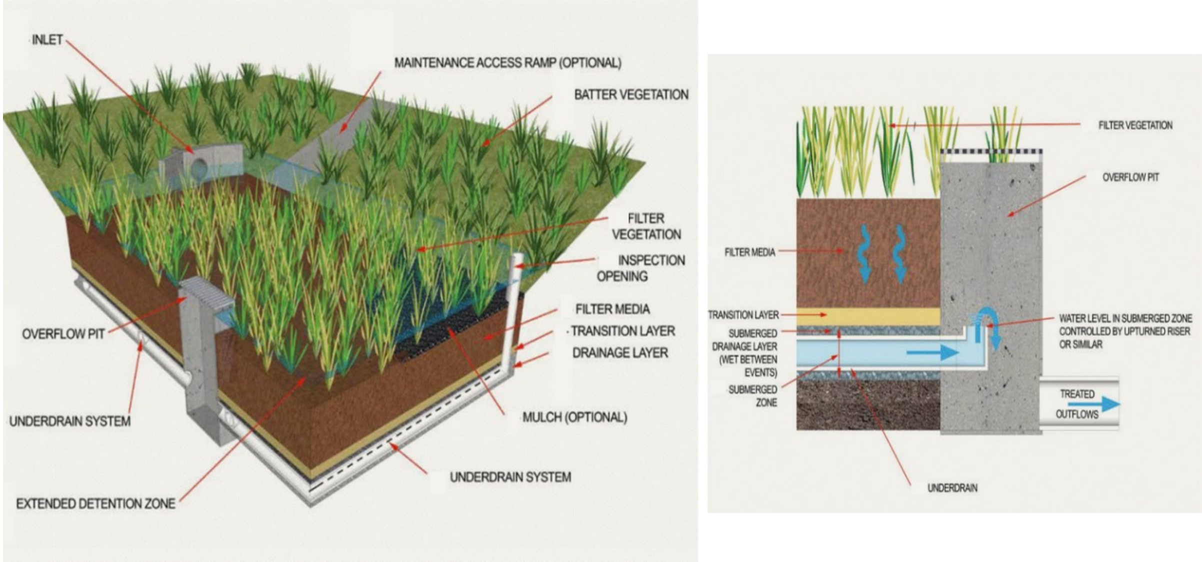

Figure (2.5): Schematic of conventional bioretention in open space (piped inflow) showing key functional elements in the right panel and panel left represent the Cross section of submerged zone bioretention outlet control adopted from (Melbourne Water, 2020)

2.3.2. Hydrological modeling of infiltration-based practices

Models expand research possibilities beyond measurements, overcoming site-specific limitations in field-based studies. The hydrologic modeling of bioretention plays a vital role by offering valuable insights into runoff quantity and quality. It is important to note that reductions in pollution are frequently associated with decreases in runoff volume rather than solely relying on biogeochemical processes (Davis et al., 2009; Jefferson et al., 2017; Li et al., 2017). Depending on the goal of SUDS modeling, several models may be classified as follows: first, planning/assessment tools, and subsequently, process-based computational models. Bioretention systems involve several hydrological processes, including evapotranspiration, infiltration, runoff generation, etc. The overall water balance equation for the entire system, as well as separate equations for the ponding zone and filter medium, can be expressed as follows Equation (2-1a), for the entire system, Equation (2-1a) for the ponding zone, and Equation (2-1a) for the filter medium Figure (2.6):

$$Q_{\mathrm{Inflow}} = Q_{\mathrm{overflow}} + Q_{\mathrm{Infiltration}} + Q_{\mathrm{Etr}} + Q_{\mathrm{Exfiltration}} + Q_{\mathrm{out}} \tag{2-1a}$$

$$A\frac{dH}{dt} = Q_{\mathrm{Inflow}} - (Q_{\mathrm{overflow}} + Q_{\mathrm{Infiltration}}) \tag{2-1b}$$

$$A\frac{dF}{dt} = Q_{\mathrm{Infiltration}} - (Q_{\mathrm{Etr}} + Q_{\mathrm{Exfiltration}} + Q_{\mathrm{out}}) \tag{2-1c}$$

Where $\frac{dH}{dt}$ is the time varying water reserved at the ponding zone, $\frac{dF}{dt}$ is the time varying water stored in the filter media. A denotes the mean area of the base of the ponding zone. In these equations, the sum of precipitation and runoff discharge is represented as Q_{Inflow}, which indicates the inflow discharge in the ponding zone. $Q_{\mathrm{Infiltration}}$ denotes the cumulative inflow rate from surface infiltration while Q_{ETr} denotes the cumulative evapotranspiration rate. Q_{Overflow} refers to the cumulative overflow from the ponding zone, Q_{Out} signifies the outflow from the drainage pipe and $Q_{\mathrm{Exfiltration}}$ is the infiltration to the subsoils or percolation.

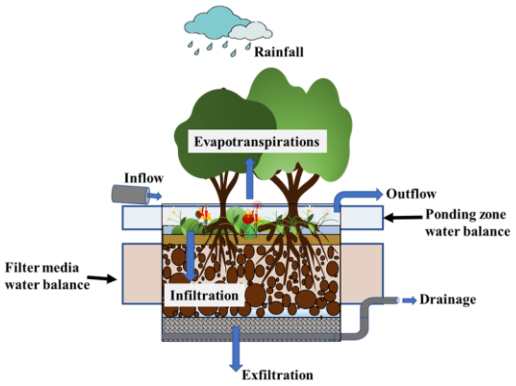

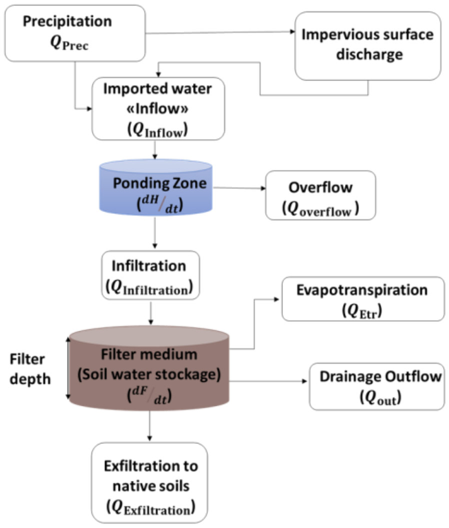

Figure (2.6): Illustration of the conceptual modeling processes for bioretention within the water balance framework.

The following mathematical equations describe the hydrological processes in bioretention modeling. The evapotranspiration Q_{ETr} from the filter media is calculated using potential evapotranspiration (assuming a crop factor of 1.0) and is modulated with a linear function between the wilting point and field capacity (Equation 2-2) (Bonneau et al., 2021; Francés, 2008; Van der Lee and Gehrels, 1990):

$$\begin{gathered} if\ \theta < \theta_w \rightarrow Q_{\mathrm{ETr}} = 0 \\ if\ \theta_w < \theta < \theta_{fc}, \rightarrow Q_{\mathrm{ETr}} = \frac{\theta - \theta_w}{\theta_{fc} - \theta_w} Q_{etp} \\ if\ \theta > \theta_{fc} \rightarrow Q_{\mathrm{ETr}} = Q_{etp} \end{gathered} \tag{2-2}$$

Where θ_w and θ_{fc} are the wilting point and the field capacity, respectively, taken as usual valued for sandy soils (FAWB., 2009), Q_{ETr} is the real evapotranspiration rate and Q_{etp} the potential evapotranspiration rate.

In the hydrological modeling proposed by Bonneau, 2021, the surface storage (‘ponding zone’) and overflow are assumed to be an empty rectangular box. To account for the presence of a weir at the surface of the storage, the user sets a threshold level. When the water level in the storage exceeds this threshold, the excess water is diverted, resulting in an overflow rate, Equation (2-3):

$$\begin{gathered} if\ h_{pond} < h_{weir} \rightarrow Q_{\mathrm{overflow}} = 0 \\ Otherwise \rightarrow Q_{\mathrm{overflow}} = Q_{\mathrm{Inflow}} - Q_{\mathrm{Infiltration}} \end{gathered} \tag{2-3}$$

Where h_{pond} is the water level in the surface storage, h_{weir} the height of the overflow weir, Q_{overflow} the overflow rate, $Q_{\mathrm{Inflow}}$the inflow into the surface storage, $Q_{\mathrm{Infiltration}}$ the infiltration flux from the surface storage into the filter.

Exfiltration or percolation from the filter to the surrounding soil and the groundwater store depends on the surrounding soil's hydraulic conductivity and the filter's wetted surface area. Therefore, it is calculated as a function of these variables (Equation (2-4)):

$$Q_{\mathrm{Exfiltration}} = K_{s\,inf}\ S_{wet} \tag{2-4}$$

Where $K_{s\,inf}$ is the saturated hydraulic conductivity of the surrounding soil and S_{wet} is the wetted area of the filter storage, i.e., the contact surface between water and the surrounding soil. The flow is considered gravity-driven since it is expected to be entirely saturated. Outflow through the underdrain can be described as an orifice equation (thus assuming the pipe itself does not limit flow), according to a hydraulic head in the filter (Equation (2-5)):

$$Q_{out} = C_{out}\sqrt{2gy} * \mathrm{A} \tag{2-5}$$

Where C_{out} is an orifice coefficient to be calibrated, g is the acceleration due to gravity, and y is the difference between the water level in filter F and the level of the underdrain orifice. Finally, the infiltration rate from the ponding zone to the filter media, is generally obtained using the Green-Ampt Equation 2-6):

$$Q_{\text{Infiltration}} = \left(1 + \Delta\theta \frac{\varphi + H}{F}\right) * K(S_e) * A \tag{2-6}$$

Where F is the cumulative infiltrated water depth, Δθ is the soil moisture deficit, φ is the matric suction at the wetting front, H is the amount of ponding water height, and $K(S_e)$ is the mean unsaturated hydraulic conductivity, where $S_e(\theta)$ can be performed for soil moisture under residual, saturated, and actual conditions. The van Genuchten (1980) and Mualem (1976) models are among the most widely used empirical approaches to compute the water retention and the unsaturated hydraulic conductivity functions for resolving Richards equations (Richards 1931, van Genuchten 1980) and read as follows Equation (2-8):

$$S_e = \frac{\theta - \theta_r}{\theta_s - \theta_r} = \left(1 + (\alpha h)^{1/(1-m)}\right)^m \tag{2-7}$$

$$K(S_e) = K_s {S_e}^\tau \left[1 - \left(1 - (S_e)^{\frac{1}{m}}\right)^m\right]^2 \tag{2-8}$$

Where S_e is the saturation degree, θ the volumetric water content, θs the saturated volumetric water content and θ_r is the residual water content, α a fitting parameter related to water pressure head; m (m = 0.5 for coarse soils, with the sand/gravels used for the filter and drainage layer) and τ (τ = 0.5, default values for tortuosity) are shape parameters, K is the unsaturated hydraulic conductivity (m/s), K_s the saturated hydraulic conductivity (m/s).

A brief summary of the existing hydrodynamic modeling as well as the governing equations used in urban hydrological models, is provided in Table (2.2). For example, the model that enhanced infiltration processes by using Richards' equation or soil water retention by adding vegetation, water uptake processes, and evapotranspiration (ET) calculations and creating output hydrographs and drainage configurations that reflect underdrains and filter media are referred to be well-suited models (Lisenbee et al., 2021b). It is important to acknowledge that a multitude of distributed models have been proposed in the literature for the purpose of modeling LID (Low Impact Developments). These models vary in the functions they employ to simulate water infiltration and movement within the vadose zone (Azam et al., 2018; Rodriguez et al., 2008; Sage et al., 2020).

2.3.3. Modeling of infiltration at the block of soil scale

Water movement in soils is a crucial process that affects water quantity and quality (Ferguson, 1994; Simůnek et al., 2009). Water in soil tends to flow from a place with high potential energy to a position with low potential energy. The total potential energy of water in the soil is constituted mainly of matrix potential, gravitational potential, and suction potential (Brady et al., 2008; Hiellel, 2003). In saturated soil, capillary forces hold water with zero potential. Increasing suction leads to outflow until the air-entry suction is reached. Coarse-textured soils show this more distinctly.

Water is tightly bound in the smallest pores and grain contact points at the wilting point. Let us define soil water potential. All matter in nature naturally seeks equilibrium with its surroundings by moving from higher to lower potential energy. Soil water flows toward decreasing potential energy, driven by the potential energy gradient. In a rigid, unsaturated soil in equilibrium with atmospheric pressure, the total soil water potential is determined by (Hillel, 2003):

$$\psi = \psi_c + \psi_g + \psi_o \tag{2-9}$$

The energy level of water retained in the soil through capillary and surface adsorption is represented by the matric or capillary potential, ψ_c. The gravitational potential is denoted by ψ_g, and the osmotic potential by ψ_o.

The unit of potential is typically measured in terms of pressure and expressed in units of length or energy per unit mass of water. The commonly used unit for potential in hydrological studies is $[m]$ Or it is equivalent in energy units such as $[Pa]$. Water hydraulic head in saturated soil can be described as following formula in which h is the hydrostatic potential:

$$H = z + h \tag{2-10}$$

The pressure head h is positive below the water table and negative above it. In the unsaturated zone, the negative pressure is called matric suction or tension, denoted by a negative value. The pressure head is positive or neutral when saturated, called the piezometric head. The pressure head can reach shallow, highly negative values in arid soils.

2.3.4. Physical-numerical-based infiltration models

2.3.4.1. Darcy’s Law

In a uniform, saturated soil with hydraulic conditions at inflow and outflow boundaries, Darcy's law states (Hillel, 2003):

$$q = -K_s \frac{dH}{dL} \tag{2-11}$$

Where q is the flux or infiltration rate $[LT^{-1}]$, K_s is the hydraulic conductivities $[LT^{-1}]$, and $\frac{dH}{dL}$ $[-]$ Is the gradient of the hydraulic head (where H is the total hydraulic head $[L]$, L is the vertical distance $[L]$). The ability of the soil to allow water to flow through it, known as hydraulic conductivity, is determined by factors such as the shape, size, and arrangement of soil particles, as well as the physical properties of the liquid, like water viscosity (Miyazaki, 2006).

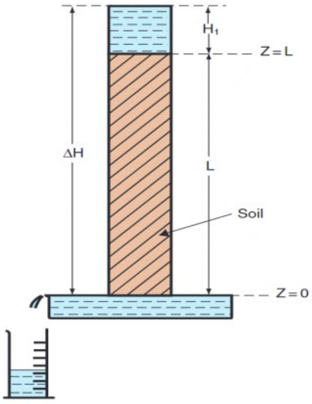

Figure (2.7): Downward flow of water in a saturated vertical column (adopted from (Hillel, 2003))

The total hydraulic head H equation is obtained by summing the gravitational pressure z and potential heads h (See Equation (2-10) and Figure (2.7), a uniform and saturated vertical column is depicted. The upper surface of the column is ponded under a constant water head H, while the bottom surface is connected to a lower reservoir with a constant water level. Consequently, there is a flow occurring from the higher reservoir to the lower reservoir through the column, which has a length z.

$$q = K \frac{(h_1 + z_1) - (h_2 + z_2)}{L} \rightarrow q = K(1 + \frac{\Delta h}{\Delta z}) \tag{2-12}$$

Table (2.2): Explanations of process-based computational models applicable for modeling of bioretention cells. To assess the ability of each model to represent the different water balance components accurately, various fields were evaluated (Lisenbee et al., 2021).

Model		**SWMM**	**MUSIC**	**RECARGA**	**HYDRUS**	**CANOE**
Recommended Use		Hydrologic, hydraulic, and water quality model with optional continuous simulation	Hydrologic, water quality, and treatment processes model	Hydraulic model for an optional event and continuous simulation or design purpose	Hydraulic model for continuous simulation or design purpose	Hydraulic model for an optional event and continuous simulation or design purpose
Brief Description		Detailed analysis of watershed with storage-focused LID (Rossman, 2010)	Evaluate drainage systems with treatment devices for optimal cost, hydrology, and water quality improvement (Hatt et al., 2009)	Design tool for evaluating the performance of Bioretention facilities, rain garden facilities, and infiltration basins (Boancă et al., 2018)	Evaluate infiltrations with treatment for optimal hydrology and water quality improvement (Šimůnek, 2005)	Simulation Detailed analysis of watershed with storage-focused LID (Bonneau et al., 2021; Chocat, 2013; Chocat and Cabane, 1999)
Inflow	**Runoff Generation**	SCS CN, Rational method, unit hydrograph, user input	simplified rainfall-runoff model	SCS CN & initial abstraction, user-input	user-input	SCS CN, Rational method, unit hydrograph, user input
	Flow Routing	Steady flow, Kinematic wave, Dynamic wave; Pipe: Hazen-Williams, Darcy-Weisbach, Manning	Muskingum Cunge; simple lag time	n/a	Dynamic wave	Muskingum Cunge; simple lag time; Saint Venant equations; Gradually varying curves
Infiltration	**Surface Infiltration**	Modified Green-Ampt	Simple bucket model	Modified Green-Ampt	Richards' Equation	Modified Green-Ampt, CANOE-Hydrobox equations (Asry et al., 2023)
	Infiltration between layers	Darcy's law uses HCO parameter to describe the slope of $K(\theta)$	Exponential equation of Ksat	$K(\theta)$ from Van Genuchten	Van Genuchten-Mualem; modified Van Genuchten; Brooks-Corey; Kosugi	Darcy's law; Van Genuchten-Mualem;
Outflow	**Drainage Equation**	Weir or Orifice equation	Orifice equation	Orifice equation	Tile drain boundary condition	Orifice equation
Overflow	**Ponding Depth**	Ponding > Max Ponding Depth	Weir equation	Ponding > Max Ponding Depth	Seepage faces boundary condition	Ponding > Max Ponding Depth
Exfiltration	**Seepage Equation**	Ksat of surrounding soil	Ksat of surrounding soil	Van Genuchten	MVG, modified VG, Brooks-Corey, Kosugi	Ksat of surrounding soil
ETP	**Equation**	User- input	user-input	user-input	Atmospheric boundary conditions	Step function according to the saturation degree of the soil, user-input

2.3.4.2. Richard's equation

The relationship between hydraulic conductivity and soil moisture content is not universal. When soil is saturated, all pores are filled, and hydraulic conductivity is highest. As the soil becomes unsaturated, some pores become filled with air, and the conductive area decreases. However, several authors have attempted to give relationships that describe this relationship satisfactorily. If we assume that we have a relationship, $K(Se)$, between the hydraulic conductivity and the potential pressure of the soil, Darcy's law can be applied as follows (Richards, 1931):

$$q = K(Se).\frac{dH}{dz} \tag{2-13}$$

As for saturated medium, Equation (2-14) is combined with the mass conservation law, so the general equation of non-saturated soil is:

$$\frac{\partial \theta}{\partial t} = \nabla[K(Se).\nabla(\mathrm{h} + z)] \tag{2-14}$$

The one-dimensional case of a vertical flow from top to bottom is:

$$\frac{\partial \theta}{\partial t} = \frac{\partial \theta}{\partial h}\frac{\partial \mathrm{h}}{\partial t} \rightarrow \mathrm{C(h)}.\frac{\partial \mathrm{h}}{\partial t} = \frac{\partial}{\partial z}\left[K(\mathrm{h}).(\frac{\partial \mathrm{h}}{\partial z} + 1)\right] \tag{2-15}$$

Substituting specific water capacity $C(h)$ is the specific retention capacity, simply the slope of the soil moisture retention curve or derivative of θ concerning h. Defined as Equation (2-15):

$$\mathrm{C(h)} = \frac{\partial \theta}{\partial h} \tag{2-16}$$

Hydraulic diffusivity of soil is then defined as the ratio of the conductivity to the specific capacity to simplify the treatment of the Equation (2-17) (Hillel, 1971):

$$\mathrm{D(h)} = \frac{K(\mathrm{h})}{C(\mathrm{h})} \tag{2-17}$$

The coefficient D is highly water content-dependent and expresses a propagation velocity for water content changes (Durner and Flühler, 2005). We can therefore take Equation (2-5) to obtain by:

$$\mathrm{q} = \mathrm{D(h)}\frac{\partial \theta}{\partial z} \tag{2-18}$$

Soils with high macro-porosity (large and continuous pores) are the most conducive in saturated conditions. It is well known that sandy soils conduct water more rapidly than clayey soils when saturated. However, the opposite may be valid under unsaturated conditions. In macropore soils, the pores quickly empty out, resulting in decreased conductivity as the suction increases. In soils with numerous micropores, many pores remain full and conductive even with significant suction, meaning the hydraulic conductivity does not decrease as much and may even be higher than that of soil with larger pores under the same suction (Hillel, 1971).

2.3.4.2.1. Saturated media

The non-permanent processes require the introduction of the law of conservation of mass, which gives the continuity equation:

$$\frac{\partial \theta}{\partial t} = -\nabla q \tag{2-19}$$

By combining this equation with Darcy's law, the general equation of the saturated flow is obtained, which is written as follows:

$$\frac{\partial \theta}{\partial t} = \nabla K_s \frac{dH}{dz} \tag{2-20}$$

Where θ $[L^3 L^{-3}]$ is the volumetric water content of the soil, q is the flux $[LT^{-1}]$, K_s is the saturated hydraulic conductivity $[LT^{-1}]$, and Z $[L]$, is the vertical height considering z is oriented upwards. In the one-dimensional case of a vertical flow by considering S as a sink term $[T^{-1}]$, following modified form of Richard's' Equation can be yielded:

$$\frac{\partial \theta}{\partial t} = \frac{\partial}{\partial z}\left(K_s\left(\frac{dH}{dz} + 1\right)\right) - S \tag{2-21}$$

2.3.4.2.2. Unsaturated media

The vadose zone between the water table and the soil surface is called the unsaturated zone. In this region, the soil's water content is lower than the saturation $(\theta < \theta_s)$, and opposing pressure heads are joint. The vadose zone is pivotal in various hydrological processes, including infiltration, soil moisture storage, evaporation, plant water uptake, groundwater recharge, runoff, and erosion. Historically, it held significant importance for agricultural water supply. Presently, there is growing concern about pollution and contamination in the unsaturated zones, affecting both urban and rural areas (Simunek et al., 2011).

In unsaturated soil, water is subject to sub-atmospheric pressure, known as suction, which also acts as a driving force. Matric suction arises from the water's attraction to soil particle surfaces and capillary pores. Water tends to flow from low-suction areas to those with higher suction. When the soil is in equilibrium, there is no driving force, and the suction remains uniform along a horizontal column. Even in a suction gradient, water will flow through pores still filled with water (Hillel, 1971).

There has long been an appreciation for the importance of the unsaturated zone in the hydrological cycle. Here, the fundamental difference from the saturated case lies in the fact that the hydraulic conductivity is not constant over time as the water content of the soil changes. Two essential functions are required to solve the Richards equation: $K(\theta)$, representing the hydraulic conductivity as a function of water content, and $\theta(h)$, representing the water content as a function of pressure head.

2.3.4.3. The Soil Water Retention Curve (SWRC)

To model and study the water movement and infiltration in non-saturated soil, assessing the relation between water content and related potential pressure is necessary, this relation also called « soil wetness » or « soil moisture retention » is the curve between water content and associated soil water potential $\theta(h)$. This curve is highly non-linear and may exhibit significant multi-scale heterogeneity in their spatial distribution (Schaap et al., 2001) (see Figure (2.8)).

The direct measurement of soil hydraulic properties can be divided into in situ and laboratory measurements. Although laboratory experiments offer speed and precision, they may not yield representative results that reflect the actual soil conditions in the field (Durner and Lipsius, 2005; Nemes et al., 2001; Van Genuchten, 1999).

Therefore, direct in situ measurements of hydraulic and retention properties remain the most reliable, albeit expensive and time-consuming, method of determining these properties (Tseng and Jury, 1993). To comparison of different soils and scenarios, it is advantageous to mathematically represent the water retention curve (WRC) using continuous functions or Indirect modeling (Durner and Flühler, 2005; Leij, 1996; Schaap et al., 2001).

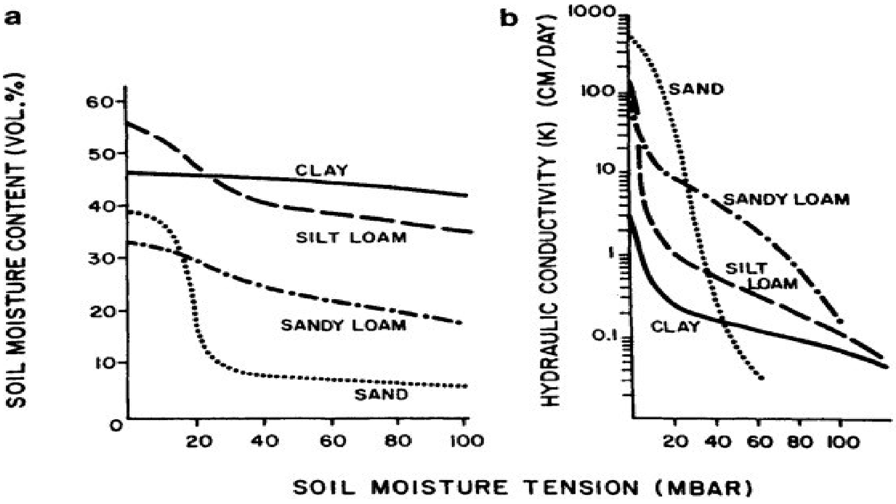

Figure (2.8): Typical soil water characteristic curves for soils of different textures adopted from (Daniel and Bouma, 1974)

Indirect modeling of soil hydraulic properties consists of two categories:

i. Semi-physical methods that use particle-size distribution and water retention characteristic shape similarity to gain insights into the physical relations between texture and pore-size distribution (Arya and Paris, 1981; Haverkamp and Parlange, 1986).
ii. Empirical methods, also called Pedotransfer functions (PTF), use basic soil survey information (such as field morphology, soil texture, structure) and to provide a predictor function for specific soil hydraulic properties (SHPs) (Rawls et al., 1991).

Soil water potential functions are typically denoted as $\theta(h)$ (see Figure (2.8) panel (a)) Describe the relationship between the soil water content (θ) and the soil water potential (h). The soil water potential represents the energy state of water in the soil and indicates how tightly the water is held within the soil matrix.

The soil water potential functions summarize this relationship and help understand the behavior of soil water movement and availability. Table (2.3) is a summary of some commonly used soil water potential functions:

Table (2.3): Statical models for unsaturated soil water potential functions

Author	**Equation**	**Definition**
Van Genuchten	$S_e(h) = [1 + (-\alpha h)^n]^{-m}$	α , m and n are the fitting parameters
Brooks and cory	$S_e(h) = 1 \quad if \quad h_a < h < 0$ $S_e(h) = \left(\frac{h_a}{h}\right)^{\lambda} \quad if \quad h < h_a$	where h_a is the air entry, and λ is the pore size distribution
Durner (1994)	$S_e(h) = \frac{(w_{\mathrm{f}} S_{\mathrm{e.t}} + w_{\mathrm{m}} S_{\mathrm{e.m}})^{\tau} B}{(w_{\mathrm{f}} \alpha_{\mathrm{f}} + w_{\mathrm{f}} \alpha_{\mathrm{f}})^2}$	Dual porosity retention model, where w_f and w_m are the weighting factors, α_f and α_m and m denotes the fitting parameters for the separate function
Dexter et al. (2008)	$\theta(h) = \theta_r + P_m e^{(-\frac{h}{h_m})} + P_s e^{(-\frac{h}{h_s})}$	P_m is the effective soil matrix porosity, $P_s$is the effective soil structure porosity, h_m , h_s is the pore water pressure head at respectively dry and wet soil.
Haverkamp (1977)	$S_e(h) = \frac{1}{1 + (\alpha h)^N}$	α and N are the fitting parameters

The hydraulic conductivity function denoted as $K(\theta)$ or $K(h)$ (see Figure (2.8) panel (b)), describes the relationship between the hydraulic conductivity K and a parameter that represents the state of water in the soil, such as the volumetric soil water content θ or the soil water potential h. It provides a mathematical representation of how the ability of soil to transmit water changes with varying soil water conditions.

Numerous models have been devised to characterize the hydraulic conductivity function across various soil types and conditions. Some commonly used models are included in Table (2.4). Empirical studies (Van Genuchten, M. Th. and Nielsen, 1985) showed that the expression proposed by van Genuchten (1980) suits the functions listed above.

These models are based on the following formula:

$$K(\theta) = K_{\mathrm{r}}(\theta) K_s \tag{2-22}$$

Where $K_{\mathrm{r}}(\theta)$ is the relative hydraulic conductivity.

Table (2.4): Statistical models for unsaturated hydraulic conductivity

Author	**Equation**	**Definition**
Burdine (1953)	$K_{\mathrm{r}}(\theta) = S_e^{\tau} \frac{\left[\int_{\theta_r}^{\theta} \frac{d\theta}{h^2}\right]}{\left[\int_{\theta_r}^{\theta_s} \frac{d\theta}{h^2}\right]}$	$\boldsymbol{\tau}$ is a dimensionless parameter interpreted as representing the tortuosity and connectivity of pores with different sizes, Bourdin given the value $\boldsymbol{\tau = 2}$.
Mualem (1976)	$\mathrm{K_r(\theta)} = \mathrm{S_e^{\tau}} \left[\frac{\int_{\theta_r}^{\theta} \frac{d\theta}{h}}{\int_{\theta_r}^{\theta_s} \frac{d\theta}{h}}\right]^2$	$\boldsymbol{\tau}$ is a dimensionless parameter interpreted as representing the tortuosity and connectivity of pores with different sizes, Mualem given the value $\boldsymbol{\tau = 0.5}$.
Brooks & Corey (1964)	$\mathrm{K_r(\theta)} = K_s S_e^{1+\tau+\frac{2}{\lambda}}$	$\boldsymbol{\tau}$ is a dimensionless parameter interpreted as representing the tortuosity and connectivity of pores with different sizes, Brook and Coery given the value $\boldsymbol{\tau = 2}$.
Van Guenchten (1980)	$\mathrm{K_r(\theta)} = \mathrm{S_e^{\tau}} \left[1 - (1 - \mathrm{S_e}^{\frac{1}{m}})^{m}\right]^2$ $m = 1 - \frac{1}{n}$	$\boldsymbol{\tau}$ is a dimensionless parameter interpreted as representing the tortuosity and connectivity of pores with different sizes, Mualem given the value $\boldsymbol{\tau = 0.5}$.
Haverkamp (1977)	$\boldsymbol{K(h) = \frac{1}{1 + \left(\frac{h}{\alpha}\right)^{N}}}$	$\boldsymbol{\alpha}$ and **N** are the fitting parameters (Fayer and Version, 2000)

The unsaturated flow equation describes water movement in soils that are not fully saturated. It considers the effects of gravity and capillary forces on water flow. The Richards equation Equation (2-13) is commonly used for unsaturated flow.

Numerical solutions of Richard’s equation are commonly used to simulate water movement in unsaturated soils over time. Richards' partial differential equation describes water flow in porous media, considering soil properties, hydraulic conductivity, and water content. Since the 1960s, numerous software tools, such as HYDRUS, have been developed for quantifying and predicting soil infiltration by numerically solving the Richards equation for different boundary conditions. Models that calculate infiltration rate and ponding in a spatiotemporal domain can be used without external empirical or semi-analytical models. For example, HYDRUS-1D has been used to simulate water infiltration into a one-dimensional soil profile in simulations by Šimůnek and van Genuchten (2008) and Šimůnek et al. (2008, 2016).

2.3.5. Physical-Empirical based infiltration models

This section discusses the moisture distribution profile during infiltration in a homogeneous soil profile under ponding conditions. At any given moment during infiltration, the profile can be described as follows: the uppermost layer of the soil, known as the surface soil, becomes saturated; below this layer, there is a transmission zone that appears uniformly saturated. This zone extends for a certain depth from the surface. Beyond the transmission zone lies the wetting soil, where the moisture content gradually decreases with depth in a steep gradient.

The wetting front is the boundary between the wetting soil above and the dry soil beneath and represents a sharp interface between the soil with moisture and the soil that remains dry. These concepts are described by (Hillel, 1972), who has extensively studied soil moisture dynamics and infiltration processes.

Overall, this moisture distribution profile provides insights into the spatial variation of water content within the soil during infiltration under ponding, highlighting the distinct zones and the sharp wetting front that separates them Figure (2.9).

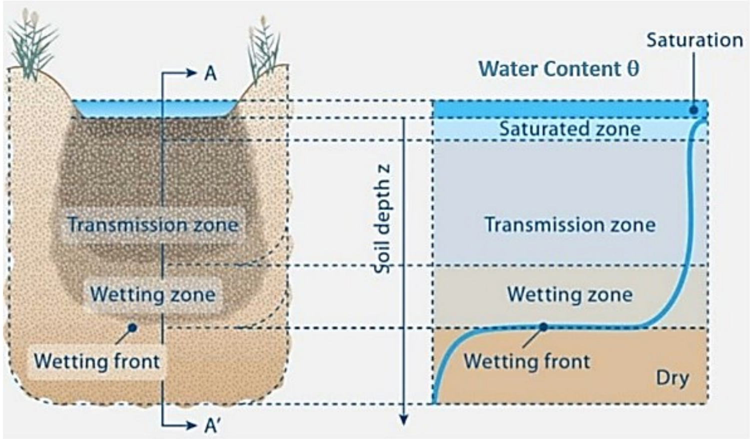

Figure (2.9): The moisture content in the soil during infiltration in the wetted soil profile (left) and the corresponding soil moisture profile (right) (adopted from Vereecken et al., 2019)

If we observe the moisture profile during infiltration at regular intervals, we will observe a continuous downward movement of both the wetting zone and the wetting front. As the wetting front progresses more profoundly into the soil profile, its steepness decreases. This behavior is depicted by typical sets of successive moisture and hydraulic head profiles, as illustrated in Figure (2.10). Two well-established mathematical solutions of Richard's equation that accurately describe physical infiltration under boundary conditions are the Green-Ampt and Philip equations. These equations provide analytical approaches to model and understand the complex process of water movement into the soil (Swartzendruber and Hillel, 1973).

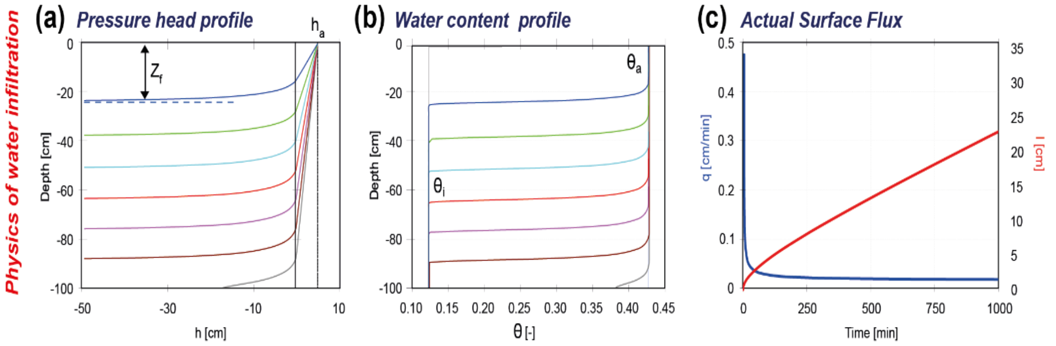

Figure (2.10): Physical principles of water infiltration based on the illustration with numerically generated data (from left to right, pressure head and water content profiles and infiltration rate, q, and cumulative infiltration, I, at the soil surface)

The Green-Ampt equation, an approximate solution to Richard's equation, explicitly addresses the dominance of capillary flow in infiltration processes. The Green-Ampt (GA) piston flow model, initially proposed by Green and Ampt in 1911, is a widely used analytical and physically-based model that simplifies the process of water infiltration into initially dry and homogeneous soils under ponded conditions, typically above the water table. The *GA* model employs the assumption of piston flow, where the soil moisture distribution is represented by a sharp and abrupt moving front that separates a saturated region above the front (wetted zone) from a dry region below it.

It is designed for scenarios involving sudden and intense infiltration events, assuming a constant hydraulic conductivity throughout the soil depth. This simplified representation allows for a straightforward characterization of the infiltration process. As mentioned above, the moisture profile in this model is assumed to exhibit a piston-like behavior, with a corresponding pressure head profile, represented by solid lines in Figure (2.11).

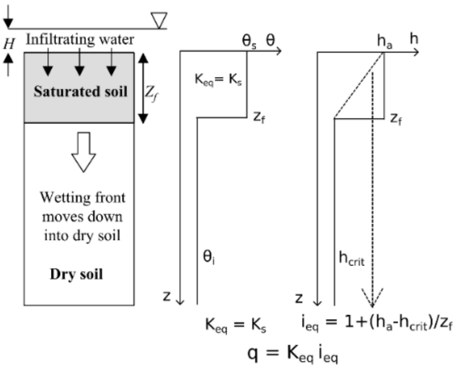

Figure (2.11): Soil moisture profile and pressure head profile of the Green-Ampt model

The smooth curve in Figure (2.11) is the actual moisture profile. For example, in the Green–Ampt model, the infiltration rate is given by:

$$i = i_c + \frac{b}{I} \tag{2-23}$$

Where b is a physically defined parameter; alternatively, this equation is written by using saturated hydraulic conductivity Ks and the pressure heads as:

$$i = K_{\mathrm{s}} \frac{H_0 - H_{\mathrm{f}} + Z_{\mathrm{f}}}{Z_{\mathrm{f}}} \tag{2-24}$$

Where H_0 is the pressure head at the land surface (which is equal to the depth of ponded water), H_{f} is the practical pressure head (negative value) at the wetting front (specific water pressure head), and Z_{f} is stands for the position of the wetting front. The increase in the volumetric water content $\Delta\theta$ in the wetted zone is defined by $(\theta_i - \theta_0)$, where θ_i is the volumetric water content in the wetted zone and θ_0 is the initial volumetric water content. The value of $\Delta\theta$ is related to the infiltration rate by:

$$i(t) = |\theta_0 - \theta_i| \times \frac{dZ_{\mathrm{f}}}{dt} = \Delta\theta \frac{dZ_{\mathrm{f}}}{dt} = K_s \frac{(H_{\mathrm{f}} - Z_{\mathrm{f}}) - H_0}{Z_{\mathrm{f}}} \tag{2-25}$$

Substitution of two following equations yields:

$$\int_0^t \frac{K_{\mathrm{s}}}{\Delta\theta} dt = \int_0^{L_f} \frac{Z_{\mathrm{f}}}{H_0 + H_{\mathrm{f}} + Z_{\mathrm{f}}} \; dZ_{\mathrm{f}} \tag{2-26}$$

$$\frac{K_i}{\Delta\theta} dt = Z_{\mathrm{f}} - (H_0 + H_{\mathrm{f}}) \ln\left(1 + \frac{Z_{\mathrm{f}}}{H_0 + H_{\mathrm{f}}}\right)$$

Substitution of Equation (2-20) into the definition of integrated infiltration $I = \Delta\theta Z_{\mathrm{f}}$ yields the Green–Ampt equation.

$$I = K_{\mathrm{s}} t + Z_{\mathrm{f}} \, ln(1 + \frac{I}{Z_{\mathrm{f}}}) \tag{2-27}$$

Where:

I = cumulative infiltration depth at time $t(L)$,

K_{s} = effective hydraulic conductivity (L/T),

t = time (T)

The wetting front could be defined as:

$$dZ_{\mathrm{f}} = \Delta\theta(H_0 - H_{\mathrm{f}}) \tag{2-28}$$

The reliability of the Green-Ampt equation hinges on the physical representation of H_{f}, which represents the effective pressure head at the assumed wetting front. However, the Green-Ampt equation faces challenges due to the lack of a precise and universally agreed-upon definition for H_{f}. This ambiguity in defining H_{f} has contributed to a decrease in the theoretical reliability of the Green-Ampt equation.

The equation assumes that a sharp wetting front propagates downward through the unsaturated zone as water infiltrates the soil. It implies that the soil above the wetting front is entirely saturated while the soil below remains dry. This assumption simplifies the modeling process by treating the wetting front as a well-defined boundary within the soil profile.

However, it is essential to note that the wetting front is not always a sharp and distinct boundary (Alastal and Ababou, 2019; Kale and Sahoo, 2011; Sage et al., 2020). Instead, it can be influenced by factors such as soil heterogeneity, preferential flow paths, and variability in hydraulic properties. These factors can lead to a more diffuse and gradual wetting front rather than a sharp interface.

The accuracy and applicability of the Green-Ampt equation heavily depend on the assumptions made regarding the wetting front and the associated pressure head. Different interpretations of H_{f} can lead to variations in the predicted infiltration behavior and may not accurately represent the actual physical processes occurring in the soil.

2.3.6. Empirical-based infiltration models

The decline in infiltration rates over time describes the phenomenon whereby the initial rate of water infiltration into the soil gradually decreases as the infiltration event progresses. Typically, in the starting phase of infiltration, when the soil is relatively dry, the infiltration rate is higher. Over a period of time, the rate of water infiltration into the soil gradually diminishes as the soil becomes increasingly saturated.

Over time, the decreasing trend of infiltration rates has practical consequences for various hydrological and environmental applications. It affects the design of drainage systems, irrigation practices, and the estimation of infiltration rates for water resource management. Understanding and accurately modeling this trend is important to capture the dynamics of water movement in the soil and make informed water management decisions. Various empirical formulas are employed to mathematically express the decrease in infiltration as a function of time, starting from an initial value that approaches a limit value, often represented as K_{s}. These formulas typically follow an exponential or quadratic function to describe the decreasing trend over time. Here is an example of an empirical equation commonly used for this purpose:

The Horton equation (1940) is one such empirical equation that describes the decrease in infiltration rate over time. It is based on an exponential decay model and is given by the equation:

$$i = i_c + (i_0 - i_c)e^{-kt} \tag{2-29}$$

Where i infiltration rate at time t, i_c denotes steady-state infiltration rate at significant times, i_0 is the initial infiltration rate at time t = 0, and k = constant for a given soil and initial condition. The values of i_0, i_c, and k can be determined experimentally for any soil. Although this equation is widely used, its practical application is limited because it can be challenging to determine the values of the parameters. i_0, i_c, and k. Several other equations are available for calculating the water infiltration rate into the soil (as shown in Table (2.5)).

It is important to note that each formulation has its own assumptions and empirical coefficients. The selection of an appropriate equation depends on the specific characteristics of the infiltration event and the available data.

Calibration and validation against field measurements are typically performed to determine the empirical coefficients.

Table (2.5): The main empirical denote and physical empirical infiltration equation is commonly used in hydrology.

Author	Function	Legend
Horton	$i(t) = i_c + (i_0 - i_c)e^{-kt}$	where i = infiltration rate at time t, i_c= steady-state infiltration rate at significant times, i_0 = initial infiltration rate at time t = 0, and k = constant for a given soil and initial condition.
Kostiakov	$I(t) = \mathrm{K}t^a$	Where I is the cumulative infiltration upon time t, and K and a are the constants parameters, which can be calibrated using measured infiltration data and did not have physical meaning.
Philip	$i(t) = 0.5. s. t^{-0.5} + A$	Where A is the gravity component function of saturated hydraulic conductivity, and S is the sorptivity.
Dooge	$i(t) = a(F_{max} - F_t)$	Where a is constant, F_{max} is the maximal water retention capacity and F_t is the water content at time t.

2.4. Modeling of infiltration affected by preferential flows

In Bioretention units, the organic aspect of these systems is probably responsible for maintaining a high hydrological capacity. The roots strongly impact the hydrological capacity of soil structure in bioretention systems, soil fauna, soil microorganisms, and hydraulic variables (e.g., wetting and drying cycles), which can be the same case for agricultural and urban bioretention basins (Rasse et al., 2000; Thomas and Mérot, 2009). Plant roots have been shown to increase soil hydraulic conductivity by creating preferential flow paths and increasing porosity (Hatt et al., 2009; Muerdter et al., 2018; Six et al., 2004).

Bioretention establishment or « bioretention maturity » or « post-construction period of Bioretention age » is a process known as pedogenesis. Pedogenesis begins when vegetation establishes itself in the soil, adding organic matter to the surface, and root exudates growth, creating an organic horizon on the soil surface over several years (Mitchell Ayers and Kangas, 2018). In several other mature bioretention studies, performance appeared to improve over time after the post-construction phase, which may also be due to soil pedogenesis and structural processes maintained by vegetation and soil fauna (Johnson and Hunt, 2019; Spraakman et al., 2020; Willard et al., 2017).

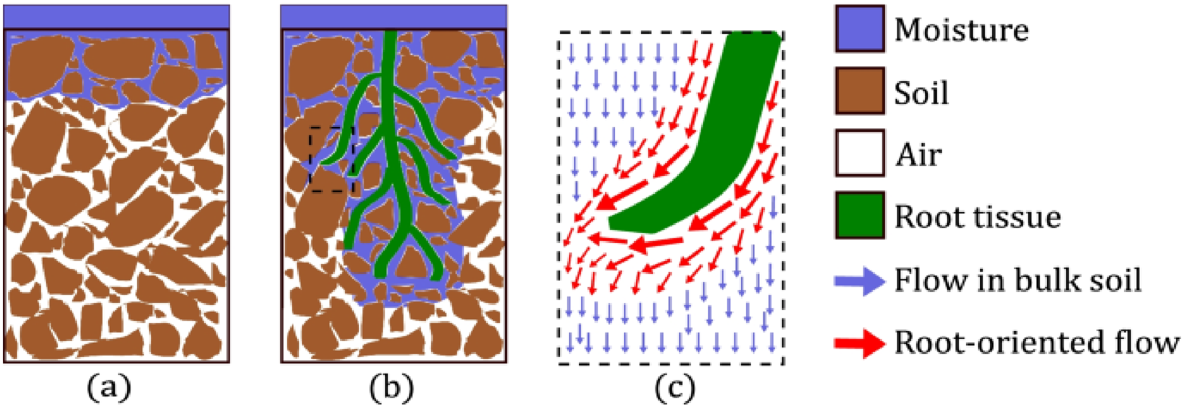

Figure (2.12): Illustration of Root-Oriented Preferential Flow (PF). a) A depiction of a fallow soil domain where no root-oriented preferential flow (PF) is taking place. b) A portrayal of a vegetated soil domain where root-oriented PF is occurring. c) A representative volume of the vegetated soil domain, comprising a bulk soil volume (depicted in blue) and a volume of soil where root-oriented PF is happening (depicted in red)

Multiple studies have demonstrated a correlation between the presence of root systems and preferential flow (PF) through the soil (Holden, 2005; Wang et al., 2020). For example, in an investigation where a dye was employed to track water infiltration beneath a tropical rainforest, (Noguchi et al., 1997) observed that the dye accumulated along the roots, indicating PF aligned with the root orientation. (Noguchi et al., 1999; Wang et al., 2020) Concluded that these PF patterns arise from areas of soil that are more easily fragmented, and the specific locations of these zones are influenced by the positioning and orientation of roots within the soil (Mair et al., 2022). A visual representation of this phenomenon can be seen in Figure (2.12).

The heightened soil heterogeneity and subsequent preferential flow process can significantly elevate the risk of groundwater pollution by reducing pollutant removal effectiveness (Flury et al., 1994a; Jarvis and Ga, 2003). Several bioretention modeling studies have assumed uniform flow (Hilten et al., 2008a; Palla et al., 2009). The hydraulic properties required for these studies were expressed by simple functions corresponding to an unimodal distribution of pore sizes (Mualem, 1986; Van Genuchten and Dalton, 1986). Few studies have considered preferential flow for modeling SUDS (Brunetti et al., 2016; Liu and Fassman-Beck, 2017).

The growing concern for non-equilibrium and preferential flow and transport in soil and agriculture is driven by the increasing speed of agricultural contaminants and urban stormwater, such as fertilizers, pesticides, microorganisms, and microplastics, moving through the unsaturated zone and reaching groundwater (Simunek, 2008). Preferential flow is a phenomenon where water and solutes move along specific pathways while bypassing a fraction of the porous matrix (Hendrickx and Flury, 2001). Published works interested in water flow in soil macropores can be classified into two main categories regarding the way macroporosity has been considered. Macropores have generally been defined according to two main criteria. Many authors have defined them by their structural organization, in other words, their diameter, their spacing, and the ratio of their volume to the total volume of the soil ((Beven and Germann, 1981) for example). Others are interested in their contribution to flow by the pressure at which they empty or their contribution to infiltration (White, 1985).

Several approaches to studying the preferential flow in structured media have been suggested, including multi-porosity and multi-permeability models dual-porosity and dual-permeability models (Gerke and van Genuchten, 1993; Jarvis, 1998). The dual-porosity model and the dual-permeability model both assume that the porous medium is divided into two interacting regions: one containing interaggregate, macropores, or fractures, and the other containing micropores, or interaggregate pores, within the rock matrix or soil aggregates, as shown in Figure (2.13). A dual-porosity model assumes that macropore space is continuous, connected pores of large dimensions and water is stagnant within the matrix (Philip, 1968), whereas a dual-permeability model allows water to move within the matrix in addition to being stagnant (Gerke and van Genuchten, 1993).

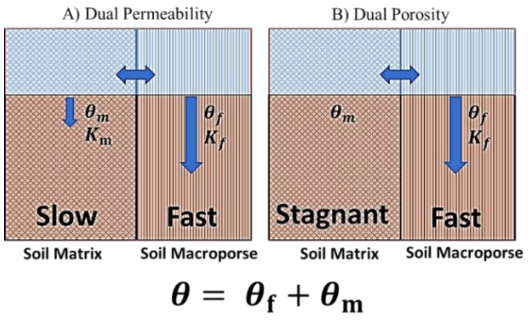

Figure (2.13): Conceptual physical non-equilibrium models for water flow. In plot a), θ the water content, θ_m , K_m and θ_f , K_f are are hydraulic conductivity and water contents of the matrix and macropore (fracture) regions in the plot b) θ_m and θ_f are water contents of the matrix and macropore (fracture) regions, K_f is the hydraulic conductivity, respectively, wetting front moved forward simultaneously

2.4.1. Dual permeability approach

The dual permeability approach can be defined as a concept that considers porous media in terms of two different pore systems, which are treated as homogeneous media with separate hydraulic properties and two distinct pore systems. The permeable interface separates these two porous media. Since dual permeable media have two distinct flow permeabilities, pressure heads, and water contents at any time or space, we can consider them dual permeable media. It is hypothesized that a medium of dual permeability will have two water retention functions, one in the matrix and one in the fracture pore system, but two hydraulic conductivity functions: $K_{\mathrm{f}}\,(h_{\mathrm{f}})$ and $K_{\mathrm{m}}(h_{\mathrm{m}})$, The flow equations for the fast-flow region (subscript f) and the matrix (subscript m) are, respectively (Gerke and van Genuchten, 1993). By assuming V_{f} as the volume of fracture medium, and V_{t} as the unit volume of medium, which is equal to $V_{\mathrm{t}} = V_{\mathrm{f}} + V_{\mathrm{m}}$,the ω weighting factor is as follows (Hilten et al., 2008):

$$\omega = \frac{V_{\mathrm{f}}}{V_{\mathrm{t}}} \tag{2-30}$$

As a result, the bulk soil water content $\theta[L^3L^{-3}]$ is then calculated by:

$$\theta = \ \omega\theta_{\mathrm{f}} + (1-\omega)\theta_{\mathrm{m}} \tag{2-31}$$

Where θ_{m} and $\theta_{\mathrm{f}}\,[L^3L^{-3}]$ is respectively the volumetric water content of matrix and fracture pore systems, the fluid density of the bulk soil at any given depth can also be expressed in the form.

$$q = \ \omega q_{\mathrm{f}} + (1-\omega)q_{m} \tag{2-32}$$

This shows that q represents the area-weighted fluid flux density, then the pore water velocities. υ_f and $\upsilon_m$in the fracture and matrix regions are defined as:

$$\upsilon_{\mathrm{f}} = \frac{q_{\mathrm{f}}}{\theta_{\mathrm{f}}} \qquad \text{(a)} \qquad \upsilon_{\mathrm{m}} = \frac{q_{\mathrm{m}}}{\theta_{\mathrm{m}}} \tag{2-33}$$

The following expression can be derived to directly calculate the bulk soil hydraulic conductivity by substituting q with Darcy's flux law:

$$K\left(\frac{\partial h}{\partial z}+1\right) = \omega_{\mathrm{f}}K_{\mathrm{f}}\left(\frac{\partial h_{\mathrm{f}}}{\partial z}+1\right) + (1-\omega_{\mathrm{f}})K_{m}\left(\frac{\partial h_{\mathrm{m}}}{\partial z}+1\right) \tag{2-34}$$

Where h is the pressure head associated with the bulk soil. Further, by assuming that the densities of the fluid and solid phases are constant, ignoring the effects of swelling and shrinking, assume no hysteresis in the hydraulic properties and consider the effect of temperature, air pressure, and solute concentration on water flow are negligible. On dimensional vertical water flow in the fracture and matrix pore systems of dual porosity medium is then described by the following equation:

$$\frac{\partial\theta_{\mathrm{f}}}{\partial t} = \frac{\partial}{\partial z}\left[K_{\mathrm{f}}(h_{\mathrm{f}})\frac{\partial h_{\mathrm{f}}}{\partial z} + K_{\mathrm{f}}(h_{\mathrm{f}})\right] - \frac{\Gamma_{\omega}}{\omega} - \varphi_{\mathrm{f}} \tag{2-35}$$

And then:

$$\boldsymbol{\frac{\partial\theta_{\mathrm{m}}}{\partial t} = \frac{\partial}{\partial z}\left[K_{\mathrm{m}}(h_{\mathrm{m}})\frac{\partial h_{\mathrm{m}}}{\partial z} + K_{\mathrm{m}}(h_{\mathrm{m}})\right] + \frac{\Gamma_{\omega}}{1-\omega} - \varphi_{\mathrm{m}}} \tag{2-36}$$

Where θ_{m} and θ_{f} $[L^3L^{-3}]$ denote water contents in the matrix and fast-flow regions, respectively; K_{m} and K_{f} $[LT^{-1}]$ are hydraulic conductivities in the matrix and fast-flow regions, respectively; h_{m} and h_{f} $[L]$ are pressure heads in the matrix and fast-flow regions, Γ_{ω} $[T^{-1}]$ is water exchange between the matrix and fast-flow regions, φ_m $[L^3L^{-3}]$ and φ_{f} $[L^3L^{-3}]$ are sink–source terms in the two regions, ω $[L^3L^{-3}]$ is the ratio of the volume occupied by the fast-flow region and the total volume, with z corresponding to the vertical coordinate. As we mentioned, the two following regions are considered to be separated by the permeable filter, which means there are exchanges between the two following regions, The exchange rate of water between the fast-flow and matrix regions, Γ_{ω}, is assumed to be proportional to the difference in pressure heads (Gerke and van Genuchten, 1993) :

$$\Gamma_{\omega} = \alpha_{\mathrm{w}}(h_{\mathrm{f}} - h_{\mathrm{m}}) \tag{2-37}$$

Where α_{w} is the first-order mass transfer coefficient. This approach requires estimating retention curves because water contents and pressure heads are needed for both regions. For porous media with well-defined geometries, the first-order mass transfer coefficient, α_{w}, can be defined as (Gerke and van Genuchten, 1993):

$$\alpha_{\mathrm{w}} = \frac{B_a}{d^2} K_a \gamma_{\omega} \tag{2-38}$$

Where $\mathrm{B_a}$ is a shape factor, d is a characteristic length of matrix elements, $\mathrm{K_a}$ is the interfacial hydraulic conductivity, and γ_{ω} is a scaling factor. Then the effective hydraulic conductivity $\mathrm{K_a}$of the fast flow matrix interface using a single arithmetic average involving both is evaluated $\mathrm{h_f}$ and $\mathrm{h_m}$:

$$K_{\mathrm{a}}(h) = \frac{1}{2}[K_a(h_{\mathrm{f}}) + K_a(h_{\mathrm{m}})] \tag{2-39}$$

2.4.2. Dual porosity approach

Dual-porosity models assume that water movement is restricted to fractures and does not occur in the matrix. This leads to two-region flow and transport models (Gerke and van Genuchten, 1993a; Philip, 1969) in which water is divided into a mobile (fractures and macropores, inter-aggregate) and an immobile (stagnant, intra-aggregate) region. The mobile region, θ_{f} permits convective flow, while the immobile region, θ_{m}, can exchange, retain, and store water but does not allow it to move.

The dual-porosity formulation for water flow is based on a mixed formulation of the Richards equation (2-32) to describe water flow in fractures (subscript f), Exchange of water and solutes dynamic in the intra-aggregate region, described as:

$$\frac{\partial \theta_{\mathrm{f}}}{\partial t}=\frac{\partial}{\partial z}\left[K_{\mathrm{f}}(h_{\mathrm{f}})\frac{\partial h_{\mathrm{f}}}{\partial z}+K_{\mathrm{f}}(h_{\mathrm{f}})\right]-\Gamma_{\omega}-\varphi_{\mathrm{f}} \tag{2-40}$$

And:

$$\boldsymbol{\frac{\partial \theta_{\mathrm{m}}}{\partial t}=\Gamma_{\omega}-\varphi_{\mathrm{m}}} \tag{2-41}$$

Where K_{m} and K_{f} $[LT^{-1}]$ are hydraulic conductivities in the matrix and fast-flow regions, respectively; h_{m} and h_{f} $[L]$ are pressure heads in the matrix and fast-flow regions, Γ_{ω} $[T^{-1}]$ is water exchange between two regions, φ_m $[L^3L^{-3}]$ and φ_{f} $[L^3L^{-3}]$ are sink–source terms in the two regions (Jarvis and Ga, 2003; Šimůnek et al., 2003).

2.4.3. Model complexity and parameterization

In contrast to single pore region models, models for dual-porosity and dual-permeability require a large number of input parameters if they characterize both pore systems simultaneously, which is one of their major disadvantages. Using the dual-permeability model of (Gerke and van Genuchten, 1993) as an example, in its full complexity, there are 16 parameters required to describe the flow of water according to the model.

There may be some interest in reducing the number of input parameters in the model to make it a well-parsimony model. Today, the more sophisticated dual permeability model involving two coupled Richards' equations is still challenging to use to describe preferential flow and transport under field conditions especially for SUDS, in part because of the large number of parameters involved and the current lack of a set of standard experimental techniques to obtain them (Šimůnek et al., 2003).

The application of such a model under field conditions is complicated. Hence, such models have been limited to theoretical applications and laboratory studies under well-defined and controlled conditions. The main reasons for the broader use of this model are that it is physically-based and numerically robust, while the challenging parameterization issue is not insurmountable (Carbone et al., 2015; Illgen et al., 2007). They used Hydrus to simulate the preferential flow in (LID) development. Nevertheless, determining input parameters and identifying the correct values remains challenging (Brunetti et al., 2016). Researchers have explored approaches such as particle swarm optimization and Monte Carlo filtering methods to address this issue to find the optimal parameters for permeable pavement in sustainable urban drainage systems. However, these methods are far from practical and user-friendly for effectively managing and modeling such systems.

2.5. Inversion methods of soil hydraulic estimation

The accurate representation of soil is crucial for the success of soil models in characterizing systems. Information about soil properties must be obtained through laboratory or field methods to describe water movement in the vadose zone effectively. However, direct experimental analyses can be time-consuming and expensive, requiring meeting specific conditions for explicitly calculating model coefficients. For example, some methods necessitate repeatedly achieving steady-state or equilibrium hydraulic conditions for different boundary conditions. Field methods like infiltration, internal drainage, and evaporation (Angulo-jaramillo et al., 2016) can be costly, especially when dealing with large areas. Integrating small-scale measurements of soil hydraulic properties into hydrologic models that can be applied across different spatial and temporal scales is a significant challenge (Grayson and Blöschl, 2001; Vrugt et al., 2004).

Determining the hydrodynamic properties of soils in sustainable urban drainage systems involves various field measurement techniques such as infiltration methods, lysimeters, and radar geology. However, soil samples collected from specific sites may not fully represent the entire catchment due to vegetation heterogeneity that develops over time. Additionally, obtaining accurate measurements can be time-consuming and costly.

Two common approaches are often employed in hydrologic studies with large spatial dimensions. The first approach is deterministic, which uses a distributed physically-based model with upscaled effective soil properties (Blöschl et al., 1995). Alternatively, a stochastic model can be used, which retains the small-scale characteristics of the measurements but incorporates spatial heterogeneity of hydraulic properties to estimate effective properties at a larger spatial scale. Two main stochastic approaches are utilized to upscale soil hydrologic processes from a local to a field scale. The first approach involves analytical models primarily based on the perturbation approximations of Richards' equation, as Zhang (2006) demonstrated. The second approach employs numerical stochastic models that utilize Monte Carlo simulations to derive effective field-scale hydraulic properties and predict field-scale hydraulic behavior based on local-scale measurements (Gill et al., 2006).

Inverse modeling is a powerful technique used in many areas of science and engineering to solve problems where the cause of an observed effect is unknown or difficult to measure directly. It involves using mathematical algorithms to estimate a system's input parameters or unknown causes that can produce the observed output or effects (Hopmans et al., 2002).

In literature, deterministic inverse modeling approaches are extensively utilized to estimate effective parameters of soil hydraulic properties. These approaches ensure consistency concerning the spatial and temporal scale of measurement and model parameter support (Hopmans and Simunek, 1999; Hopmans, 1999; Hopmans et al., 2002; Köhne et al., 2006, 2006; Van Dam et al., 1994). Inverse models involve numerical inversion of the unsaturated flow equation and optimization algorithms to indirectly determine unknown parameters by minimizing deviations between measured and simulated flow attributes such as infiltration flow, soil water content, or pressure head. There are several different approaches to inverse modeling in soil physics, including mathematical optimization-based methods or traditional parameter optimization (Vrugt et al., 2008, 2004).

2.5.1. Mathematical Optimization-based methods

These methods involve minimizing an objective function that measures the difference between the model output and the observed data. The objective function is typically a measure of the distance or error between the model output and the observed data, and the optimization algorithm seeks to find the set of input parameters that minimize this error. Such as the simplest local-search optimization method, which is commonly used in the field of soil hydrology, is a Gauss–Newton type of derivative-based search Levenberg-Marquardt algorithm (Abbaspour et al., 2004, 2001; Arora et al., 2011; Hopmans et al., 2002; Köhne et al., 2006), genetic algorithms (Ines and Droogers, 2002), particle swarm optimization (Brunetti et al., 2016b; Gill et al., 2006, 2006; Parsopoulos and Vrahatis, 2002), artificiel neural networks (Jain et al., 2004; Moreira de Melo and Pedrollo, 2015), etc.

2.5.2. Traditional parameter optimization

Traditional parameter optimization algorithms focus on finding a single optimal set of parameters without considering any uncertainty estimates. However, this approach is questionable because our modeling efforts often involve various sources of uncertainty, including input (boundary conditions), output (calibration data), and model structural errors (since models are simplifications of reality) (Bertrand-Krajewski and Muste, 2008; Šimůnek and Hopmans, 2002). To address the issue of over-conditioning, one solution is to abandon the search for a single "best" parameter combination and adopt a Bayesian perspective (Bayes, 1763), which enables the identification of a parameter distribution that is commonly used in the literature for the urban hydrology and soil hydrology (Deletic et al., 2012, 2012; Vrugt et al., 2009, 2008).

2.5.3. Markov Chain Monte Carlo (MCMC)

To estimate the input parameters of a model using probability theory, it is essential to integrate inverse parameter estimation within a probabilistic framework based on Bayesian statistics. This approach combines prior knowledge of the system with observed data, such as soil water content, matric potential, and outflow, to obtain posterior probabilities of the model parameters. Incorporating this statistical inference approach can achieve a statistically robust information and uncertainty analysis. Monte Carlo-based methods are commonly employed to evaluate the posterior probabilities. However, these methods have certain limitations when applied to data-worth analysis with soil hydrological models. They need to be compatible with strongly non-linear and discontinuous models. Ideally, they should allow for the quantification of information gain in terms of relative entropy (also known as Kullback-Leibler divergence) between prior and posterior from data assimilation (Brunetti et al., 2020, 2016b; Schübl et al., 2022).

2.5.4. Bayesian

In recent years, Bayesian inference has become widely adopted for modeling soil processes, enabling reconciliation of system models with data through prediction in space (interpolation), prediction in time (forecasting), assimilating observations and deterministic/stochastic model output, as well as inference of model parameters (Brunetti et al., 2020; Schübl et al., 2022; Vrugt et al., 2009; Zou et al., 2019).

The Bayesian method is based on Bayes' theorem. The Bayes' theorem was discovered by the mathematician Thomas Bayes in the XVIII century as a probability theorem, P(A|B), of some hypothesis, B, is proportional to the product of the prior probability, P(A), of this hypothesis and the likelihood, L(A|B), of the same hypothesis given the observations, B, or (Bayes, 1763):

$$P(A|B) = \frac{L(A|B) * P(A)}{P(B)} \tag{2-42}$$

In Bayesian inference, the marginal likelihood, P(B), serves as a normalization constant for the posterior distribution, ensuring that it integrates to unity (Bingham, 1933). While the evidence may be ignored during parameter inference, it is crucial for model selection. The hypothesis or model, B, typically consists of a numerical model, F(x), which captures the system's state variables and fluxes through algebraic and differential equations. The unknown parameter values, x, are estimated using the observed data, and B. is for errors in model inputs such as boundary conditions. However, for complex soil models, the posterior distribution, P(A|B), can be high-dimensional and analytically intractable, requiring Monte Carlo simulation methods to approximate the target distribution (Vrugt et al., 2009, 2008). Hydrologic modeling encompasses various sources of uncertainty, including model structure, parameters, initial conditions, and observational data utilized for model input and evaluation (Liu and Gupta, 2007). The Bayesian calibration involves an optimization search through parameter domains to identify local minimum errors and may identify several parameter combinations that result in local minimum errors. Such methods often achieve lower error rates than calibration based on expert knowledge (Vrugt et al., 2005).

In addition, by accounting for uncertainties in model parameter calibration data and model structural errors (epistemic), the Bayesian approach offers a quantitative framework to address all potential sources of uncertainty explicitly. The model structural error represents the impact of incomplete knowledge on soil processes and system heterogeneities (Vrugt and Sadegh, 2013).

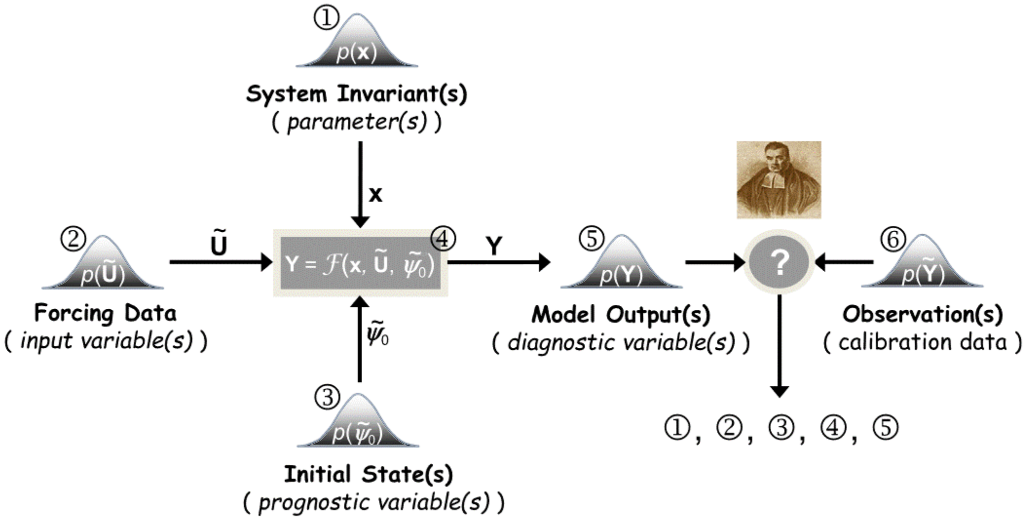

Figure (2.14): A schematic representation is provided to highlight the significant sources of uncertainty in environmental systems modeling, which include (1) parameter uncertainty, (2) input data uncertainty (also known as forcing or boundary conditions), (3) initial state uncertainty, (4) model structural uncertainty, (5) output uncertainty, and (6) calibration data uncertainty, Adopted from (Vrugt, 2016)

2.6. Overview and positioning of the thesis

The effectiveness of SUDS in managing water flow largely depends on the infiltration capacity of the soils within these systems. This infiltration capacity is influenced by various soil hydraulic properties, including water retention and unsaturated hydraulic conductivity curves.

The result of the literature review shows that accounting for infiltration and hydraulic properties of soils into hydrological modeling of SUDS is challenging in terms of the following:

1. Numerical infiltration models like Richards' equations incorporated in HYDRUS software are contingent upon having knowledge of the complete unsaturated hydraulic properties of soils, which necessitates prior characterization of soils using hydraulic methods such as the Beerkan estimation of soil transfer parameters (BEST) method (Angulo-Jaramillo et al., 2016; Bouarafa et al., 2019; Di Prima et al., 2020; Kanso et al., 2018; Lassabatère et al., 2006). The complexity and data requirements of these models can often pose challenges, preventing operational and scientific staff from utilizing them effectively.
2. The conceptual and physically-based models, such as Horton and Curve Number Green-Ampt, incorporate parameters that are either conceptual or not readily obtainable in the field.

Considering the extensive literature, the objective of this thesis is to delve into the models employed for estimating infiltration and assess their suitability for integration into a physically-based urban hydrological models.

From a methodological point of view, urban water management software such as SWMM (Rossman,2010), Infoworks (Solvi et al.,2005), or RECHARGE, etc. are supposed to be based on parameters that can be measured theoretically in the fields. However, these models have proven to be difficult to calibrate for several reasons:

- Measurement complexities: some parameters, such as the water pressure head at the wetting front in the Green-Ampt model, can be challenging to measure accurately in field conditions. Obtaining reliable measurements for these parameters adds to the complexity of the calibration.
- Number of parameters: these models typically require more than 15 parameters for accurate modeling. Estimating such a large number of parameters can be time-consuming and may require extensive data collection and analysis.
- Scope of urban planning: urban catchments often include many SUDS for effective management. In order to include these systems in the models, a large number of parameters

need to be extended, which adds to the complexity of the calibration. These parameters often need to be calibrated for use in practical management and planning tools. Soil parameterization accuracy is well known for the Bayesian method, which is often used in SUDS to estimate soil hydrodynamic parameters (Vrugt, 2016).

- Preferential flow: SUDS are implemented to effectively manage stormwater and minimize runoff. However, it's important to recognize that stormwater often carries diverse pollutants into infiltration basins. Over time, the soil characteristics within these systems change due to the growth of plant roots, resulting in the formation of macropores and pathways that promote preferential flow. Consequently, pollutants transported by stormwater can potentially migrate to deeper soil layers during the infiltration process. While in the cadre of this thesis pollution transfer and filtration didn't cover.

The three methodological developments proposed in this thesis are discussed in the corresponding chapters: a user-friendly physically-based parsimony model (Infiltration-Mod) approach in Chapter 3, the physically-based dual-permeability infiltration modeling and sensitivity analysis of this model in Chapter 4. , the sensitivity analysis and parameters calibration using Bayesian interface in Chapter 5.

Chapter 3

Sets of infiltration models for modeling and management of sustainable urban drainage systems

Chapter 3. Sets of infiltration models for modeling and management of sustainable urban drainage systems

Preface

In this chapter, our main focus is on the development of the INFILTRON-MOD tool. This tool offers three simplified physically-based infiltration models (*CH1*, *CH2*, *CH3*) within the Canoe-Hydrobox (*CH*) platform, which are utilized for simulating the water balance and evaluating SUDS (Asry et al., 2023). These models are based on the Green-Ampt (*GA*) approach, where the water flow is determined by the equivalent hydraulic gradient and the equivalent hydraulic conductivity, with variations in how they relate to moisture conditions and soil parameters. To assess the performance of the INFILTRON-Mod tool (Lassabatere and Asri, 2022). We compared the results obtained from the tool under different moisture conditions with the numerical solutions derived from the Richard equation. Furthermore, we evaluated the adjusted *CH* models using data from six infiltration experiments to determine their ability to fit real-world data accurately and predict hydrodynamic parameters, particularly the saturated hydraulic conductivity.

Asra Asry[a], Gislain Lipeme Kouyi[a], Tim D Fletcher[c], Jeremie Bonneau[a,b], Damien Tedoldi[a], Laurent Lassabatere[d]*

[a] Univ. Lyon, INSA Lyon, DEEP Laboratory, EA7429, Villeurbanne cedex, France.
[b] INRAE, UR HHLy, Hydrology and Hydraulics, 5 rue de la Doua, 69100 Villeurbanne, France.
[c] School of Ecosystem and Forest Sciences, University of Melbourne, 500 Yarra Boulevard, Burnley, Victoria, 3121, Australia.
[d] Univ. Lyon, Univ. Claude Bernard Lyon 1, CNRS, ENTPE, UMR5023 LEHNA, F-69518, Vaulx-en-Velin, France

This chapter has been published in the journal of hydrology.
https://doi.org/10.1016/j.jhydrol.2023.129477

Contents

3.1. Abstract

Infiltration is a key process in various fields such as hydrology, particularly for Sustainable Urban Drainage Systems (SUDS) management, agriculture, and urban soils. Over the past century, much effort has been invested in the comprehension of the physics of infiltration employing developing quantitative predictors of infiltration dynamics. In this study, three physically-based infiltration models developed within the Canoe-Hydrobox (*CH*) platform (models labeled *CH1*, *CH2*, *CH3*) were developed for modeling the water budget and evaluating SUDS. The three models rely on a Green-Ampt (*GA*) approach with the description of the water flux as the product of the equivalent hydraulic gradient and the equivalent hydraulic conductivity, with different ways to relate these to hydric conditions and soil parameters. These models were first subjected to preliminary mathematical and analytical analysis. Subsequently, they were used to model water infiltration into dry, intermediately wet, and wet soils, and were compared to numerical resolution based on Richard's equation, using the Hydrus software. The differences between the proposed models and the numerically generated reference data were then discussed to assess the capability of the *Canoe-Hydrobox (CH)* models to comply with the key principles of the physics of water infiltration into soils. Finally, we evaluated the revisited models using data derived from six experimental infiltration campaigns to assess their capability to fit real data and predict accurate values of hydrodynamic parameters, in particular the saturated hydraulic conductivity. The results show that the *CH1* model was not able to fully represent the physical principles of water infiltration into soils. Conversely, the new *CH3* model seemed more appropriate to comply with the principles of the physics of water infiltration and should be preferred in this context. Lastly, the *CH2* model reproduces a shape more in accordance with water infiltration disturbed by water repellence, depending on the initial water infiltration, and thus less appropriate. Our findings will provide the basis for further developments in the hydrological modeling of SUDS and their hydraulic performance.

Keywords

Urban hydrology, modeling, new models, water infiltration, SUDS

3.2. Introduction

Urbanization affects the physical properties of urban soils and, as a result, water movement and soil's capacity to act as a sink for water-transported pollution (Fletcher et al., 2015; O'Loughlin et al., 1996). These changes dramatically change the hydrological cycle, as infiltration capacity is reduced (Woltemade, 2010), changing river and stream flow and sedimentation levels (Marsalek et al., 2008; Miller and Hess, 2017). On the other hand, an increased rate of impervious surfaces reduces the infiltration process into the ground and surface storage capacity, increasing surface runoff (Booth DB, 1991). To mitigate effects arising from the generation of runoff in urban areas, sustainable urban drainage systems (SUDS) are widely implemented for stormwater management (Bertrand-Krajewski et al., 2000; Liu et al., 2012). SUDS aims to shift the water cycle back towards its natural cycle by reducing runoff volumes, attenuating peak flows, and improving water quality, through various processes including infiltration and evapotranspiration. These practices include filter strips, grassed swales, bioretention facilities, green roofs, permeable pavements, and water treatment systems (Chocat, 2008; Davis, 2008, 2005).

The hydrological performance of SUDS devices relies, in part, on the infiltration capacity of soils, which in turn is dependent on the soil hydrodynamic properties, such as the water retention and permeability curves, initial water content, and the saturated hydraulic conductivity (Bockhorn et al., 2017; Rinderer and Seibert, 2012; Zhu et al., 2012). A proper quantification and modeling of water infiltration in SUDS is therefore of prime importance. The models developed for water infiltration may be either empirical or theoretical, like Richard's, Philip, Meyer and Warrick's, Brooks and Corey's, Gardner, Brutsaert, Haverkamp models (Angulo-Jaramillo et al., 2016; Marinoschi, 2006). Among these approaches, the conceptual physically-based Green-Ampt model has been the subject of several investigations (Warrick and Broadbridge, 1992) and is widely used for the modeling of SUDS. For instance, the Green-Ampt approach is incorporated in the widely used SWMM software package, among other options including the Hortonian or the Curve-Number infiltration models, to simulate water infiltration into SUDS (Roesner, 2009; Rossman, 2010). However, these modeling tools are far from perfect, especially regarding the description of the effects of base and sub-base layers on the infiltration processes (Hilten et al., 2008). The newly added low-impact development (LID) module in SWMM Version 5.1 aimed to improve the simulation of the stormwater management performance of various types of LID practices. There is also an increasing emphasis on the development and use of physical process-based models to improve the modeling of infiltration systems (Carbone et al., 2015).

Numerical solving of the Richards equation has been developed for decades to predict water infiltration processes in many contexts, including the investigation of SUDS hydraulic performance (Tedoldi et al., 2016). HYDRUS is perhaps the best-known software for solving the Richards equation, allowing for many types of initial and boundary conditions and types of soils (Radcliffe and Simunek, 2018). The HYDRUS suite has been widely used in the literature for the description of the hydraulic behavior of various types of LID practices (Brunetti et al., 2016; Hilten et al., 2008; Li and Babcock, 2015; Newcomer Michelle E. et al., 2014; Osman, 2013; Palla et al., 2009). However, HYDRUS requires knowledge of the entire unsaturated hydraulic properties of soils, requiring the prior characterization of soils with hydraulic methods like the Beerkan estimation of soil transfer parameters (BEST) method (Angulo-Jaramillo et al., 2016; Bouarafa et al., 2019; Di Prima et al., 2020; Kanso et al., 2018; Lassabatère et al., 2006). Such a requirement drastically increases the level of complexity of these models and requires a large amount of specific data, precluding their use by decision-makers, designers, and practitioners. Consequently, there is a need for physically-based models that are easy to use and require less effort for calibration, based on data relatively easy to collect and monitor (e.g., water levels and fluxes). The availability of such models is critical for urban water management practitioners in current and future cities. With this aim, Bonneau et al. (2021) implemented a physically-based simplified model for the prediction of water fluxes in bioretention systems (named here *CH1* – *CH* stands for Canoe-Hydrobox, Hydrobox being the LID module integrated into the Canoe software, see Chocat (2013)). This model was designed to avoid over-parametrization and simulate hydraulic fluxes in the bioretention system after calibration using two contrasting rainfall events. This model predicts the following variables: water infiltration at the soil surface, soil water storage, vertical gravity-driven infiltration in the filter media, exfiltration, underdrain, and outflow fluxes. However, the results from this study proved that some parts of physics were not properly represented, and that improvement was still needed (Bonneau et al., 2021). These authors related these inconsistencies to the inaccurate quantification of the infiltration component, among others.

The aim of the present study was therefore to improve the relationship between the infiltration rate, on the one hand, and the hydraulic gradient, hydric conditions, and soil hydraulic parameters, on the other, to better capture the variability of infiltration components, by proposing and validating three alternatives for the modeling of the infiltration in urban soils. A set of two physically-based models, *CH2* and *CH3* were designed as improvements of *CH1* for water infiltration in SUDS. The three models (*CH1*, *CH2,* and *CH3*) were assessed regarding their capability to predict infiltration fluxes accurately. The three models consider Darcy's law as their basis but differ in their ways of computing the equivalent hydraulic gradient and the equivalent hydraulic conductivity. These models were tested against both numerically generated data (simulation with Hydrus software of infiltration for different synthetic soils and initial saturation degrees) and real experimental data (real infiltration runs performed in the field). The models were assessed concerning their capability to fit the synthetic and real infiltration data, comply with the physics governing water infiltration into soils, and provide accurate estimates of hydraulic parameters (e.g., saturated hydraulic conductivity) when used in the inverse mode. The final goal of this study is to give insight into the selection of the best model with regard to the modeling of water infiltration into soils, before their implementation into the broader numerical platform for the design and evaluation of SUDS.

3.3. Theoretical analysis

3.3.1. Water infiltration into soils

Infiltration at the soil surface and water redistribution in the soil are ruled by the Richards equation (Equation 3-1c) that combines Darcy's law (Equation 3-1a) with the mass conservation equation (Equation 3-1b):

$$q = -K(\theta)\left(1 + \frac{\partial h}{\partial z}\right) \quad \text{(3-1a)}$$

$$\frac{\partial \theta}{\partial t} = -\frac{\partial q}{\partial z} \quad \text{(3-1b)}$$

$$\frac{\partial \theta}{\partial t} = \frac{\partial}{\partial z}\left(K(\theta)\left(1 + \frac{\partial h}{\partial z}\right)\right) \quad \text{(3-1c)}$$

Where q (L T^{-1}) stands for the water flux, h (L) for the water pressure head, θ (L^{3} L^{-3}) for the water content, and $K(\theta)$ (L T^{-1}) for the unsaturated hydraulic conductivity. Solving Equation (3-1c) requires the knowledge of the hydraulic functions, i.e. the water retention curve and the unsaturated hydraulic conductivity. Several models were developed for these functions (Angulo-Jaramillo et al., 2016). The van Genuchten (1980) model with the Mualem condition $m = 1 - \frac{1}{n}$ is often considered for the description of the water retention curve, where m (-) and n (-) are hydraulic shape factors. The Mualem (1976) model for unsaturated hydraulic conductivity is also among the most frequently used models. These models are as follows:

$$\theta(h) = \theta_r + (\theta_s - \theta_r)(1 + (\alpha h)^n)^{-m} \tag{3-2a}$$

$$K(S_e) = K_s\, S_e^l \left(1 - \left(1 - S_e^{\frac{1}{m}}\right)^m\right)^2 \tag{3-2b}$$

Where $S_e = \frac{(\theta - \theta_r)}{(\theta_s - \theta_r)}$ (-) is the saturation degree, θ_r ($L^3\ L^{-3}$) and θ_s ($L^3\ L^{-3}$) stand for the residual and the saturated water contents, α (L) is the scale parameter for the water pressure head, K_s ($L\ T^{-1}$) is the saturated hydraulic conductivity, n, $m = 1 - \frac{1}{n}$ and l (-) are hydraulic shape parameters.

Solving Equation (3-1) for given water retention and hydraulic conductivity functions allows the determination of flow variables, leading to the type of results described in Figure (3.1 a-c) for the case of water infiltration into a uniform profile with uniform initial water contents and water pressure heads and for a constant water pressure head imposed at the soil surface. Figure (3.1 a-c) describes the typical features of variables during water infiltration into homogeneous soils, including the water pressure head Figure (3.1 a) and the water content Figure (3.1 b) profiles describing the wetting front displacement through the soil profile, and the infiltration rate and the cumulative infiltration Figure (3.1 c) describing water infiltration at the soil surface.

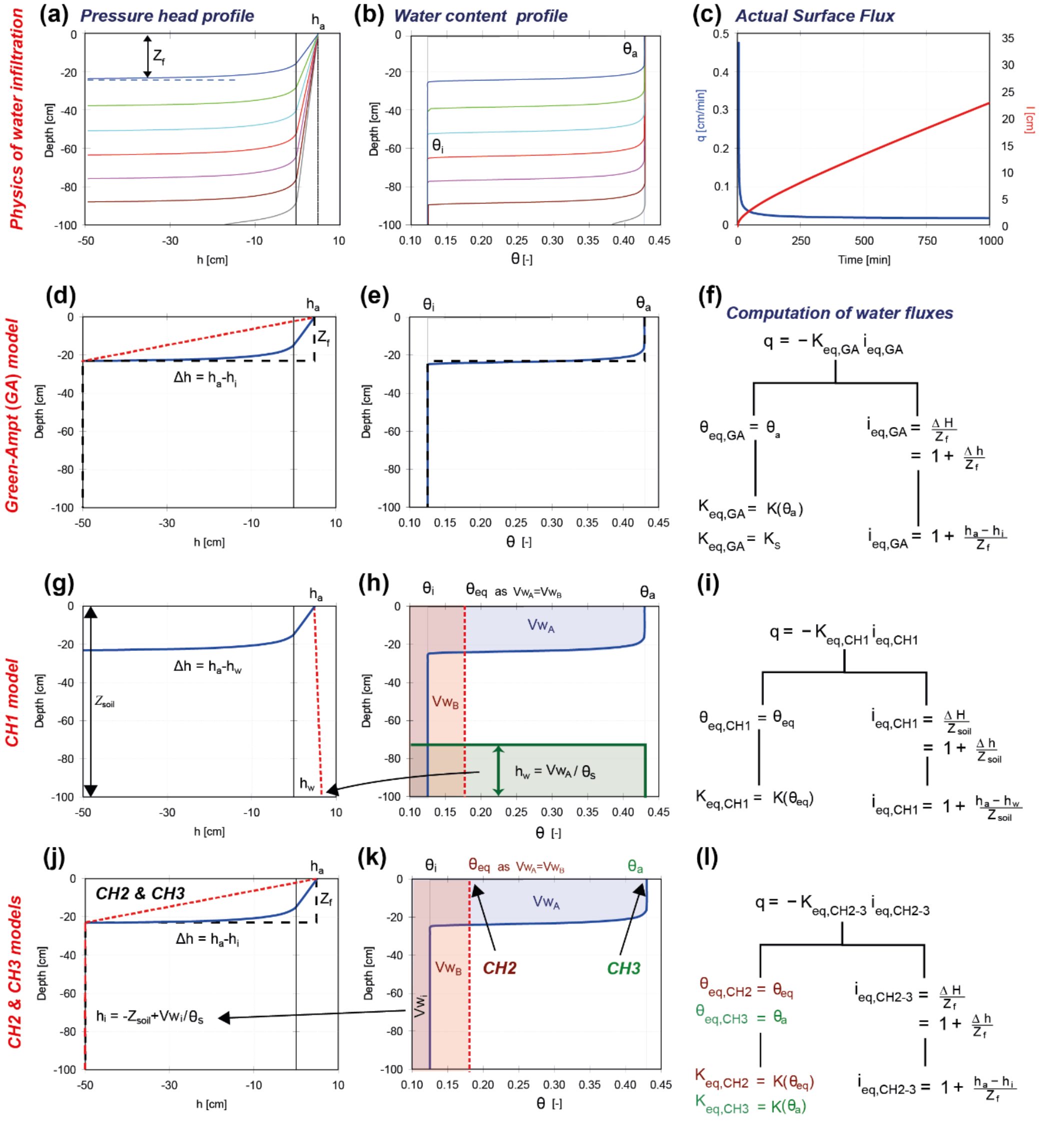

Figure (3.1): *CH* models developments: first row: physical principles of water infiltration based on the illustration with numerically generated data (from left to right, pressure head and water content profiles and infiltration rate, q, and cumulative infiltration, I, at the soil surface); second row: the case of the Green-Ampt model (from left to right, simplification of the water pressure head profile, the water content profile, and computations of fluxes with Darcy's law), third row: same illustration for the *CH1* model, 4th row: same illustrations for the *CH2* & *CH3* models. (where h_a is the water pressure head on upper soil, Z_f is the wetting front position, h_w is the water pressure head present in the soil, h_i is the initial water pressure head, θ_s, the saturated water content, θ_i the initial water content, θ_{eq} the equivalent water content, Z_{soil}, the soil depth, V_w is the volume of water present in the soil)

At the beginning, the difference in water pressure head $\Delta h = h_a - h_i$ between the surface and the soil applies on a very thick soil layer, above the wetting fronts positioned at small depths, z_f (Figure 3.1 a). The capillary part of the hydraulic gradient $\frac{\partial h}{\partial z} \approx \frac{\Delta h}{Z_f}$ then takes very large values close to infinity. With time, the wetting front moves downwards thus increasing the depth of the wetting front z_f and then decreasing the capillary part of the hydraulic gradient. Given that the gravity part of the hydraulic gradient remains the same, i.e., 1, the total hydraulic gradient follows the same decreasing trend. For very long times, when the wetting front reaches quasi-infinite values, $z_f \to +\infty$, the capillary part of the hydraulic gradient tends towards zero, $\frac{\partial h}{\partial z} \approx \frac{\Delta h}{z_f} \to 0$ and, consequently, the hydraulic gradient tends towards unity, meaning that the infiltration tends towards K_s. Consequently, the infiltration rate decreases from infinity to the value of the saturated hydraulic conductivity at steady state, Figure (3.1 c), $q(z = 0, t = +\infty) = K_s$, giving the cumulative infiltration, $I(t)$, its specific shape with a concave part for the transient state followed by a linear part for the steady state (Figure 3.1 c). These features result from the principles of the physics of water infiltration into homogeneous soils (Angulo-Jaramillo et al., 2016; Lassabatere et al., 2009).

3.3.2. Design of the proposed sets of infiltration models

Numerically solving Richards equation predicts flow and the water flux $q(z,t)$ continuously along the whole soil profile, with no restriction in terms of depth limits and spatial precision, provided that numerical options (mesh, boundary conditions, etc.) are properly chosen (Radcliffe and Simunek, 2018). Conversely, the model developed by Bonneau et al. (2021) is based on the reservoir approach, assimilating the soil profile to a block of given depth, z_{soil} (L), and a given area at the surface, A=1 m^2 (L2) (Figure 3.1 g-l). The water flux $q(t)$ (L T-1) is averaged at the scale of the block and related to an equivalent hydraulic gradient, i_{eq} (L L-1), and equivalent hydraulic conductivity, K_{eq} (L T-1):

$$q(t) = -K_{eq} i_{eq} \tag{3-3}$$

Assumptions and options for the choice of the block of soil (value of z_{soil}) provide several expressions of K_{eq} and i_{eq} depending on the considered model. Those assumptions allow us to relate the averaged infiltration rate, $q(t)$ to the cumulative infiltration at the surface, $I(t)$ (L), leading to the definition of a characteristic function $q(I)$. The Green and Ampt model is also based on the same approach but with specific definitions of K_{eq} and i_{eq}. The design of K_{eq} and i_{eq} and the characteristic function $q(I)$ are described for all the models in the dedicated part.

3.3.2.1.1. Hydraulic conductivity, K_{eq}

For the hydraulic conductivity, K_{eq} is either equal to the saturated hydraulic conductivity, $K_{eq} = K_s$, like for the Green and Ampt model (Green and Ampt, 1911), or is equal to the unsaturated hydraulic conductivity $K_{eq} = K(S_e) \leq K_s$, needing the quantification of the saturation degree $S_e$at the scale of the soil block.

In this study, we consider the approach implemented by Bonneau et al. (2021) for the estimation of the profile averaged saturation degree, $S_{e,eq}$. These authors considered that the total volume of water present in the profile $V_{w,A}$ (L^3) could be converted into an equivalent volume of water, $V_{w,B}$ (L^3) in the same profile with a homogeneous saturation degree $S_{e,eq}$ (-) Figure (3.1 h). Then, at any time *t*, the total water content θ ($L^3\ L^{-3}$) in the profile is computed as the sum of the initial water content and the contribution of infiltration from the surface see Figure (3.1 h):

$$\theta = \theta_i + \frac{V_{w_{added}}}{A\, z_{soil}} \tag{3-4}$$

Where θ_i ($L^3\ L^{-3}$) corresponds to the initial water content (assumed homogeneous over the entire soil depth), and $V_{w_{added}}$ (L^3) to the volume of water added to the soil block due to the water infiltration at the surface. In this study, we consider no fluxes at the base of the soil block.

To go further, $V_{w_{added}}$ can be easily related to the cumulative infiltration I (L) in the equation (3-4), considering that it corresponds to $V_{w_{added}}$ divided by the infiltration surface, i.e., $I = \frac{V_{w_{added}}}{A}$, leading to:

$$\theta = \theta_i + \frac{I}{z_{soil}} \tag{3-5}$$

and thus one obtains the following expression for the saturation degree, $S_{e,eq}$:

$$S_{e,eq} = S_{e,i} + \frac{I}{z_{soil}(\theta_s - \theta_r)} \tag{3-6}$$

Where $S_{e,i}$ (-) stands for the initial saturation degree. Then, the equivalent saturation degree, $S_{e,eq}$, can be injected into the hydraulic conductivity function as defined by the Mualem (1976) model, $K(S_e)$ (Equation 3-2 b), to compute the hydraulic conductivity $K_{eq,CH1}$ ($L\ T^{-1}$) as a function of the cumulative infiltration I:

$$K_{eq,CH1}(I) = K_s\left(S_{e,i} + \frac{I}{z_{soil}(\theta_s - \theta_r)}\right)^l \left(1 - \left(1 - \left(S_{e,i} + \frac{I}{z_{soil}(\theta_s - \theta_r)}\right)^{\frac{1}{m}}\right)^m\right)^2 \tag{3-7}$$

For the specific case of the saturation degree description with the equation (3-6). The subscript "*CH1*" in $K_{eq,CH1}(I)$ refers to the fact that this function was developed for the design of the *CH1* model.

Considering the case of no leakage at the base of the soil block, the volume of water added to the soil block cannot exceed the volume of voids initially filled with air and thus available for the water entering the soil block, i.e., $A\, z_{soil}(\theta_s - \theta_i)$. The maximum infiltration corresponds to, $I_{max} = Z_{soil}(\theta_s - \theta_i)$, and no quantities should be computed for larger cumulative infiltration, $I > I_{max}$, corresponding to the saturation degrees $S_e > 1$ (which is meaningless with regard to the principles of soil physics).

3.3.2.2. Hydraulic gradient, i_{eq}

Green-Ampt model:

The Green and Ampt (1911) model considered the saturated region of the soil between the surface and the position of the wetting front to compute the hydraulic gradient over this region (Figure 3.1 d-e). At the surface, the water pressure head corresponds to the value imposed at the soil surface, h_a. If one considers infiltration experiments, h_a corresponds to the water height in the ring. Just below the wetting front, the water pressure head corresponds to the initial water pressure head h_i. Then, the difference in the water pressure head can be considered, $\Delta h = h_a - h_i$ (L), and the equivalent hydraulic gradient $i_{eq,GA}$ (L L^{-1}) can be easily computed from the gravity-driven (+1) and capillary-driven gradient, $\frac{\partial h}{\partial z} \approx \frac{\Delta h}{z_f}$, where z_f (L) corresponds to the depth of the wetting front:

$$i_{eq,GA} = 1 + \frac{\Delta h}{z_f} \tag{3-8}$$

The replacement of the position of the wetting front as a function of the cumulative infiltration, $z_f = \frac{I}{\Delta\theta}$ (mass conservation), leads to the following final expression:

$$i_{eq,GA}(I) = 1 + \frac{\Delta\theta \Delta h}{I} \tag{3-9a}$$

$$i_{eq,GA}(I) = 1 + \frac{(\theta_s - \theta_i)\,(h_a - h_i)}{I} \tag{3-9b}$$

***CH1* model and related hydraulic gradient:**

The *CH1* model developed by Bonneau et al. (2021) computes the hydraulic gradient between the surface and the lower depth of the soil column, z_{soil}. The water pressure head gradient $\frac{\partial h}{\partial z}$ considers that the water pressure head is fixed at the surface at h_a and that the water pressure head at the lower boundary is in equilibrium with the column of water above. In other words, the water in the profile is allowed to drain till the lower boundary at $z = z_{soil}$, and to form a saturated zone with a specific height h_w imposing the lower water pressure head Figure (3.1 h). These assumptions were considered for coarse materials, like in the base of bioretention systems, with water drainage and storage layers**.** Then, the depth of saturated soil is computed from the total quantity of water in the profile V_w (L^3) and the saturated water content, θ_s , considering a stepwise distribution into the profile for water content $\theta(z)$ Figure (3.1h):

$$V_w(t) \ = A\int_0^{Z_{soil}} \theta(z,t)dz \ \ = A\int_0^{h_w(t)} \theta_s dz \ \ \approx A\, h_w(t)\, \theta_s \tag{3-10}$$

Equation (3-10) is an approximation since it considers that the water content above the saturated zone is negligible and that all the water present in the profile saturates the soils over the depth h_w. The depth h_w (L) can then be easily derived from the volume of water, V_w:

$$h_w \approx \frac{V_w(t)}{A\theta_s} \tag{3-11}$$

Then, the volume V_w is equal to the initial volume added with the volume of infiltrated water, leading to:

$$V_w(t) = A\, Z_{soil}\, \theta_i + A\, I(t) \tag{3-12}$$

$$h_w(t) = \frac{V_w(t)}{A\theta_s} = \frac{A\, z_{soil}\, \theta_i + A\, I(t)}{A\theta_s} \tag{3-13}$$

$$h_w(t) = \frac{\theta_i}{\theta_s} z_{soil} + \frac{I(t)}{\theta_s} \tag{3-14}$$

Then, the equivalent hydraulic gradient, $i_{eq,CH1}(t)$ (L L^{-1}), can be computed by dividing the difference in water pressure head $\Delta h = h_a - h_w$ (L) by the total distance z_{soil} (L) Figure (3.1), leading to:

$$i_{eq,CH1}(t) \ = 1 + \frac{h_a - h_w(t)}{z_{soil}} \tag{3-15}$$

$$i_{eq,CH1}(t) \ = 1 + \left(\frac{h_a}{Z_{soil}} - \frac{\theta_i}{\theta_s} - \frac{I(t)}{Z_{soil}\, \theta_s}\right) \tag{3-16a}$$

$$i_{eq,CH1}(I) \; = 1 + \left(\frac{h_a}{Z_{soil}} - \frac{\theta_i}{\theta_s} - \frac{I}{Z_{soil}\,\theta_s}\right) \tag{3-16b}$$

Again, Equation (3-16) is valid as long as there are no water leaks at the lower boundary of the soil block. Otherwise, additional fluxes should be added to the expression of $h_w(t)$.

<u>Alternative hydraulic gradient for *CH2* and *CH3*:</u>

The water pressure head gradient previously computed for the *CH1* model may lead to $\left(\frac{h_a}{Z_{soil}} - \frac{\theta_i}{\theta_s} - \frac{I}{Z_{soil}\,\theta_s}\right) \leq 0$, meaning a hydraulic gradient lower than unity, $i_{eq} \leq 1$ (see equation (3-16)). This implies that the infiltration rate may be lower than the gravity-driven infiltration, which is meaningless with regard to the physics of water infiltration into soils. Two enhanced *CH2* and *CH3* models are developed as alternative ways for the quantification of the hydraulic gradient. As previously assumed for *CH1*, the water initially present in the soil profile is still allowed to drain and create a saturated zone of a depth of $h_{w,i}$ at time zero. However, the computation of the initial water pressure head at the surface and over the profile, h_i, was modified. In this new version, h_i (L) equates to the initial isostatic water pressure head, and then relates to the initial water pressure head at the base of the soil block, $h_{w,i}$ (L), leading to:

$$h_i = -\left(z_{soil} - h_{w,i}\right) \tag{3-17}$$

$$h_i = z_{soil}\left(\frac{\theta_i - \theta_s}{\theta_s}\right) \tag{3-18}$$

$$\Delta h = (h_a - h_i) \tag{3-19}$$

$$\Delta h = h_a + z_{soil}\left(\frac{\theta_s - \theta_i}{\theta_s}\right) \tag{3-20}$$

To compute the hydraulic gradient, we divide the difference of water pressure head Δh with the position of the wetting front, as suggested by Green and Ampt (1911), instead of the soil block depth z_{soil}. This leads to the following expressions:

$$i_{eq,CH2-3}(t) \; = 1 + \frac{h_a + z_{soil}\,\left(\frac{\theta_s - \theta_i}{\theta_s}\right)}{z_f(t)} \tag{3-21}$$

$$i_{eq,CH2-3}(t) \; = 1 + \frac{\left[h_a + z_{soil}\,\left(\frac{\theta_s - \theta_i}{\theta_s}\right)\right](\theta_s - \theta_i)}{I(t)} \tag{3-22a}$$

$$i_{eq,CH2-3}(I) \; = 1 + \frac{\left[h_a + z_{soil}\,\left(\frac{\theta_s - \theta_i}{\theta_s}\right)\right](\theta_s - \theta_i)}{I} \tag{3-22b}$$

In Equations (3-22a) and (3-22b), the position of the wetting front z_f is replaced by its expression as a function of cumulative infiltration, i.e., $z_f(t) = \frac{I(t)}{(\theta_s - \theta_i)}$.

3.3.2.3. Summary of the set of models

***CH1* model:** The equivalent hydraulic conductivity is taken as the unsaturated hydraulic conductivity, $K_{eq,CH1}(I)$ as defined by the Equation (3-7), and the hydraulic gradient, $i_{eq,CH1}(I)$, as defined by the Equation (3-16).

New *CH2* model: The *CH2* model considers only the change in hydraulic gradient, $i_{eq,CH2-3}(I)$, as defined by the Equation (3-22), instead of $i_{eq,CH1}(I)$, while the equivalent hydraulic conductivity remains defined by the unsaturated hydraulic conductivity $K_{eq,CH2}(I) = K_{eq,CH1}(I)$ using the Equation (3-7).

New *CH3* model: The hydraulic gradient relies on the alternative function $i_{eq,CH2-3}(I)$ defined by Equation (3-22), like the *CH2* model, whereas the equivalent hydraulic conductivity is fixed at the saturated hydraulic conductivity, $K_{eq,CH3}(I) = K_s$.

Once the options are selected for the equivalent hydraulic conductivity, K_{eq}, and hydraulic gradient, i_{eq}, all the models define the infiltration rate as the product of $K_{eq}$and i_{eq}, leading to the function $q(I)$.

3.4. Material and methods

The verification of the *CH* models was performed using both simulated and experimental data. Regarding the comparison against numerically generated data, the predictions by the *CH* models were compared with the numerical data obtained by solving Richards' equations for different scenarios (soils and initial saturation degrees). In addition, the analytical features of the *CH* models were discussed regarding the physics of water infiltration into soils. For the validation using experimental data, the *CH* models were fitted to water infiltration data obtained with the single-ring procedure (Angulo-Jaramillo et al., 2016), and the quality of the fits and the plausibility of estimates were discussed.

3.4.1. Field Experiments

The experimental data involve six infiltration tests realized on vegetated soils with a large ring infiltrometer that is under development within the framework of the INFILTRON project (www.infiltron.org). The ring, 50 cm in diameter, was directly inserted into the ground (5cm insertion), and a constant height of water between 5 and 10 cm was imposed in the ring, corresponding to a water pressure head of approximately $h_a \approx 0.1$ m. Two big reservoirs located nearby supplied the water needed to maintain constant the level of water in the ring (Figure 3.2). The operators monitored the drop in water level in the reservoirs to measure the infiltration rates. The cumulative infiltrations were then deduced by dividing the volume of infiltrated water by the ring surface. These experiments were performed at two different but comparable sites Figure (3.2), on the campus of the ENTPE located in Vaulx-en-Velin (Lyon, France). More details on the characterization of the loamy soil may be found in previous works (Concialdi et al., 2020).

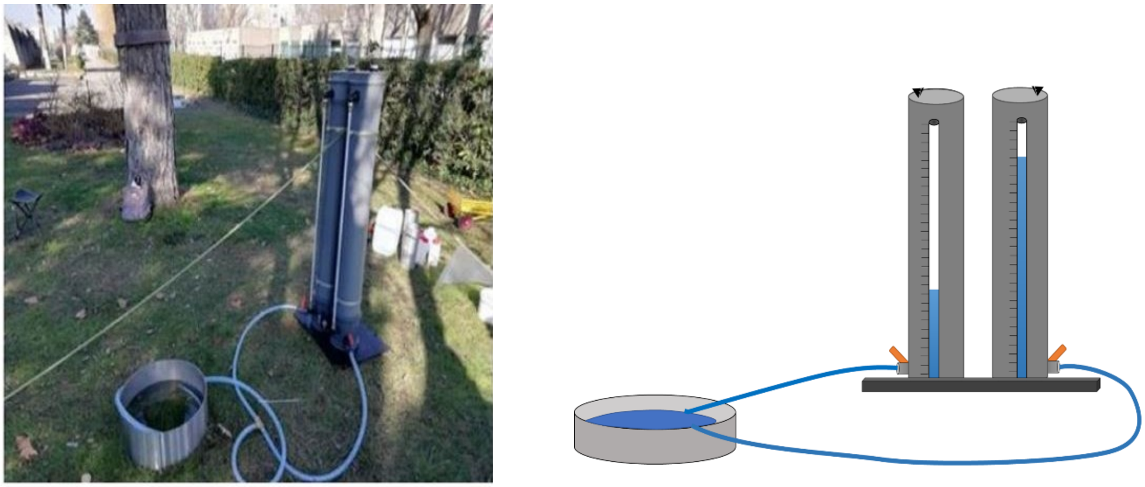

Figure (3.2): Picture of the field and experimental device; large ring infiltrometer with two large reservoirs

We also sampled the soil to get the value of the initial water content and the soil bulk density, leading to the following derivations of initial water content and porosity:

i. ENTPE 1 site: The initial averaged water content value was measured at 0.31. The dry bulk density was measured at 1.24 g cm^{-3}, which corresponds to a value of porosity of 53.1%, assuming the by-default value of the mineral density, i.e., 2.65 g cm^{-3}.

ii. ENTPE 2 site: The initial averaged water content value was measured at 0.40. The dry bulk density was measured at 1.28 g cm^{-3}, which corresponds to a value of porosity of 51.7%, assuming the by-default value of the mineral density, i.e., 2.65 g cm^{-3}.

Given the large dimension of the ring (*i.e.*, 50 cm in diameter), we consider that the lateral flux is negligible, this flux being proportional to the inverse of the ring radius (Smettem et al., 1994), and then expected to be negligible for our large ring. Consequently, we consider that the water infiltration is mainly 1D, instead of 3D, and that the data can be modeled by the proposed models, that were designed for 1D infiltration into soils.

3.4.2. Numerically generation of data and numerical inversion with Hydrus

We considered the numerically generated data as the reference since they are directly based on the numerical solving of Richards equation Equation (3-1) without any simplification. In this study, we modeled 1D vertical infiltration processes with HYDRUS-1D software (Šimůnek and van Genuchten, 2008). For a thorough test, the models were evaluated considering twelve typical synthetic soils with contrasting hydraulic behaviors from the Carsel and Parrish database (Carsel and Parrish, 1988). Their water retention and hydraulic conductivity curves are described by Equation (3-2) and related hydraulic parameters are listed in Table (3.1).

Table (3.1): Van Genuchten-Mualem (VG-M) and related hydraulic parameters for the twelve studied synthetic soils (Carsel and Parrish, 1988)

Soil Texture	θ_r $[cm^3\ cm^{-3}]$	θ_s $[cm^3\ cm^{-3}]$	α $[mm^{-1}]$	$\boldsymbol{n}$	K_s $[mm\ h^{-1}]$	l
Sand	0.045	0.43	1.45E-02	2.68	2.97E+02	0.5
Loamy Sand	0.057	0.41	1.24E-02	2.28	1.46E+02	0.5
Sandy loam	0.065	0.41	7.50E-03	1.89	4.42E+01	0.5
Loam	0.078	0.43	3.60E-03	1.56	1.04E+01	0.5
Silt	0.034	0.46	1.60E-03	1.37	2.50E+00	0.5
Silt loam	0.067	0.45	2.00E-03	1.41	4.50E+00	0.5
Sandy Clay Loam	0.10	0.39	5.90E-03	1.48	1.31E+01	0.5
Clay loam	0.095	0.41	1.90E-03	1.31	2.60E+00	0.5
Silty Clay Loam	0.089	0.43	1.00E-03	1.23	7.02E-01	0.5
Sandy Clay	0.10	0.38	2.70E-03	1.23	1.20E+00	0.5
Silty Clay	0.07	0.36	5.00E-04	1.09	2.00E-01	0.5
Clay	0.068	0.38	8.00E-04	1.09	2.00E+00	0.5

The water infiltration was computed considering a numerical domain of 2.5 m deep for all the soils, with a step discretization of 5 mm. We considered a constant water pressure head of 5 mm at the soil surface and uniform initial water contents and water pressure heads, with several values to mimic contrasting scenarios (initially dry or wet soils). The lower boundary was designed as free drainage and is usually considered for an unsaturated soil profile with small depths (Šimůnek, 2006; Šimůnek and van Genuchten, 2008). The time steps were managed with the Hydrus adaptive method, considering a minimum time step fixed at values between 10^{-9} and 10^{-3} minutes depending on the soil and the difficulty of convergence. The total time was designed to allow the numerical modeling of water infiltration until the attainment of the lower boundary of the numerical model. More details regarding the numerical modeling may be found in previous studies (Bouarafa et al., 2019; Lassabatère et al., 2006).

For the inverse method, we reduced the number of parameters to two, in order to avoid non-uniqueness and equifinality (Pollacco et al., 2013; Šimůnek and van Genuchten, 1997), by inverting the value of the saturated hydraulic conductivity, K_s, and the value of the scale parameter for the water pressure head, α. The shape parameter n was fixed at the value of loamy soils, $n = 1.56$, since this value represents an average value among all types of soils. The shape parameter m was then deduced considering that $m = 1 - \frac{1}{n}$. The shape parameter l was fixed at its default value, $l = 0.5$. Lastly, the residual water content was considered null and the saturated water content was equaled to the soil porosity. The fitting procedure implemented in HYDRUS-1D was then applied (Šimůnek and van Genuchten, 2008). Hydrus software considers an objective function defined as the sum of the square errors and minimizes the objective function by using the Levenberg-Marquardt nonlinear optimization method (Simůnek et al., 2009).

3.4.3. Inverse modeling using *CH* and *GA* models

The inverse modeling approach was used to fit the studied models, including the *GA* model and the proposed *CH* models to the experimental data and to determine the related hydraulic parameters and the soil properties. Solving the inverse problem consists of the optimization of an objective function that corresponds to minimizing the difference between observed and simulated values. In this study, we considered the *NSE* Sutcliffe Efficiency coefficient (NSE) which is defined as follows:

$$NSE = 1 - \frac{\sum_{i=1}^{n}(O_i - S_i)^2}{\sum_{i=1}^{n}\left(O_i - \underline{O}\right)^2} \quad (3\text{-}23)$$

Where O_i and S_i are the observed and simulated values, respectively, n is the total number of paired values, $\underline{X}$ refers to the mean of the variable *X*. In this study, we used the Monte Carlo optimization technique. This technique consists of generating a random sample of 1 million sets of parameters (based on plausible intervals of values), computing the *NSE* objective function for all the sets, and selecting the "best one", i.e., the set of the parameter that maximizes the *NSE* function (Eckhardt, 1987). Note that the maximization of the *NSE* objective function corresponds to the minimization of the distance between the observed and the simulated data.

For the fits of *CH* and *GA* models, we considered two options: (i) optimization of K_s, the other parameters being derived from field measures or fixed *a priori*, (ii) optimization of more parameters to allow better fits.

The *GA* model has the following input parameters: the difference in water content, $\Delta\theta = \theta_s - \theta_i$, the difference in water pressure head between the ring and the soil profile before water infiltration, $\Delta h = h_a - h_i$, and the saturated hydraulic conductivity, K_s. As a first step, we only optimized the saturated hydraulic conductivity, $\Delta\theta = \theta_s - \theta_i$ being deduced from the field measures, and $\Delta h = h_a - h_i$ being deduced from the estimation of the initial water pressure head, h_i. The value of h_i was deduced from the initial saturation degree considering Equation (3-2a) for the case of a loamy soil ($\alpha = 3.6\ 10^{-3}$ mm^{-1} and $n = 1.56$). For the second option, we also optimized the value of h_i to improve the model fits.

Regarding the *CH* models, *CH1* and *CH2* models depend on residual and saturated water contents, θ_r and θ_s, the saturated hydraulic conductivity, K_s, the shape parameters n (or equivalently m) and l, the initial water content, θ_i, and the water pressure head imposed at the soil surface, h_a. The *CH3* model involves fewer hydraulic parameters since the equivalent hydraulic conductivity is fixed at $K_{eq} = K_s$ implying that parameters θ_r, n and l are no longer needed. Note that, by design, none of the *CH* models requires the scale parameter for water pressure head α. In addition to the hydraulic parameters, all the *CH* models have a specific parameter that corresponds to the depth of the soil profile, z_{soil}. This last parameter may be varied to fit data but should remain high enough to allow the storage in the soil profile of the total amount of infiltrated water. That leads to the following condition: $z_{soil} \geq \frac{I_{tot}}{(\theta_s - \theta_i)}$. Otherwise, some observed cumulative infiltrations may not be modeled by the *CH* models which provide predictions only over the following interval: $I \in [0, I_{max} = z_{soil}(\theta_s - \theta_i)]$.

The first optimization option, option (i), involved the following simplifications aimed at reducing the number of parameters to estimate: the residual water content was fixed at zero, $\theta_r = 0$, the saturated water content, θ_s, was computed from the bulk density, the shape parameter n was fixed at the value of loamy soils, $n = 1.56$, and the shape parameter l was fixed at its by-default value, $l = 0.5$, as for the case of numerical inversion (Hydrus). Then, we optimized only the remaining hydraulic parameter, i.e., K_s. For this first option, we assigned a large value to the *CH* model parameter $z_{soil} = 10$ m, to ensure that the soil profile was deep enough to store the total amount of infiltrated water and that the positions of the wetting fronts remained far above the lower limit of the soil profile.

For the second option, option (ii), we varied more hydraulic parameters. We considered that the hydraulic parameters, n, and thus m, could be also optimized, for *CH1* and *CH2*. For *CH3*, we allowed the initial water content, θ_i, to be optimized in order to improve the fits. For these three models, we also allowed the parameter z_{soil} to be varied.

Lastly, in addition to the *NSE* objective function that was used for the fits, additional criteria were also considered to assess the quality of fits and the alignment of *CH* models on experimental data or the numerically generated data (Hydrus). In addition to the *NSE* function, we considered the Normalized Root Mean Square Error, *NRMSE*, the P-Bias indicator, *PBIAS*, and the coefficient of determination, R^2:

$$PBIAS = \frac{\frac{1}{n}\sum_{i=1}^{n}(O_i - S_i)}{\underline{O}} \quad NRMSE = \frac{\sqrt{\frac{1}{n}\sum_{i=1}^{n}[O_i - S_i]^2}}{\sqrt{\frac{1}{n}\sum_{i=1}^{n}\left[O_i - \underline{O}\right]^2}} \qquad (3\text{-}24)$$

$$R^2 = \frac{cov(O,S)^2}{V(O)\,V(S)}$$

All computations were done using R-free software. The scripts for the computation of results illustrated in Figure (3.6) can be downloaded online at https://zenodo.org/record/7190966 (Lassabatere and Asri, 2022).

3.5. Results and discussion

3.5.1. Comparison of the *CH* models to numerically generated data

The simulated data with *CH1* do not fit well with the synthetic infiltration rate curve (Figure 3.3 a-i). The *CH1* model predicted very small values, close to zero in comparison to the synthetic curves. The *CH1* model provides values strictly positive but very low, which appear only when the scale of the x-axis is adapted. Consequently, this model is biased with a bias around 95-100% for most cases (Table (3.2), *PBIAS* for $qCH1$ model). This means that *CH1* misses around 95-100% of the average synthetic data. The other statistics of the *CH1* model are very close to those corresponding to a null cumulative infiltration (Table (3.2), $qCH1$ versus $I(t) = 0$).

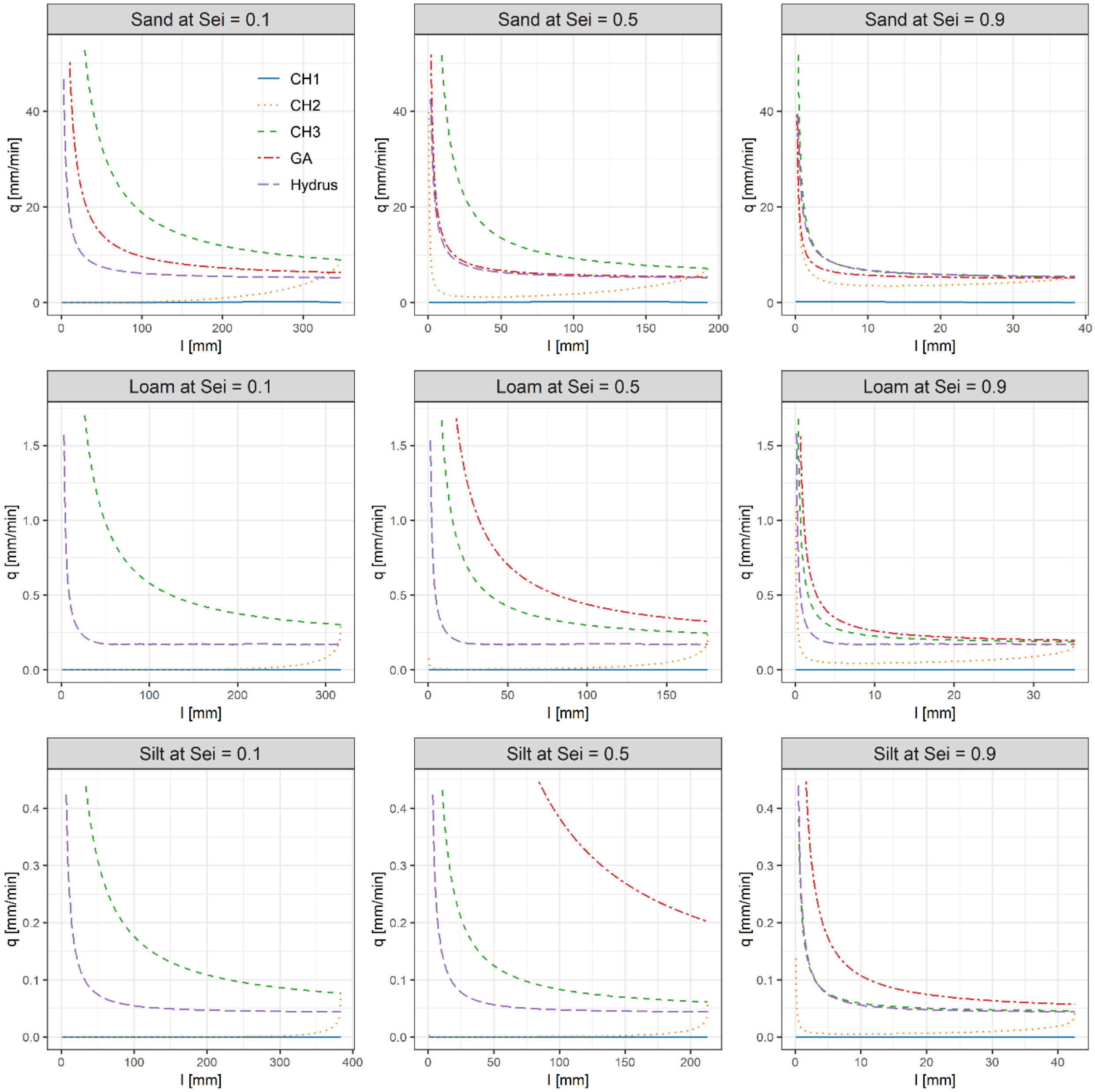

Figure (3.3): Comparison of the data modeled with *CH1*, *CH2*, *CH3,* and *GA* models with the reference synthetic infiltration rates (Hydrus) as a function of the cumulative infiltration, for various types of soil and initial saturation degree. Data corresponds to the case of a 5 mm water pressure head imposed at the surface (h_a = 5 mm) and a uniform initial water content and water pressure head profiles. In the case of loam and silt at S_{ei} = 0.1, the *GA* model is out of the scale

The *CH2* model also provides much smaller values than the synthetic infiltration rate function Figure (3.3 a-i). The *CH2* model gets closer to the reference synthetic curves for the sandy soils, in particular for the largest values of the initial saturation degrees Figure (3.3 b,c) or the loam at the largest initial saturation degree Figure (3.3 f). The large underestimation is confirmed by the very low values of the *PBIAS* for the *CH2* models, with values in the range of 90-100% for the Silt soil, Table (3.2). The situation improves, in particular for the sandy soil, at the largest values of the initial saturation degree (Table (3.2), Sand at $S_{e,i}$ = 0.5 or 0.9). However, the *CH2* model continues to underestimate the reference synthetic curve, with *PBIAS* values in the range of 35-65%. For the case of sandy soil with an initial saturation degree of 0.9, the situation improves, reaching quite a good fit in Figure (3.3 c). The related values of *NSE* become positive (*NSE* = 0.52) and a small value for the *NRMSE* (*NRMSE* = 69.5%). However, this model presents a typical shape, with a substantial increase at the end of the cumulative infiltration, which does not comply with the physics of water infiltration into soils. In addition, it remains less accurate than the *GA* model. The *CH3* model and the *GA* models present a shape in compliance with the physics of water infiltration into soils, with a decrease in the infiltration rate with the cumulative infiltration. The two models present good alignments with synthetic curves, in many situations. However, for other situations, the *GA* model performs very poorly, in particular for fine soils at low initial saturation degrees. Conversely, the *CH3* model never deviates too much from the reference synthetic data. The comparison of the statistics of goodness of fit illustrates the robustness of the *CH3* model (less variation between cases) and the better alignments in many cases (See Table 3.2). The alignment of the *CH3* model is particularly accurate for the cases of the silt and the sand at $S_{e,i}$ = 0.9, Figure (3.3 c, i) and Table (3.2). The development of *CH3* based on reformulation of *GA* by rewriting h_i by means of initial and final water contents and the soil depth, z_{soil}, seems promising. Reformulating the *GA* model in such a way is compatible with the common “linear reservoir” models that are easily implemented in modeling tools.

Table (3.2): Statistics of the goodness of fits (*NSE,* R2, *NRMSE*, and *PBIAS*) for the assessment of the capability of *CH1*, *CH2*, *CH3,* and *GA* models to fit the simulated infiltration rates for synthetic soils depicted in Figure 3.3 (considered as the reference). The lines highlighted in grey delineate the best models for each case. The value of the statistics corresponding to a perfect fit (model = observations) or to a model that provides only null values (I(t)=0 were added).

	NSE	***NRMSE %***	***PBIAS %***	**R2**	**NSE**	***NRMSE %***	***PBIAS %***	**R2**	**NSE**	***NRMSE %***	***PBIAS %***	**R2**
Perfect fit	1	0	0	1	1	0	0	1	1	0	0	1
	Sand at Sei = 0.1				**Sand at Sei = 0.5**				**Sand at Sei = 0.9**			
I(t) = 0	-1.28	151	-100	NA	-1.45	157	-100	NA	-1.72	165	-100	NA
qCH1	-1.25	150	-98.5	0.11	-1.39	155	-97.6	0.15	-1.65	163	-98.1	0.14
qCH2	-1.01	142	-78.6	0.05	-0.23	111	-62.7	0.38	0.52	69.5	-35.7	0.76
qCH3	-293	17134	349	0.83	-97.3	990	183	0.79	-1.17	147	9.1	0.8
qGA	-25.8	517	97.5	0.83	-0.97	140	14	0.79	0.75	49.5	-14.8	0.8
	Loam at Sei = 0.1				**Loam at Sei = 0.5**				**Loam at Sei = 0.9**			
I(t) = 0	-0.09	104	-100	NA	-0.35	116	-100	NA	-2.12	177	-100	NA
qCH1	-0.08	104	-99.7	0.01	-0.35	116	-99.5	0.03	-2.08	175	-99	0.02
qCH2	-0.08	104	-93.6	0	-0.28	113	-88.6	0	-0.25	112	-63.2	0.78
qCH3	-10.1	333	316	0.91	-20.4	462	204	0.98	-4.07	225	41.7	0.96
qGA	-9.33E+03	9.65E+03	7.90E+03	0.91	-116	1081	451	0.98	-18.24	438	76.6	0.96
	Silty clay loam at Sei = 0.1				**Silty clay loam at Sei = 0.5**				**Silty clay loam at Sei = 0.9**			
I(t) = 0	-0.02	101	-100	NA	-0.08	104	-100	NA	-0.57	125	-100	NA
qCH1	-0.02	101	-99.9	0	-0.08	104	-99.8	0.02	-0.57	125	-99.6	0
qCH2	-0.02	101	-98.2	0	-0.08	104	-96.2	0	-0.28	113	-84.6	0.52
qCH3	0.79	45.6	130	0.83	-0.05	103	113	0.95	0.85	38.1	5.5	0.96
qGA	-1.55E+05	3.93E+04	7.33E+04	0.83	-233	1527	1284	0.95	-15.5	406	122.5	0.96

3.5.2. Study of the consistency of the *CH* models concerning the physics

The illustration of the models proved that they exhibit different types of shapes, in particular, the specific shapes of the *CH1* and *CH2* models. Conversely, the *GA* and *CH3* models present a more usual shape with a decrease in the infiltration rate till stabilization when the steady state is reached in Figure (3.4 c,f, i,l). These shapes are in line with the physics of water infiltration into soils (Angulo-Jaramillo et al., 2016). Indeed, water infiltration is characterized by a decrease in the infiltration rate with time and the attainment of the value equal to the saturated hydraulic conductivity, K_s, at a steady state, as illustrated in Figure (3.1 c). Such a decrease results in a typical shape for the cumulative infiltration, with a concave shape followed by a linear part.

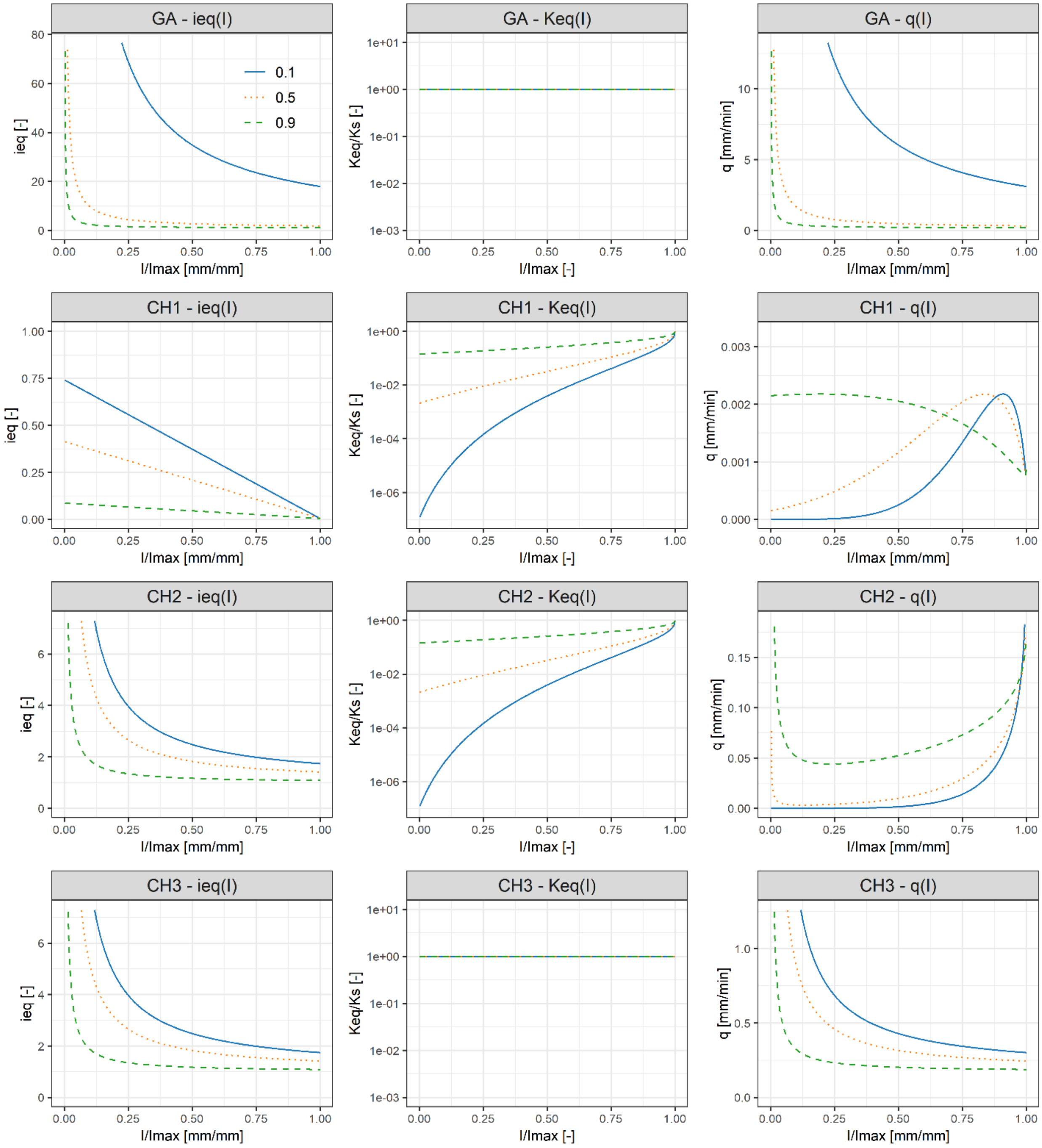

Figure (3.4): Study of the hydraulic gradient, i_{eq}, the hydraulic conductivity, K_{eq}, and the resulting function, q(I), for the four models (*GA*, *CH1*, *CH2*, and *CH3*), computation for the case of the synthetic loam defined by Carsel and Parish (1988), for an initial saturation degree of $S_{e,i}$ of 0.1, 0.5, and 0.9 with a water top soil pressure head imposed as h_a= 5 mm

Conversely, for the *CH1* model, the curve $q_{CH1}(I)$ presents an increasing shape over a large part of the time interval (or equivalently cumulative infiltration interval) for the two lower values of the saturation degree interval (Figure (3.4 f), $S_{e,i}$ = 0.1 & $S_{e,i}$ = 0.5). This shape comes from its analytical features that can be characterized by considering the analytical expression of the function $q_{CH1}(I)$. This function can be retrieved directly considering $q_{CH1}(I) = K_{eq,CH1}(I) \times i_{eq,CH1}(I)$ combining the equations (3-7) and (3-16):

$$q_{CH1}(I) = K_s \left(S_{e,i} + \frac{I}{z_{soil}(\theta_s - \theta_r)}\right)^l \left(1 - \left(1 - \left(S_{e,i} + \frac{I}{z_{soil}\,(\theta_s - \theta_r)}\right)^{\frac{1}{m}}\right)^m\right)^2 \times \left(1 + \left(\frac{h_a}{z_{soil}} - \frac{\theta_i}{\theta_s} - \frac{I}{z_{soil}\,\theta_s}\right)\right) \tag{3-25}$$

Note that the Equation (3-25) must be restricted to the interval [0, I_{max}]. The values of $q_{CH1}(I)$ can easily be computed at the lower and upper boundaries of the interval [0, I_{max}] to determine the two values between which the function $q_{CH1}(I)$ varies. At the beginning of the infiltration, the cumulative infiltration is null I =0, leading to:

$$q_{CH1}(0) = K_s\, S_{e,i}^l \left(1 - \left(1 - S_{e,i}^{\frac{1}{m}}\right)^m\right)^2 \times \left(1 + \left(\frac{h_a}{z_{soil}} - \frac{\theta_i}{\theta_s}\right)\right) \tag{3-26}$$

Instead of taking infinite values, as required by the physics of water infiltration, the infiltration rate takes finite values and is even close to zero for very dry soils. Indeed, $q_{CH1}(0)$ tends towards zero when the initial saturation degree $S_{e,i} \to 0$, since $K_s\, S_{e,i}^l \left(1 - \left(1 - S_{e,i}^{\frac{1}{m}}\right)^m\right)^2 \to 0$ while $1 + \left(\frac{h_a}{z_{soil}} - \frac{\theta_i}{\theta_s}\right) \to 1 + \left(\frac{h_a}{z_{soil}} - \frac{\theta_r}{\theta_s}\right)$, which remains bounded. Consequently, these small values for very small times (or, equivalently, cumulative infiltrations) are inconsistent with the physics of flow that imposes an infinite infiltration rate at small times (or, equivalently, cumulative infiltrations).

At the opposite bound, $I = I_{max}$, the reservoir is full and the saturation degree equals unity. Consequently, the apparent hydraulic conductivity equals $K_{eq} = K_s$, while the equivalent hydraulic gradient takes the value of $i_{eq} = \frac{h_a}{z_{soil}}$, leading to:

$$q_{CH1}(I_{max}) = K_s \times \frac{h_a}{z_{soil}} \tag{3-27}$$

Again, the formulation of the value of the infiltration rate diverts from the regular values of infiltration rates corresponding to steady state, i.e., $q_{+\infty} = K_s$. Another shortcoming of this formulation is that $q_{CH1}(I_{max}) = 0$, when the water pressure head imposed at the surface is null, $h_a = 0$, which is even more meaningless. In between those two values, the infiltration rate varies, following a non-monotonous variation depicted by Figure (3.4 d-f) with two opposing influences: an increase in the equivalent hydraulic conductivity Figure (3.4 e) and at the same time a decrease in the equivalent hydraulic gradient Figure (3.4 d). In the case of $S_{e,i}$ = 0.1 or 0.5, the bulk variation involves the first increase of $q(I)$, as the result of the increase in the hydraulic conductivity, followed by a decrease resulting from the decrease of the hydraulic gradient Figure (3.4 f). This type of shape is not in agreement with the expected decrease in infiltration rate with time. This trend is less marked when the initial saturation degree is $S_{e,i}$ = 0.9, with a shape of $q(I)$ that defines a slight decrease with a concave shape Figure (3.4 f), ($S_{e,i}$ = 0.9), instead of the regular convex shape (Figure (3.1 c)).

The disagreement between the *CH1* model and the features required to comply with the physics of water infiltration is not that surprising. Bonneau et al. (2021) designed their models to represent the dynamic of outflow in bioretention systems. In these systems, a drain allows the rapid depletion of water in the structure, thus allowing for much more infiltration than the maximum stated here, $I_{max} = Z_{soil}(\theta_s - \theta_i)$. As a consequence, the function $q(I)$ is always used far from the maximum limit I_{max}, and the observed shortcomings may not arise.

A similar analysis may be done for the *CH2* et *CH3* models. The combination of the equivalent hydraulic conductivity $K_{eq,CH2}(I)$, and hydraulic gradient $i_{eq,CH2}(I)$, leads to the following expression:

$$q_{CH2}(I) = K_s\left(S_{e,i} + \frac{I}{z_{soil}(\theta_s - \theta_r)}\right)^l \left(1 - \left(1 - \left(S_{e,i} + \frac{I}{z_{soil}(\theta_s - \theta_r)}\right)^{\frac{1}{m}}\right)^m\right)^2 \times \left(1 + \frac{\left[h_a + z_{soil}\left(\frac{\theta_s - \theta_i}{\theta_s}\right)\right](\theta_s - \theta_i)}{I}\right) \quad (3\text{-}28)$$

As previously explained above for the *CH1* model, the equivalent hydraulic conductivity increases from $K(S_{e,i})$ at the beginning of the infiltration to K_s at the end of the infiltration (Figure 3.4 h). The equivalent hydraulic gradient evolves from $+\infty$ down to $1 + \left(\frac{h_a}{Z_{soil}} + \frac{\theta_s - \theta_i}{\theta_s}\right)$. The combination of the two opposite trends (increase and decrease), leads to an initial decrease, followed by an increase, defining then a minimum value (Figure 3.4 i). However, it depends on the initial saturation degree, with mostly an increase for low initial saturation degrees (Figure 3.4 i, $S_{e,i}$ = 0.1), and the succession of a decrease and an increase for larger values of initial saturation degrees Figure (3.4 i), ($S_{e,i}$ = 0.5 or 0.9). At the end of the infiltration, when $I \rightarrow I_{max}$, the final values of the infiltration rate tend towards $q_{CH2}(I) = K_s\left(1 + \frac{h_a}{Z_{soil}} + \frac{\theta_s - \theta_i}{\theta_s}\right)$.

Lastly, the model *CH3* has the following expression:

$$q_{CH3}(I) = K_s \times \left(1 + \frac{\left[h_a + z_{soil} \left(\frac{\theta_s - \theta_i}{\theta_s} \right) \right] (\theta_s - \theta_i)}{I} \right) \tag{3-29}$$

In this case, the equivalent hydraulic conductivity is constant in Figure (3.4 k) and the variation of the equivalent hydraulic gradient makes the monotony of the function Figure (3.4 l) versus Figure (3.4 k). The infiltration rate $q_{CH3}(I)$ varies between infinite values at the beginning to the minimum values of $q_{CH3}(I) = K_s \left(1 + \left(\frac{h_a}{z_{soil}} + \frac{\theta_s - \theta_i}{\theta_s} \right) \right)$. It must be noted that for larger infiltrations $I \rightarrow +\infty$, the infiltration rate should tend towards K_s, following the principles of water infiltration into soils.

The analysis of the three models shows that model *CH1* is less compatible with the usual shapes of water infiltration rate and the physics of water infiltration into pseudo-infinite soils. Conversely, the model *CH3* appears to be the best candidate. Lastly, the *CH2* model exhibits an intermediate behavior but may present a two-step monotony (increase following the regular decrease) that may divert from the principles of water infiltration into soils. The series of models *CH1* and *CH2* do not address properly the modeling of water infiltration under regular and classic conditions. However, their use may become more appropriate for the modeling of more complex physics like infiltration into water-repellent soils. Indeed, in this case, water infiltration is slowed down initially, before returning to the regular case, with the humidification of the soil and the disappearance of water repellency (Abou Najm et al., 2021; Beatty and Smith, 2013).

3.5.3. Inverse modeling with *CH* models using real experimental data

For the inversion of infiltration data with the *CH* models, we need to assume that water infiltration is mainly 1D in the soil profile since the *CH* models are designed for 1D water infiltration. However, it must be borne in mind that water infiltration under any single ring is in reality 3D, with the combination of 1D vertical and 2D axisymmetric horizontal flow, the horizontal cumulative infiltration being linear to the inverse of the source radius (Smettem et al., 1994). Consequently, for large rings, and in particular for the case of our study (rings with a diameter of 50 cm), the infiltration is considered 1D with a negligible horizontal component. The infiltration data are then inverted with the Hydrus numerical model, the *CH,* and the *GA* models to estimate the soil hydraulic parameters. We consider that Hydrus, based on the resolution of the

Richards equation, provides estimates close to the real values and thus constitutes the reference for comparison.

3.5.3.1. Numerical inversion and strategy of fits for *CH* and *GA* models

The numerical model (Hydrus) was fitted to the experimental data by optimizing the hydraulic parameters related to the hydraulic functions (See Material and Method section). The numerical inversion provided accurate fits for the six experiments (See Figures 3.5 and 3.6). The values of the statistics of the goodness of fit confirmed the accuracy for the fits in all cases, with values of the *NSE* between 0.671 and 0.892, *NRMSE* between 32% and 56%, *PBIAS* between -1.8% and 6.3%, and coefficient of determination R^2 between 0.735 and 0.933 (Table (3.3) and Table (3.4)). The optimized values for the hydraulic conductivity do not vary to a large extent and have an average of 182.7 mm/h, with a standard deviation of 162.4 mm/h. The optimized values of the scale parameter, α, have an average value of 0.203 mm^{-1} and a standard deviation of 0.256 mm^{-1}. Those values correspond to a soil between sand and loamy sand, for the estimation of K_s, and to a loamy sand for the parameter α considering the soil databases defined by Carsel and Parrish (1988). These data point to a typical behavior of coarse material, with high hydraulic conductivity and little water retention by capillarity (high value of α, see Di Prima et al. (2020)).

3.5.3.2. The first optimization option for the inversion of data with *GA* and *CH* models

Optimizing only the saturated hydraulic conductivity was not enough to provide satisfactory fits for all the models Figure (3.5). *CH1* fails to fit the experimental data, particularly the maximum infiltration rate at the beginning of the experimental tests. The infiltration rate curve predicted with *CH1* increases, while the observed data reveals decreasing infiltration rates. Consequently, the statistics of goodness of fit are not satisfactory (Table (3.3), *CH1* model). The best indicator is the *PBIAS* which remains low, below 2.5%. However, the wrong trend of the model which utterly misses the decreasing feature of the observations leads to low values of coefficient of determination R^2 (below 0.50 except for ENTPE-1_3) and low values of *NSE* values, with values below -0.1 (Table (3.3)). Lastly, the estimations of the saturated hydraulic conductivity are very far from the reference values provided by Hydrus with relative errors in the order of 10^4 (Table (3.3), *Er_Ks*). Indeed, for a given value of saturated hydraulic conductivity, the *CH1* model predicts very low infiltration rates in comparison to the reference infiltration (see Figure (3.3)).

Consequently, the fit of the *CH1* model to observations requires to increase in the values of K_s to be able to align the model with the observations. Large over-estimations of K_s are then expected to be systematic when inverting with the *CH1* model.

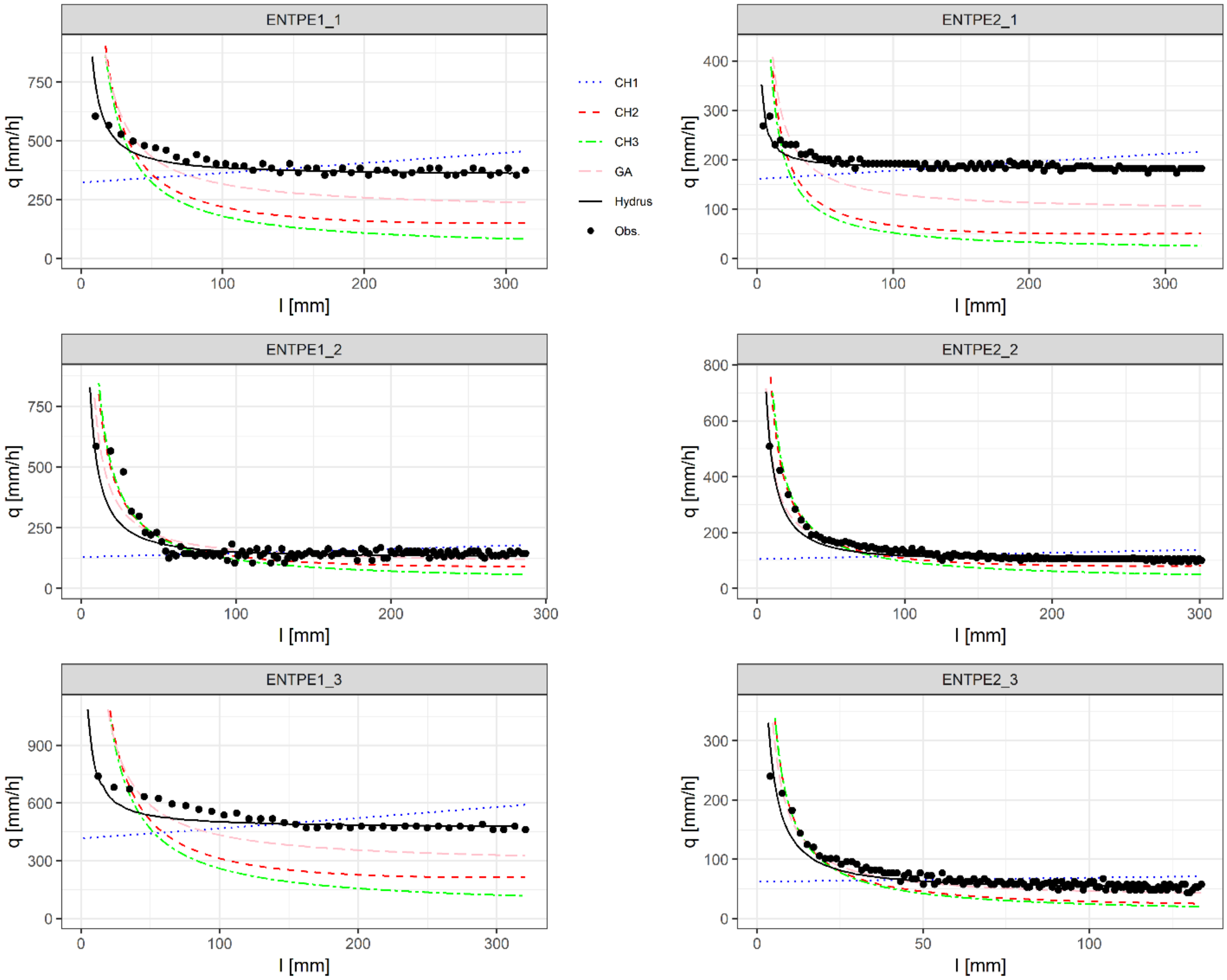

Figure (3.5): Fits of the *CH1*, *CH2*, *CH3*, *GA,* and Hydrus model – first optimization option, optimization of K_s. Related values of K_s and values of statistics of the goodness of fits are indicated in Table (3.3) for the six experimental cumulative infiltrations

The use of the *CH2* and *CH3* models improves at least the shapes of the curves with a classical decrease of infiltration rate with the cumulative infiltration, in compliance with the physics of water infiltration into soils. However, if for some experimental data, the *CH2* and *CH3* models are close to the observations (Figure (3.5), ENTPE1-2, ENTPE2-2, and ENTPE2-3), for others, these models underestimate the observed data (Figure (3.5), ENTPE1-1, ENTPE1-3, and ENTPE2-1). In these cases, the statistics of the goodness of fit demonstrate the deviation with very low values of *NSE,* high values of *NRMSE,* and high absolute values of *PBIAS* for the two models *CH2* and

CH3. The improvement of the shape in comparison to *CH1*, improves the values of the coefficient of determination (Table (3.3), R^2 for *CH2* and *CH3* models versus *CH1* model).

Regarding the quality of estimations of saturated hydraulic conductivity, the *CH2* model provides estimates much higher than the reference values, with relative errors in the order of 100%-500% (Table (3.3), *Er_Ks*). Conversely, the *CH3* model predicts estimates of K_s lower than the estimates provided by Hydrus, with relative errors in the order of -75%. These findings can be related to the analytical properties of the *CH* models and their comparison to Hydrus in the context of direct modeling (section 3.4.1).

Table (3.3): Results of the optimization process – first optimization option: statistics of goodness of fit (NSE, R2, NRMSE, and PBIAS) for the models CH1, CH2, CH3, GA, and Hydrus numerical models; optimized saturated hydraulic conductivity, Ks, relative errors considering the estimates by Hydrus as the reference values, E_r_K_s, and optimized values of the scale parameter for water pressure head. (only for Hydrus). The asterisk points to the values that were optimized.

		NSE	***NRMSE* (%)**	***PBIAS* (%)**	**R2**	**Ks (mm/h)**	**Er_Ks**	**n**	**□ (1/m)**	**θi (-) / hi (m)**	**zsoil (m)**
ENTPE1-1	*CH1*	-1.48	156%	-1.80%	0.576	4.48E+04*	12641%	1.56	N.A.	0.378	10.0
	CH2	-16.9	418%	-39.1%	0.793	1.42E+03*	305%	1.56	N.A.	0.378	10.0
	CH3	-23.0	485%	-51.3%	0.812	3.68E+01*	-89.5%	NA	N.A.	0.378	10.0
	GA	-4.81	239%	-14.6%	0.812	2.25E+02*	-36.0%	1.56	3.60	0.378 / -0.347	NA
	Hydrus	0.714	52.9%	-2.30%	0.794	3.51E+02*		1.56	10.0*	0.378	NA
ENTPE1-2	*CH1*	-0.175	108%	-2.20%	0.156	1.78E+04*	13824%	1.56	N.A.	0.378	10.0
	CH2	0.421	75.7%	-15.6%	0.769	8.55E+02*	567%	1.56	N.A.	0.378	10.0
	CH3	-0.026	101%	-27.4%	0.756	2.41E+01*	-81.2%	NA	N.A.	0.378	10.0
	GA	0.756	49.2%	0.30%	0.756	1.08E+02*	-15.9%	1.56	3.60	0.378 / -0.347	NA
	Hydrus	0.703	54.3%	-3.90%	0.774	1.28E+02*		1.56	1.25*	0.378	NA
ENTPE1-3	*CH1*	-1.69	162%	-2.10%	0.713	5.78E+04*	12238%	1.56	N.A.	0.378	10.0
	CH2	-16.0	407%	-35.3%	0.737	2.03E+03*	333%	1.56	N.A.	0.378	10.0
	CH3	-22.8	481%	-48.1%	0.766	5.31E+01*	-88.7%	NA	N.A.	0.378	10.0
	GA	-4.07	222%	-12.0%	0.766	3.07E+02*	-34.3%	1.56	3.60	0.378 / -0.347	NA
	Hydrus	0.671	56.5%	-3.30%	0.764	4.68E+02*		1.56	500*	0.378	NA
ENTPE2-1	*CH1*	-2.07	174%	-1.10%	0.449	1.75E+04*	9590%	1.56	N.A.	0.400	10.0
	CH2	-64.9	808%	-56.8%	0.704	3.75E+02*	107.4%	1.56	N.A.	0.400	10.0
	CH3	-77.5	882%	-66.9%	0.721	1.39E+01*	-92.3%	NA	N.A.	0.400	10.0
	GA	-26.6	523%	-25.2%	0.721	9.75E+01*	-46.1%	1.56	3.60	0.400 /-0.288	NA
	Hydrus	0.697	54.8%	-1.80%	0.735	1.81E+02*		1.56	500*	0.400	NA
ENTPE2-2	*CH1*	-0.248	111%	-2.40%	0.408	1.12E+04*	10933%	1.56	N.A.	0.400	10.0
	CH2	0.580	64.6%	-14.6%	0.949	5.95E+02*	486%	1.56	N.A.	0.400	10.0
	CH3	0.0333	98.0%	-27.5%	0.958	2.62E+01*	-74%	NA	N.A.	0.400	10.0
	GA	0.944	23.6%	1.70%	0.958	9.53E+01*	-6%	1.56	3.60	0.400 / -0.285	NA
	Hydrus	0.892	32.7%	-6.30%	0.933	1.02E+02*		1.56	0.70*	0.400	NA
ENTPE2-3	*CH1*	-0.123	106%	-1.20%	0.500	6.54E+03*	13343%	1.56	N.A.	0.400	10.0
	CH2	-0.169	108%	-31.4%	0.894	1.57E+02*	224%	1.56	N.A.	0.400	10.0
	CH3	-0.439	120%	-37.0%	0.897	6.48E+00*	-86.7%	NA	N.A.	0.400	10.0
	GA	0.695	55.0%	-10.2%	0.897	3.28E+01*	-32.7%	1.56	3.60	0.400 /-0.285	NA
	Hydrus	0.867	36.3%	-6.10%	0.888	4.86E+01*		1.56	2.10*	0.400	NA

Both the *CH1* and *CH2* models predict cumulative infiltrations much lower than the numerical model (Hydrus) at given values of saturated hydraulic conductivity (see Figure (3.3)). Consequently, these models need to increase the values of K_s to reach accurate fits, which is in line with the overestimations of K_s. Conversely, the *CH3* model provides much higher infiltration rates than Hydrus in a direct mode (see Figure (3.3)).

Then, the *CH3* model needs to decrease this parameter artificially to reach accurate fits, resulting in a systematic under-estimation of the saturated hydraulic conductivity, K_s. We also note that, in terms of order of magnitude for K_s, the *CH3* model offers the best options, in comparison to *CH2*, with final estimates in the same order of magnitude as the target, whereas *CH2* predicts values one or two orders of magnitude higher.

Lastly, we fitted the *GA* model to the same experimental data. The *GA* model fails to properly fit the data when the difference in water pressure head is fixed at the difference between the final and the initial states $\Delta h = h_a - h_i$, and when only the saturated hydraulic conductivity is optimized. Most cases are unproperly fitted (Figure (3.5), ENTPE1-1, ENTPE1-3, ENTPE2-1). However, for two cases (ENTPE1-2 and ENTPE2-2), the fits are better and the *GA* model approaches in terms of quality of the fits (Table (3.3), *NSE, NRMSE*, *PBIAS,* and *R*2). In addition, for these two cases, the estimations of K_s are very close to the reference values provided by Hydrus, with relative errors in the order of 5-15% (Table (3.3), *Er_Ks*).

3.5.3.3. The second optimization option for the inversion of data with *GA* and *CH* models

In this section, we allow all the parameters to be varied, apart from those that can be robustly derived from field measures (water content and bulk density). We aim to investigate if giving more degrees of freedom improves the fits the estimations of the hydraulic conductivity, K_s.

For the *CH1* model, we noticed a slight improvement in the fit and the shape. The additional optimizations of parameter n and z_{soil} changes the shape of the curve, with a decreasing trend instead of an increase (e.g., Figure (3.6 c) versus Figure (3.5 c)). However, the decrease remains very light and the *CH1* model remains unable to properly capture the marked observed decrease (e.g., Figure (3.6 c)). Consequently, the statistics of fit do not reveal a drastic improvement, with low values of *NSE, NRMSE*, and R^2 remaining (Table (3.4)). In terms of quality of estimates, the *CH1* model still largely overestimates the saturated hydraulic conductivity (Table (3.4), *Er_Ks*).

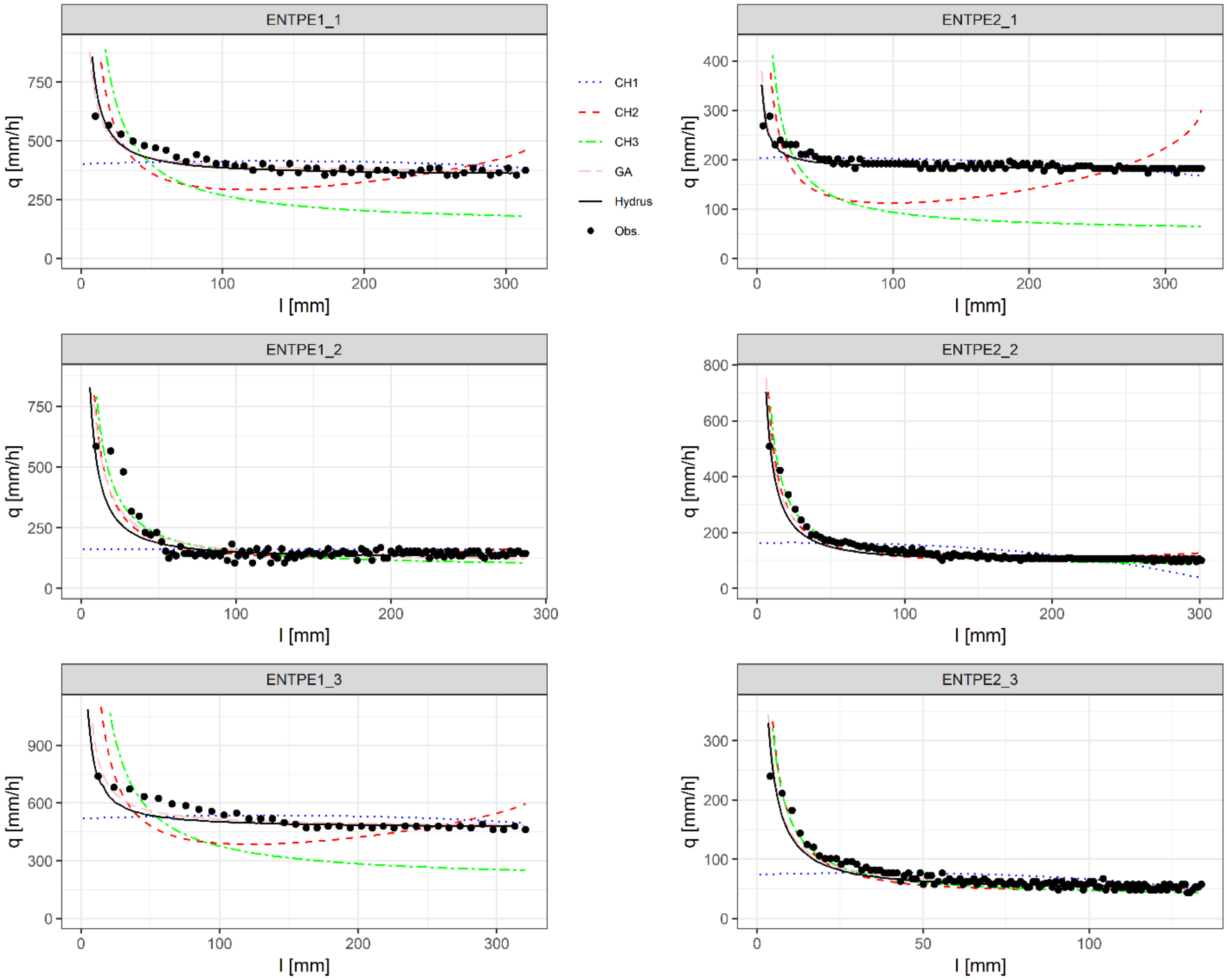

Figure (3.6): Fits of the *CH1*, *CH2*, *CH3*, *GA,* and Hydrus model – second optimization option, optimization of all model parameters. Related values of optimized parameters and statistics for the goodness of fit are tabulated below (Table (3.4)) for the six experimental cumulative infiltrations

The increase in the degrees of freedom for the *CH2* model significantly changes the fits, with an improvement of the statistics of fit. Values obtained for *NSE* and R^2 increase and the values of *NRMSE* decrease, getting closer to the statistics related to Hydrus (Table (3.4)). This is particularly the case of ENTPE1-2, ENTPE2-2, and ENTPE2-3, for which we may consider that the *CH2* model provides accurate fits. In comparison to the previous case (first optimization option), the statistics of the goodness of fit reveal that the fits are accurate, with $NSE > 0.7$, $NRMSE < 50\%$, $PBIAS < 10\%$ (in absolute value), and $R^2 > 0.7$. We can conclude that fits were significantly improved in most cases and that the optimization of n and z_{soil} improves model performance (Table (3.4) versus Table (3.3)). In all cases, the saturated hydraulic conductivity K_s was overestimated with *CH2*.

For the other experimental data (ENTPE1-1, ENTPE1-3, and ENTPE2-1), the addition of the optimization of n and z_{soil} also improved the fits, but not enough to get accurate fits, as revealed by the values of the statistics of goodness of fit (Table (3.4)). The addition of parameters n and z_{soil} allowed to reshape the model to better fit the last part of the curves (Figure 3.6 a,c,d, ENTPE1-1, ENTPE1-3, and ENTPE2-1). However, this results in a typical shape, with a decrease in the infiltration rate (e.g., Figure 3.6 a, I < 100 mm) followed by a final increase (e.g., Figure 3.6 a, I < 100 mm). This shape was already depicted in the section related to the study of the analytical properties of the model (section 3.5.2, Figure 3.4). The optimization procedure has varied the parameter z_{soil} to be able to represent the last part of the curve. The optimized value of z_{soil} equals the lower threshold $z_{soil} = \frac{I_{tot}}{(\theta_s - \theta_i)}$ (Table (3.4), underlined values of z_{soil}). Sensitivity analysis proves that the fit would have been improved with lower values of z_{soil} and fit to sub-datasets of experimental data. However, in this study, we wanted to fit the whole set of experimental data and consider the threshold $z_{soil} = \frac{I_{tot}}{(\theta_s - \theta_i)}$.

Table (3.4): Results of the optimization process – second optimization option: statistics of the goodness of fits (NSE, R2, NRMSE, and PBIAS) for the fits with models CH1, CH2, CH3, GA and the numerical model (Hydrus); optimized values of saturated hydraulic conductivity, K_s, with relative error in comparison with Hydrus estimates (E_r_K_s), optimized values of shape parameter n, model parameter z_{soil} (only CH models), and initial water content θ_i (CH3 model), or initial water pressure head, h_i (GA model). Underlined values denote inaccurate fits for the statistics of goodness of fit and when the optimized values of z_soil equal the lower limits of the optimization interval. The asterisk points to the values that were optimized.

		NSE	*NRMSE* (%)	*PBIAS* (%)	*R2*	K_s (mm/h)	Er_Ks	*n*	(1/m)	θ_i (-) / hi (m)	z_{soil} (m)
ENTPE1-1	*CH1*	0.009	98.5%	0.0%	0.010	4.67E+03*	1229%	5.00*	N.A.	0.378	4.75*
	CH2	-2.54	186%	-8.5%	0.448	3.52E+02*	0.3%	4.80*	N.A.	0.378	2.23*
	CH3	-0.675	128%	-4.8%	0.812	3.01E+02*	-14.3%	N.A.	N.A.	0.450*	2.23*
	GA	0.811	43.0%	-0.2%	0.812	3.64E+02*	3.7%	N.A.	N.A.	0.378 / -3.98E-03*	N.A.
	Hydrus	0.714	52.9%	-2.3%	0.794	3.51E+02*		1.56*	10.0*	NA	N.A.
ENTPE1-2	*CH1*	-0.005	99.8%	0.0%	0.177	1.97E+03*	1436%	4.90*	N.A.	0.378	50.0*
	CH2	0.785	46.1%	-0.3%	0.787	6.24E+02*	387%	1.80*	N.A.	0.378	4.56*
	CH3	0.755	49.3%	-0.7%	0.756	1.04E+02*	-19.2%	N.A.	N.A.	0.410*	2.04*
	GA	0.754	49.4%	-0.3%	0.756	1.04E+02*	-19.2%	N.A.	N.A.	0.378 / -0.316*	N.A.
	Hydrus	0.703	54.3%	-3.9%	0.774	1.28E+02*		1.56*	1.25*	NA	N.A.
ENTPE1-3	*CH1*	0.051	96.1%	-0.7%	0.062	6.06E+03*	1195%	5.00*	N.A.	0.378	4.79*
	CH2	-2.48	184%	-8.0%	0.315	4.58E+02*	-2.3%	5.00*	N.A.	0.378	2.28*
	CH3	-0.467	120%	-4.2%	0.766	3.97E+02*	-15.1%	N.A.	N.A.	0.450*	2.28*
	GA	0.765	47.8%	-0.2%	0.766	4.73E+02*	1.1%	N.A.	N.A.	0.378 / -1.26E-02*	N.A.
	Hydrus	0.671	56.5%	-3.3%	0.764	4.68E+02*		1.56*	500*	NA	N.A.
ENTPE2-1	*CH1*	0.235	87.0%	0.0%	0.257	2.42E+03*	1235%	4.95*	N.A.	0.400	5.25*
	CH2	-18.30	437%	-17.3%	0.281	2.24E+02*	23.7%	2.40*	N.A.	0.400	2.76*
	CH3	-17.85	432%	-17.8%	0.721	1.17E+02*	-35.5%	N.A.	N.A.	0.450*	2.76*
	GA	0.704	54.1%	-0.6%	0.721	1.82E+02*	0.8%	N.A.	N.A.	0.400 / -1.00E-07*	N.A.
	Hydrus	0.697	54.8%	-1.8%	0.735	1.81E+02*		1.56*	500*	N.A.	N.A.
ENTPE2-2	*CH1*	0.129	93.0%	-2.8%	0.204	1.84E+03*	1707%	5.00*	N.A.	0.400	2.58*
	CH2	0.882	34.2%	-2.6%	0.907	2.45E+02*	141.2%	2.20*	N.A.	0.400	5.07*
	CH3	0.958	20.4%	-0.1%	0.958	8.81E+01*	-13.3%	N.A.	N.A.	0.450*	5.07*
	GA	0.955	21.0%	0.9%	0.958	9.17E+01*	-9.8%	N.A.	N.A.	0.400 / -0.316*	N.A.
	Hydrus	0.892	32.7%	-6.3%	0.933	1.02E+02*		1.56*	0.70*	N.A.	N.A.
ENTPE2-3	*CH1*	0.165	91.0%	1.7%	0.186	6.84E+02*	1305%	5.00*	N.A.	0.400	1.14*
	CH2	0.663	57.8%	-9.5%	0.852	5.70E+02*	1072%	1.45*	N.A.	0.400	3.72*
	CH3	0.895	32.2%	0.2%	0.897	4.87E+01*	0.1%	N.A.	N.A.	0.440*	1.14*
	GA	0.896	32.1%	-0.8%	0.897	4.69E+01*	-3.5%	N.A.	N.A.	0.400 / -0.100*	N.A.
	Hydrus	0.867	36.3%	-6.1%	0.888	4.86E+01*		1.56*	2.10*	N.A.	N.A.

Varying the last parameter, θ_i in model *CH3* improved model performance Figure (3.6 a) versus Figure (3.5)) and improved the statistics of goodness of fit (Table (3.4) versus Table (3.3)). For the experiments ENTPE1-2, ENTPE2-2, and ENTPE2-3, the improvement provided accurate fits with a very satisfactory alignment of the model to the observations and resultant high values of *NSE,* low values of *NRMSE* and *PBIAS* and high values of R^2 (Table (3.4)). Conversely, the improvement was not enough for the other cases. The values of parameters show that the optimized values of z_{soil} remained close to their lower threshold $z_{soil} = \frac{I_{tot}}{(\theta_s - \theta_i)}$ (Table (3.4), z_{soil} column, underlined values). For these cases, the model remained far below the observations for the 2/3 of the data, thus revealing an inadequate concavity (Figure 3.6), as already discussed for the first optimization option. Regarding the quality of estimates, the predictions of the saturated hydraulic conductivity are close to the reference values (Hydrus), with relative errors, *Er_Ks*, below 25% in all cases. This is much better than the other models (*CH1* and *CH2*). The conclusion is that model *CH3* is a very good candidate with good fits and related estimates in many cases when its parameters z_{soil} and θ_i are optimized. If one considers the use of the *CH3* model for SUDS hydrological simulations, z_{soil} is equivalent to the total soil layer of the SUDS. Hence, only 2 parameters have to be estimated: the initial water content and the saturated hydraulic conductivity. *CH3* appears to be easy to calibrate (only two parameters) and performs well for both direct and inverse simulations.

Lastly, the *GA* model performed well at all times, providing very good fits for all the experiments (Figure 3.6). The values of the statistics of the goodness of fits were similar to those of the Hydrus model, revealing accurate fits (Table (3.4)). Similarly, the values of the estimated saturated hydraulic conductivity were also similar, with relative errors in the order of 5% in absolute value for most experiments and never higher than 20%. The additional degree of freedom (optimization of h_i) significantly improves the fits and the quality of estimates and is then necessary to get accurate fits (Figure 3.6 versus Figure (3.5) and Table (3.4) versus Table (3.3)).

3.6. Conclusions

In this study, alternative formulations of hydrological infiltration models have been elaborated, tested, and evaluated using a large data set gathering Hydrus outputs and experimental data of infiltration rates and cumulative infiltration. Within the context of the model framework developed by Bonneau et al. (2021) leading to the initial *CH1* model, we propose two alternatives, the *CH2* and *CH3* models. The results show that the best analytical models among the list of studied models are the *GA* followed by the *CH3* model. *CH1* and *CH2* models are not appropriate for the direct simulation of the water infiltration into soil. Those two models have similar features that prevent them from providing accurate prediction (direct mode). *CH1* poorly predicts water infiltration in the direct mode and a better design of the equivalent hydraulic gradient $i_{eq}(I)$ allows the *CH2* model to give better performance. However, the specific design of the equivalent hydraulic conductivity induces typical curve shapes that are inconsistent with the physics of water infiltration. It also affects the quality of estimations of the saturated hydraulic conductivity (inverse mode). Nevertheless, they could be considered as a good basis for future development, to better simulate water repellence during water infiltration. Indeed, both experimental data and modeling approaches predict dynamics similar to that captured by the *CH1* or the *CH2* models, with either increasing or increasing-decreasing trends (Abou Najm et al., 2021; Beatty and Smith, 2013).

The results indicated that the proposed *CH3* model, based on the reformulation of the *GA* model, is more convenient in both direct and inverse simulations. *CH3* avoids the problems of non-decreasing infiltration rates since its equivalent hydraulic conductivity is fixed to the saturation hydraulic conductivity, $K_{eq} = K_s$. We then consider that this choice, with its explicit formulation in a generic way, is the best alternative for modeling water infiltration into soils. However, the equivalent hydraulic gradient should be improved. Indeed, direct modeling using *CH3* and even *GA* is not always optimal, with discrepancies between their prediction and the reference numerical synthetic infiltration rates. This discrepancy impacts the quality of their performance in inverse mode, with significant misestimations in some cases. For the *CH3* model, we note that the optimization of the initial water content θ_i improves its performance. Indeed, *CH3* and *GA* are based on a similar modeling concept and approach regarding their hydraulic gradient, with the following expression $1 + \frac{[h_a - h_i]}{z_f}$ where the value of h_i is rewritten to set the *CH3* model. Our results clearly show that *CH3* may be suitable. Further investigations are conducted to improve the definition of the term h_i in *CH3* model.

The testing of the *CH* suite demonstrates that the third option, *CH3*, designed by analogy with the *GA* model, seems to be the best. However, it requires the optimization of the way to input the initial conditions, i.e., to rewrite the parameter h_i, which will be the subject of future research. We will then implement the enhanced version of the framework dedicated to the modeling of bioretention systems. In addition to that, we intend to broaden the situations and physics addressed by our model. In this study, we focused mainly on the water infiltration into homogeneous soils with single permeability behaviors and no water repellence. However, in the field, more complex physics may affect water infiltration in real soils, like air entrapment, water repellency, or preferential flow. We will thus continue the adaptation of the *CH* suite to consider water-repellent soils. We also intend to extend our suite to the case of preferential flows and water infiltration into dual permeability soils (Lassabatere et al., 2019, 2014), among others.

Chapter 4

Dual-permeability infiltration models for modeling and management

Chapter 4. Physically based dual-permeability model for modeling and management of SUDS

Preface

In this chapter, we have developed and tested a new model, as a part of INFILTRON_Mod tool, for infiltration simulation accounting for macroporosity in soil. The proposed model has been programmed in R and used to simulate a bioretention system as well as infiltration processes in a column of soil (experiments described in Chapter 3 at infiltrometer scale). We performed model calibration using the Bayesian inference approach and conducted sensitivity analysis for both models. The chapter will be submitted to the Journal of Hydrology-X for publication.

Asra Asry[a], Gislain Lipeme Kouyi[a], Tim D Fletcher[c], Jeremie Bonneau[a,b], Damien Tedoldi[a], Laurent Lassabatere[d]*
[a] Univ. Lyon, INSA Lyon, DEEP Laboratory, EA7429, Villeurbanne cedex, France.
[b] INRAE, UR HHLy, Hydrology and Hydraulics, 5 rue de la Doua, 69100 Villeurbanne, France.
[c] School of Ecosystem and Forest Sciences, University of Melbourne, 500 Yarra Boulevard, Burnley, Victoria, 3121, Australia.
[d] Univ. Lyon, Univ. Claude Bernard Lyon 1, CNRS, ENTPE, UMR5023 LEHNA, F-69518, Vaulx-en-Velin, France
This chapter will be submitted to the Journal of Hydrology-X.

Contents

Physically-based dual-permeability models infiltration models for modeling and management the sustainable urban drainage systems

Asra Asry[a], Gislain Lipeme Kouyi[a], Tim D Fletcher[b], Jeremie Bonneau[a], Damien Tedoldi[a], Laurent Lassabatere[c]*

a INSA Lyon, DEEP Laboratory, EA7429, Villeurbanne cedex, France.
b School of Ecosystem and Forest Sciences, University of Melbourne, 500 Yarra Boulevard, Burnley, Victoria, 3121, Australia.
c Univ. Lyon, Univ. Claude Bernard Lyon 1, CNRS, ENTPE, UMR5023 LEHNA, F-69518, Vaulx-en-Velin, France, corresponding author

* **Corresponding author:** Laurent Lassabatere

Keywords: Infiltration, stormwater, preferential flow, hydrology, Soils, SUDS.

4.1. Abstract

The preferential flow and transport through unsaturated zones have received considerable attention in the soil and agricultural fields, particularly in relation to risks of increased discharge rates and amounts and the subsequent transportation of pollutants to groundwater. Over the past century, traditional stormwater control has been replaced by a new low-impact development (LID) approach called " on-site alternative design strategy," which aims to restore or maintain the hydrological functions of urban watersheds by using the capacity of soil and vegetation to retain and filter wastewater pollution, such as bioretention facilities. Therefore, obtaining an accurate estimation of water infiltration within bioretention basins is crucial. The Bioretention modeling usually refers to the implicit reservoir base model, which is based on the mass balance and interaction between all the components of the hydrologic cycle (evapotranspiration, overflow, exfiltration to surrounding soils, infiltration through filter media or non-saturated zone, and underdrain discharge) during the time.

Among the existing bioretention models, the unsaturated zone or filter medium is considered a homogeneous medium, and the flow is calculated with conceptual infiltration models, such as the Green-Ampt model, the Horton model, etc. Despite our knowledge that the soil reservoir medium is heterogeneous (e.g., coarse materials, plant root systems), it is, therefore, necessary to use a physically-based infiltration model that considers the impact of non-equilibrium and preferential flow on the hydrological and hydrogeochemical performance of bioretention facilities. The INFILTRON-Mod, a generic physically-based, has been proposed for this aim.

This module consists of infiltration models, including the Green-Ampt model and three other specific custom-made models, for uniform and non-uniform flows in soils based on the Darcian approach and mass balance. Uniform and non-uniform flows are modeled using the single and dual-permeability porous media approaches, respectively. The dual-permeability concept assumes that the soil consists of two reservoirs, i.e., the general matrix and fast-flow regions, each obeying the Darcian approach. We assumed instantaneous exchange between the two regions. Consequently, we assumed that the wetting fronts in the two reservoirs advanced at the same rate. Then the different sets combined with the single or dual-permeability porous media approaches were tested against numerically synthetics data using HYDRUS and experimental data obtained with INFILTRON-exp, a specific large ring infiltrometer" deployed at several experimental sites.

The results indicate that incorporating dual-permeability models enhanced the fitting of experimental data obtained from the infiltrometer. Subsequently, the refined dual-permeability model was employed to simulate observations from the Wicks Reservoir bioretention basin (Melbourne, Australia), encompassing water head levels in the filter layer and outflow rates, yielding satisfactory outcomes in terms of filter water head modeling. The results obtained from this study will be used to develop the INFILTRON-Mod package that can be easily integrated into the LID modeling performance for calculating the infiltration capacity of bioretention systems.

Keywords: Infiltration, stormwater, preferential flow, hydrology, Soils, SUDS.

4.2. Introduction

The projected increase in the urban population is expected to reach 68% of the world's population within the next 20 years (Habitat, 2022). Cities need to prioritize the development of infrastructure at an increased rate to accommodate the growing population and urban developments, which may increase impervious surfaces. This highlights the urgent need for managing wastewater due to urbanization. Additionally, climate change is anticipated to bring more intense and shorter-duration rainfall (Lenderink and Fowler, 2017; O'Gorman, 2015). Historical data has already shown an increase in the intensity and frequency of extreme rainfall events (Fischer and Knutti, 2016; Lenderink and Fowler, 2017). More and more frequent and intense precipitation events, as meteorological features of climate change, lead to higher rates of runoff and increased flood frequency in impervious cities and periurban areas, which inhibits water infiltration into the soil (Min et al., 2011).

Sustainable urban stormwater management or smart stormwater management (Webber et al., 2020) is an essential approach for mitigating the negative impacts of urbanization. Its primary objective is to control urban stormwater flooding, thereby preserving the integrity of public safety, as well as preserving both soil and groundwater quality. In fact, by preventing pollution and degradation caused by stormwater runoff and related pollutants transport, smart stormwater management plays a critical role in protecting the environment and conserving water resources (Bertrand-Krajewski, 2021; Fletcher et al., 2015a).

The use of ecosystem-based adaptation strategies (known as low impact development (LID) controls, SUDS) is highly advised in the Intentional Panel of Climate Change Report 2022 (GIEC, 2022) to establish a source of fresh water in urban and suburban areas and create a green corridor with a cooler temperature in future cities (Pörtner et al., 2022). The efficiency of low-impact development practices can be determined by assessing their hydrological function and their ability as "Sinks" to intercept pollutant fluxes (Ahiablame et al., 2012; US-EPA, 2000). Stormwater carries a variety of pollutants, micropollutants, and suspended matter (Göbel et al., 2007; Tedoldi et al., 2016).

Infiltration-based LID systems such as swales, rain gardens, infiltration basins, or bioretention systems are commonly used due to their suitability for integration within urban areas where hydrogeological conditions promote the ability of soil- or media-based SUDS to retain, degrade or pollutants removal as the result of various physical, physicochemical and biological processes that occur during water infiltration into the soil or other reactive porous medium (Tedoldi et al., 2016). Soil macroporosity and preferential pathways may be due to the lithological heterogeneity of the soil or engineered substrate used to support the filter-based LID (Ben Slimene et al., 2015) or, in other cases, bioturbation including the actions of macrofauna and plant root systems. The vegetation roots thriving in a filter media can create large porous interstices that permit the development of preferential pathways and allow contaminants to move quickly and to deeper soil layers (Alaoui, 2015; Ben Slimene et al., 2015; Brunetti et al., 2020; Goutaland et al., 2013; Liu and Fassman-Beck, 2017; Morvannou et al., 2013; Roulier et al., 2008, 2007; Winiarski et al., 2013). Preferential paths present within the infiltration-based LID can enhance the risk of contaminants reaching the subjacent vadose zone, potentially leading to significant impacts on groundwater quality (Clark et al., 2010).

The potential for non-equilibrium mass flow can be influenced by the presence of macropores and large features like voids or cracks in soils (Allaire et al., 2009; Chen and Wagenet, 1992; Flury et al., 1994a; Germann and Beven, 1982a; Greco, 2002; Hendrickx and Flury, 2001; Jarvis, 1998; Jarvis and Ga, 2003; Köhne et al., 2006). Preferential flow occurs when water moves more quickly through certain parts of the soil profile, creating non-uniform wetting fronts and shortening the travel time of pollutants, increasing the risk of soil and groundwater contamination in urban and peri-urban environments (Hendrickx et al., 1993; Dekker et al., 1999; Flury et al., 1994; Wang et al., 1998). These issues have already been addressed in the literature for hydrological and hydrogeological modeling of karstic aquifer basins (large-scale hydrological studies) (Bakalowicz, 2005; Bonneau et al., 2017; Bresinsky et al., 2023; Delbart, and; Fleury et al., 2007; Robineau et al., 2018). Physically-based models are extensively utilized for hydrological analysis, groundwater management, and predicting pollution infiltration.

These modeling approaches can be classified into two main categories: (1) numerical modeling, which involves dividing soil systems into two or three-dimensional mesh and necessitates the assignment of hydraulic parameters to each node, and (2) lumped models which conceptualizes physical processes at the scale of the entire soil system without explicitly considering spatial variability or separate compartments in the soils (Fleury et al., 2007).

Several different process-based models have been developed and may been employed for the modeling of LID performance, each with a different level of complexity like SWMM, MUSIC, RECHARGE, CNAOE, MIDUSS, STORM, GIFmod, RISURSIM, Hydrus, Macro, etc. (Elliott and Trowsdale, 2007; Niazi et al., 2017). Within the range of models employed for modeling LID, the infiltration module can be categorized into two groups.

The first category includes finite-element variably-saturated models that numerically solve Richards' equation for the prediction of the movement of water in unsaturated soils and for some of them, their extension to the case of dual-permeability soils like the Macro model (Alaoui, 2015) or the dual-permeability module implemented in Hydrus (Nimmer et al., 2010), These models can estimate the influence of macroporosity and preferential flow on water infiltration. However, their implementation requires a thorough knowledge of the unsaturated hydraulic properties of the soil, which can be challenging to measure accurately in field conditions (e.g., Lassabatere et al., 2014).

The second category of physically-based water infiltration models utilized in LID modeling comprises straightforward empirical equations such as Hortonian, Green-Ampt, or Curve-Number (Roesner et al., 2010a; Rossman, 2010). These equations are frequently employed in models such as SWMM (Sage et al., 2020). Despite their utility, these models have been found to be less precise in estimating the infiltrated water budget due to their lack of consideration for the impact of preferential flow, which plays a major role in the modeling of the infiltration compartment.

Numerical modeling of systems with their heterogeneity presents intricate challenges. However, limited studies found in the literature have specifically addressed the modeling of preferential flow in infiltration-based LID facilities (Ben Slimene et al., 2015; Brunetti et al., 2016; Dawson et al., 2009; Goutaland et al., 2013; Liu and Fassman-Beck, 2017; Roulier et al., 2008; Winiarski et al., 2013).

Infiltration is a crucial factor of hydrological response of LID systems, as well as the water level present in the filter and the system outflow fluxes. It is, therefore, important to develop a physically-based infiltration model, capable of considering the soil heterogeneity and related preferential flow pathways in LID and SUDS.

The objective of this study is to validate and improve the understanding of infiltration flow mechanisms within LID through flow simulations employing a double medium approach. The results of this study can be used to improve the flow simulations in LID, which may, in turn, bring help to LID design and monitoring.

4.3. Theory and modeling

Recent advancements in stormwater management have centered around infiltration-based urban management systems. A key element of these approaches is restoring water balance at a small scale, utilizing LID, which intercept runoff from impervious surfaces and promote water loss (evapotranspiration, storage), infiltration, and water quality improvement. A typical LID is a plant-based system such as rain gardens and bioretention basins, which reduce stormwater volume and peak flow (Brown et al., 2010; Davis et al., 2009; Roy-Poirier et al., 2010). The purpose of bioretention cells is to collect and filter stormwater runoff, which is then exfiltrated into the surrounding soil (and eventually into groundwater aquifers), discharged to receiving waters (for systems with underdrains) or absorbed by plants (i.e., by evapotranspiration, ETP) (Fletcher et al., 2015a; Lisenbee et al., 2021b). Bioretention has been shown to be effective in reducing the impacts of development on urban hydrologic regimes according to the results of a study comparing field-scale bioretention facilities (Bonneau et al., 2021; Davis, 2008; Dietz and Clausen, 2005; Hunt et al., 2006).

Bioretention system modeling is essential to accurately predict the hydrological and water quality performance of bioretention systems and verify the adequacy of current guidelines. The development of improved bioretention hydrologic will lead to improved water quality modeling, as the amount, peak, and timing of flows have a direct impact on contaminant loads, plant uptake, and microbiology. There are only a few models available to describe the hydrology and hydraulics of bioretention cells (Davis, 2008; Jefferson et al., 2017; Wilson et al., 2015). RECHARGE, HEC-RAC, Hydrus, MUSIC, and SWMM are among the most important models that works on hydrological process of bioretention systems at the event scale (Dotto et al., 2011; Dussaillant et al., 2003; Heasom et al., 2006; Li et al., 2018; Meng et al., 2014; Roesner et al., 2010b). As the complexity of a model grows, the number and complexity of inputs also grow. An ideal model will balance between assumptions, simplification, and input parameter sophistication requiring less time and effort from the end-user. Bonneau et al. (2021a) have developed a simplified physically-based model to model the bioretention systems with application to field monitoring data provided by the Wicks project in Australia (Bonneau et al., 2021a).

As already discussed formerly, bioretention systems have been used to reduce stormwater runoff and eliminate pollutants carried by stormwater. An important factor that has been seen to impact the retention of pollutants is the impact of macropores (and related preferential flows). These are large continuous openings in soil, that are formed by the macrofauna or plants and can result in the rapid downward movement of solutes and pollutants through the soil profile (Germann and Beven, 1982b). The result of model simulations by Bonneau et al. (2021a) was found to be particularly sensitive to bioretention soil drainage properties and antecedent soil water content. Although the model produced useful total outflow estimates, the prediction of water levels in the filter remained poor for most storms. We expect such discrepancy by the existence of preferential flow paths within the soil media in the bioretention system, which would allow a fraction of the influent to reach the underdrain structure without any delay. This study aims to give more insight into the impact of preferential flow on the crucial component of the water budget which is 'the infiltration component' and on the hydraulic performance of bioretention cells. Our objective in this paper is to develop a more accurate model for the simulation of hydrological processes by incorporating preferential flow while keeping an easy-to-calibrate hydrological model.

4.3.1. Model development and mathematical approach

In the following, we remind the main principles and equations associated with the dual-permeability approach (in addition to the concepts presented in the first chapter). The concept of dual permeability can be described as a concept that considers porous media in terms of two distinct pore systems, which can be treated as homogeneous media with separate hydraulic properties. In this conceptual model, the permeable interface acts as a boundary between the two porous media. The exchange of flow between these media is controlled by the pressure difference and follows Darcy's law.

The flow rate is influenced by a shape factor that takes into account the shape and size of the matrix blocks and the fracture/macropore network between the matrix blocks. Since dual-permeability media exhibit two different hydraulic conductivities, pressure heads, and water contents at any point in time or space. It is hypothesized that a dual permeable medium will have two water retention functions, one in the matrix and one in the fracture pore system, $\theta_f(h_f)$ and $\theta_m(h_m)$, as well as two hydraulic conductivity functions: $K_f(h_f)$ and $K_m(h_m)$.

The preferential flow or fast-flow (subscript f) and matrix (subscript m) flow equations are given by assuming $V_{t.f}$ as the volume of fracture medium, and V_t as a per unit volume of the medium. The volume fraction occupied by the fracture pore system, ω_f is obtained as follows (Hilten et al., 2008):

$$\omega_f = \frac{V_{t.f}}{V_t} \qquad (4\text{-}1)$$

$$\theta_f = \frac{V_{w.f}}{V_{t.f}} \quad (1\text{-}2a) \qquad \theta_m = \frac{V_{w.m}}{V_{t.m}} \quad (4\text{-}2)$$

As a result, the bulk soil water content θ $[L^3L^{-3}]$ is then calculated by the following equation:

$$\theta = \omega_f \, \theta_f + (1 - \omega_f)\theta_m \tag{4-3}$$

Where θ_m and θ_f $[L^3L^{-3}]$ are respectively the volumetric water cotenant of matrix and fracture pore systems, the water flow at any given depth can also be expressed in the form:

$$q = \omega_f q_f + (1 - \omega_f)q_m \tag{4-4}$$

This shows that q represents the area-weighted water flux, assuming identical water pressure head in the matrix and the fracture pore system, The equality in fluxes leads to the expression of the bulk soil hydraulic conductivity:

$$K_{2K}(\theta) = \omega_f \, K_f(\theta_f) + (1 - \omega_f) \, K_m(\theta_m) \tag{4-5}$$

Further, by assuming that the densities of the fluid and solid phases are constant, ignoring the effects of swelling and shrinking, assuming no hysteresis in the hydraulic properties, and considering that the effect of temperature, air pressure and solute concentration on water flow are negligible, the concatenation of the mass conservation and Darcy's law at the scale of each pore system leads to the following one-dimensional (1D) equation that governs water flow in dual-permeability systems:

$$\frac{\partial \theta_f}{\partial t} = \frac{\partial}{\partial z}\left[K_f(\theta_f)\frac{\partial h_f}{\partial z} - K_f(\theta_f)\right] - \frac{\Gamma_\omega}{\omega_f} - \varphi_f \tag{4-6}$$

And

$$\frac{\partial \theta_m}{\partial t} = \frac{\partial}{\partial z}\left[K_m(\theta_m)\frac{\partial h_m}{\partial z} - K_m(\theta_m)\right] + \frac{\Gamma_\omega}{1-\omega_f} - \varphi_m \tag{4-7}$$

where θ_m and θ_f $[L^3L^{-3}]$ denote water contents in the matrix and fracture pore systems, K_m and K_f $[LT^{-1}]$ are hydraulic conductivities in the matrix and fracture pore systems, respectively; h_m and h_f $[L]$ are the pressure heads in the matrix and fracture pore systems, Γ_ω $[T^{-1}]$ is water exchange between the matrix and fracture pore systems, φ_m $[L^3L^{-3}]$ and φ_f $[L^3L^{-3}]$ are sink–source terms in the two regions z are the Cartesian coordinates, corresponding to the vertical coordinate oriented downwards. The exchange rate of water between the preferential flow and matrix regions, Γ_ω, is assumed to be proportional to the difference in pressure heads (Gerke and van Genuchten, 1993a):

$$\Gamma_\omega = \alpha_w(h_f - h_m) \tag{4-8}$$

Where α_w is the first-order mass transfer coefficient. For well-defined geometries of the matrix blocks, the first-order mass transfer coefficient, α_w, can be defined as (Gerke and van Genuchten, 1993a):

$$\alpha_w = \frac{B_a}{d^2} K_a \gamma_\omega \tag{4-9}$$

Where B_a (dimensionless) is a shape factor that depends on the geometry of the fractures (3 for rectangular matrix blocks equally spaced orthogonal fractures, 8 for solid cylinders, and 15 for spheres, Gerke et al., 1996), d is a characteristic length of matrix elements, K_a is the interfacial hydraulic conductivity, and γ_ω is a scaling factor. Then the interfacial hydraulic conductivity K_a may be computed using a single arithmetic average of hydraulic conductivities corresponding to water pressure heads in the matrix and fracture pore system h_f and h_m:

$$K_a(h) = \frac{1}{2}\left[K_a(h_f) + K_a(h_m)\right] \tag{4-10}$$

The use of Equation (4-10) implies that the medium contains geometrically well-defined rectangular or other types of elements (Haverkamp et al., 1990; Van Genuchten and Dalton, 1986).

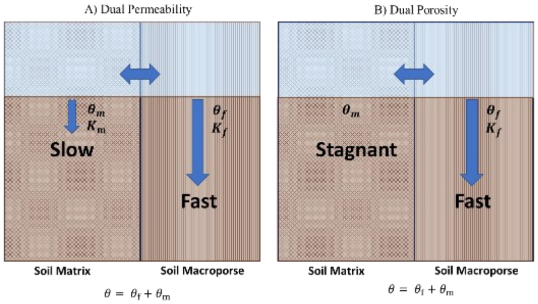

Figure (4.1): Conceptional physical nonequilibrium models for water flow and solute transport. In the figures, θ is the water content; θ_m and θ_f are the water contents of the matrix and macropore (fracture) domains, respectively. Panel A) represents the Dual permeability and B) represents the Dual porosity approaches.

To ease the computation, we set the interfacial hydraulic conductivity to a null value to ensure that water does not transfer between the two pore systems, as suggested by Lassabatere et al. (2014). Therefore, the infiltration into the dual-permeability medium can be derived from infiltration into the two single-permeability domains, i.e., the matrix and fracture pore systems. As a result, water infiltrates independently in the two-pore systems and then can be modeled with any analytical model dedicated to water infiltration into single-permeability systems. In addition, infiltration fluxes into dual-permeability media can simply be written as a linear combination of fluxes into individual regions with proportionality coefficients that correspond to their respective surface fractions (Lassabatere et al., 2014). Considering the surface and volume fractions are considered equivalent (isotropic porous media), the bulk infiltration can be described by Equation (4-10) as proposed by Lassabatere et al. (2014):

$$I_{1D.2K}(t) = \omega_f I_{1D.f}(t) + (1 - \omega_f) I_{1D.m}(t) \tag{4-11}$$

In Equation (4-10), Lassabatere et al. (2014) replaced $I_{1D.f}(t)$ and $I_{1D.m}(t)$ with the quasi-exact implicit formulation proposed by Haverkamp et al., (1994). If the infiltration of water is done separately in the two-pore systems without any interaction, one can expect a much deeper wetting front to be formed in the fracture pore system. The depth of the wetting front in both pore systems $z\ [L]$ can be estimated using the assumption that the movement of water into the soil is driven by a piston-like displacement. The volume of water that enters the soil $I(t)$ has the shape of a piston with $z\ [L]$ as height and the difference between final and initial water contents as width. The depth of the wetting front can be expressed in units of length, leading to the following equation (Lassabatere et al., 2019):

$$z= \frac{I(t)}{(\theta_s-\theta_i)} \tag{4-12}$$

Where $\theta_s\ [L^3L^{-3}]$ and $\theta_i\ [L^3L^{-3}]$ are the final and initial water contents, respectively. By applying these equations to each system (matrix and fracture network), the following equations come out:

$$z_f = \frac{I_{1D.f}(t)}{(\theta_{s.f}-\theta_{i.f})} \quad \text{(4-13a)} \qquad z_m = \frac{I_{1D.m}(t)}{(\theta_{s.m}-\theta_{i.m})} \quad \text{(4-13b)}$$

In which $z_f\ [L]$ is the position of the wetting front for the fracture pore system, $z_m[L]$ is the position of the wetting front for the soil matrix, $I_f(t)$ and $I_m(t)$ are cumulative infiltrations over the fracture and matrix pore systems, respectively, $\theta_{s.f}$ and $\theta_{i.f}\ [L^3L^{-3}]$ is the saturated (final) and initial water contents in the fracture pore system, and where $\theta_{s.m}$ and $\theta_{i.m}$ and $[L^3L^{-3}]$ in the soil matrix.

Now, we consider the opposite hypothesis stating that the water exchange between the two regions is infinite meaning water exchange instantaneously compensates for the difference in water pressure head between the two pore systems. Under those circumstances, wetting fronts move downwards together, as is referenced by the high interaction between intra and inter-aggregated pores in the well-developed coarse soil structure. Therefore, $z_f = z_m$, and then the combination with Equation (4-14) demonstrates that the cumulative infiltration in the fracture pore system can be calculated as:

$$I_{1D.f} = I_{1D.m}\frac{(\theta_{s.f}-\theta_{i.f})}{(\theta_{s.m}-\theta_{i.m})} \tag{4-14}$$

This equation may be rewritten as:

$$I_{1D.f} = I_{1D.m} \times \frac{(\theta_{s.f}-\theta_{i.f})}{(\theta_{s.m}-\theta_{i.m})} = I_{1D.m} \times R_{\Delta\theta} \tag{4-15}$$

Where $R_{\Delta\theta}$ is a dimensionless ratio of water content difference between the two regions. The equation of cumulative infiltration can be rewritten by substituting the following equation into Equation (4-13), leading to:

$$I_{1D.2K}(t) = \left(\omega_f\, R_{\Delta\theta} + \omega_m\right) I_{1D,m}(t) \tag{4-16}$$

Where ω_m=1-ω_f (volume fraction occupied by the matrix). Now, the total cumulative infiltration of each section can be separately calculated as follows:

$$I_{1D.f}(t) = \frac{R_{\Delta\theta}\, I_{1D.2K}(t)}{\left(\omega_f\, R_{\Delta\theta} + \omega_m\right)}\; I_{1D.m}(t) = \frac{I_{1D.2K}(t)}{\left(\omega_f\, R_{\Delta\theta} + \omega_m\right)} \tag{4-17}$$

The previous set of Equation (4-17) allows the determination of cumulative infiltration into each pore system as a function of the total cumulative infiltration. Doing so helps with the use of the analytical *CH* models presented in Chapter 3. Let's consider that each pore system has a specific function that defines infiltration rate as a function of cumulative infiltration, $q_{1D}\big(\mathrm{I}(t)\big)$, the following developments come out:

$$q_{1D,2K}(t) = \omega_f\, q_{1D.f}(t) + \omega_m q_{1D.m}(t) \tag{4-18a}$$

$$q_{1D,2K}(t) = \omega_f\, q_{1D.f}\left(I_f(t)\right) + \omega_m q_{1D.m}\big(I_m(t)\big) \tag{4-18b}$$

We deduce the final relationship as:

$$q_{1D.2K}(I) = \omega_f\, q_{1D.f}\left(\frac{R_{\Delta\theta} I_{total}}{(\omega_f\, R_{\Delta\theta} + \omega_m)}\right) + \omega_m q_{1D.m}\left(\frac{I_{total}}{(\omega_f\, R_{\Delta\theta} + \omega_m)}\right) \tag{4-19}$$

Where $q_{1D.f}$ and $q_{1D.m}$ stand for the studied model $q_{1D}(I)$ (i.e., *CH3*) applied to the fracture and matrix pore systems, respectively.

This model will serve as a starting point for us as it proved to be the best model among the proposed alternatives (see Chapter 3). The *CH3* model is based on: *CH3* based on the reformulation of *GA* by rewriting h utilizing initial and final water contents and the soil depth, z_{soil}, seems promising. Reformulating the *GA* model in such a way is compatible with the typical "linear reservoir" models that are easily implemented in modeling tools. The application of the model to the fast-flow compartment leads to:

$$q_{CH3.f}\left(I_f\right) = K_{s.f} \times \left(1 + \frac{\left[h_{a.f} + z_{soil.f}\left(\frac{\theta_{s.f} - \theta_{i.f}}{\theta_{s.f}}\right)\right]\left(\theta_{s.f} - \theta_{i.f}\right)}{I_f}\right) \tag{4-20}$$

The $q_{CH3.f}$ is the infiltration rate in the preferential flow region for the *CH3* model, $h_{a.f}$ is the water pressure head on the preferential flow region, which is the same for the matrix, $h_{a.m} =$

$h_{a.f}$ =h_a. The application of the *CH3* model to the matrix region leads to the following equations and developments:

$$q_{CH3.m}(I_m) = K_{s.m} \times \left(1 + \frac{\left[h_{a.m} + z_{soil.m}\left(\frac{\theta_{s.m}-\theta_{i.m}}{\theta_{s.m}}\right)\right](\theta_{s.m}-\theta_{i.m})}{I_m} \right) \tag{4-21}$$

$$q_{CH3.2K}(I) = \omega_f \; q_{CH3.f}\left(I_f\right) + \omega_m \; q_{CH3.m}(I_m) \tag{4-22}$$

$$q_{CH3.2K}(I) = \omega_f \; q_{CH3.f}\left(\frac{R_{\Delta\theta} \; I}{\omega_f \; R_{\Delta\theta} + (1-\omega_f)}\right) + (1-\omega_f) \; q_{CH3.m}\left(\frac{I}{\omega_f \; R_{\Delta\theta} + (1-\omega_f)}\right) \tag{4-23a}$$

$$q_{CH3.2K}(I) = \omega_f \; q_{CH3.f}\left(\frac{R_{\Delta\theta} \; I}{\omega_f \; R_{\Delta\theta} + (1-\omega_f)}\right) + (1-\omega_f) \; q_{CH3.m}\left(\frac{I}{\omega_f \; R_{\Delta\theta} + (1-\omega_f)}\right) \tag{4-23b}$$

This last equation relates the infiltration rate, $q_{CH3.2K}$, to the the bulk cumulative infiltration into the dual-permeability media, I. It corresponds to the *CH3* model in Chapter 3, with adaptation to the dual-permeability behavior dedicated to the modeling of preferential flows. In the following, we study its properties and capability to reproduce analytically generated data and to invert experimental data.

4.3.2. Application of CH3-2K infiltration model to the Bioretention modeling

4.3.3. Preferential flow in bioretention model

The modeling of preferential flow in soils and soil infiltration dual-permeability approach at the scale of the basin watershed has been investigated for the non-saturated zone as part of the hydrological study of the karst basin (Birkholzer and Tsang, 1997; Fleury et al., 2007; Robineau et al., 2018). In urban hydrology, the application of dual permeability for water infiltration to evaluate the performance of SUDS has already been studied (Ben Slimene et al., 2015; Coutinho et al., 2015; Goutaland et al., 2013). Physically-based representations of preferential flow in hydrological models have the potential to help understand and evaluate how these complex physical processes can affect natural base stormwater system hydrologic behavior under different land use and climate conditions. Accordingly, the objectives of this study were to develop and evaluate a dual-permeability description for variably non-saturated flow in soils for the modeling of bioretention systems. The formulation presented in the last section was incorporated into the bioretention model developed by Bonneau et al. (2021) to model data from the Wick bioretention system with the final aim to predict accurately water outflow and water level in the filter medium at the same time. Indeed, Bonneau et al. (2021) had tremendous difficulties to mimic properly the two signals at the same time, suggesting that the physical processes were not well represented.

4.3.3.1. Governing equations of the bioretention model

The hydrological behavior of the bioretention basin was extensively modeled in Bonneau et al., (2021) using the hydrologic model implemented in R-codes. The authors provide a detailed description of the modeling approach in their paper. The model used in this study is a process-based computational hydrological model, based on the interconnected reservoirs concept. The model incorporates physical processes, such as precipitation, evaporation, and infiltration, to predict water flow and fluxes within the system. The schematic of the hydrological model used for modeling the bioretention basin is shown in Figure (4.1). The equations used in the model have been discretized using a first-order, explicit numerical scheme and a fixed 6-minute timestep to match observed data.

The modeling of subsurface flow involves two primary reservoirs: the ponding zone and the filter medium. A water balance model is used to simulate the filling and emptying of the surface basin (ponding zone) and the filter media which predicts the time-dependent depth of water ponded at the basin surface Equation (4-24) and water height in the filter Equation :

$$A\frac{dH_i}{dt} = Q_{IN_{i-1}} - Q_{OVER_{i-1}} - Q_{INF_{i-1}} \tag{4-24}$$

$$A\theta_S \frac{dF_i}{dt} = Q_{INF_{i-1}} - Q_{EX_{i-1}} - Q_{OUT_{i-1}} - Q_{ETP_{i-1}} \tag{4-25}$$

Where F_i is the water height available in the filter within the given time i, $dF_i = F_i - F_{i-1}$ and $dH_i = H_i - H_{i-1}$. The Q_{INF} is the recharge flux from the ponding zone into the filter media, Q_{OVER} denote the overflow in surface of the basin, Q_{IN} is the imported water in the basin, Q_{EX} is the exfiltration of water by infiltration into the surrounding native soil, Q_{OUT} is the outflow from the underdrain, Q_{ETP} is the potential evapotranspiration rate, and $dt = \Delta t$ is considering a fixed 6 min time step. The infiltration component of bioretention was evaluated in this study using the first-order Canoe Hydrobox model (*CH1*), as described in more detail in (Asry et al., 2023).

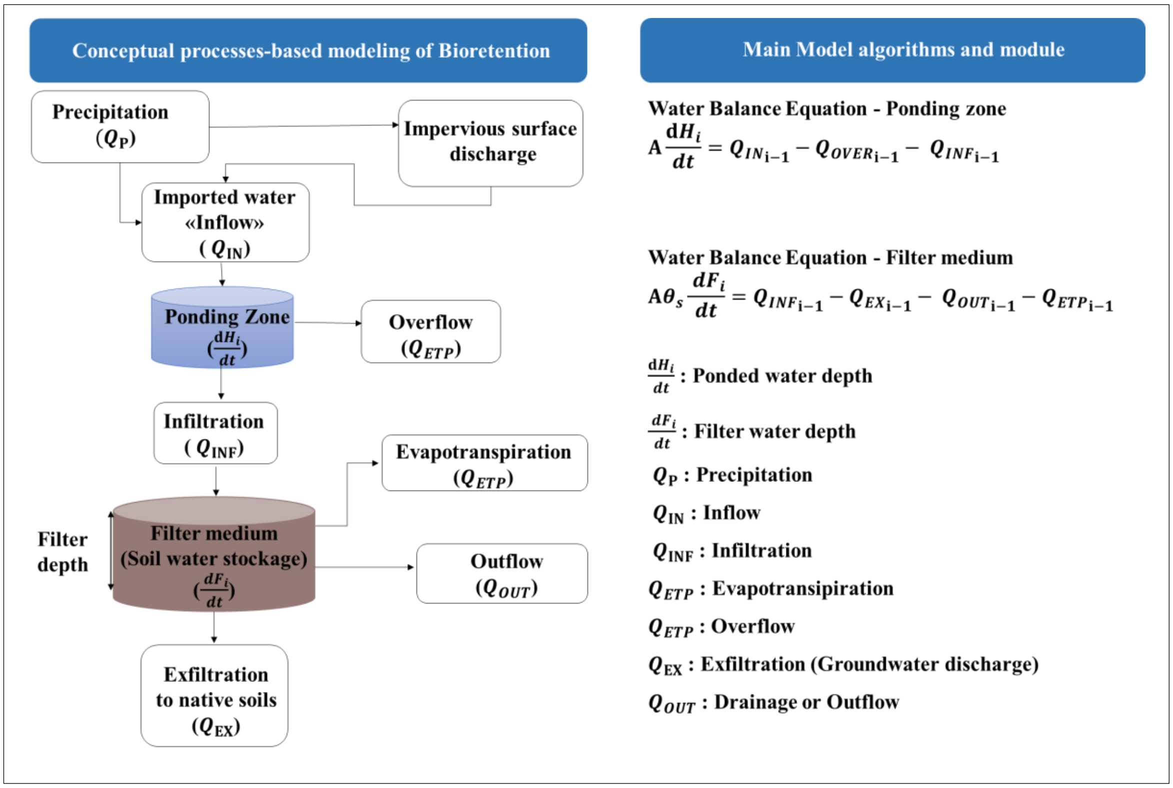

Figure (4.2): Conceptual schematic of the hydrological model used for modeling the bioretention basin.

4.3.3.2. Modification of Bioretention Modeling for Current Study

To accurately represent site-specific conditions in our study, we have made several modifications to the bioretention modeling approach. In the original version proposed by Bonneau et al. (2021), the overflow was calculated by comparing the water level in the ponding zone with a predetermined threshold. However, we have revised this approach in our new version.

Instead of calculating the overflow based on the difference between the inlet flow and infiltration rate, we now directly utilize the water level in the ponding zone. This new calculation takes into account the mass balance in the ponding zone. This modification was necessary because, for certain scenarios, when the filter is already ponded with water, the infiltrated water can exceed the inlet flow rate. This situation could potentially result in a negative value for the overflow which is unrealistic regarding the real world, therefore model returns zero in the same situation, even if the overflow is present. By implementing this modification, we can accurately represent the behavior of the bioretention system and improve the reliability of our modeling results in capturing site-specific conditions. The preliminary test, which involved modifying only the overflow term, revealed that the model's performance remained largely unchanged, particularly in terms of modeling water height in the filter. In the second step, the infiltration model with dual-permeability porous media was implemented.

The hydrological processes in Wick's model are described by the following mathematical equations: The evapotranspiration (ET) from the filter media is calculated using potential evapotranspiration (assuming a crop factor of 1.0) and is modulated with a linear function between the wilting point and field capacity (Francés, 2008; Van der Lee and Gehrels, 1990):

$$\begin{gathered} if\ \theta < \theta_w, Q_{etr} = 0 \\ if\ \theta_w < \theta < \theta_{fc}, Q_{etr} = \frac{\theta - \theta_w}{\theta_{fc} - \theta_w} Q_{etp} \\ if\ \theta > \theta_{fc}, Q_{etr} = Q_{etp} \end{gathered} \tag{4-26}$$

Where θ_w and θ_{fc} are the wilting point and the field capacity, respectively, taken as usual valued for sandy soil (FAWB., 2009; Payne et al., 2015), Q_{etr} is the real evapotranspiration rate and Q_{etp} the potential evapotranspiration rate, sourced from a nearby meteorological station of the Australian Bureau of Meteorology (BoM, 2021; SILO, 2020).

In this model, the surface storage" ponding zone" and overflow are assumed to be a rectangular empty box. To account for the presence of a culvert weir at the surface of the storage, the user sets a threshold level. When the water level in the storage exceeds this threshold, the excess water is diverted, resulting in an overflow rate Equation (4-27):

$$\begin{gathered} if\ h_{pond} < h_{weir}, Q_{ovf} = 0 \\ Otherwise, Q_{ovf} = h_{pond} - h_{weir} \end{gathered} \tag{4-27}$$

Where h_{pond} is the water level in the surface storage, h_{weir} the height of the overflow weir, Q_{ovf} the overflow rate.

Exfiltration from the filter to the surrounding soil and the groundwater is dependent on the hydraulic conductivity of the surrounding soil and the wetted surface area of the filter. It is calculated as follows:

$$Q_{exf} = K_{s\,inf}\ S_{wet} \tag{4-28}$$

Where $K_{s\,inf}$ is the saturated hydraulic conductivity of the surrounding soil and S_{wet} is the wetted area of the filter storage, i.e. the contact surface between water and the surrounding soil. The flow is considered gravity-driven since it is expected to be entirely saturated. Outflow through the underdrain can be described as an orifice equation (thus assuming the pipe itself does not limit flow), involving the hydraulic head in the filter:

$$Q_{out,i} = C_{out}\sqrt{2gH_{i-1}} * A \tag{4-29}$$

Where C_{out} is an orifice coefficient to be calibrated, g is the acceleration due to gravity, and H is the difference between the water level in the filter F_i and the level of the underdrain orifice. The water height in the filter at the time step $(i-1)$ can be calculated using:

$$F_{i-1} = \frac{VF_{i-1}}{\theta_s \times A} \tag{4-30}$$

Where VF_{i-1} is the volume of water in the filter and A the horizontal surface considered to compute the volumes.

Dual-permeability porous media infiltration modeling is used for modeling the infiltration from the ponding zone into the filter media. The proposed model assumes that wetting fronts move downward at the same rate and simultaneously in both pore systems, matrix, and fracture as stated above (see Equation 4-14).

During the considered time step, no more than the volume of water available in the surface storage can infiltrate. In addition, no more than the volume available in the filter can be filled by the infiltrating water. These two conditions impose two limitations. Finally, the discharges from the ponding zone $Q_{inf\,(i)}$ into the filter media was obtained using the following equation:

$$Q_{inf\,(i)} = min \begin{Bmatrix} Q_{2K,CH3}(I) = \omega_f Q_f + \omega_m Q_M & (a.) \\ (F_{max} - F_{i-1}) \frac{A}{\Delta t} \theta_s & (b.) \\ h_{pond,_{i-1}} \times \frac{A}{\Delta t} + Q_{in,i} & (c.) \end{Bmatrix} \tag{4-31}$$

Equation (4-31) in the function “min” corresponds to the application of the dual-permeability infiltration model and Equation (4-31b-c) is set to respect the mass balance of the system. Equation (4-31b) enables to computation of infiltration rate when the storage capacity within the filter is limiting the amount of water allowed to infiltrate (typically at the end of an event). Equation (1-30a) enables us to compute infiltration rates when all the ponded water can infiltrate during time step i, typically at the start of an event with dry initial conditions. In the proposed *CH3-2K* equation, as shown in the Equation (4-17), I_{total} is given by the cumulative infiltration depth since the beginning of the rainfall event, then:

$$I_{total,i_{(i)}} = \sum_{i=1}^{n} Q_{\inf(i)} * \Delta t_i$$

$$I_{m,i} = \frac{I_{total,i_{(i)}}}{R_{\Delta\theta} \times \omega_f + (1-\omega_f)} \tag{4-32}$$

$$I_{f,i} = I_{m,i} \times R_{\Delta\theta}$$

Then the total flux, $Q_{2K,CH3}(I)$, can be computed using Equation (4-32 a) and considering the definition of specific cumulative infiltration computed with (4-31). The following model for preferential flow was tested to evaluate the outflow and water level in Wicks' Bioretention filter media.

4.3.4. Model performance assessment

The performance of the model has been evaluated for two study scales. **a)** at the infiltration scale: Firstly, the results of the synthetic infiltration generated using numerical modeling (Hydrus-2K) for three saturation scenarios (Hydrus-2K model) were compared to the predictions by our *CH3*-2K model. Secondly, the CH3-2K model was used to invert real experimental data corresponding to the 6-infiltration data collected in the field. **b)** at the scale of the bioretention system: the performance of the model in terms of prediction of the water fluxes in the bioretention system was calculated. To evaluate the effectiveness of the model's predictive capability, four indices are used: the root-mean-square error ($RMSE$) to assess a type of standard deviation of the difference between observed and modeled data, the percent bias ($PBIAS\%$), the NSE-Sutcliffe Efficiency (NSE) (Nash and Sutcliffe, 1970), and coefficient of determination (R^2). By applying the indices, we can compare the observed (O_i) and modeled (S_i), values, which enables us to calibrate and validate the model (D. N. Moriasi et al., 2007, 2015; Khan et al., 2013)

$$\begin{gathered}
NSE = 1 - \frac{\sum_{i=1}^{n}(O_i - S_i)^2}{\sum_{i=1}^{n}\left(O_i - \underline{O}\right)^2} \\
KGE = 1 - \sqrt{(r-1)^2 \times (\alpha - 1)^2 \times (\beta - 1)^2} \\
PBIAS = \frac{\frac{1}{n}\sum_{i=1}^{n}(O_i - S_i)}{\underline{O}} \\
NRMSE = \frac{\sqrt{\frac{1}{n}\sum_{i=1}^{n}[O_i - S_i]^2}}{\sqrt{\frac{1}{n}\sum_{i=1}^{n}\left[O_i - \underline{O}\right]^2}} \qquad (4\text{-}33) \\
R^2 = \frac{cov(O,S)^2}{V(O)\,V(S)}
\end{gathered}$$

Where n is the total number of paired values, $\underline{O}$ refers to the mean of the variable O_i, and where r is s the linear correlation coefficient between O_i and S_i , α is the variability ratio or ratio between the standard deviation of simulated values and standard deviation of observed values and β is the ratio between the mean of the simulated and observed values (Althoff and Rodrigues, 2021). The chosen evaluation indices cover three major categories of model evaluation techniques, standard regression, dimensionless, and error index. Standard regression, measured by R^2, assesses the linear relationship between modeled and measured data and describes the model's ability to explain the observed data's variance. An R^2 value above 0.50 is considered acceptable. The dimensionless NSE-Sutcliffe efficiency evaluates how well the plot of observed against modeled values by comparing the relative magnitude of the residual variance, with *NSE* values above 0.6 indicating an acceptable performance. Moriasi et al. (2007) provided criteria for satisfactory, good, and very good performance for each index for watershed-scale models, although they may not perfectly fit the evaluated model here. For example, *NSE* > 0.35, > 0.5, and > 0.65 for satisfactory, good, and very good performance, respectively (Moriasi et al., 2015; Moriasi et al., 2007). The Kling-Gupta Efficiency (KGE) index, introduced by (Gupta et al., 2009), is a valuable metric that allows for a comprehensive assessment of three key components: correlation, bias, and measure of variability, ensuring that the model captures the observed variations in different basins more accurately during the optimization process (Wöhling et al., 2013). The KGE index ranges from -inf to 1, where a value of 1 indicates a perfect match between the simulated and observed values. Higher values of KGE indicate better model performance in capturing the variability, timing, and magnitude of the modeled variable. Conversely, lower values indicate poorer model performance. The error indices, including $RMSE$, and $PBIAS$, quantify the error in the units of observed values. As stated above, $RMSE$ quantifies a kind of standard deviation between the model and the observations. The index $PBIAS$ has an optimal value of 0% with positive values indicating that the model tends to overestimate and negative values indicating that the model tends to underestimate (Moriasi et al., 2007; Moriasi et al., 2015).

4.4. Material and Methods: Site study and field data

To validate the proposed models, this study made use of a big-data base including several types of data, observed experimentally or numerically generated.

4.4.1. Application of CH3-2K in infiltrometer scale

4.4.1.1. Direct modeling - illustrative examples

In this study, the model's performance was evaluated using the blind test direct approach under various saturation scenarios. The results were then compared with synthetic numerical infiltration data from Hydrus 1D-2K. The initial input parameters used for modeling are detailed in Table (4.1). The study assumed that 10% of the entire domain was occupied by the fracture pore system ($\omega_f = 10\%$), with zero residual water content in the preferential flow region ($\theta_{r.f} = 0.0$) and high porosity ($\theta_{s.f} = 0.60$) based on the work by Lassabatere et al. (2014). Other parameters were obtained according to the absolute pressure head required to activate the pores in the fracture pore system, which is determined by the average pore size r_{max} $[L]$. The hydraulic conductivity in the fracture was adopted from Lassabatere et al. (2014), with $K_{s.f} = 3.13\ mm/min$. A soil depth of one meter is assumed for the matrix while for the macropores, the soil depth is assumed to be three times that of the matrix soil depth. The initial water content in the soil is estimated based on the soil saturation, using the formula $\theta_{i.2K} = (\theta_{s,2k} - \theta_{r,2k}) \times S_e + \theta_r$. The distribution of initial water content in each region is estimated based on the partition coefficient (ω_f) and the following assumptions. It is assumed that the initial water content in the fractures is very low $\theta_{i.f} = \theta_{r.f} + 0.001$. The soil water content in the matrix can then be determined from mass balance consideration $\theta_{i.m} = \frac{\theta_{i.2K} - \omega_f \times \theta_{i.f}}{1 - \omega_f}$.

Table (4.1): Hydraulic parameter for modeling the dual permeability of loamy soil with large and intermediate pores (Carsel and Parrish, 1988a; Lassabatere et al., 2014a).

Parameter	Matrix	unit	Source	Preferential flow region	unit	Source
	Loam			$pore\ Dia. = r_{1000}$		
h_a	5	mm	Assumed	5	mm	Assumed
θ_r	0.078	-	(Carsel and Parrish, 1988)	0	-	(Gerke and van Genuchten, 1993)
θ_s	0.43	-	(Carsel and Parrish, 1988)	0.5	-	(Gerke and van Genuchten, 1993)
θ_i	$\frac{\theta_{i.2K} - \omega_f \times \theta_{i.f}}{1 - \omega_f}$	-	Estimated	$\theta_{i.f} = \theta_{r.f} + 0.001$	-	Estimated
K_s	17×10^{-2}	mm/min	(Carsel and Parrish, 1988)	3.13	mm/min	(Lassabatere et al., 2014b)
z_{soil}	1000	mm	Assumed	$3 \times z_{soil.m}$	mm	Assumed

4.4.1.2. Inverse modeling using Monte Carlo

The *CH3-2K* model was evaluated using data from six infiltration experiments conducted on the ENTPE campus. The inverse modeling approach was utilized to determine the relevant hydraulic parameters and soil properties as often performed in the literature (Kim et al., 2015; Köhne et al., 2006; Vrugt et al., 2008). Specifically, for fitting the *CH3-2K* model, the hydraulic properties of the matrix and fractures $K_{s.f}$ and $K_{s.m}$ were optimized using the Monte Carlo optimization technique and *NSE* objective function, while other parameters were either derived from field measurements or fixed a priori using pedotransfer functions. One million sets of parameters were generated based on plausible intervals of values, and the *NSE* objective function was computed for all sets. The set of parameters that maximized the *NSE* function was selected as the "best one". For more details, please refer to Table (4.2). Note that we considered a large value of z_{soil} to simulate water infiltration into a quasi-infinite soil.

Table (4.2): Model parameterization using the measured and optimization for indirect modeling.

	Matrix					**Preferential flow region**				
Ex.	h_a (mm)	θ_i	θ_s	K_s (mm/min)	z_{soil} (mm)	h_a (mm)	θ_i	θ_s	K_s (mm/min)	z_{soil} (mm)
	Field Measure	Field Measure	Field Measure	Optimized(MC)	Fixed	Field Measure	Fixed	Fixed	Optimized(MC)	Fixed
1	58	0.37	0.5184		10000	58	0.01	0.6		10000
2	75	0.37	0.5184			75				
3	53	0.37	0.5184			53				
4	30	0.40	0.5184			30				
5	53	0.40	0.5171			53				
6	83	0.40	0.5171			83				

4.4.1.3. Numerical data with Hydrus

Our study used the HYDRUS-1D software for modeling vertical Dual-Permeability porous media infiltration processes (Šimůnek and Genuchten, 2008). A finite-element software package known as HYDRUS-1D is designed to solve the Richards equation numerically for saturated-unsaturated water flows. HYDRUS-1D offers the opportunity to use the hydraulic parameters listed in the Carsel and Parrish database for the description of most types of soils. We selected van Genuchten (1980) for the description of the water retention curve combined with the Mualem condition ($m = 1 - \frac{1}{n}$) with Mualem's (1976) capillary model for the prediction of hydraulic conductivity. To mimic different scenarios (initial wet or dry soil), we used a 5 mm water pressure head at the soil surface and uniform initial .This means HYDRUS assumes two different mobile domains to account for preferential flow.

The theory of that approach describes the preferential flow in the way that the effective flow space is decreased due to the immobile fraction and thus the same volume flux is forced to flow through this decreased flow space, resulting in higher porewater velocities and consequently also in a deeper percolation of water and solutes (Šimůnek and van Genuchten, 2008). For the parameterization of these two domains, we select an immobile soil water content $\theta_{r.f}$ of 0 and hydraulic conductivity between two regions are considered as $Ksa = \infty$. Indeed, such hypothesis corresponds to the hypothesis of identical wetting front progression in the matrix and the fracture pore systems.

4.4.1.4. Field Experiments data using Infiltrometers

The INFILTRON project utilized infiltrometers to measure the infiltration of grassed soils at the ENTPE campus in Vaulx-en-Velin, France. Sampling the soil at two different locations on the site, the average water content and dry bulk density were determined, resulting in an estimated porosity of 53.1% and 54.6%, respectively. The field experiment measurements reveal that the hydraulic conductivity of the soil medium within a bioretention SUDS can vary significantly, up to six orders of magnitude (Kanso et al., 2018), across different spatial areas (Asleson et al., 2009). This variability can be attributed to the impact of macropores formed by vegetation and the age of the bioretention system post-development. Consequently, when measuring soil infiltration, it is highly recommended to employ infiltrometers with larger diameter rings. The larger ring size increases the likelihood of encountering larger macropores, thereby providing a more accurate assessment of infiltration rates (Rose, 2004).

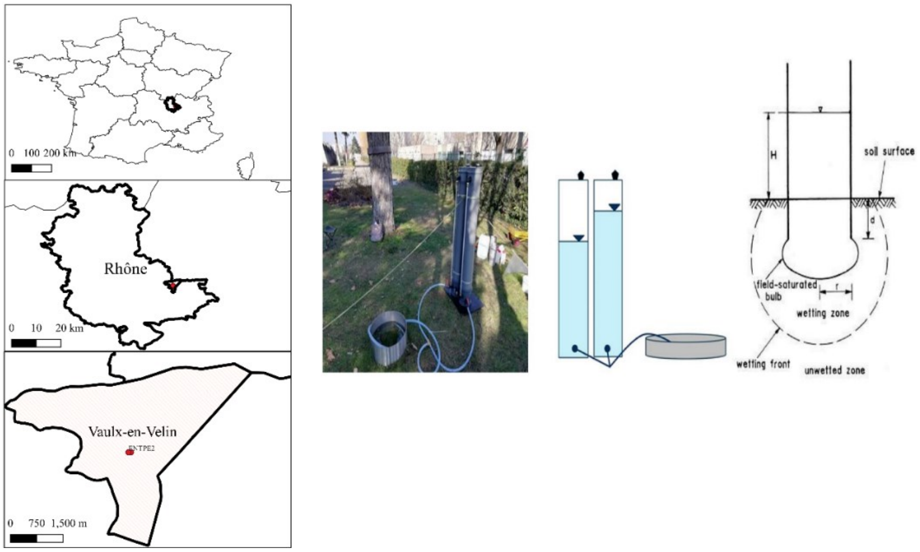

Figure (4.3): Map of field infiltration experiment locations and the right panel is the dual reservoir large ring infiltrometer that was used for the experiments

The Infiltron project aimed to design a large-ring infiltrometer for the assessment of the filtration and infiltration functions (infiltron.org). Within this framework, a specific infiltrometer was designed with a ring of a diameter of 50 cm and two large reservoirs to supply the volume of water needed to provide a total cumulative infiltration of 250-300 mm. As explained above, six water infiltration experiments were performed under intermediate dry conditions (initial water around 38-40%). A water height of around 5-10 cm was maintained at the soil surface and the level of water in the reservoirs was monitored to compute the cumulative infiltration into the soil. Meanwhile, regular-size ring infiltrometers were deployed on the site (Concialdi et al., 2020), but this work is not detailed in this study.

4.4.1.5. Field experimental data from Wicks Reserve infiltration basin

The field monitoring data presented in this study were collected in the Wicks Reserve Infiltration Basin, also known as "the Wicks Infiltration Basin". The Wicks Reserve Infiltration Basin is located in the eastern suburbs of Melbourne, Australia Figure (4.4). Constructed in 2011, the basin covers a surface area of 1,800 m^2 and serves three main purposes: 1) to reduce the frequency and intensity of high runoff flows, 2) to improve the quality of the discharged stormwater, and 3) to infiltrate the stormwater locally to recharge the groundwater and improve the base flow of the nearby Dobsons Creek. In terms of topography, it is anticipated that the infiltrated stormwater will naturally follow the slope from the basin to Dobsons Creek, which is approximately 75m away. The slope is estimated to be approximately 10% (Bonneau et al., 2020). It receives an average annual rainfall of 730 mm and has a potential evapotranspiration (PET) of 1050 mm. This catchment has a quick response to rainfall, with a time response of 30-45 minutes. A traditional stormwater drainage system in the catchment collects and drains runoff from approximately 5 hectares of impervious surfaces, which is then discharged into the basin via inlet pipes. The infiltration basin is covered with a variety of vegetation, including prickly shrubs, sedges, swamp grasses, and common spike rush.

An overflow weir is installed to allow excess water from rainfall events to exit the basin without being filtered. Stormwater percolates through the 0.8 m deep filter medium of loamy sand and scoria gravel and then empties into a discharge pit with an elevated orifice. When the water level in the basin is below the orifice level, no water leaves through the underdrain, and only infiltration and evapotranspiration help to reduce the water level in the basin. For a period of two years, the flow rate, water level, and rainfall of the basin were monitored at a 6-minute time step. From this data, 22 rainfall-runoff events were selected for the calibration (2 events) and validation (20 events) of the model (Bonneau et al., 2021). The inflow and outflow of the basin were monitored, and the flow rate and water levels in the ponding zone were measured with a low-cost sensor. The water level stored in the filter media was also measured with a piezometer. All details regarding basin information, calibration, and data collection are explained in detail in (Bonneau, 2018; Bonneau et al., 2020).

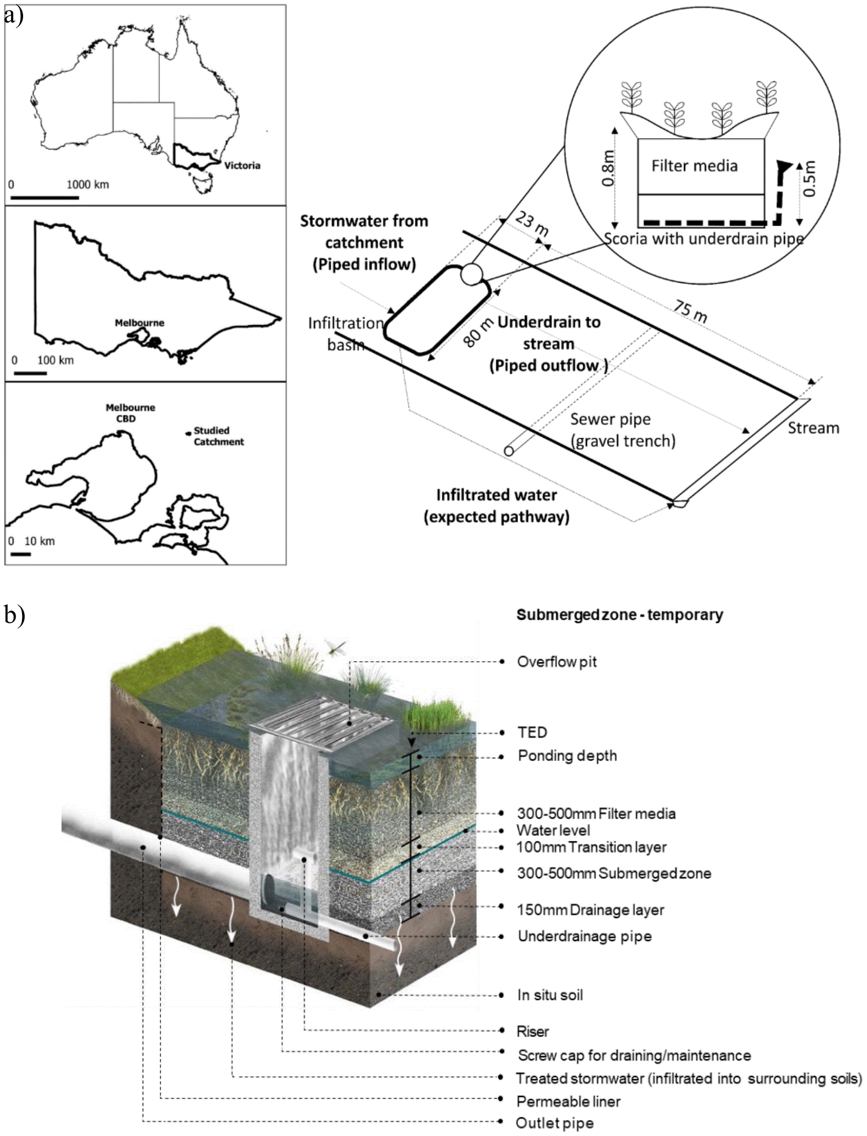

Figure (4.4): The upper panel (a) displays a map of the catchment that supplies water to the bioretention basin, as adopted by Bonneau et al. (2021). The lower panel (b) presents a schematic representation of the bioretention basin, adopted from Melbourne Water (2020)

4.5. Result and discussion

4.5.1. Model sensitivity assessment: setting up and limitations of the model

To begin with, the initial phase involves an evaluation of the proposed model concerning infiltration in both matrix and macropores reservoirs. Through these analyses, it is possible to demonstrate that there are disparities in flow between the two reservoirs, both in terms of volume and water flux. While the wetting front is assumed to progress simultaneously through the reservoir and matrix (with an indefinite exchange between the two reservoirs), the volume of infiltration is slightly in relation to different values of $\Delta\theta$ in the macropore and the matrix.

This can be mathematically represented by the Equation. (4-17) and (4-18). The equation below allows us to determine how the infiltration in each region can be altered by two fundamental coefficients in a Dual-Permeability porous media medium: $\omega_f = \frac{V_{t,f}}{V_t}$, the volume fraction occupied by the fracture pore system, and $R_{\Delta\theta} = \frac{(\theta_{s,f}-\theta_{i,f})}{(\theta_{s,m}-\theta_{i,m})}$ the ratio of the water content between pore systems. The system of equations is defined above Equation. (4-17) leads to the following expressions for the ratios of respective infiltrations and the total infiltration.

$$\begin{aligned} \frac{I_{1D,m}(t)}{I_{1D,2K}(t)} &= \frac{1}{(\omega_f\, R_{\Delta\theta} + (1-\omega_f))} = \frac{1}{1+\omega_f(\,R_{\Delta\theta}-1)} = inf_m \\ \frac{I_{1D,f}(t)}{I_{1D,2K}(t)} &= \frac{R_{\Delta\theta}}{(\omega_f\, R_{\Delta\theta} + \omega_m)} = \frac{R_{\Delta\theta}}{1+\omega_f(\,R_{\Delta\theta}-1)} = inf_f \end{aligned} \tag{4-34}$$

For ω_f = 0.1, inf_m ranges from 0.55 to 1. This behavior indicates that when $R_{\Delta\theta}$=1, the cumulative infiltration in the matrix is equal to the total cumulative infiltration. As $R_{\Delta\theta}$ increases, implying an increase in the initial water content in the matrix, inf_m "exponentially" decreases. For $R_{\Delta\theta} = 10$, inf_m reaches approximately 0.55, indicating that the cumulative infiltration in the matrix is equal to half of the total cumulative infiltration. Similar patterns are observed for other values of ω_f, but with more intensity for larger values.

In the fracture pore system, the ratio of water infiltration into the system to the total water flow increases. The cumulative infiltration in the fracture varies, reaching up to five times the cumulative infiltration. Assuming any value for $R_{\Delta\theta}$ ($R_{\Delta\theta}$= 2.5 is considered in Figure (4.5), when ω_f increases, the total water flow in the matrix decreases, while the total water flow in the fracture increases.

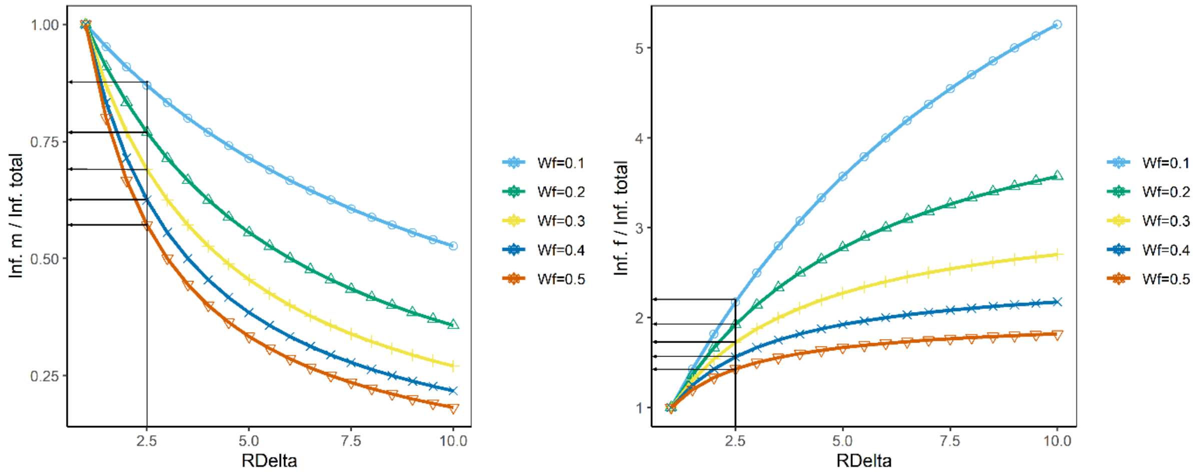

Figure (4.5): Analytical assessment of infiltration ratio between matrix and fracture and the total infiltration as a function of ratio $R_{\Delta\theta}$ and ω_f.

To gain a deeper understanding of the model's behavior concerning various parameters, an analytical demonstration of the infiltration rate in the matrix and fracture regions in response to changes in the parameters can be provided. Let's consider the following parameters: the ratio of water content deficit $R_{\Delta\theta} = \frac{(\theta_{s,f}-\theta_{i,f})}{(\theta_{s,m}-\theta_{i,m})}$, hydraulic conductivity $R_{k_s} = \frac{K_{sf}}{K_{sm}}$, volume fraction occupied by the fracture, ω_f and soil depth $R_{zsoil} = \frac{Zsoil_f}{Zsoil_m}$.

As the ratio of water content deficit increases, meaning the water content deficit in macropores is greater compared to the matrix, the infiltration rate in both the matrix and fracture regions increases Figure (4.6). Consequently, the overall infiltration rate in the system is enhanced. In this part, we considered a moderate ratio of water content deficit, in agreement with regular values and common scenarios ($R_{\Delta\theta} \in [0,2.8]$). Note that in the previous figure, we considered larger values of $R_{\Delta\theta}$ (Fig. 1.2, $R_{\Delta\theta} \in [0,10]$). The values of $R_{\Delta\theta}$ should be bounded by the value $\frac{1}{(\theta_{s,m}-\theta_{i,m})}$. Indeed, the initial water content in the fracture pore system cannot be lower than zero and the maximum water content cannot exceed 1. Very large values of $R_{\Delta\theta}$ may be obtained when the initial water pressure head is just below the value needed to activate the fracture pore system. In that case, the matrix is expected to be quasi-saturated while the fracture pore system is expected to be dry. The application of the final water pressure head may trigger a slight change in water content in the matrix, $(\theta_{s,m} - \theta_{i,m}) \simeq 0$ versus a large drop of water content in the fracture pore system, $(\theta_{s,f} - \theta_{i,f}) \simeq (\theta_{s,f} - \theta_{r,f})$, leading to large values of $R_{\Delta\theta} = \frac{(\theta_{s,f}-\theta_{i,f})}{(\theta_{s,m}-\theta_{i,m})}$.

As the fracture volume increases, the infiltration rate in the fracture pore system tends to increase Figure (4.6). However, the infiltration rate in the matrix region may decrease due to reduced available volume for infiltration. The overall impact on the final infiltration rate depends on the relative magnitudes of the fracture volume and matrix volume. Note that for both input parameters, $R_{\Delta\theta}$ and ω_f, their impact on infiltration can be related to their impact on the distribution of infiltration between the matrix and the fracture pore system. The system decreases water infiltration in the two regions Figure (4.6), whereas $R_{\Delta\theta}$ decrease, the infiltration into the matrix but increase it for the fracture pore region.

The ratio of hydraulic conductivity between the matrix and macropores does not significantly affect the infiltration rate in the matrix by design since we consider the hydraulic conductivity of the matrix as constant. Conversely, the hydraulic conductivity ratio does impact the infiltration rate in the macropores Figure (4.6). Consequently, the final infiltration rate in the combined matrix and fracture pore system is influenced by the hydraulic conductivity contrast, with a large increase when K_s increases.

Lastly, regarding the parameter $Zsoil$, if the soil depth in the macropores exceeds one times the soil depth in the matrix, the infiltration rate in the matrix decreases. Conversely, the infiltration rate in the macropores increases. The balance between these two rates determines the overall change in the final infiltration rate.

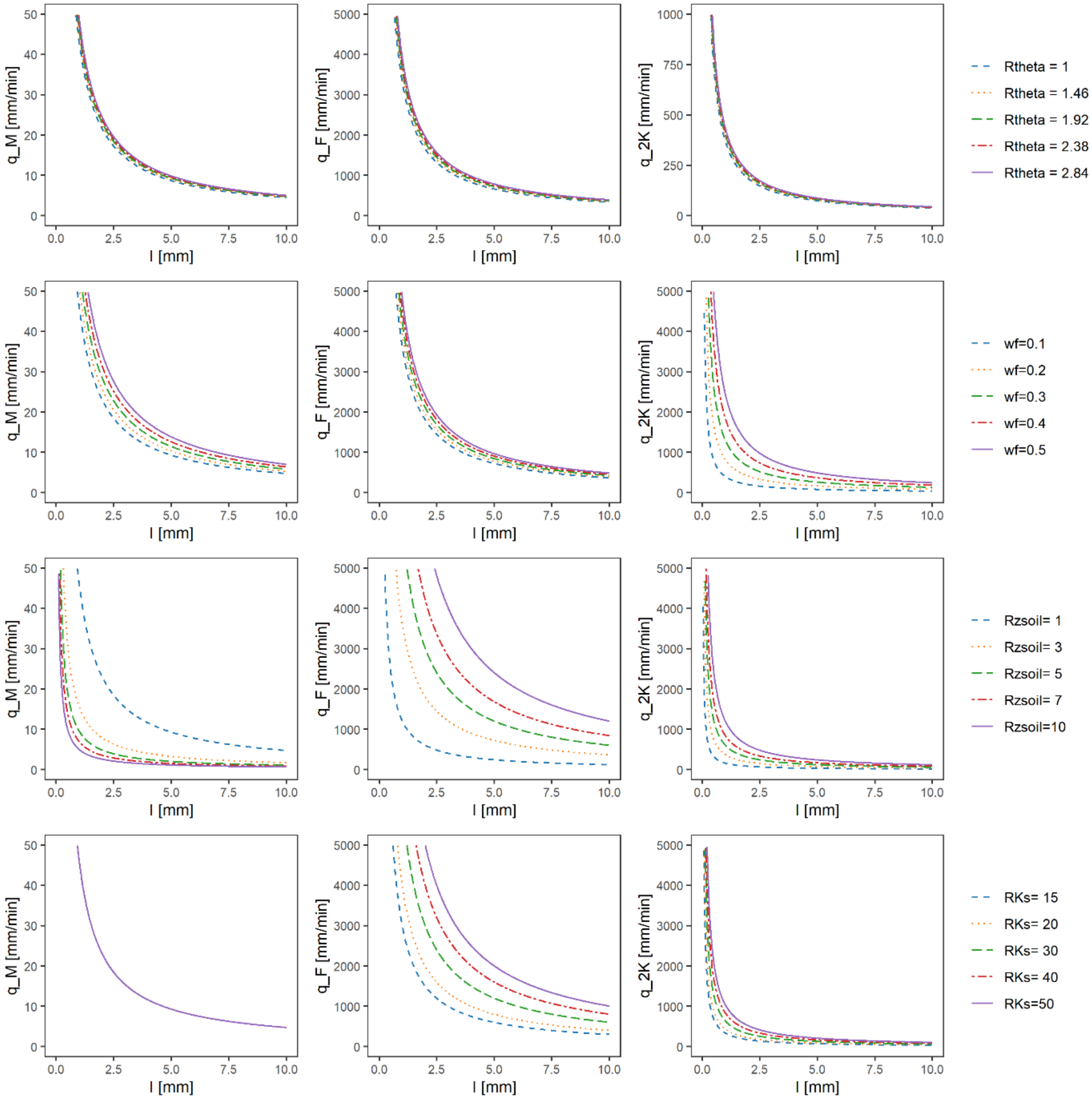

Figure (4.6): Sensitivity analysis of infiltration rate in matrix and fracture regarding the change in the parameters

4.5.2. Preliminary results

4.5.2.1. Analysis of the accuracy of *CH3-2K* models using numerically generated data

The performance and domain validity of the dual-permeability model in different saturation conditions using synthetic infiltration data from $Hydrus\_2K$ is investigated in this study. The hydraulic parameters of loamy soil were for the matrix using a pedotransfer assumption approach, as presented and explained in detail in section 4.4.1.1.

The volume fraction occupied by the fracture pore system was set at 10% and the other hydraulic parameters of the 2K system are described in Table (4.1). Preferential flow can be induced by a variety of factors, and one of these factors is antecedent moisture conditions and water pressure head conditions applied at the surface (Torres, 2002). The rate of water infiltration can change from a slow displacement process to a much faster acceleration rate relative to the initial water content, which is closely related to the occurrence of preferential flow. A small change in soil water pressure head in the near-zero range can activate soil water movement and store it in larger macropores, creating favorable conditions for preferential flow (Tymchak and Torres, 2007).

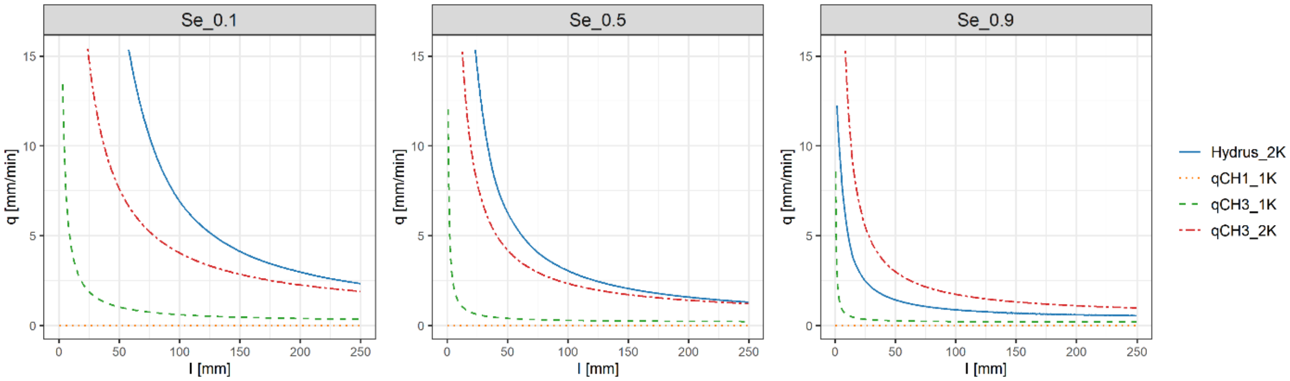

Figure (4.7): Result of direct infiltration modeling using the ($CH1\_1K$, *CH3*-1K, *CH3*-2K) models for Loam compared to numerical infiltration modeled using Hydrus-2K for three different saturation scenarios (Dry soil (Se=0.1), intermediate soil (Se=0.5), saturate soil (Se=0.9))

To determine the validity of the model, the impact of preferential flow on water infiltration rate was studied by considering three different degrees of initial saturation and a positive water pressure head at the surface. Figure (4.7) displays the result of a physically-based infiltration model ($CH1$, $CH3\_1K$, $CH3\_2K$) that were tested for loamy soils, amended with macropores with three different saturation levels (dry, intermediate, and saturated) and their comparison with reference numerically generated data (Hydrus_2K).

The results present three key outcomes. Firstly, the initial version of the infiltration model ($CH1$) was unable to replicate the shape of synthetic infiltration curves for any saturation scenarios, as indicated by low R^2, *NSE* values and a high value of $PBIAS$ of 99-100%, which means this model missed around 99-100% of the average of synthetic data Table (4.3). On the other hand, the last version of the Infiltration model set in simple permeability $CH3\_1K$ which is a reformatted Green-Ampt model, closely matches the physics of water infiltration into soils, with the onset of infiltration decreasing as a function of cumulative infiltration, highlighting the importance of model evaluation (more detail can be found in Asry et al., (2023)). Secondly, the figure compares $CH3\_1K$ and $CH3\_2K$ in terms of their agreement with the physics of infiltration and agreement with the reference numerically generated data. The static analysis shows a high degree of model agreement R^2 between (0.87 to 0.95) for the model $CH3$ in both homogeneous and heterogeneous modeling in terms of shape: it decreases all the time. Even if most users consider the single permeability approach to model water flow in soils, most cases involve heterogeneous soils, requiring the use of dual-permeability media. $CH1\_1K$ and $CH3\_2K$ in terms of agreement with the Hydrus 2K data, which can be used to represent real soil media, underestimate the infiltration for the two lower degrees of saturation Figure (4.7).

Finally, the $CH3\_1K$ model exhibits a negative NSE for soil at intermediate and high degrees of saturation and a high value of $NRMSE$ indicating a poor fit. Additionally, the model's significantly negative $PBIAS$ indicates that it consistently underestimates the reference infiltration curve. In contrast, the $CH3\_2K$ model, designed to account for soil heterogeneity in dry and intermediate soils, performs well with an NSE of 0.87 and $NRMSE$ of 40%. However, $PBIAS$ analysis shows that the model still underestimates infiltration values by around 28% for dry soils. The $CH3\_2K$ model seems appropriate for loamy soil conditions with median and dry conditions, making it useful for hydrological modeling to simulate preferential flow impacts in such types of soil. The comparison with reference analytically generated data shows that $CH3\_2K$ overestimates infiltration values for the saturated condition, which may be due to the imperfect parametrization of fractured reservoirs. These findings are supported by the results presented in Figure (4.7) and Table (4.3).

The $CH3\_2K$ model is an appropriate model for median and dry saturation conditions in a coarse filter medium. This allows for its use and integration in hydrological modeling to simulate the impact of preferential flow in such systems. The results are in line with the study of (Bond and Thompson, 2013; Tymchak and Torres, 2007) who shows in the experimental stand for the loamy soil, the wetting front can move forward at the same time.

In cases where the initial water content of the soil is low, the activation of macropores in bimodal soil media occurs more rapidly. This leads to a higher level of infiltration, as indicated by the results obtained from the HYDRUS 2K model. Additionally, the performance of the $CH3\_2K$ model, which incorporates more complex permeability characteristics, demonstrates a better fit compared to the simple permeability model.

Table (4.3): Statistics of the goodness of fits (NSE, R^2, $NRMSE$, and $PBIAS$) for the assessment of the capability of *CH1*, *CH3_1K*, and *CH3_2K* models to fit the simulated infiltration rates for synthetic soils depicted in Figure (4.7) (considered as the reference). The lines highlighted in grey delineate the best models for each case. The value of the statistics corresponding to a perfect fit (model = observations) or to a model that provides only null values were added).

	NSE	$NRMSE$ %	$PBIAS$ %	R^2
Perfect model	**1**	**0**	**0**	**1**
$S_{ei} = 0.1$ $Loam\ and\ r_{avrage}$ (1000µm)				
$q(I)_{CH3\_2K}$	0.33	81.8	-55.4	0.95
$q(I)_{CH3\_1K}$	0	99.9	-80.6	0.95
$q(I)_{CH1\_1K}$	-0.23	110.7	-100	0.15
$S_{ei} = 0.5$ $Loam\ and\ r_{avrage}$ (1000µm)				
$q(I)_{CH3\_2K}$	0.83	40.7	-28.2	0.94
$q(I)_{CH3\_1K}$	-0.02	100.8	-76.9	0.94
$q(I)_{CH1\_1K}$	-0.46	120.8	-99.9	0.23
$S_{ei} = 0.9$ $Loam\ and\ r_{avrage}$ (1000µm)				
$q(I)_{CH3\_2K}$	-9.95	330.7	140.2	0.87
$q(I)_{CH3\_1K}$	-0.17	107.9	-61.2	0.87
$q(I)_{CH1\_1K}$	-0.68	129.6	-99.8	0.71

4.5.3. Inverse modeling with *CH3*-2K model using experimental data

The *CH1* model does not match the experimental data in all cases, and the statistics measuring the model's fit to the data are poor. In contrast, the $CH3\_1K$ model effectively replicates the typical decrease in infiltration rate with cumulative infiltration, consistent with the principles of water infiltration into soils. The $CH3\_1K$ models accurately depict some experimental data but may underestimate observations at the end of the infiltration for other data sets. However, the statistics measuring the fit of the $CH3\_1K$ model to the data ($NSE, NRMSE$, and $PBIAS$) indicate moderate performance, with very low *NSE* values, high $NRMSE$ values, and high absolute values of *PBIAS*. The *CH3_2K* model shows an improvement compared to the $CH1$ model, as seen in the increased coefficient of determination (R^2) values in Table (4.4) and in Figure (4.8).

Overall, the $CH3\_1K$ model is considered a strong candidate with good fits in the context of SUDS hydrological simulations. Despite this, the $CH3\_1K$ model is easy to calibrate (only two parameters) and performs well for both direct and inverse simulations. Assumptions during modeling, such as considering soil as homogenous instead of heterogenous, can result in inadequate goodness of fit statistics and also bad values of estimates.

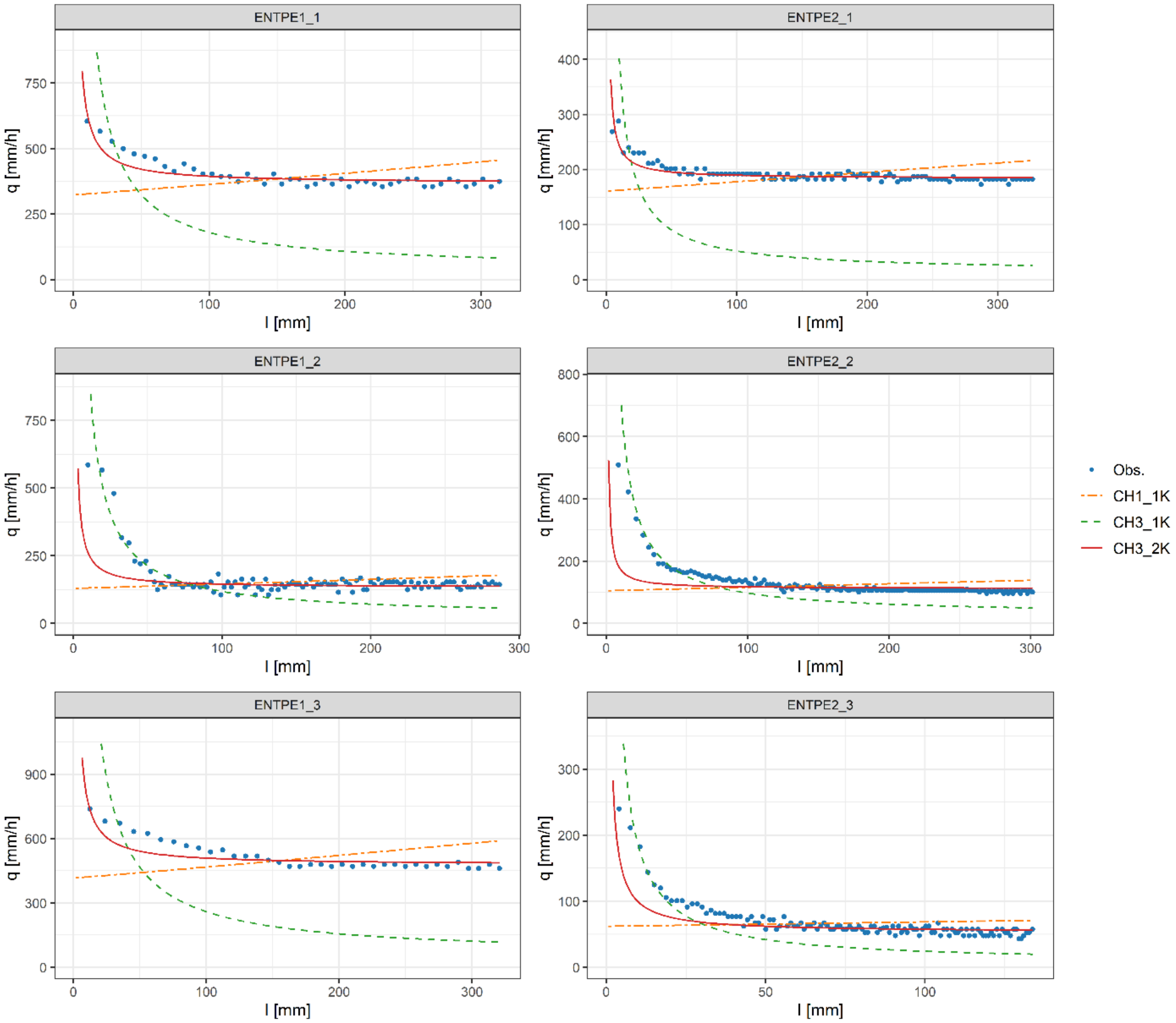

Figure (4.8): Infiltration rate simulated using inversion modeling for six experiments

The comparison between $CH3\_1K$ and field data in six infiltrations showed that the $CH3\_1K$ model underestimates the observed infiltration, which may be explained by the presence of macroporosity and preferential infiltration flow.

On the other hand, $CH3\_2K$, as shown in Figure (4.8) achieved accurate fits in all infiltration scenarios and provided good results in terms of goodness of fit Table (4.4). However, *CH3-2K* had an underestimation at the beginning of the curve in cases *ENTPE*1-1, *ENTPE*1-3, and *ENTPE*2-1 which may be related to the error of data measurement in the first point of infiltration, given the very slight decrease in infiltration rate at the beginning of the infiltration. In conclusion, the $CH3\_1K$ model, which is an improved version of the dual permeability model, is a strong candidate for use in SUDS in which soils are prone to preferential flows. The statistics of the goodness of fit, with high NSE values, low $NRMSE$ values, and low absolute values of $PBIAS$, prove that the $CH3\_2K$ model provides satisfactory results.

The $CH3\_2K$ model may be an important and effective physically-based model candidate for preferential infiltration modeling in field conditions and SUDS. It is relatively simple to calibrate since only 4 parameters are needed. It also performs well for both direct and inverse simulations. When using the $CH3\_2K$ model for SUDS hydrological simulations, we considered that z_{soil} was equivalent to the total soil layer of the SUDS. Only 2 parameters need to be estimated for each region, the initial water content, and the saturated hydraulic conductivity, making it an efficient option for modeling.

Table (4.4): Results of the optimization process–optimization of the saturated hydraulic conductivity in the fracture pore system and the matrix); statistics of the goodness of fits (NSE, R^2, $NRMSE$, and $PBIAS$) for the fits with models (*CH3*-2K, *CH3*-1K, *CH1*_1K). Underlined values denote inaccurate fits for the statistics of the goodness of fit and when the optimized values equal the lower limits of the optimization interval.

		ENTPE1_1	ENTPE1_2	ENTPE1_3	ENTPE2_1	ENTPE2_2	ENTPE2_3
NSE	*CH3-2K*	0.83	0.85	0.76	0.8	0.84	0.87
	CH3-1K	-23.04	-0.03	-22.76	-77.47	0.03	-0.44
	CH1-1K	-1.48	-0.18	-1.69	-2.07	-0.25	-0.12
$NRMSE$%	*CH3-2K*	45.3	84.9	54.3	52.7	87.6	62.7
	CH3-1K	485.1	100.8	480.8	881.5	98	119.5
	CH1-1K	155.8	107.9	161.7	174.4	111.3	105.5
$PBIAS$%	*CH3-2K*	-0.9	-8.9	-1.7	-0.3	-8	-8.4
	CH3-1K	-51.3	-27.4	-48.1	-66.9	-27.5	-37
	CH1-1K	-1.8	-2.2	-2.1	-1.1	-2.4	-1.2
R^2	*CH3-2K*	0.82	0.76	0.77	0.72	0.96	0.9
	CH3-1K	0.81	0.756	0.766	0.72	0.95	0.89
	CH1-1K	0.58	0.16	0.71	0.45	0.41	0.5
CH3-1K	K_s	36.78	24.07	53.08	13.92	26.25	6.48
CH3-2K	$K_{s.F}$	3663.2	1328.7	4755.2	1834	1113.1	526.3
	$K_{s.M}$	1.2	0	2.1	0.4	0	0.3

When using *CH3-2K* models to invert infiltration data, it is important to remember that these models are designed for 1D water infiltration in soil. However, in reality, water infiltration is 3D, with both vertical and horizontal flow. For large rings like the 50--in diameter rings used in our study, the horizontal component of infiltration is considered negligible, and the infiltration can be considered 1D. That is the reason why we fitted our 1D model to our experimental data.

4.5.4. Model calibration and parameters adjustment in bioretention modeling

The main focus of this chapter is to present our findings on three key objectives: evaluating the hydrological performance of the bioretention model, adjusting the model to match measurement data, and assessing how changes in its parameters impact the model's output. We developed infiltration models that incorporate the concept of preferential flow and applied them to the case of bioretention modeling to simulate outflows and water level dynamics using data collected from the Wicks Reserve Bioretention Basin. The primary objective of the model is to accurately replicate the measured outflows, as this is the variable of one of greatest concern for stormwater managers. The behavior of soil medium is affected by seven parameters, of which the parameter C_{out} related to the underdrain and the hydraulic parameters of matrix and macropores, $K_{s.m}$, $K_{s.f}$ are primary and four soil characteristic parameters $\theta_{s.m}$, $\theta_{s.f}$ and, $\theta_{i.m}$, $\theta_{i.f}$ are secondary. The primary parameters directly affect the water balance of the bioretention basin and have readily observable and dynamic effects, while the other four model parameters have much less effect on the mass balance.

The soil bulk porosity was derived from basin physical characteristics and allowed us to set the saturated water contents in the matrix, assuming a value of 0.6 for the saturated water content in the fracture pore system. The values of $\theta_{s.f}$, $\theta_{s.m}$ was calibrated using 2 rainfall events out of 22, meaning 1/11 of the dataset to fit observations. In addition, $\theta_{i.m}$ was yielded from the initial water level present in the system and $\theta_{i.f}$ was set to a very low value, assuming no capillarity in the fracture pore system.

The soils surrounding the basin involve a clay matrix with extremely low hydraulic conductivity, determined through the application of rising stage slug tests in nearby piezometers (Bouwer and Rice, 1976). As a result, $K_{s.inf}$ was set to a value less than 1 mm/day. In this study, it was assumed that the ponding zone was initially dry before the beginning of a storm. The primary parameters were determined by calibration by comparing the computed values of the outflow rate Q_{out} by checking the overall mass balance.

The calibrated events were selected to represent a range of precipitation levels, including both small and high levels. The remaining data was then used to evaluate the model's accuracy and robustness by comparing simulated results to actual measurements. Then, a significant number of random parameters (primary) sets are generated, and the model is run using each set of parameters. The results of the simulation are compared to the observed data, and the set of parameters that gives the highest match, as determined by the value of NSE_Q, is selected. These parameters were adjusted to simulate outflows, but the model's ability to replicate the dynamics of water levels was also evaluated to determine its accuracy in capturing the hydraulic gradient dynamics within the filter.

Table (4.5): Bioretention basin parameters for model calibration

Parameters	**Values**	Source	Unit
Filter depth	1	Visual observation	m
Area of the ponding zone	900	Visual observation	m^2
Wilting point θ_w	0.1	FAWB 2015	-
Field capacity θ_{fc}	0.2	FAWB 2015	-
Surrounding soil hydraulic conductivity	1.5×10^{-7}	Measured	$\frac{m}{s}$
Area of the filter	1800	Visual observation	m^2
Filter porosity $\theta_{s.m}$	0.45	Measured	-
Filter porosity $\theta_{s.f}$	0.6	(Gerke & VG, 1993)	-
Saturated filter media hydraulic conductivity K$_{s.m}$	3.72×10^{-7}	Calibarted	$\frac{m}{s}$
Saturated filter media hydraulic conductivity K$_{s.f}$	4.8×10^{-4}	Calibarted	$\frac{m}{s}$
volumetric weighting factor ω_f	0.1	Assumed	-
Initial hydraulic conductivity $\theta_{i.f}$	$(\frac{F_1}{F_{max}} \times \theta_{s.f})$	Calculated	-
Initial hydraulic conductivity $\theta_{i.m}$	$(\frac{F_1}{F_{max}} \times \theta_{s.m})$	Calculated	-
Orifice coefficient C$_{out}$	2.3×10^{-3}	Calibarted	-

4.5.4.1. Model calibration

The calibration process is a critical step, particularly when dealing with highly non-linear processes like unsaturated flow modeling (Ritter et al., 2003). Calibration of the model was conducted by evaluating the goodness of fit between model predictions and field observations over a range of plausible parameter values from the literature. Bonneau et al. (2021) used the systematic Monte Carlo (MC) approach for model calibration with the NSH as the optimization objective function. Figure (4.9) represents the space of response using the Monte Carlo approach.

However, as the number of parameters increases, the uniform Monte Carlo sampling approach becomes computationally inefficient and is unable to maintain an adequate sampling density, which can lead to unreliable results.

As a result, the MCMC (Markov chain Monte Carlo) sampler approach is an attractive method for the evaluation of the uncertainty of the model parameters in continuous multi-variable problems (Vrugt and Bouten, 2002). To avoid any uncertainty regarding the multiple local optima, the nonlinear interactions between the model parameters, and the complex shape of the response surface defined by the objective function (Feyen et al., 2007), the Bayesian approach has been recommended in the literature for the hydrological model calibration (Bertrand-Krajewski et al., 2021; Laloy et al., 2010; Yang et al., 2017).

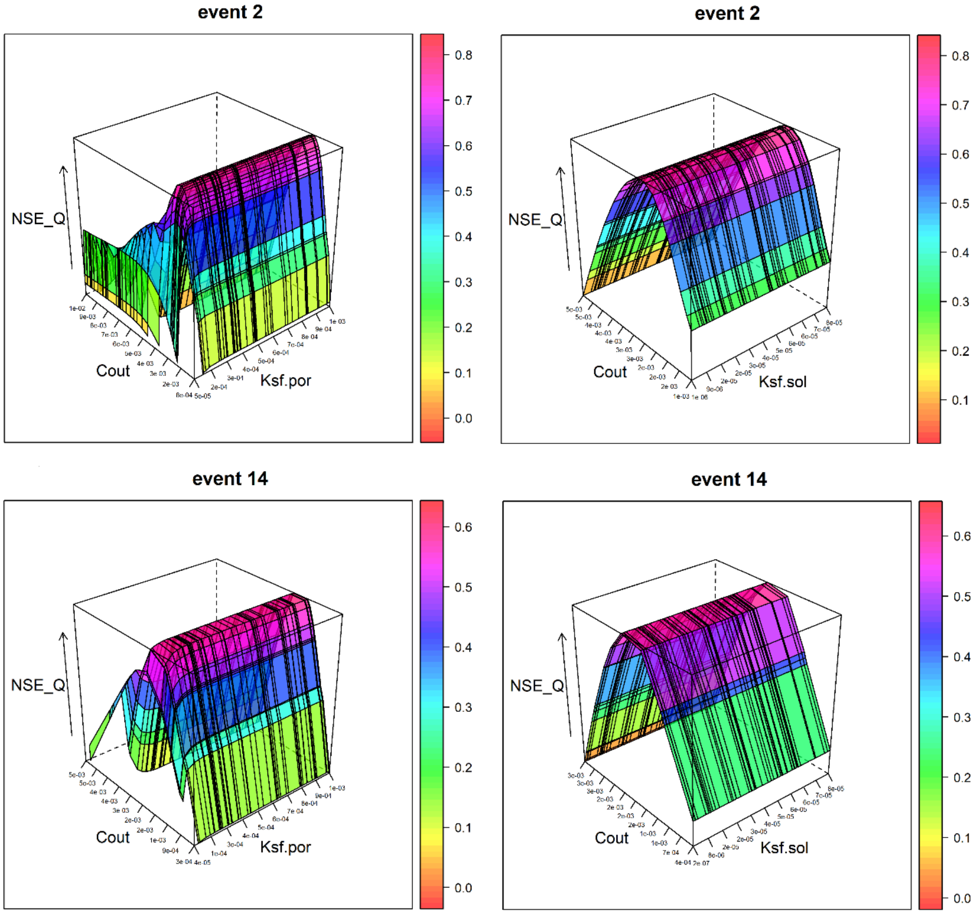

Figure (4.9): Schematic of the surface of response reproduced by Monte Carlo for two calibration events, with respect to the NSE-Sutcliffe Efficiency (NSE), The values of C_{out} was selected within the range of of 0.0001 to 0.01, while $K_{s.m}$ was varied between 10^{-10} to 10^{-4} m/s, and $K_{s.f}$ was varied between 10^{-5} to 10^{-3} m/s

An inverse problem can be effectively addressed using Bayesian inference, as it allows rigorous determination of nonlinear quantitative uncertainty distributions of parameters treated as random variables rather than point estimates (Dosso et al., 2009). The self-adaptive Monte Carlo Markov chain (MCMC) approach is a useful method for sampling from a posterior probability density function (PDF). By conducting a random walk within the Markov chain, it explores the prior space and provides an approximate estimation of the posterior probability distribution (Vrugt et al., 2003). During the random walk, new parameter values are proposed based on the current state of the chain, and their acceptance or rejection is determined by the posterior probability.

The likelihood function refers to the probability of observing a set of data given a specific model and its parameter values. Bayesian inference goes beyond maximum likelihood estimation by incorporating prior information into the analysis. In this study, a multi-objective optimization approach was employed to optimize modeling objectives, specifically for estimating flow or water height in the filter media. It considers both the outflow and filter depth as objectives. The Differential Evolution Adaptive Metropolis (DREAMzs) algorithm, a Bayesian optimization technique, was utilized to calibrate the three parameters: C_{out}, $K_{s.m}$ and $K_{s.f}$. DREAMzs dynamically adjusts the proposal distribution's scale and shape based on the chain's past performance, aiming to improve exploration and convergence properties over time. Two chains of modeling and 25,000 iterations were carried out. A prior probability distribution is formed for the model parameters by assuming a uniform distribution over the range of data intervals. The values of C_{out} were tested between 0.0001 to 0.01, while $K_{s.m}$ was varied between 10^{-9} to $10^{-4}\ m/s$, and $K_{s.f}$ was tested between 10^{-5} to $10^{-3}\ m/s$. The parameters C_{out} reached a threshold of around, 2.8×10^{-3}.

The calibrated orifice coefficient C_{out} was found to be within the expected range based on literature values for perforated PVC pipes. However, estimating this value accurately in real-world scenarios can be challenging. The expected value of the orifice coefficient for perforated pipes would be 0.064. Nevertheless, the field conditions in the Wicks study deviated from ideal conditions due to the possibility of plant roots penetrating the orifices and an unknown degree of clogging in the PVC pipe. Consequently, the literature value could not be relied upon, and calibration of the orifice coefficient was necessary. It is important to note that there is some uncertainty surrounding the design value for C_{out}, but the calibrated value appeared to align well with the characteristics of the site. Similarly, while soil properties of fine sandy loam are generally established in the literature, a site-specific value was required for calibration purposes in this study. The parameter of $K_{s.f}$ and $K_{s.m}$ reached $4.48\ 10^{-04}$ (m/s) and 3.72×10^{-7} (m/s) respectively.

To assess the convergence of Bayesian statistics using the Markov chain Monte Carlo (MCMC) method, the Gelman-Rubin indicator is used. A Gelman indicator value of 1.04 and 1.1 indicates that the MCMC chains have achieved convergence and the sampling process has reached a stable state. Generally, a value less than 1.1 is considered indicative of convergence, while values greater than 1.1 suggest that further iterations may be required to achieve convergence.

Table (4.6): The result of model calibration using Monte Carlo for two events derived by two chains and two events

Calibration Event	Mean inflow (l/s)	Mean outflow (l/s)	Mean water height (m)	Initial water height (m)	Optimization Objective	$K_{s.f}$ (m/s)	$K_{s.m}$ (m/s)	C_{out}	Gelman-Rubin
(Event 2) 2013/9/18	4.89	3.795	0.661	0.5357	Multiobjective	3.60e-04	5.60e-08	0.0032	1.04
(Event 14) 2015/4/24	1.63	0.939	0.540	0.4809	Multiobjective	5.36e-04	6.88e-07	0.0024	1.1

4.5.4.2. The sensitivity of the model regarding the C_{out}

In previous studies of basin hydrology, the estimation of the weir coefficient was commonly based on established hydraulic formulas. For two calibration events, the model behavior using different values of C_{out} are examined through the goodness of fit for outflow and water level in the filter media Figure (4.10). The mean of optimal value for C_{out} was 2.8×10^{-5} gives an overall best fit for both high- and low-peak events calibration regarding satisfying the objective of NSE_Q and NSE_H. We then can see that we can find a value of C_{out} that provides high values of *NSE* functions for both water heights in the filter and water fluxes. This is the first step towards optimizing at the same time water fluxes and water height in the filter. That was one of the drawbacks of the modeling proposed by Bonneau et al. (2021). These authors reproduced accurately water fluxes but with a poor fit of water heights. By implementing the dual-permeability model, we expected to improve the modeling of both parameters, indicating an improvement in the simulation of physical processes.

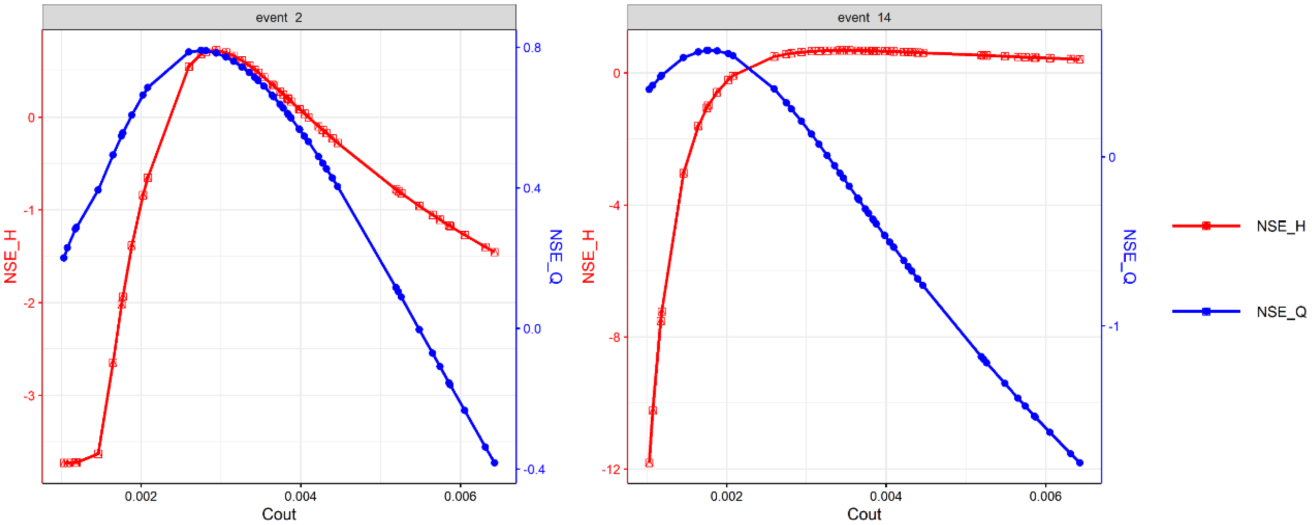

Figure (4.10): NSE-Sutcliffe Efficiency (NSE) values for overflow rate (Q) and water level in filter medium (H), for calibration of orifice coefficient (C_{out}) (with $K_{s.m}$ and $K_{s.f}$ held constant at 4.48× 10^{-4} m/s and 3.72e-07 m/s respectively) for the rainfall events 2 and 14 .

4.5.4.3. The impact of C_{out} on model estimation

The orifice coefficient C_{out}, which controls the outflow through the culvert pipe, plays a significant role in regulating the water level in the filter media. which is in line with those of (Bonneau et al., 2021b). By increasing C_{out}, the culvert discharge can be increased, allowing more water to flow out of the basin. This directly affects the water balance within the basin and produces observable and dynamic effects.

The study results demonstrated that the orifice coefficient had a more substantial impact on the model's performance compared to the hydraulic conductivity of the matrix and macropores reservoirs. This suggests that accurate calibration and optimization of this parameter are crucial for accurately simulating and predicting the behavior of the system. To gain a deeper understanding of the model's behavior with respect to the orifice parameter, a sensitivity analysis was conducted. In Figure (4.11), the influence of the orifice coefficient on the dynamics of outflow for two specific events has been investigated. By systematically adjusting the value of C_{out} and observing its impact on the model outputs, insights were gained into the sensitivity and responsiveness of the system to changes in the orifice parameter.

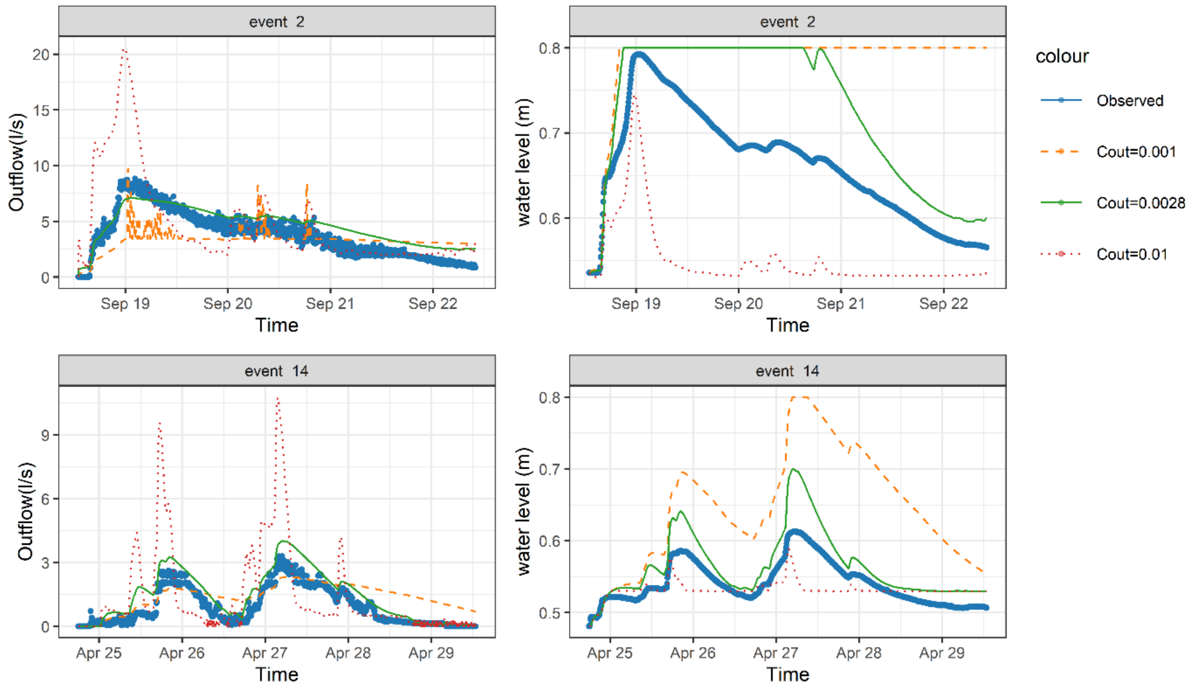

Figure (4.11): Sensitivity analysis for two calibration rainfall events (top/bottom), Left: Modeled and observed outflows, right: Modeled and observed water level in the filter medium depending on C_{out} (hydraulic conductivity for matrix and porosity are fixed to calibrated values).

The calibrated value of $C_{out} = 2.8 \times 10^{-3}$ for high- and low-peak events, provides the best overall fit, and gives a realistic peak flow time. As shown in Figure (4.11), a higher value of orifice coefficient at 0.01 results in peak-outflow values that are higher than observed, but also causes the filter media to empty quickly through the culvert, lower peak-water water level in the filter; the model initially overestimates the peak flow and then rapidly decreases after the peak due to the quick drainage of the structure. A smaller value of C_{out}, specifically 0.001, leads to an underestimation of peak outflow and results in a higher water level within the filter media. The model predicts a larger accumulation of water within the basin until the filter media becomes saturated. Once saturation occurs, the water starts to pond at the surface, leading to the combination of ponded water and water within the filter. This behavior transforms the system into a pool-like state, where the outflow and potential overflow discharge (if the ponded water exceeds a specific threshold) govern the water dynamics in the system. The anomaly observed in Event 2, at the C_{out}=0.001, indicates that the ponded water in the system exceeded the threshold level, leading to an overflow. Over time, the modeled water height in the filter exceeds the height of the filter itself, indicating complete saturation of the filter. After this point, all the incoming water is stored in the ponding zone. When the filter water level reaches the height of internal water storage, the underdrain controls the whole system. This response of the model aligns with findings from other studies, which could be attributed to the construction of the basin (Bonneau et al., 2021b; Fournel et al., 2013). This behavior can be attributed to the hydraulic characteristics and design elements of the basin, including the presence of an internal water storage system and the configuration of the underdrain (a pipe outflow with an upturned outlet to form IWS).

4.5.4.4. The impact of $K_{s.f}$ and $K_{s.m}$ on model estimation

In this section, the impact of hydraulic conductivity of macropores on the system response has been studied. After determining the optimum values for the parameters, C_{out} and $K_{s.m}$ were fixed, and then the $K_{s.f}$ was systematically changed to observe its impact on the model response. As shown in the Figure (4.12), choosing a small value for $K_{s.f}$ leads to less infiltration in the system. Even though the matrix is unable to infiltrate more water, the outflow and the water level in the filter are smaller than expected. In Event 14, an anomaly can be observed in the curve when the infiltration decreases.

This anomaly indicates that when infiltration decreases, water accumulates, and in this case, the water surpasses the threshold. Choosing a higher conductivity value for $K_{s.f}$ does not result in any change in the plot because, although it increases infiltration, the model regulates the infiltration based on the mass balance Equation (4-24) instead of applying Darcy's law (or equivalently the dual-permeability equation). In that case, the value of the saturated hydraulic conductivity does not play any role. The variation in the small pores does not appear to have a significant impact on the model's response. This is because the macropores have a high infiltration capacity that can be controlled primarily through the drainage coefficient.

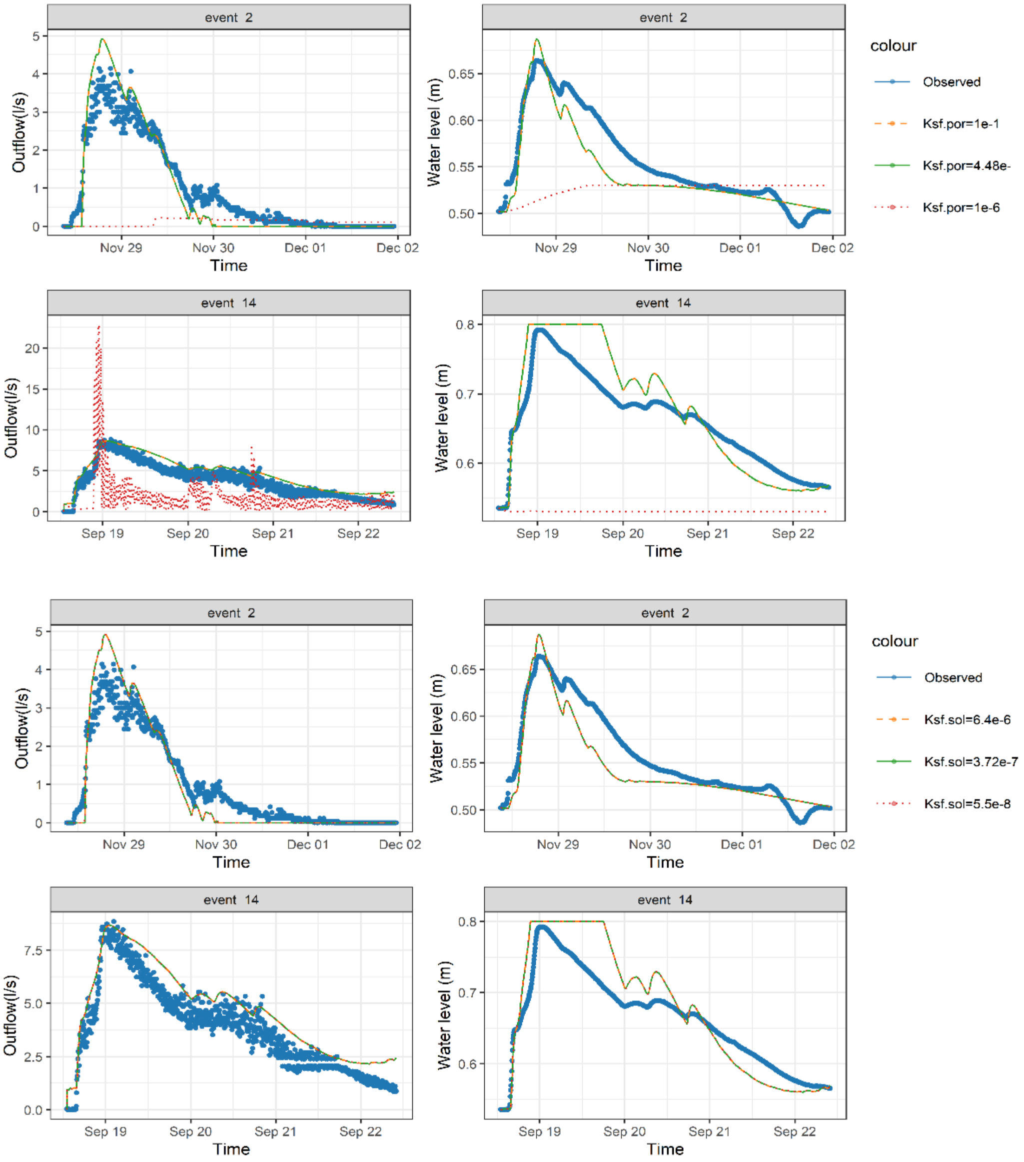

Figure (4.12): The sensitivity analysis of the model regarding the conductivity hydraulic of macropores and matrix

4.5.5. Comparison against validation data

The performance of the model was evaluated using several metrics, including KGE, *NSE,* R2, and RMSE, for both outflow and water height in the filter media. The summary of the model's performance can be found in Table (4.7) and a visual representation of the results is presented in Figure (4.13). The outflow is of great interest due to its significant impacts on water quality and the flow patterns of receiving waters (DeBusk et al., 2011).

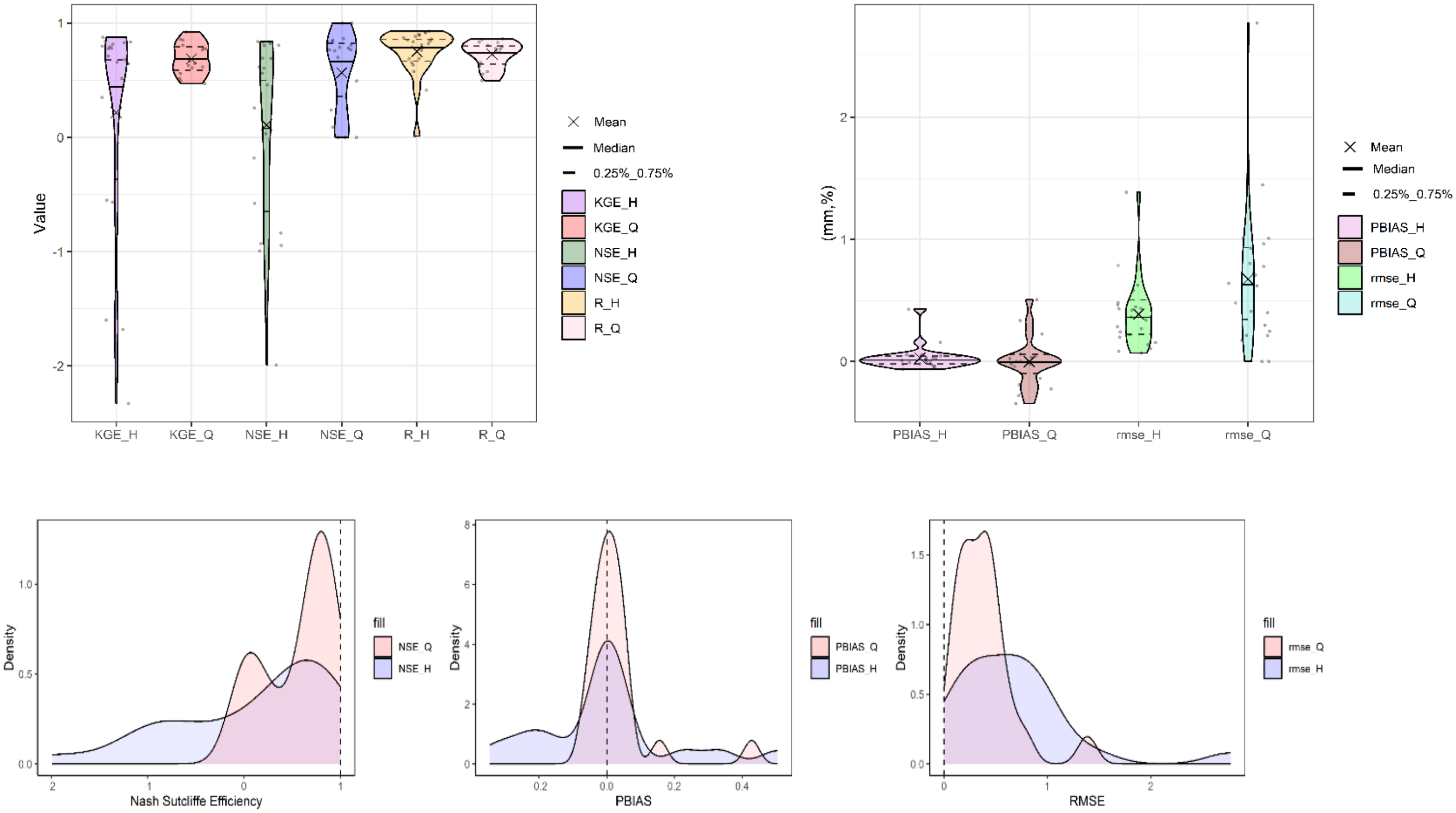

Figure (4.13): Distribution of the *NSE* Sutcliffe efficiencies, *PBIAS,* and RMSE for outflows for all the rainfall events

Table (4.7): The summary result of goodness of fit for outflow and filter water height

NSE-Q	NSE-H	KGE-Q	KGE-H	RMSE-Q	*PBIAS*-Q
Median: 0.76	Median: 0.51	Median: 0.65	Median: 0.66	Median: 0.62	Median: 0
Mean: 0.56	Mean: 0.10	Mean: 0.68	Mean: 0.21	Mean: 0.67	Mean: -0.002

Regarding the outflow simulation, the model showed a slight improvement in comparison to the further developed model in the study of Bonneau et al. in 2021, in terms of the *NSE* criterion, with a mean value of 0.76 Figure (4.13). In most events, the model was able to reach and represent the observed curve more accurately. However, there were some events where the overflow was shown to be non-satisfactory, which can be attributed to the simplification of the equation used to calculate the overflow discharge. To assess the accuracy and variability of the model predictions, the KGE metric also was estimated. A mean KGE value of 0.68 suggests that, on average, the model captures approximately 68% of the variability and patterns observed in the data. Additionally, the RMSE criterion showed a median value of 0.62 l/s and a *PBIAS* of 0, indicating a good fit between the model and the observed data.

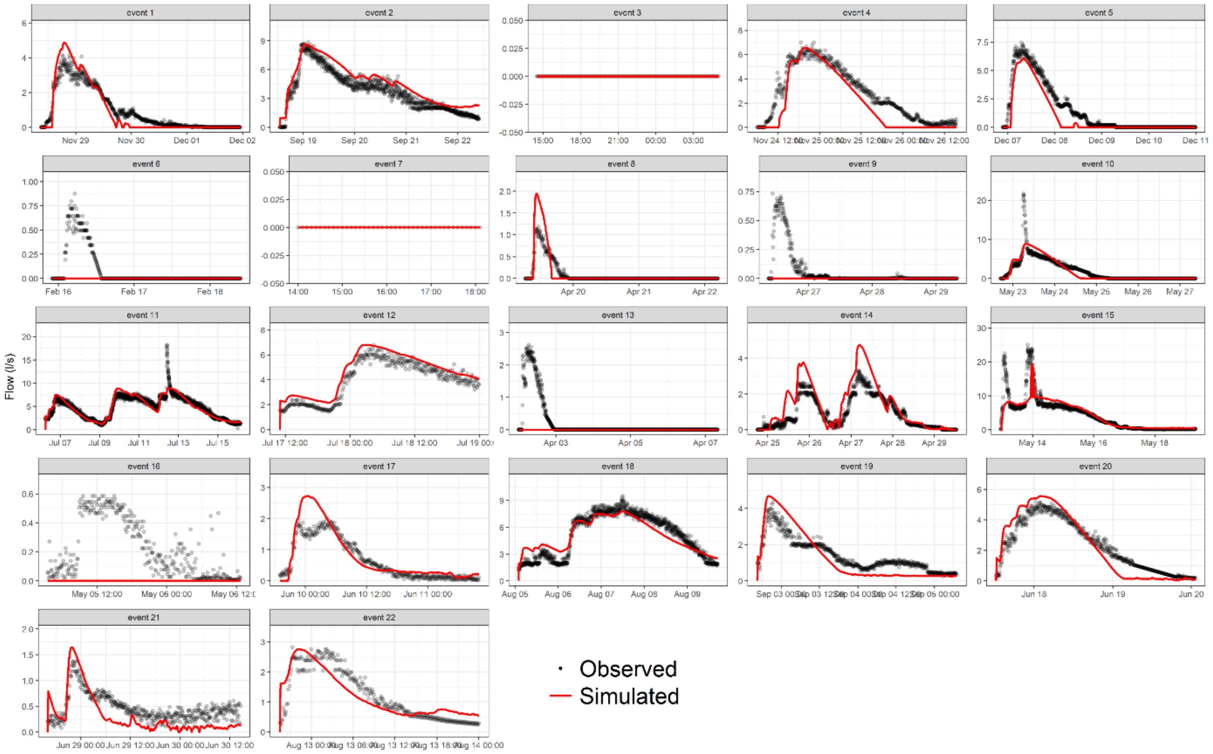

Figure (4.14): Observed and modeled outflow hydrographs for the studied 22 rainfall events (black line with points = measured; red line = simulated with the proposed model)

The simulation of water height in the filter media significantly improved with the new model that incorporated the dual-permeability porous media infiltration model. The median *NSE* value was 0.51, the KGE value was 0.68, and the mean *NSE* value was 0.10. However, the model tended to underestimate the water high, as indicated by a median *PBIAS* of -22% Figure (4.13). To improve the representation of observed water levels, additional complexity, such as adding new soil layers of modeling soil or capturing soil hydrodynamic parameters, would be necessary. However, obtaining such detailed information is not always feasible or readily available (Fournel et al., 2013).

One plausible explanation for the observed outcomes is the development of preferential flow paths. The mentioned cases were observed in temperate climates, and it is speculated that preferential flow in green roofs could be more prevalent in dry-summer subtropical/tropical climates (Guo and Luu, 2015). However, further research is necessary to monitor water movement in field configurations and gather solid evidence regarding the occurrence and characteristics of preferential flow.

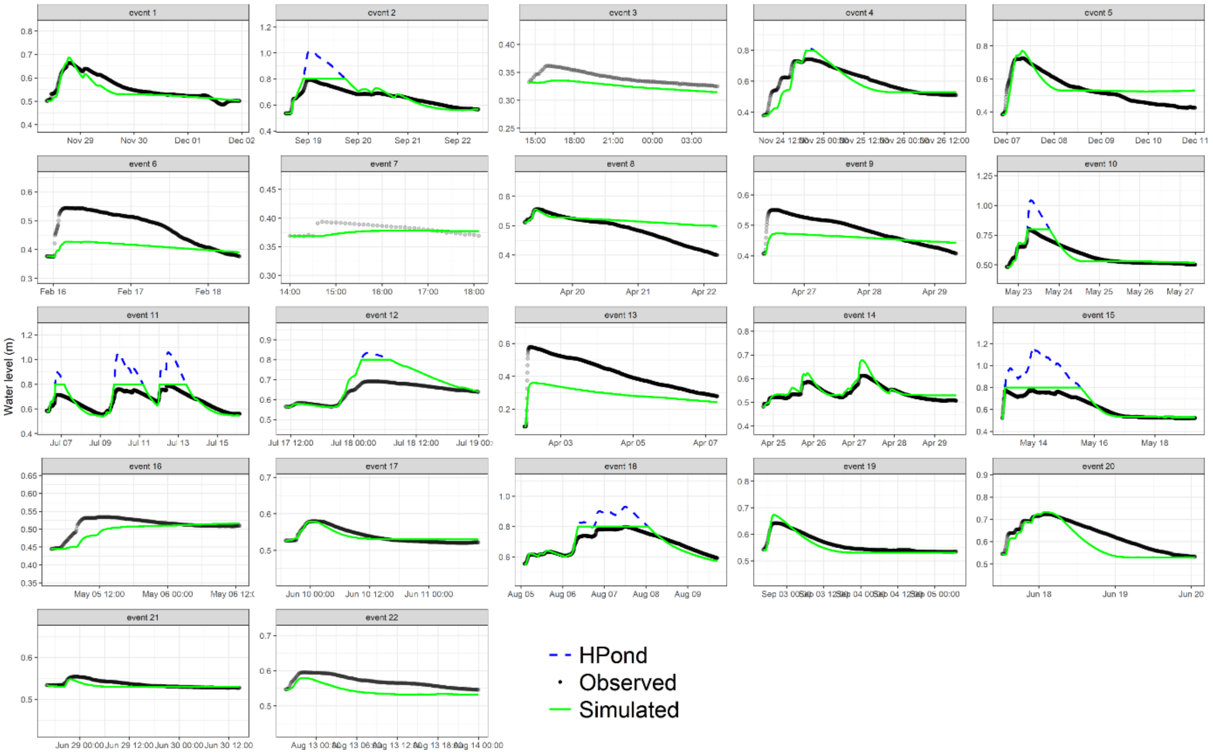

Figure (4.15): Illustration of the comparison between observed and modeled water levels in the filter. The black line with points represents the measured data, while the green line represents the simulated water levels using the proposed model, and the blue line corresponds to the ponded water depth

4.6. Discussion and conclusion

In this study, we focused on enhancing and developing the (*CH3*) model, (see Asry et al., 2023) for dual-permeability porous media modeling in a bioretention basin, based on modified Green Ampt modeling. The model was tested for three saturation scenarios (dry, wet, medium) and compared to the numerical model using Hydrus. The results demonstrated that the model effectively represented the dual-permeability porous media approach, particularly for dry and medium initial saturated soils. Subsequently, the model was inverted for six infiltration experiments conducted on the campus of the ENTPE using a specific large-ring infiltration device.

The results confirmed that the dual permeability modeling proposed in this study accurately represented infiltration through the calibration of two parameters (hydraulic conductivity in matrix and macropores). The simplified physically-based infiltration model in this study showed its capability to account for complex aspects of infiltration, including the position of the wetting front during the infiltration process and the influence of preferential flow, however, the model needs just three calibration parameters. The infiltration model implemented in the hydrological modeling proposed by Bonneau et al. in 2021 has been enhanced with the new dual permeability module. Contrary to SWMM or RECHARGE which needs more than 16 parameters for calibration, this model requires fewer parameters, with only three principal parameters needing optimization and the other parameters used in the bioretention modeling are physically measurable field parameters, making the model practical and applicable. The new version of the bioretention model, incorporating the dual permeability module, was initially calibrated using two specific events and validated using the remaining 20 events. This calibration and validation procedure ensured that the model's parameters were appropriately adjusted to accurately reflect the observed data.

The results of the modeling demonstrated a slight improvement in Outflow and an interesting improvement in simulating the filter water height in comparison with the simple-permeability approach. It is important to note that C_{out}, is a key parameter controlling the hydrologic performance of the model, which may influence the design of bioretention systems. The use of an elevated underdrain outflow pipe, by producing an internal saturated zone, simulates a pool-like system where the outflow coefficient becomes the hydraulic control of the system.

Nonetheless, the rapid arrival of the wetting front in the internal saturated zones occurs so quickly that the current 6-minute time steps are inadequate to observe its progression during infiltration. To accurately model the advancement of the wetting front, a finer time step is required to capture the intricate dynamics and movements (Lassabatere et al., 2009, 2014). It is suggested that using a non-elevated outflow pipe would allow for the observation of how different soil infiltration parameters affect system performance.

Additionally, the Mean and Median of *NSE* (NSE-Sutcliffe efficiency coefficient) for the filter water height were influenced by certain events that resulted in negative *NSE* values.

In event 13, there was a notable and rapid rise in water level within the filter. This increase can be attributed to the maturation of Wick's system which has been more pronounced in the absence of soil tillage. This leads to the soil water repellency and activation of macropores which are connected to the soil surface, facilitating a significant volume of water infiltration in the system. This finding is consistent with observations by researchers such as (Doerr et al., 2006; Hallett et al., 2004), who have shown that water repellency is more evident in undisturbed no-till arable or permanently vegetated soils like grassland, where macropores often extend continuously to the soil surface.

Furthermore, the initial water content in the system was observed to be below field capacity, which aligns with the results of (Edwards et al., 1993) who found that water flow in earthworm channels under no-till maize was highest during intense storms that occurred on initially dry soil (water shrinkage impact). While our model did not accurately simulate soil shrinkage and water repellency in the system, and considered that wetter soils will generate more macropore flow (Jarvis, 2007), then, it attempted to capture the overall curve. Therefore, it is recommended to model dry and wet events separately, considering the previous water content in the system as highlighted by Guo and Luu, (2015).

Another aspect that was not considered was the preexisting ponded water in the system (Wang et al., 2019). Despite our initial assumption of a precedent ponded water height of zero, the actual measurement data revealed a different scenario. This discrepancy had a noticeable impact on the model's performance for specific events (e.g., events 3, 6, 13).

As a result, our simplified model necessitates additional refinement and the incorporation of specific inputs to effectively replicate the curve, taking into account water repellency and soil shrinkage phenomena. To address these concerns, we suggest testing the proposed model using data with a finer time step and considering the spatial aspects for the bioretention without the IWS (Internal Water Storage) zone at the bottom of the filter.

Moreover, we have also suggested introducing more complexity by adding additional soil layers to the filter. However, this brings challenges in terms of handling a larger number of input parameters, as recommended by (Dussaillant et al., 2005).

Data availability statement

All data, models, or codes that support the findings of this study are available from the corresponding author upon reasonable request.

Acknowledgments

This research was funded by the french government scholarship (Campus France scholarship), ANR-INFILTRON. The authors thank Jérémie Bonneau for providing the original R-Code and Wick’s data. Thanks to H2O Lyon for their support during this work. We thank anonymous reviewers who have contributed greatly to improve this manuscript.

Declaration of competing interest

The authors declare that they have no known competing financial interests or personal relationships that could have appeared to influence the work reported in this paper.

Authors' contributions

All the authors significantly contributed to this research paper. The specific contributions to the paper lists as follows: A.A.: Conceptualization, Formal analysis, Investigation, Methodology, Software, Validation, Visualization, Writing - original draft; G.L.K.: Conceptualization, Funding acquisition, Methodology, Supervision, Validation, Reviewing and editing; T.F.: Conceptualization, Validation, Reviewing and editing; J.B.: Methodology, Validation, Reviewing and editing; D.T.: Validation, Reviewing and editing; L.L.: Conceptualization, Formal analysis, Funding acquisition, Investigation, Methodology, Software, Supervision, Validation, Visualization, Writing - original draft.

Chapter 5

Model parametrization, uncertainty, and sensitivity analysis

Chapter 5. Model uncertainty and sensitivity analysis

Preface

This chapter provides an overview of model uncertainty and sensitivity analysis for the models presented in Chapter 3. It aims to assess the reliability and robustness of these models by exploring the impact of uncertainties and variations in input parameters. Through sensitivity analysis, the chapter examines how changes in these parameters affect the output of the model. Examining model uncertainties and carrying out sensitivity analysis provide a deeper understanding of the reliability and limitations of the models, allowing more informed decision-making based on their results. It helps also to define the best strategies for its use in inverse mode (fitting experimental data).

Contents

Abstract

Cities across the globe are progressively embracing Low Impact Development strategies (LID) to restore the urban hydrological cycle and combat the impacts of global changes. Advanced, eco-friendly stormwater techniques effectively reduce runoff per numerous modeling studies, but knowledge gaps persist in hydraulic functionality and modeling. The study globally assesses the sensitivity of INFILTRON-Mod, a set of three physically-based infiltration models for LID modeling. It examines parameter changes' impact on the model output, enhancing understanding of reliability and limitations for informed decision-making. Multivariate Global Sensitivity Analysis using Extended Fourier Amplitude Sensitivity Test (FAST) is employed to assess the influence of INFILTON-Mod parameters on model estimation. Coupling FAST with the Bayesian interface conducts an uncertainty analysis of the model's parameters and evaluates its ability to replicate real LID hydraulic behavior. Bayesian inference proves useful in refining the model's parameters and enhancing reliability. The study's findings offer valuable insights for urban hydrologists on the statistical accuracy and computational efficiency of the studied models. It addresses influential and non-influential parameters, reducing uncertainty, and simulation time, and highlighting model limitations. Our results will also help to define an optimized strategy for the design of inversion algorithms for our models.

5.1. Introduction

Cities across the globe are progressively embracing Low Impact Development strategies (LID) to restore the urban hydrological cycle and combat the impacts of global warming. Advanced, eco-friendly stormwater techniques effectively reduce runoff per numerous modeling studies (Brattebo and Booth, 2003; Davis et al., 2009), but gaps of knowledge persist in hydraulic functionality and modeling. The efficacy of individual infiltration based-LID cells and the consequences of various design factors can both be better understood by site-scale modeling (Brown et al., 2013; Ding et al., 2019; Li and Davis, 2008; M. Li et al., 2017).

The key principle of LID modeling is soil infiltration. Richards' equation is frequently regarded as the most complete infiltration model and was used as the basis for several numerical tools like HYDRUS (modeling water fluxes in soil profiles) (Šimůnek and van Genuchten, 2008), GIFmod (Massoudieh et al., 2017), and DRAINMOD (infiltration based-LID modeling) (Brown et al., 2013, 2010).

The soil water characteristic curve (SWCC) and the unsaturated hydraulic conductivity curve (HCC) K(θ) are two soil functions that are required for modeling water fluxes but that are difficult to characterize (Angulo-Jaramillo et al., 2016). These numerical models present a series of equations for the soil hydraulic functions (SWCC and HCC), as demanded by Richards' equation, including Van Genuchten-Mualem (1980), modified Van Genuchten, Brooks Corey (1964), and Kosugi (1996) equations. The ROSETTA tool can be used to infer the input data for these equations from particle size distribution or texture data (Šimůnek and van Genuchten, 2008). Based on readily accessible soil textures, ROSETTA calculates the water retention parameters needed in the Van Genuchten flow equations (Schaap et al., 2001). However, acquiring water retention parameters in the field proves to be quite intricate, and the calibration of these parameters amplifies the uncertainty in the model outcomes. This heightened complexity in the model's output uncertainty could pose challenges for decision-makers, as it may entail substantial uncertainty to contend with.

There is a direct correlation between the number and complexity of input variables and model complexity. We need to strike a balance between intricate models that incorporate a multitude of complex input variables and simplistic models with only a few inputs that fail to capture the intricacies of the modeled physical processes. The complexity of the model directly relates to the number and complexity of the input variables (Sage et al., 2020). Given so, numerous models opt to use the simpler Green-Ampt equation as opposed to the more intricate Richards' equation.

The input requirements and computing demands are reduced by the Green-Ampt equation (Lisenbee et al., 2021b; Zhang and Chui, 2019). This simplification comes with some assumptions, such as one-dimensional vertical flow and complete saturation behind a clear piston-like wetting front. Although infiltration based-LID cells function in a variety of saturated and unsaturated contexts, these assumptions can occasionally be unappropriated (Barbu and Ballestero, 2015; Brown et al., 2013).

In theory, a physically-based model uses field-measurable parameters to represent processes (Niehoff et al., 2002; Zégre et al., 2010). Practically speaking, the model needs to be calibrated when data for the particular case study is lacking. The Green-Ampt infiltration model is a physical-empirical model that needs physical inputs like the initial water contents as well as typical soil characteristics like porosity, field capacity, and wilting point (Zhang and Chui, 2019). Determining the parameter of pressure head on the wetting front in the Green-Ampt equation can be challenging and not easily obtained from field experiments, especially due to the heterogeneity of soil and the dynamic nature of water movement over time (Kale and Sahoo, 2011; Ogden and Saghafian, 1997). This study introduces the INFILTRON-Mod, (see Chapter 3. for more results) which comprises three physically-based parsimonious models designed for simulating infiltration in LID. These models consider soil physics and have demonstrated effectiveness in accurately simulating infiltration rate and underdrain outflow. In limited infiltration, these modules can be easily calibrated using inversion approaches. The users need to comprehend the level of detail required for each infiltration model specific to their modeling application. It is crucial to establish a domain of model validity for parameter calibration and determine the model sensitivity within the calibration interval, which can be applied to these models. Additionally, understanding the sensitivity of the model to different parameters, especially input variables defining the state of the system, is important. In order to quantify and compare the effect of uncertain parameters or input variables on a given model's output, modelers must use global sensitivity analysis. By considering these factors, the user can make informed decisions during parameter calibration and ensure the model's reliability and applicability under both direct and inverse modes.

The majority of physically-based models contain a large number of input parameters, which causes an important challenge for implementing these since parameter estimation becomes a high-dimensional and mostly nonlinear problem (Vrugt and Sadegh, 2013). To overcome this problem, numerous optimization algorithms have been developed (Beven and Binley, 2014;

Vrugt et al., 2003). The Generalized Likelihood Uncertainty estimate (GLUE) frameworks have frequently been encouraged for parameter forecasting due to their simplicity and adaptability. Nevertheless, unlike Bayesian approaches, these techniques do not necessitate assumptions about error structure. This absence of requirements enhances their accessibility and versatility (Beven and Binley, 2014; Sage et al., 2017).

Furthermore, the equifinality problem (Beven, 2006), where different parameter combinations might produce equivalent results, is frequently encountered in environmental optimization investigations. This problem is made more difficult when there are many parameters and little knowledge of how they interact and affect the output of the model. Although certain model parameters can be measured or approximated, others may not always need to be included in the optimization process. The primary aim of this research is to explore multivariate sensitivity analysis techniques in conjunction with the INFILTON-Mod module. The study follows a specific approach to address the research objective. Firstly, Multivariate Global Sensitivity Analysis using Extended Fourier Amplitude Sensitivity Test (FAST) is applied and compared to assess the influence of INFILTON-Mod parameters on modeled infiltration data and parameter calibration. Then, this study couples FAST with the Bayesian approach to conduct an uncertainty analysis of the model's parameters and evaluate the model's ability to replicate the hydraulic behavior of LID. The research also includes a comparison of results between Monte Carlo and Bayesian methods.

Moreover, the integration of multivariate variance-based sensitivity analysis (E-FAST) with the Bayesian approach provides valuable information for urban hydrologists concerning the statistical accuracy and computational efficiency of their models. This approach could lead to significant advancements in understanding and managing infiltration-based LID within urban environments.

5.2. Material and Methods

The INFILTRON-Mod is the hydrological infiltration model which has been tested against a dataset comprising experimental infiltration rate, cumulative infiltration data, and numerically generated data (Hydrus outputs). The models used in INFILTRON-Mod are concise and based on physical governing processes. These models will be incorporated into the Hydrobox module of the Canoe model (Chocat, 2013) to facilitate their utilization in urban water infiltration modeling.

The infiltration models integrated into INFILTRON-Mod encompass parameters that are readily available in the field. However, when field parameters are lacking, the inversion (more information in Chapter 3.) of the subsequent models continues to be the optimal approach for deducing soil parameters from data readily gathered in the field.

In this study, the Monte Carlo Inversion (MCI) method was initially applied to the data (see Chapter 3) for inverse problem-solving. The MCI method involves generating model outputs by randomly selecting input parameters within predetermined upper and lower bounds. Each generated output is then compared to the available data using the *NSE* criteria, which was used in this study (Beven, 2006). Then, the set of input parameters corresponding to the best fit is selected.

Monte Carlo filtering is relevant when dealing with inversion models that contain ill-defined parameters and are thus referred to as overparameterized models (Draper and Smith, 1998). When dealing with ten or fewer unknown parameters, utilizing a simple deterministic grid search with MCI can be practical and efficient (Cambridge and Mosegaard, 2002). (Vrugt, 2016) has also pointed out that standard Monte Carlo simulation methods are computationally inefficient, except for very low-dimensional problems. However, we have also explored a Bayesian approach in relation to model uncertainty and the ill-posed nature of inverse modeling with MCI. This approach has already facilitated its implementation in the dual permeability approach. An inverse problem becomes ill-posed when the identified parameters are correlated to each other or exhibit instability or non-uniqueness. The process of estimating parameters of unsaturated soil hydraulic functions through inverse problems is often ill-posed but can be converted into a well-posed problem through well-designed experiments for homogeneous soils with minimal measurement and model errors (Hopmans and Simunek, 1999).

The lack of identifiability arises when various parameter combinations result in a similar system response, thereby rendering it unachievable to obtain a singular solution. Then, additional information is required to decorate input variables. Stability is achieved when optimized parameters remain insensitive to measurement errors, such that small errors in system response do not lead to significant changes in optimized parameters. To tackle this issue, first, the model uncertainty and sensitivity assessment are conducted. Finally, one possible solution is to abandon the search for a single optimal parameter combination and instead utilize the Bayesian theorem.

5.2.1. Uncertainty and sensitivity assessment

Our understanding of how computer models represent physical reality is improved significantly by quantifying model uncertainty. Parameter uncertainty and model discrepancy are the two main sources of uncertainty that contribute to the differences between a computer model and the actual physical system. The model discrepancy results from the absence of some physical components and other errors in the computer model, whereas parameter uncertainty is caused by unknown calibration parameters within the computer model (Ghanem et al., 2017).

A technique for measuring and quantifying uncertainty in model outputs that results from ambiguities in model parameters is known as uncertainty quantification. Uncertainty quantification gives each model parameter a distribution of possible values as opposed to deterministic models, which assume fixed parameter values (as shown in Figure (5.1 A). A distribution of potential outcomes for the model output results from this propagation of uncertainty in the model's parameter values (as shown in Figure (5.1 B). This method enables a more thorough comprehension of the range of potential outcomes and the corresponding uncertainties in the model predictions.

The Monte Carlo simulation (see Chapter 3) is a straightforward method for solving stochastic partial differential equations. It involves generating a significant number of random realizations of parameter fields, which are equally probable. For each realization, deterministic infiltration rate equations are solved, and the results are averaged across all realizations.

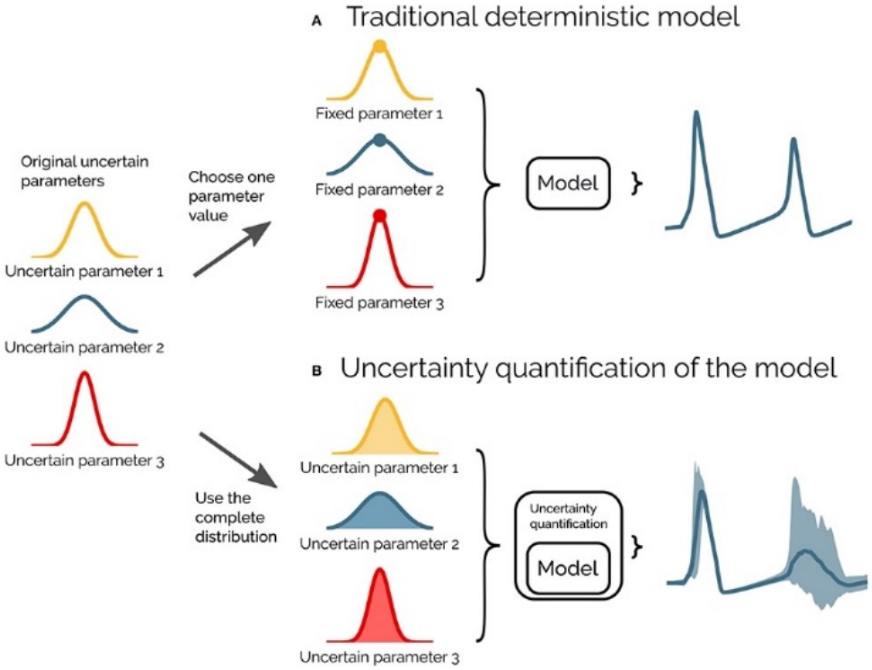

Figure (5.1): Illustration of uncertainty quantification of a deterministic model (adopted from Tennøe et al., 2018)

This process allows us to obtain sample moments of the solution (Giles, 2015; Lu and Zhang, 2003). In the context of uncertainty associated with real-valued measurements of a system, it is frequently assumed that the parameters follows a normal probability distribution. This assumption of normality enables the distribution to be characterized by the mean (μ) and variance (σ^2) of the normal distribution.

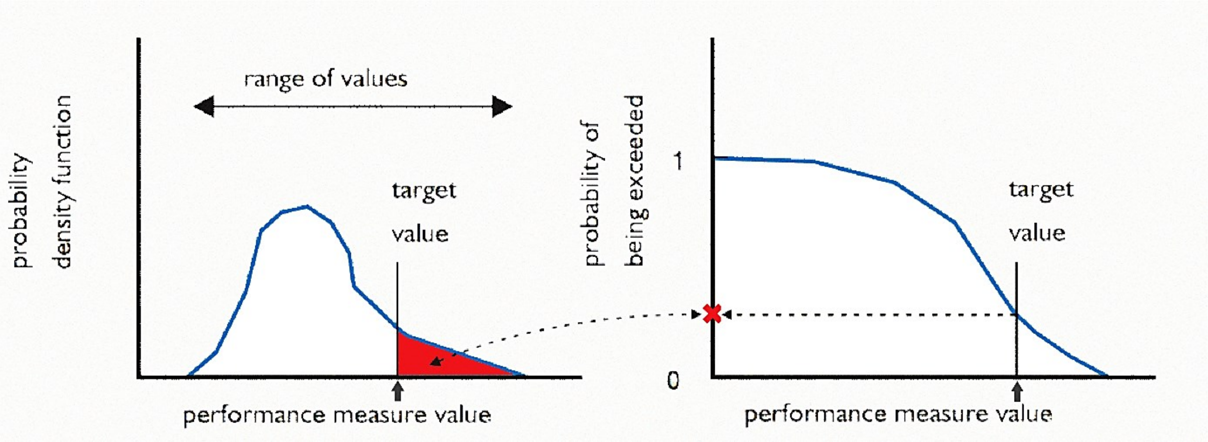

Figure (5.2): The distribution of performance measures defines a range of potential values and the likelihood that a specified target value will be exceeded. The shaded area under the density function on the left represents the probability that the target value will be exceeded. This probability is shown in the probability of exceedance plot on the right

The uncertainty can be represented by a percentage confidence interval, which indicates the range within which the measurement is likely to fall with a certain probability. The uncertainty of the model studied by the elliptical confidence zone of a variable represented by a bivariate normal distribution is illustrated in Figure (5.3) (Balas et al., 2009; Friendly et al., 2013).

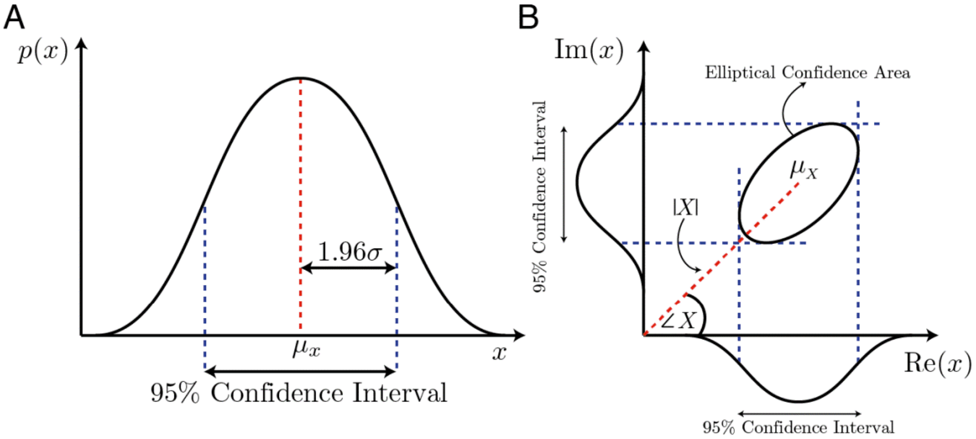

Figure (5.3): The uncertainty in a complex variable can be represented by a bivariate normal distribution creating an elliptical uncertainty area in the real imaginary space. A) The probability distribution of a real-valued univariate variable with its 95% confidence intervals. B) The elliptical confidence area of a complex variable represented by a bivariate normal distribution. Adopted from (Jacobs et al., 2018)

When we rely on a single set of fixed parameter values despite the presence of uncertainty, it becomes challenging to assess the reliability of the model results. Uncertainty quantification is essential in accounting for the effects of uncertain parameters and determining the level of confidence we can place in the model output (Deletic et al., 2012). By incorporating uncertainty quantification, we can effectively model the inherent variation in system parameters, thereby enhancing our understanding of how these uncertain parameters influence the model output. Moreover, conducting an uncertainty quantification allows for more informative comparisons between two model outputs or between model output and experimental results, as we gain insight into the distribution of the model output and can quantify their similarity or dissimilarity (Marino et al., 2008).

Sensitivity analysis plays a crucial role in understanding the relationship between input variables, parameters, and model outputs, providing valuable insights into how each parameter impacts various aspects of the model. It guides experimental focus by identifying parameters with high sensitivity, requiring accurate measurement, while parameters with low sensitivity can be estimated with less precision (Mishra, 2009).

Sensitivity analysis (SA) finds utility in model reduction scenarios and parameter estimation tasks, enabling the identification of parameters that have minimal impact on the variance of the model output, thus allowing them to be fixed at any value within the explored distribution. By leveraging sensitivity analysis and uncertainty quantification techniques, we gain a deeper understanding of the model, enhance the interpretability of results, and make informed decisions about parameter estimation and model reduction strategies (Zi, 2011).

SA methods can be categorized according to their scope, applicability, and characteristics. The two primary classifications are local SA and global SA, which have been widely discussed in the literature (Saltelli, 2004; Saltelli and Annoni, 2010). These classifications provide a basic and commonly used framework for understanding SA methodologies. Analyzing the effects of unknown inputs close to a certain point or base case is the main goal of local SA. Within a specific range, it seeks to comprehend how changes in these inputs impact the model's output. While considering a wider variety of input variations, global SA focuses on analyzing the effects of uncertain inputs over the whole input space. A more thorough knowledge of the system is made possible by Global SA, which offers insights into the general behavior and sensitivity of the model to various input combinations (Tian, 2013).

The Monte Carlo filtering is often coupled with the local sensitivity analysis. The LSA (Local Sensitivity Analysis) generally requires two tasks: (a) a qualitative description of the system behavior and (b) a binary classification of the model output that divides solutions into two behavioral and non-behavioral groups. However, the main drawback of the LSA is that no higher-order analysis is performed and thus interactions between parameters are not investigated.

The 'one-at-a-time' (OAT) method is a frequently employed sensitivity analysis technique in the field of environmental sciences. In this strategy, each parameter's value is changed while the values of the other parameters are held constant (Rezaei et al., 2016; Wesseling et al., 2020). However, the results of an OAT analysis can be inconsistent when a model considers interactions between parameters. This is so that parameter interactions can only be discovered when several parameters are changed at once. As a result, the OAT analysis may not fully account for parameter interactions, producing incomplete and sometimes inaccurate sensitivity estimates. In hydrological modeling applications, global SA (GSA) methods are commonly preferred due to their inherent advantages over local SA methods (Song et al., 2015) and several studies have highlighted their advantages (Baroni and Tarantola, 2014; Makler-Pick et al., 2011). GSA methods offer a broader perspective by considering the entire input space, enabling the identification of parameter interactions and nonlinear effects that may be missed by LSA. GSA provides a more comprehensive understanding of the system's behavior and enhances the ability to capture complex relationships between inputs and outputs.

In this study, a two-step approach is employed for sensitivity analysis. Firstly, LSA is combined with a basic Monte Carlo filtering technique, this last being the chosen protocol for the selection of sets of input parameters. The objective of this step is to identify behavioral regions in the parameter space and reduce uncertainty in the subsequent parameter estimation step using the same sample and runs of the LSA. The objective function (NSE and $RMSE$) values are calculated for each parameter set. Based on these values, potential solutions are divided into two groups: behavioral solutions with $NSE > 0.0$ and non-behavioral solutions with $NSE < 0.0$.

After the filtering step, uncertainty analyses are performed on the filtered sample. The relative cumulative probability distribution is then calculated against the parameter values. Finally, a variance-based method is employed for the sensitivity analysis. Various variance decomposition techniques, such as Sobol's method, the Fourier Amplitude Sensitivity Test (FAST), and the extended FAST methods, can be utilized for this purpose. The variance-based approach is considered global as it simultaneously varies all sources of uncertainties. It is also regarded as a model-free method, as it can compute sensitivity indices without relying on assumptions about the linearity, monotonicity, or other generic properties of the underlying model. Within this approach, the first-order sensitivity indices (Si) and total-order sensitivity indices (ST) are estimated using:

$$S_i = \frac{V[E(Y|X_i])}{V(Y)} \tag{5-1}$$

$$S_T = \frac{E[V(Y|X\sim_i])}{V(Y)} \tag{5-2}$$

In the sensitivity analysis, the first-order sensitivity index (S_i) and total-order sensitivity index (S_T) are used to quantify the importance of input variables. The notation $X\sim_i$ represents the array of all inputs except for the variable X_i. The variance (V) and expectation (E) operators are used in the calculations. Higher values of S indicate higher sensitivity. First-order sensitivity indices assess the significance of an individual input variable in isolation.

This index quantifies the importance of a single input by itself. Total-order sensitivity indices measure the overall importance of a specific input, considering its interactions with all other possible inputs. Global sensitivity analysis is commonly employed in models that have multivariate or functional outputs. In such cases, conducting separate sensitivity analyses on each output individually or on a few specific scalar functions of the output may not provide sufficient information, as highlighted by Campbell et al., (2006). Instead, it becomes more valuable to perform sensitivity analysis on the multivariate output as a whole. This necessitates the development of criteria and methods tailored specifically for the sensitivity analysis of multivariate or functional outputs.

To perform sensitivity analysis on a multivariate dynamic model, the "multisens" package in R is utilized (Lamboni et al., 2011). This package is specifically designed to handle sensitivity analysis of dynamic models. Since the infiltration rate is a dynamic variable, the "multisens" package offers suitable tools and methods to conduct sensitivity analysis on such models. By using this package in R, researchers can effectively analyze the sensitivity of the infiltration rate in a multivariate dynamic model and gain valuable insights into its behavior and interactions with other variables.

5.2.1.1. Bayesian parameter inference

This approach relies on the idea of integrating a priori knowledge of the system in the statistical inference, to combine it with the observed data (i.e., measurements of soil water content, matric potential, and outflow) to derive the posterior probabilities of model parameters. In a hydrologic context, this method is admirably suited for systematically addressing and quantifying the various error sources within a single cohesive, integrated, and hierarchical manner (Vrugt et al., 2003; Liu and Gupta, 2007).

The Markov Chain Monte Carlo (MCMC) methods or Bayesian inversion have been given more attention over the past decades by geophysicists and soil physicists for soil parameter derivation. It is the preferred model for both optimization and uncertainty estimation (Sambridge and Mosegaard, 2002). The inverse problem is solved by incorporating both prior knowledge of the model and observed data, resulting in a posterior probability density function (PDF) for the model parameters. This PDF is considered the "complete solution" to the problem (Gelman et al., 2013). In addition, it is a controversial issue as to whether prior information can be adequately represented probabilistically (see Scales and Snieder [1997] and Gouveia and Scales [1998] for a discussion). Note that probabilistic prior information is often called “soft” and differs from strict inequalities on the model parameters, which are referred to as “hard” prior information. Within a Bayesian context, then, the emphasis is less on optimization and more on sampling the most probable regions.

In contrast to the MCI model utilized earlier in this study, the Bayesian approach employs important sampling to identify the most probable regions of parameter space based on the posterior PDF. While the MCI model focused on exploring the acceptable regions of parameter space as defined by data and prior constraints (Sambridge and Mosegaard, 2002). In the context of an optimization framework, the results of the GSA can be used to extract useful information about the problem structure. The GSA preliminarily identifies the subset of input factors that drive most of the variation in the model output; to establish their optimal values, these sensitive parameters can be further investigated by using a Monte Carlo filtering approach. Filtering techniques are used to explore the parameter space about the single or multiple optima. This is particularly relevant when dealing with mechanistic models that almost always contain ill-defined parameters and are thus referred to as overparameterized models (Draper and Smith, 1981).

In this study, we employed the Markov Chain Monte Carlo (MCMC) of Bayesian inference. The MCMC approach generates candidate samples independently, allowing for easy distribution of sampling across multiple processors. The Metropolis algorithm, the foundation for many MCMC samplers, is a simple yet effective method for generating samples (Liu, 2001). In the Metropolis algorithm, samples are generated from a proposal distribution, and a probabilistic decision is made to accept or reject each candidate sample based on its probability relative to the current state of the process. The procedure for generating samples using the proposal PDF is:

Algorithm: Rejection sampler

```
• For $i = 1,2,3, \dots, N$
repeat
    1. Generate $\theta'$ from the prior distribution $\mathrm{P}(\theta)$
    2. Simulate $Y$ from the model, $Y = \mathrm{H}(\theta'|.)$
    3. Where $\epsilon \to 0$
Until the distance function is smaller than $\epsilon$
    $\boldsymbol{\rho}(\boldsymbol{S}(\widehat{\boldsymbol{Y}}), \boldsymbol{S}(\boldsymbol{Y}(\boldsymbol{\theta}))) = \left|\boldsymbol{mean}(\widehat{\boldsymbol{Y}}) - \boldsymbol{mean}(\boldsymbol{Y}(\boldsymbol{\theta}))\right| \leq \boldsymbol{\epsilon}$
Set $\theta_i = \theta'$
    End for
```

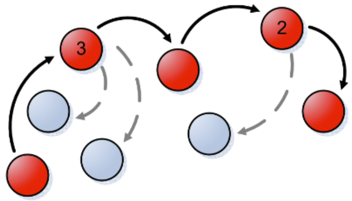

Figure (5.4): Metropolis algorithm schematic: The depicted image demonstrates how the Metropolis algorithm generates samples using a random walk. The samples that are rejected are displayed in gray. If a candidate sample gets rejected, the current sample in the Markov chain is duplicated, and the frequency of duplicated models is indicated by the numbers.

If the probability of the target for a candidate sample is higher than that of the current sample, it will be accepted. Nevertheless, even if the probability is lower, it could still be accepted based on the value of a random variable. This characteristic permits the random walk to transition between peaks of a multimodal posterior probability density function (PDF) by accepting both better and worse models.

The plausible prior range of all evaluated parameters is shown in Table (5.1) for the studied *CH* models. Generally, increasing the number of parameters in a model can improve its goodness of fit, regardless of the model's complexity (Brunham 2002). However, this also increases the uncertainty or variance of the model. To strike a balance between the bias and variance of a model, the principle of parsimony dictates that the model should have "the smallest possible number of parameters for adequate representation of the data" (Anderson and Burnham, 2004). Therefore, in the present study, some available and obtained parameters are fixed for modeling, but the parameters that should be optimized in the response spaces are assumed to vary in the following priority range mentioned in Table (5.1).

Table (5.1): Ranges of parameters used in the Bayesian computation.

Fixed (Soil parameters measured on the field)						**Variables**							
Experiment	**ha [mm]**	θ_s	θ_i	θ_r	τ	$K_s\ [mm/h]$		m		θ_i(CH3)		$h_g\ [mm]$ (GA)	
ENTPE1_1	58	0,5184	0,3778	0	0.5	Lower	Upper	Lower	Upper	Lower	Upper	Lower	Upper
ENTPE1_2	75	0,5184	0,3778	0	0.5	30	10000	0,0476	0,8	0	0.51	2900	30000
ENTPE1_3	53	0,5184	0,3778	0	0.5								
ENTPE2_1	30	0,5184	0,4001	0	0.5								
ENTPE2_2	53	0,5171	0,4001	0	0.5								
ENTPE2_3	83	0,5171	0,4001	0	0.5								

The Bayesian statistical analysis developed for this thesis was run using the MCMC function in the R package MCMC DREAMzs algorithm (Markov chain Monte Carlo) (Joseph and Guillaume, 2013). Two Markov Chains were simultaneously executed, each comprising 60,000 iterations, following the specification of a prior distribution for the parameters. Running multiple Markov chains (usually more than 1 chain for simpler models) is recommended to explore the entire range of possible parameter values.

The Bayesian method generates a sequence of samples for the parameter values in each iteration. It considers the previous result to generate a new sample that is closer to the observations based on the range of possible parameter values. This enables the method to update its prior guess about the parameters to the posterior, considering the new data (van de Schoot et al., 2021). The algorithm first sets a prior distribution for each parameter and then selects a value from these distributions for each parameter. Next, the algorithm uses one of the models (*CH1*, *CH2*, *CH3*, GA) to compute data. After this, the likelihood of this set of parameters is determined by calculating the probability of the difference between the simulated and observed data. To accomplish this, the appropriate probability density function is used to represent the distribution of differences more accurately, and the normal distribution is commonly selected as there is limited prior information available. Finally, the posterior distribution is obtained by multiplying the prior distribution by the likelihood function and normalizing the result. The resulting distribution is referred to as the posterior distribution. The Markov chain will reach a stable state where the parameter values remain within the stable distribution. The initial iterations of the chain before reaching its steady-state distribution are typically disregarded, which is referred to as “burn-in”(van de Schoot et al., 2021).

Achieving convergence to the desired distribution is crucial for obtaining precise estimates of parameter values. Theoretically, a chain's duration in a particular area of the parameter space will be proportional to its posterior probability. Thus, a chain that is long enough and exhibits good behavior will closely approximate the posterior distribution. To ensure that the algorithm is functioning correctly, and since we are limited in practice by the finite number of iterations, we execute multiple chains and verify that they all converge to the same distribution, despite being initialized with different starting values (Muth et al., 2018). Running multiple independent chains can help identify potential convergence issues and ensure that the MCMC algorithm effectively generates samples from the target distribution.

5.2.1.1.1. Model evaluation

To determine the parameters of the (*CH1, CH2, CH3, GA*) models, we need to run the MCMC approaches code with two chains and 60,000 iterations. The convergence of the models can be assessed by examining the R̂ diagnostics, which should be greater than one for all chains, and the experimental data from the infiltration test. The Gelman Rubin statistic, $\hat{R}$ −Statistics the potential scale reduction factor is the most frequently used method to evaluate the convergence of a Markov chain to its stationary distribution. This statistic measures the ratio of the within-chain variability to the between-chain variability (Gelman et al., 2013), considering N different chains. This diagnostic compares for each parameter j ¼ {1,…,d} the within-chain (Gelman and Rubin, 1992):

$$W_j = \frac{2}{N(T-2)} \sum_{r=1}^{N} \sum_{i=[\frac{T}{2}]}^{T} (X_{i,j}^r - \bar{X}_j^r)^2 \qquad \bar{X}_j^r = \frac{2}{T-2} \sum_{i=[\frac{T}{2}]}^{T} X_{i,j}^r \tag{5-3}$$

and between-chain variance:

$$B_j/T = \frac{1}{2(N-1)} \sum_{r=1}^{N} (X_{i,j}^r - \bar{X}_j^r)^2 \qquad \bar{X}_j^r = \frac{1}{N} \sum_{r=1}^{N} X_j^r \tag{5-4}$$

Using:

$$\hat{R}_j = \sqrt{\frac{N+1}{N} \frac{\widehat{\sigma_+}^{2(j)}}{W_j} - \frac{T-2}{NT}} \tag{5-5}$$

Where T signifies the number of samples in each chain, and $\widehat{\sigma_+}^{2(j)}$ is an estimate of the variance of the jth parameter of the target distribution:

$$\widehat{\sigma_+}^{2(j)} = \frac{T-2}{T} W_j + \frac{2}{T} B_j \tag{5-6}$$

To officially declare convergence, the value $\hat{R}_j \leq 1.2$ for each parameter, j ∈{1,…,d}, the value of T should be increased and the chains run longer. As the N different chains are launched from different starting points, the $\hat{R}$ −Diagnostic is a relatively robust estimator. If this is not the case, increase the value of T and run the chains for a longer period. The $\hat{R}$ −Diagnostic is a fairly robust estimator since the N chains are initialed from different starting points (Vrugt, 2016).

If the behavior and convergence of all chains are similar, then the variance between the chains is expected to be approximately equal to the average variance within chains, resulting in an estimated $\hat{R}$ Close to 1. In practice, it is commonly recommended that $\hat{R}$ be less than 1.1 for all model parameters, which indicates that the model has converged. Failure to achieve convergence may result from insufficient iterations. If increasing the iterations fails to resolve the issue and non-convergence persists, it may be due to poor parameter initialization or a need to reconsider and revise the model.

Once convergence and sampling quality have been assessed by R̂ diagnostics, the posterior predictive fit of the model should be verified. This can be achieved by using the efficiency criteria function. The posterior prediction of the model parameters should be compared with the measured data to conclude the efficiency of the model and its fit to the data. Many verification criteria can be checked to confirm that the parameters give the best fit. The most commonly used in hydrology are the *NSE-Sutcliffe* model efficiency criteria (*NSE*), Normalized Root Mean Square Errors (*NRMSE*), the coefficient of determination (R^2), and the P-Bias indicator (*PBIAS*) are studied:

$$NSE = 1 - \frac{\sum_{i=1}^{n}(O_i - S_i)^2}{\sum_{i=1}^{n}(O_i - \bar{O})^2} \qquad NRMSE = \frac{\sqrt{\frac{1}{n}\sum_{i=1}^{n}(O_i - S_i)^2}}{\sqrt{\frac{1}{n}\sum_{i=1}^{n}(O_i - \bar{O})^2}} \tag{5-7}$$

$$R^2 = \frac{cov(O,S)^2}{V(O)V(S)} \qquad PBIAS = 100 * \frac{\frac{1}{n}\sum_{i=1}^{n}(S_i - O_i)}{\bar{O}}$$

$$CRMSE = \sqrt{\frac{1}{n}\sum_{i=1}^{n}[(O_i - \bar{O}) - (S_i - \bar{S})]^2}$$

Where S_i is the simulated value, O_i is the observed value, $\bar{O}$ is the mean observed value and n is the number of simulations. The δ_s and δ_O are the standard deviations of the simulated and observed data, respectively. The coefficient of determination, R^2, is the square of the Pearson correlation (R). The maximization of the *NSE* coefficient corresponds to the minimization of the difference between observed and simulated values; it describes the model's dynamic. As for the *NSE* coefficient, the R^2 value for a perfect fit is 1.

On the contrary, *NRMSE* and *PBIAS* give values in percent, and the perfect fit would give a value of 0% for both criteria. The *PBIAS* criterion indicates whether the model is underestimated or overestimated on average compared to the observed data, while the *NRMSE* criterion describes the distribution of errors in the model (regarding the modeled data). If the value of *PBIAS* is negative, the model underestimates the observation. Conversely, if it is positive, the model overestimates the observations. According to (Moriasi et al., 2015), a value of *PBIAS* inferior or equal to 10%, between 10% and 15%, denotes very good and good respectively, and over 25% is unsatisfactory. For the *NRMSE* criteria, a value inferior to 60% is considered valid. The centered root-mean-square error (C*NRMSE*) difference between the simulated and observed patterns is proportional to the distance to the point on the x-axis identified as "observed."

Finally, a visual approach to quickly assess the model's validity with its optimal parameters is to superimpose the observed and simulated data on a graph and assess how well they overlap. This last method is the best to assess the capability of the model to simulate the dynamics of the process. However, it shouldn't be the only way to check the optimization.

5.3. Result and discussion

5.3.1. Assessment of uncertainty and sensitivity

The *CH1, CH2, CH3*, and Green Ampt models were estimated using the Monte Carlo algorithm for over 60,000 iterations. For the event ENTPE2-2, the *NSE, PBIAS*, and *NRMSE* were calculated for the ensemble of iterations, comparing the simulation results to the measurement data. The uncertainty analysis was performed for the input series that resulted in

NSE values greater than 0 (behavioral solutions), using the multivariate Student's t-distribution, as depicted in the Figure (5.3). The figure also illustrates the statistical scores for the infiltration rate estimated by different models and parameter sets. The selection of parameter sets was performed using a Monte Carlo method based on a normal distribution for all the parameters. The inversion results obtained through the Monte Carlo approach for the *CH1* model in the behavioral space solution had an average *NSE* of approximately 0.073, an uncertainty ellipse spanning two standard deviations with a length of about 0.15, and a mean *NRMSE* of around 95 mm with an uncertainty of about 9 mm. These findings suggest that the *CH1* model is not a suitable choice for modeling infiltration. The ellipse, or probability contour, is in the Figure (5.5). represents the parameter sets encompassing a 95% probability under the assumption of a normal distribution. This depiction visually illustrates how the ranges, lengths, and orientations of the ellipses change depending on the chosen confidence level and the specific model. The confidence ellipses, based on the provided confidence levels, can be employed to assess the bivariate Normal nature of a given distribution (Friendly et al., 2013). The uncertainty analysis of the model was conducted using the Monte Carlo approach, which involved selecting random input values. These inputs, which may include parameter values, were then utilized in a model or transfer function to obtain distributions or statistical measures of the resulting outputs. Uncertainty analyses are commonly employed to make general inferences, such as estimating the mean and standard deviation of the outputs, determining the probability of a performance measure surpassing a specific threshold, assigning a reliability level to a function of the outputs (e.g., the range of function values likely to occur with a certain probability), describing the likelihood of different potential outputs from the system, and estimating the relative impacts of uncertainties in input variables (Ghanem et al., 2017; Liu and Gupta, 2007; Wesseling et al., 2020).

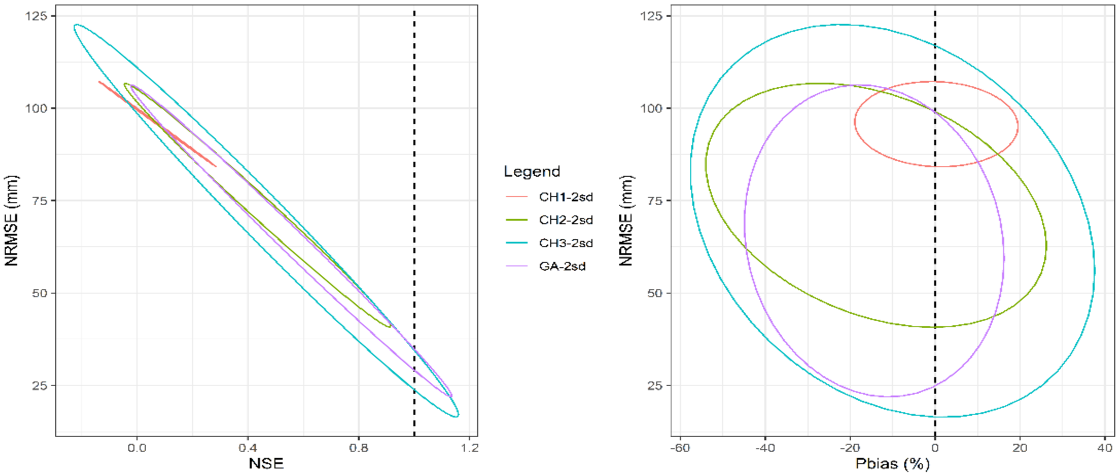

Figure (5.5): The depiction of confidence (error) ellipses at a confidence level of 95% or (2*Standard deviation). These ellipses are generated based on the cases where the random variables are obtained using the Monte Carlo algorithm for experiment ENTPE 2-2. Each model approach is represented by ellipses, which follow the multivariate Student's t-distribution according to (Fisher, 1970)

In this study, behavioral output results were specifically chosen for uncertainty assessment. The obtained output distributions can describe the potential range of outputs that the system may produce at a certain probability level and provide the probability of the output exceeding a specific threshold or target performance measure.

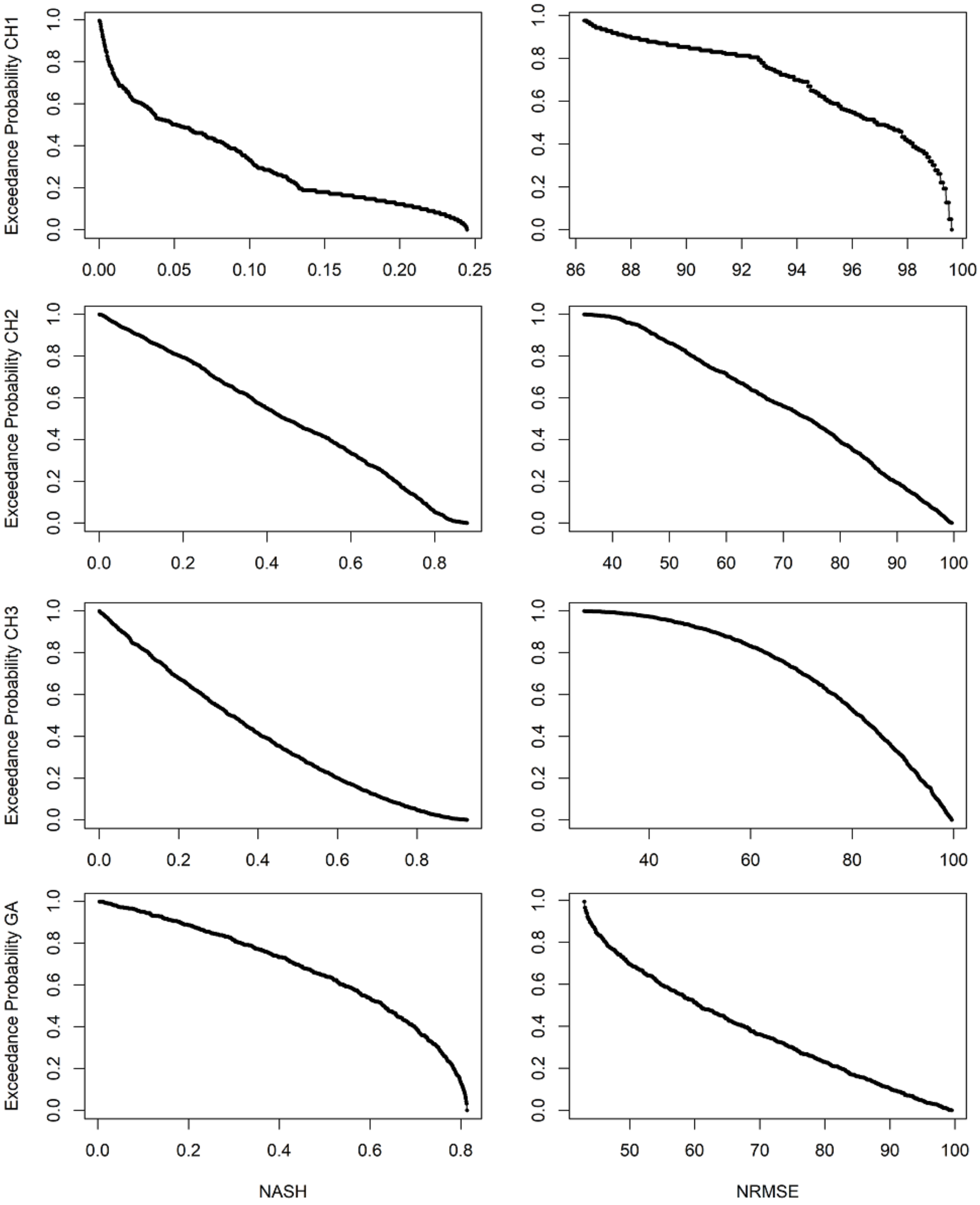

Figure (5.6): Uncertainty and exceedance probability distribution curve of a range of potential values and the likelihood parameters range for *CH1*, *CH2*, *CH3,* and *GA* models, in this figure NASH=NSE and exceedance probability is defined as the probability of the statistics values exceeds a given value “x”: Fc(x) = P(X > x)

Figure (5.6) illustrates that both models *CH2* and *CH3* have an equal probability of achieving an *NSE*-Sutcliffe Efficiency (*NSE*) greater than 0.7. On the other hand, the *GA* model consistently demonstrates a higher probability of achieving an *NSE* greater than 0.75. It is important to note that the maximum *NSE* value achievable is approximately 0.8 for the *GA* model. However, for *NSE* values greater than 0.8, the results show even better performance for models *CH2* and *CH3*. Then the set of parameters which are chosen for each model, are evaluated regarding the data.

To provide a summary of the results, Taylor diagrams are utilized to assess the level of agreement between the modeled and observed data, based on three statistics: the Pearson correlation coefficient, the centered root-mean-square error, and the normalized standard deviation. These scores are calculated for all infiltration events, resulting in a single value for each model (*CH1*, *CH2*, *CH3*, and GA). Their values provide a global assessment for all the infiltration tests.

Normalized standard deviation of models *CH2* and *CH3* reveals that their results are very close. However, model *CH3* demonstrates an improvement when comparing the normalized standard deviation and the centered root mean square score. This suggests that model *CH3* performs better in terms of capturing both the variability and overall agreement with the observed data. By comparing the Taylor diagrams (as shown in Figure (5.7)) and considering the statistics presented in Table (5.2), it is evident that the *CH3* and *GA* model approaches accurately replicate the infiltration rate curve with similar precision. The parameters used for producing the simulation reaching the best score are presented in Table (5.3). These parameters can be considered as optimized parameters.

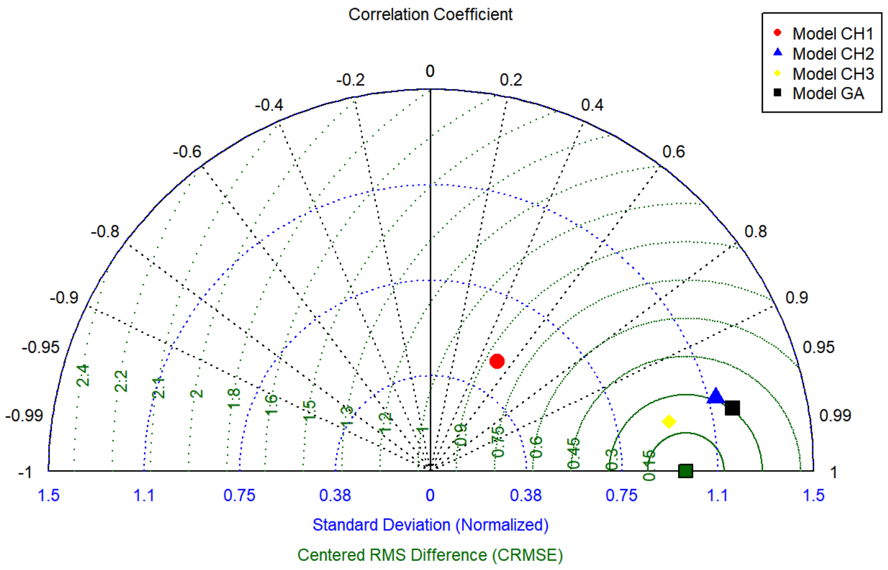

Figure (5.7): Taylor diagrams for infiltration rate modeling by *CH1*, *CH2*, *CH3,* and *GA* models. The Pearson correlation coefficient, the centered root-mean-square error (CRMSE), and the normalized standard deviation are summarized in this diagram. The perfect situation is represented by the green square

Table (5.3): Parameters chosen via model calibration within the Monte Carlo approach (max NSE)

	Model	θ_s	K_s (mm/h)	m	tau	θ_i	h_a(mm)	Z_{soil} (mm)	NSE
ENTPE2_2	*CH1*	0.5171	4952.601	0.5	0.5	0.45	53	2576	0.24
	CH2	0.5171	232.85	0.5	0.5	0.448	53	9254.7	0.91
	CH3	0.5171	55.93	0.5	0.5	0.45	53	4757.56	0.95
	GA	0.5171	90.13	0.5	0.5	0.45	53	-	0.81

After considering the score, consistency, and uncertainty analysis of the chosen parameters, sensitivity indices for each parameter were examined using the FAST method. The global sensitivity analysis results revealed that in the *CH1* model, the parameter Z_{soil} exhibited high sensitivity (Figure (5.8) and However, overall, the CH2 model exhibited higher sensitivity to K_s. Regarding the CH3 model, as mentioned earlier, K_s was identified as the most important parameter in terms of sensitivity, followed by soil layer depth as the second influential parameter. Table (5.4). During the primary sensitivity analysis, it was noted that while holding all other factors constant, variations in Z_{soil} had an insignificant influence on the model's results. Nevertheless, in conjunction with other parameters, Z_{soil} exhibited a noteworthy impact on the model's output. Notably, the model demonstrated low sensitivity to parameter m, with a global index of <0.1.

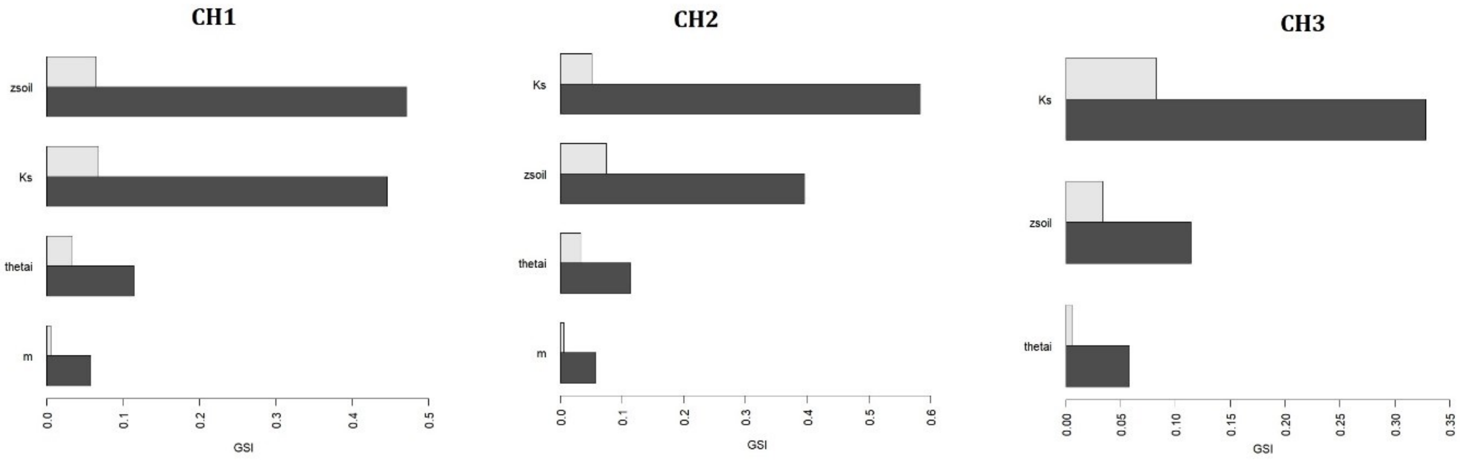

Figure (5.8): Global and main sensitivity analysis results for the *CH1*, *CH2*, and *CH3* models. The light grey pattern represents the main sensitivity or analysis or first-order indices, while the dark grey color represents the global sensitivity analysis or total indices

In contrast, the *CH2* model was highly sensitive to hydraulic conductivity (GSI>0.4), and soil layer depth was the most influential parameter for both the *CH2* and *CH1* models (GSI>0.5). Specifically, for the *CH2* model, the sensitivity index (MSI) for soil depth was higher than that for hydraulic conductivity. However, overall, the *CH2* model exhibited higher sensitivity to K_s. Regarding the *CH3* model, as mentioned earlier, K_s was identified as the most important parameter in terms of sensitivity, followed by soil layer depth as the second influential parameter.

Table (5.4): Global and main sensitivity analysis indices for the *CH1*, *CH2*, and *CH3* models.

Model	Parameters	Main sensitivity indices	Total sensitivity indices
GSI ***CH1***	Z_{soil}	0.0553	0.5557
	K_s	0.0544	0.5490
	θ_i	0.0333	0.1143
	m	0.0053	0.0580
GSI ***CH2***	Z_{soil}	0.0740	0.5830
	K_s	0.0511	0.396
	θ_i	0.0333	0.114
	m	0.0053	0.058
GSI ***CH3***	K_s	0.0823	0.328
	Z_{soil}	0.0333	0.114
	θ_i	0.0053	0.058

The model did not show significant sensitivity to θ_i (GSI<0.1), which aligns with the findings of the *CH2* model. Consequently, during the calibration of the model (performed in the previous section), parameters $m = 0.5$ and θ_i were kept fixed, since they have very little impact on the model, and thus estimating them by inverting data would lead to very imprecise estimations.

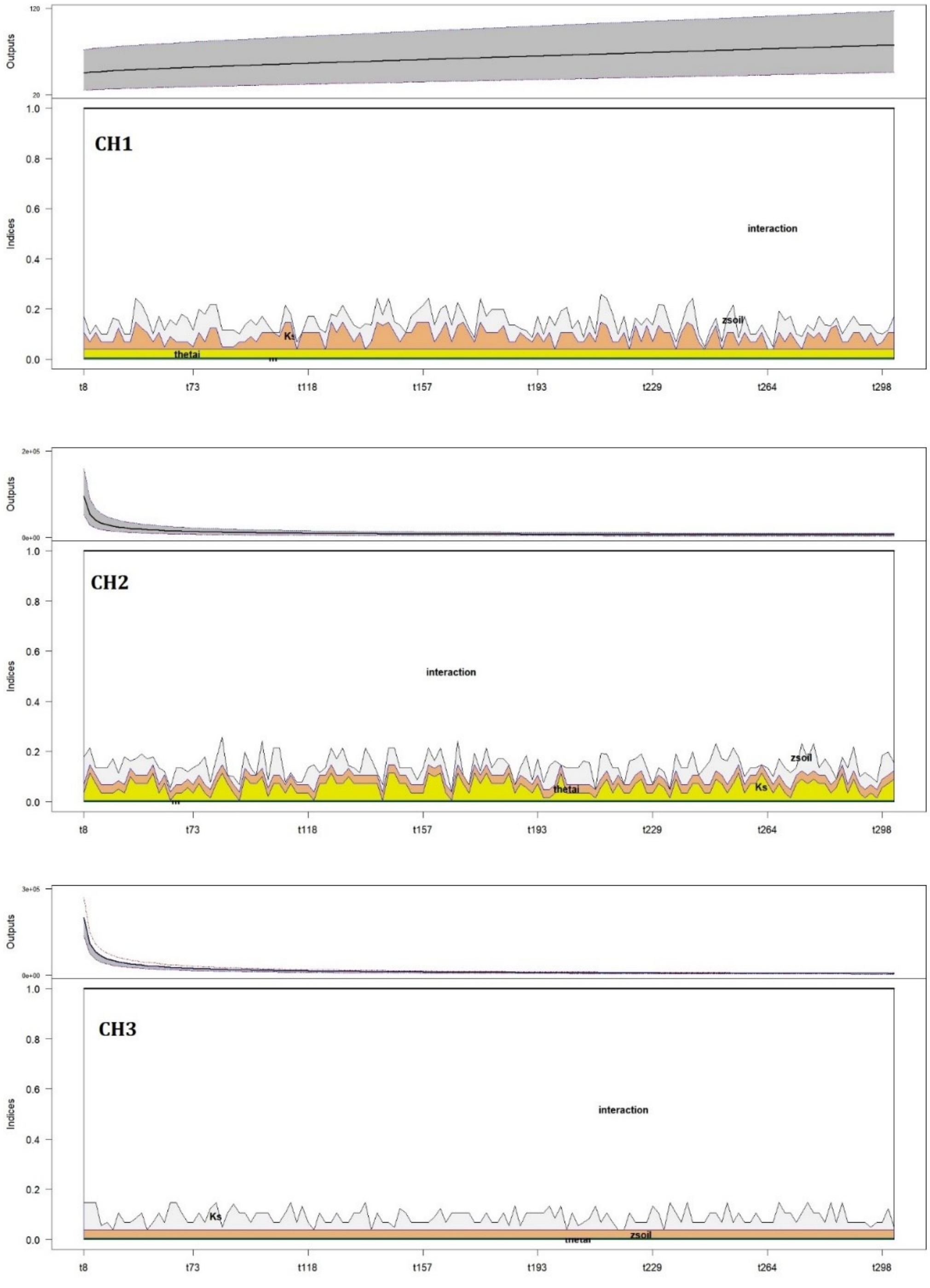

Figure (5.9): Evolution of the FAST main sensitivity indices of the three-infiltration model (*CH1, CH2,* and *CH3*) model from I = 8mm to I = 298mm. The upper subplot shows the extreme, inter-quartile (grey), and median (bold line) output values at all time steps. The lower subplot represents the sensitivity indices at all time steps for the main effects and the first-order interactions

These results of model sensitivity for model *CH3* for Dual-Permeability porous media are presented in the Chapter 4. These results are consistent with the sensitivity assessment of the *CH3* model for simple permeability, where it was found to be sensitive to K_s and particularly to $K_{s,f}$, the hydraulic conductivity of the fracture compartment in spatial terms. To assess the sensitivity of the model to parameter selection, we conducted Bayesian inference on the model parameterization. This approach was employed to mitigate the uncertainty associated with model parameterization and improve its accuracy for *CH1, CH2, and CH3* in simple and *CH3* in dual-permeability.

5.3.1. Bayesian inference applied to the studied models

The parameters were estimated using 60,000 iterations using the MCMC algorithm. A range for each parameter is given in Table (5.1). To verify the estimates' reliability, the MCMC samplers' convergence must be confirmed. The convergence of each model was assessed using the Gelman and Rubin criterion. The results presented in Table (5.5) indicate that the parameters estimated by Bayesian inversion converge for *CH1, CH3*, and *GA* in all experiments, as their values are less than (1.1). However, there was no convergence for the *CH2* model in any of the experiments. The non-convergence can be due to poor parameter initialization or due to too few iterations (van de Schoot et al., 2021). For this purpose, the number of iterations is increased with more iterations (200,000) in the case (one experiment, ENTPE1_2), but the Gelman value remained above ($R^2 \geq 1.1$), which indicates the non-convergence of MCMC model. These non-convergences are then attributed to an overly restricted prior parameter range, specifically the z_{soil} parameter which has a prior range of 2900 to 30000 mm. A range of at least 2900 mm is necessary for the correct functioning of the *CH2* model and the avoidance of errors in the calculation of q_{CH2}. Additional investigations would be required to change the strategy of variation of model parameters.

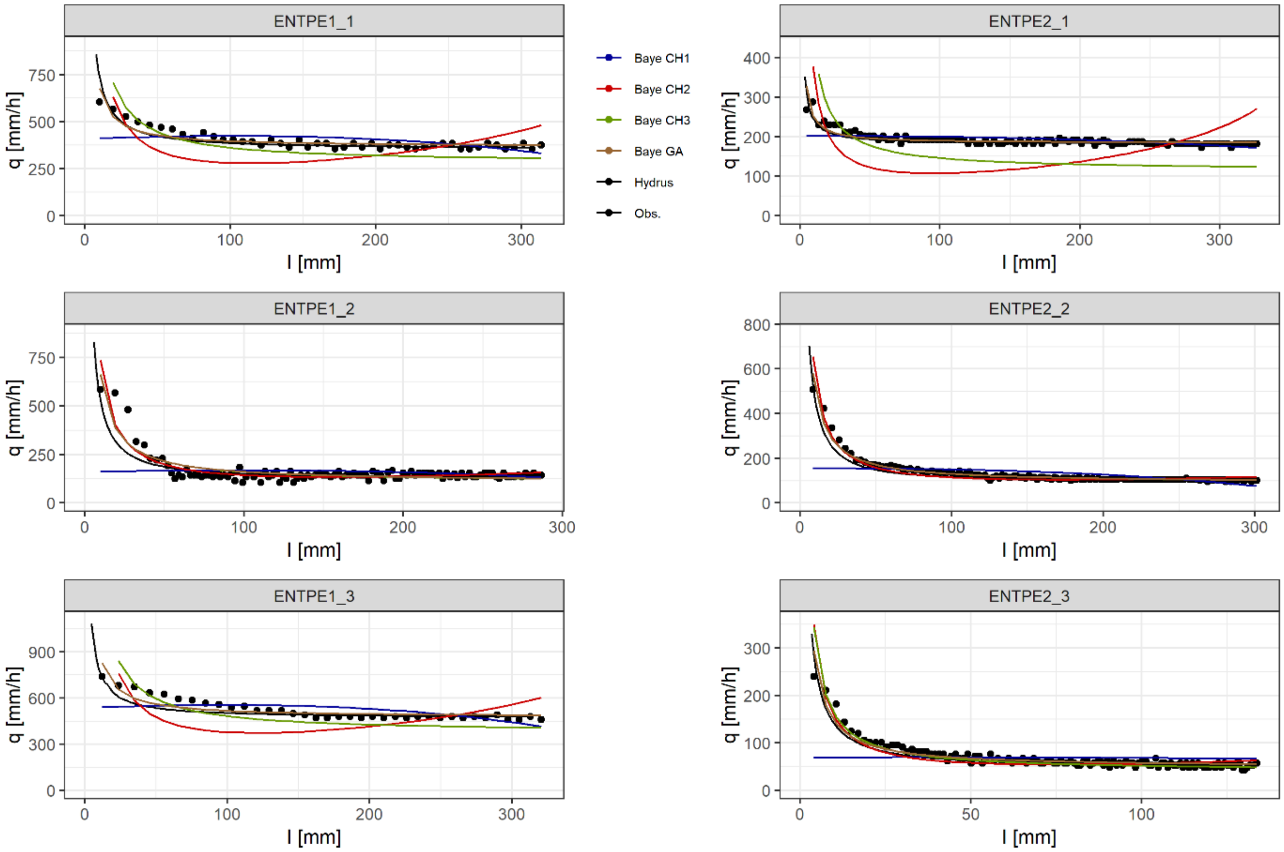

Figure (5.10): curve fit for the optimized parameters by using the Bayesian inference

The *CH1* model cannot correctly capture the infiltration curve spatially for the recession phase or the decrease remains very slight or negligible. As a result, the improvement in terms of shape can be considered to be marginal, with a shape that is still not adequate. This first phase describes the water that quickly infiltrates into the soil because it has not yet reached saturation, and the hydraulic gradient is high at the beginning of the experiment. Conversely, the pattern described by the *CH1* model is likely to occur where there is an exceptionally high degree of water repellency or water infiltration into hydrophobic soils (Abou Najm et al., 2021), but not for water infiltration under regular conditions. As depicted in Figure (5.10), the *CH2* also, as the *CH1* model, presents a pattern that is not valid for representing the transient state of water infiltration. The typical shape of the *CH2* model involves a two-step decreasing-increasing pattern, that could be more in line with water infiltration into soils with weak water repellency, as observed in water-repellent stratified profiles by Beatty and Smith, (2013). It can be seen in the cases of experiments ENTPE1_1, ENTPE1_3, and ENTPE2_1 in Figure (5.10). *CH3* and *GA* models are those that best describe the observed data in terms of infiltration curve shape: at the beginning, the infiltration rate is high, then decreases as the soil becomes saturated to reach a constant rate at saturation (K_s). These differences in shape will be taken into account in the interpretation of verification criteria. Table (5.5) presents the results with 60,000 iterations and a computation time of 25 minutes. Note also that we have investigated the dual-permeability behavior and its capability to improve the fits (See Chapter 4).

Table (5.5): Result of the optimization process with Bayesian inference (60 000 iterations)

		NSE	*NRMSE* (%)	*PBIAS* (%)	R^2	Gelman	K_s mm/h
ENTPE 1-1	*CH1*	0.125	92.500	0.000	0.138	1.011	4743.572
	CH2	-3.011	198.100	-8.200	0.367	1.215	749.658
	CH3	-1.694	162.400	-7.300	0.812	1.018	278.597
	GA	0.812	43.000	0.000	0.812	1.003	365.804
	Hydrus	**0.714**	**52.900**	**-2.300**	**0.794**	**N.A.**	**351.000**
ENTPE 1-2	*CH1*	-0.007	99.900	-0.400	0.188	1.010	1927.787
	CH2	0.786	46.100	-0.700	0.787	1.334	545.954
	CH3	0.756	49.200	0.100	0.756	1.009	106.809
	GA	0.756	49.200	0.000	0.756	1.003	106.809
	Hydrus	**0.703**	**54.300**	**-3.900**	**0.774**	**N.A.**	**128.000**
ENTPE 1-3	*CH1*	0.236	86.200	-0.100	0.246	1.011	6259.952
	CH2	-2.950	196.000	-7.500	0.290	1.246	804.389
	CH3	-1.292	149.300	-5.800	0.766	1.013	372.892
	GA	0.766	47.800	0.000	0.766	1.005	474.446
	Hydrus	**0.671**	**56.500**	**-3.300**	**0.764**	**N.A.**	**468.000**
ENTPE 2-1	*CH1*	0.259	85.600	-0.100	0.260	1.009	2377.745
	CH2	-18.223	436.300	-16.30	0.230	1.785	294.668
	CH3	-19.079	445.900	-18.90	0.721	1.015	113.883
	GA	0.707	53.800	-0.200	0.721	1.003	183.309
	Hydrus	**0.697**	**54.800**	**-1.800**	**0.735**	**N.A.**	**181.000**
ENTPE 2-2	*CH1*	0.209	88.600	0.000	0.209	1.020	1726.783
	CH2	0.904	30.800	-1.400	0.916	3.494	124.361
	CH3	0.958	20.400	0.000	0.958	1.013	88.722
	GA	0.958	20.400	0.000	0.958	1.007	88.711
	Hydrus	**0.892**	**32.700**	**-6.300**	**0.933**	**N.A.**	**102.000**
ENTPE 2-3	*CH1*	0.030	98.100	-0.500	0.189	1.035	735.870
	CH2	0.746	50.200	-4.600	0.807	1.282	488.243
	CH3	0.832	40.800	-5.200	0.897	1.010	39.555
	GA	0.897	32.000	-0.100	0.897	1.002	47.725
	Hydrus	**0.867**	**36.300**	**-6.100**	**0.888**	**N.A.**	**48.600**

Model fitting to the observed data was carried out to estimate the unknown parameters of the following models using the Bayesian approach. The fit of the model is evaluated according to

NSE, NRMSE, PBIAS and R^2 criteria. The models *CH3* and *GA* perform better than *CH1* and *CH2* in terms of the R^2 criterion, which describes the shape of the model and its agreement with the observed data. R^2 for *CH1* gives a low value on average (0.3) which may be explained by the shape of the curve, which does not simulate the transient phase of water infiltration. The R^2 for *CH2* does not reveal a good fit for experiments ENTPE1-1, ENTPE1-3, and ENTPE2-1. This is due to the slope of the curve at the end of the graph. As the shape is more realistic (closer to a typical infiltration curve) for the remaining experiments, the criterion is increased to 0.9. In each experiment, *CH3* and *GA* have a high value for R^2. This is because these models can follow the shape of the observed curve.

The *NSE* coefficient provides an assessment of the model dynamics. It is a good criterion for comparison with the real curve shape. For example, the *NSE* is never greater than 0.259 and can be negative (-0.007) for the *CH1* model. This result is similar to those provided with R^2. It can be interpreted in the same way. Furthermore, an *NSE* close to 0 means that the simulated values are similar to the mean of the observed values, i.e., the model is not better than assigning the average values at all times and with no gains in terms of explanation of the variable dynamic (time-evolution). *CH1* follows well the steady state phase where most of the observations were made but misses the three or four initial higher values describing the transient state. Another strength of the *NSE* is that it can assess the actual shape of the curve but also considers the difference between estimated and measured values. For example, in experiment ENTPE2_1, the R^2 for the *CH3* model is 0.72, which can lead to the conclusion that the fit is good, whereas the *NSE* is -19, which is a very poor result for this criterion. Whereas R^2 only quantifies the correlations between the model and observations, *NSE* assesses the equality between modeled and observed data. The *CH3* simulation shows a classical shape for the infiltrate curve but completely misses the observations because of its lower value (e.g., Figure (5.10), ENTPE1_1). On the contrary, experiments ENTPE2_2 and 2_3 both have very good results with low values of *NSE* for the *CH2, CH3,* and *GA* models. The *GA* model gives the best results for all experiments with values between 0.707 and 0.958, and it is even better than the Hydrus model in each case.

The *PBIAS* criterion quantifies whether a model tends to overestimate or underestimate observations' averages. For the majority of models, there is a tendency to underestimate the uncertainty associated with their predictions.

Indeed, the *PBIAS* values are predominantly negative (or at least 0). The sole exception is ENTPE1_2, where *PBIAS* stands at 0.1% for *CH3*. For ENTPE2_1, it applies to *CH2* and *CH3*, with 92% classified as excellent (below 10%), while 8% fall within the satisfactory range, encompassing two values ranging from 15% to 25%.

The *NRMSE* is a statistical error indicator that compares the model predictions with the actual values and expresses the difference as a normalized root mean square error. Thus, if the value of *NRMSE* is less than 60%, the model is accurate for this criterion. Table (5.5) shows that *CH2, CH3,* and *GA* have satisfactory *NRMSE* when experiments have many observations. Indeed, the higher *NRMSE* for ENTPE1_3, ENTPE2_2, and ENTPE2_3 is 50%. The criterion rises to 445% for *CH3* in ENTPE2_1 from the time when the tests are less well performed. Regardless of the experiments, it is never less than 60% for the *CH1* model, proving that this model is inadequate.

Based on these findings, *CH1* doesn't model the turnaround well because it completely ignores the decrease during the transient period. Nevertheless, as stated above, it may be used in the case of water-repellent soils with string water repellency. The relevance of the *CH2* model can be questioned by analyzing the curve and the verification criteria. There are many uncertainties. The curve cannot be explained as an infiltration curve because it tends to rise during the saturation phase. Therefore, the very physics of the model needs to be re-examined. This could be investigated in the context of water-repellent soils displaying strong hydrophobicity. A comparison of the *CH3* model to Hydrus and *GA* could be undertaken using a broader set of observations, including ENTPE1_2, ENTPE2_3, and ENTPE2_4 (Figure (5.10) and Table (5.5)).

5.3.2. Assessment of model convergence for parameter uncertainty

KDE (Kernel density estimation) plots are employed to locate areas with a high density of behavioral solutions. This is accomplished using a non-parametric probability density function (PDF) estimator for a given random variable (Silverman, 1981). Using kernel density estimation, a non-parametric smoothing method that approximates a probability density function, it is possible to compare the prior distribution with the posterior distribution (van de Schoot et al., 2021). We may have a look at the parameter estimation when the optimized parameter results from the Bayesian approaches for the different models are logical or not. In this section, the parameters, i.e., the saturated hydraulic conductivity K_s, have been studied. The range of parameters for each experiment is given in Table (5.5) to allow comparison with Hydrus.

The range of K_s According to Hydrus is between 48 and 351 mm/h. Bayesian inference using the *CH1* model gives a minimum of 736, and a maximum of 6259 mm/h, for the 6 experiments Table (5.5) which is not realistic compared to the reference value obtained by (Carsel and Parrish, 1988), for example, and has a saturated hydraulic conductivity of 290 mm/h, which is one of the highest possible values. The values of K_s for *CH1* are therefore overestimated, as the model struggles to compensate for the missing recession phase, and K_s has to be increased substantially to produce a curve close to the observations. The straightforward calculation of uncertainty bounds is one of the advantages of Bayesian inverse modeling. The probability distribution of K_s Figure (5.11) provides information on the uncertainty of the parameter. The *CH2* overestimates the K_s in most of the experiments with a minimum of 124 and a maximum of 804 mm/hr. Finally, *CH3* is the model that tends to agree more with those obtained using Hydrus and *GA*. The saturated hydraulic conductivities calculated range from 40 mm/h to 373 mm/h. These findings seem correct and in accordance with the Hydrus model, considered as the reference data. The uncertainty in K_s for *CH3* and *GA* is significantly lower than for *CH1* and *CH2*, as can be seen from the previous results. The kernel prior and posterior distribution for K_s are illustrated below for one infiltration experiment for the four models Figure (5.11). This figure shows that the posterior distribution of K_s for *CH1* model is narrow and presents only one peak, but the density remains low (0.03), indicating that the model doesn't fit the observation. In the posterior probability distributions of the *CH3* and *GA* models (depicted in subfigures b and c), a prominent single peak of dense concentration (falling between 3 and 3.5) is evident. This signifies the program's strong confidence in the computed values and affirms the alignment of prior knowledge with the recently acquired data. It is consistent with the performance of *CH3* and *GA* models, as discussed Table (5.5) previously. K_{s-CH2} is more uncertain because its posterior distribution is not clustered with several peaks Figure (5.11 b). The shape of the distribution is an indication of the lack of convergence in the estimation process. The results of this model are also less reliable as the density is lower (around 0.0012).

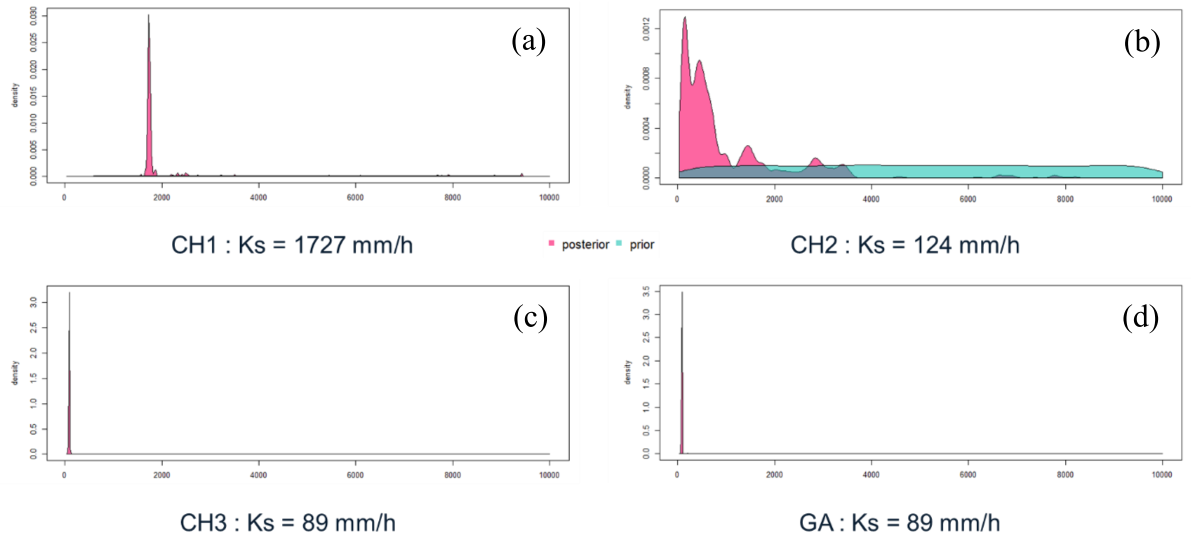

Figure (5.11): Distribution of probability on prior (green) and posterior (pink) values of K_s for experiment ENTPE2_2 with *CH1* (a), *CH2* (b), *CH3* (c) and *GA* (d)

5.4. Conclusions

The study focuses on conducting an uncertainty analysis of both parameterization and output sensitivity for the INFILTRON-Mod package model. The research initiates by investigating the model's behavior with simple permeability to comprehend uncertainties tied to model validity and potential errors in model fitting. The findings indicate that model *CH1* demonstrates limited behavioral response while models *CH2*, *CH3*, and *GA* exhibit acceptable behavioral responses within the same number of iterations. On the other hand, the *CH1* model lacks certainty due to its oversimplified nature, struggling to capture the physical process of the exponentially decreasing infiltration rate. This limitation is evident in the error estimation shown in the Taylor diagram. The uncertainty surrounding the model is depicted within confidence and exceedance curves, failing to achieve an *NSE* value exceeding 0.2. However, the *CH1* model shows promising estimations for an entrenched bioretention basin with an IWS zone at its base, necessitating further study on hydraulic functionality and model compatibility. In addition, side applications are envisioned for the case of water-repellent soils.

Global sensitivity analysis, utilizing multivariate variance-based FAST analysis was used to evaluate INFILTRON-Mod models' sensitivity to input parameters. This analysis is conducted based on six experiments at the ENTPE campus. The results underscore hydraulic conductivity as the predominant sensitive parameter across all models, with shape parameters (*m*) showing minimal influence thus requiring it to be fixed at a typical value. The analysis exposes strong parameter interactions and nonlinearity in all three models, particularly in the *CH1* and *CH2* models. Among all uncertainty assessments for the simple permeability model considering Zsoil, θ_i, and m, *CH2,* and *CH3* models stand out as robust candidates. Sensitivity analysis emerges as a dependable and computationally efficient preliminary step before model calibration, offering insights before more quantitative Bayesian analysis. It is important to highlight that the *CH2* model yields favorable results when its sensitive parameters (K_s and Z_{soil}) are calibrated. When Z_{soil} remains constant, this model could be a suitable candidate for non-repellent soils. As for the *CH1* model, its specific shape for specific cases points more to the dynamics of water infiltration into water-repellent soils.

Given the models' sensitivity to hydraulic conductivity, as confirmed through Bayesian inference, it is suggested that field quantification of parameters would enhance model calibration precision, although parameter heterogeneity (K_s) remains a challenge (Kanso et al., 2018). Comparing Monte Carlo (MC) inversion with Bayesian inversion for *CH3* model calibration reveals similar outcomes, indicating that these models, despite their simplifications and fewer than 10 parameters, are not ill-posed. Addressing heightened parameter uncertainty requires additional measurements to constrain the model. Bayesian techniques and physically-based optimal experimental design assist in selecting data to minimize model uncertainty, particularly for influential parameters such as hydraulic conductivity, which consistently emerges as the principal influencing parameter.

By combining accurate modeling tools, reliable measurements, and modern statistical techniques, physically-based models may be developed for LID, leading to broader adoption of LID. Future studies should prioritize reducing parameter uncertainty, optimizing data information content, and comprehending uncertainty propagation in Low Impact Development (LID) modeling on a catchment scale. Integrating the INFILTRON-Mod module into watershed-scale models for urbanized basins is then proposed, taking into account the insights gained from parameter uncertainty and sensitivity analyses. Specifically, the *CH3* module could be a valuable addition to the hydrological modeling of urbanized basin slopes, replacing empirical models like Horton and SCS that require calibration with non-physical parameters and thus introducing additional uncertainty.

Chapter 6

General discussion and conclusion

Chapter 6. General discussion and conclusion

Urbanization has the potential to disrupt the natural water cycle in watersheds, emphasizing the importance of implementing SUDS for infiltrating water into soils. SUDS aims to manage stormwater runoff, promote sustainability, and mitigate the adverse effects of impermeabilization and global warming. While watershed-scale modeling provides sustainable solutions for urban environmental issues, site-scale modeling focuses on evaluating SUDS cells and their design implications. Prominent models for urbanized watersheds include SWMM and MUSIC. Improving predictions and stormwater management relies on accurately considering soil infiltration in hydrological modeling. While Richards' equation is comprehensive, it can be quite complex, thus limiting its use and simpler models like Green-Ampt have their limitations. Nevertheless, obtaining Green-Ampt characteristics can still be challenging due to the complexity of soil and dynamic water movement and the difficulty of fixing the GA model parameters properly.

The main goal of this thesis was to create a complete model based on physical equations at the crossroads of Soil physics and Urban hydrology to depict water movement inside the soil filter medium of SUDS. The proposed models make use of easily accessible soil parameters to try to balance simplicity and accuracy.

The research was structured into four chapters: Chapter 2 encompassed a comprehensive literature review. In Chapter 3, a set of physically-based models was proposed and studied with regard to their capability to model water infiltration in SUDS under both direct and indirect modes. Chapter 4 aimed at implementing the dual permeability approach to the models pointed out in Chapter 3 dedicated to single permeability soils, to account for soil microporosity and heterogeneity and subsequent preferential flow paths. The model's sensitivity was examined in Chapter 5 along with parameterization and several calibration techniques. In this last chapter, I highlight the thesis' main conclusions, go over their theoretical and practical implications, and suggest some possible directions for further investigations.

6.1. Summary

6.1.1. Overview of the analysis of infiltration modeling through SUDS

The literature analysis done for this work demonstrates a discrepancy between hydrological modeling of urbanized watersheds and physically-based soil physics models, particularly when it comes to the application of SUDS in response to urbanization and climate change adaptations. Although physically-based urban water management software is theoretically designed based on measurable parameters, it faces difficulties during calibration due to the complexity of measurements, the abundance of parameters, and the incorporation of multiple SUDS in urban catchments. Additionally, the presence of preferential flow paths in SUDS can have a big impact on how pollutants move during infiltration processes and the related risk of groundwater pollution. This study emphasizes the need for improved models for SUDS application and urban water management at the crossroads of soil science and urban hydrological modeling. In general, this research looks at strategies to enhance SUDS infiltration modeling and addresses the difficulties of including soil characteristics and SUDS complexity in hydrological models, which could potentially improve urban water management and planning.

6.1.2. Proposed sets of infiltration models for modeling SUDS

In this chapter, the INFILTRON-Mod module is developed and tested to explore alternative formulations of hydrological infiltration models. The module utilizes a substantial dataset comprising both Hydrus outputs and experimental data of infiltration rates and cumulative infiltration. This physically-based module can be easily calibrated using readily available field data, making it suitable for integration into the hydrological modeling of SUDS.

Based on the framework introduced by Bonneau et al. (2021), which led to the initial CH1 model, two alternative models, CH2 and CH3, were proposed and examined. In a few words, CH2 and CH3 changed the expression of the hydraulic gradient, and CH3 replaced the description of the unsaturated hydraulic conductivity with the value for the saturated hydraulic conductivity. The models were also tested against the Green-Ampt (GA) approach. Furthermore, six infiltration experiments were conducted on campus soil using the twin reservoirs and a large ring infiltrometer setup at the ENTPE campus. While the fits were less satisfactory for 1K, the results indicated the necessity of dual permeability (2K). These outcomes substantiate the credibility of the dual permeability model proposed in this study. Through the evaluation process, it was found that the GA and CH3 models demonstrated the highest accuracy among the studied models, specifically for directly simulating water infiltration into the soil. However, the CH1 and CH2 models exhibited certain limitations and inaccuracies in their direct mode predictions, primarily due to specific design issues related to equivalent hydraulic gradients and conductivity. Despite the shortcomings of the CH1 and CH2 models, they still provide valuable foundations for future development, particularly when simulating water repellence during water infiltration. The CH3 model, which is based on a reformulated GA model, showed significant improvements in both direct and inverse modes. By fixing the equivalent hydraulic conductivity to the saturation hydraulic conductivity, the CH3 model effectively addressed issues with the non-decreasing feature of the infiltration rates predicted by CH1 and CH2.

Nonetheless, there's potential for enhancing the equivalent hydraulic gradient, given the existing disparities between CH3 and reference numerical synthetic infiltration rates. We aim to enhance the physical model by transitioning to the dual permeability approach in our efforts to improve it.

6.1.3. Implementation of the dual-permeability approach to the *CH* model suite

In this chapter, we implemented the dual-permeability approach to the previously designed CH3 model to account for preferential flow. The goal of this method is to improve bioretention basin modeling in terms of soil biological activity (bioturbation and creation of macropores).

The model was evaluated under three saturation circumstances (dry, wet, and medium) and compared to a numerical model using Hydrus to determine its efficacy. In particular for dry and medium initial hydric conditions, the findings showed that the model well reproduced the reference synthetic data. For the validation against real experimental data, we used the same set of experimental data and the reference synthetic data to test the new version of the CH3 model, CH3-2K. The model accurately reflected infiltration, including the position of the wetting front during the process and the impact of preferential flow, by calibrating just two parameters (hydraulic conductivity in matrix and macropores). Following that, the enhanced infiltration model was integrated into the hydrological modeling proposed by Bonneau et al. in 2021, resulting in a considerable reduction in the number of calibration parameters compared to other models such as SWMM or RECHARGE. The only two parameters that must be optimized for this useful and relevant model are the hydraulic conductivity and the depth of soil, and the other parameters are taken from field data that is easily accessible.

The results of the modeling showed marginal improvements in Outflow and interesting gains in simulating the filter water height. Careful consideration was paid to the parameter C_{Out}, which corresponds to the orifice feature, regulates the model's hydrologic performance, and affects the design of bioretention systems. The use of a raised underdrain outflow pipe mimicked a pool-like system, with the outflow coefficient serving as the hydraulic control. Our results also indicate the need for improving the time step. More frequent time steps are advised for reliable observation, to better describe the wetting front's quick arrival time in the internal saturated zones. Smaller time steps may allow a better description of processes, in particular at the beginning of rainfall events.

In general, the chapter introduces a novel method for comprehending infiltration through macropores in soil used in bioretention systems, providing important new information about the efficiency and layout of bioretention systems.

6.1.4. Summary of model uncertainty and sensitivity analysis

The study delves into an uncertainty analysis of parameterization and output sensitivity for the INFILTRON-Mod package model. The initial investigation involves assessing the model's behavior with simple permeability, revealing limitations in model CH1's response and oversimplification in capturing infiltration rate curves. However, CH2, CH3, and GA models display acceptable behaviors. Global sensitivity analysis highlights hydraulic conductivity as a key parameter, while CH2 and CH3 models emerge as robust options in uncertainty assessments. Sensitivity analysis proves useful for preliminary insights before quantitative Bayesian analysis. Field-based parameter quantification is recommended to enhance model calibration precision, despite challenges posed by parameter heterogeneity. Reducing parameter uncertainty and integrating INFILTRON-Mod into urban basin models are recommended, enhancing hydrological modeling. Particularly, the incorporation of the CH3 module holds the potential as a valuable enhancement for the hydrological modeling of urbanized basin slopes.

This could supplant empirical models such as Horton and SCS, which necessitate calibration with non-physical parameters, consequently introducing supplementary uncertainty and sources of errors. The study also introduces Bayesian inference as a powerful statistical method for inverse modeling which aims to determine the parameter set that best fits the observed data, and estimate distribution, while considering uncertainty and prior knowledge.

6.2. Perspectives

All of these studies have provided evidence for supporting the effectiveness of physically-based infiltration modeling in understanding the principal hydraulic and water movement in SUDS. The challenge lies in developing physical models with fewer and easily obtainable parameters.

Nevertheless, infiltration, particularly regarding soil heterogeneity, remains a key aspect of all hydrological models. These modules should be easy to calibrate and integrate into the watershed scale of urbanized areas. The model has undergone thorough testing across various scenarios, including changes in scale, time steps, calibration methods, and soil parameters. Chapter 5 highlighted the significant impact of scale on model performance and calibration techniques. The choice of scale and calibration strategy in the model should be driven by the intended application, considering factors like prioritizing output volumes or targeted hydraulic performances.

The perspective of this study is to focus on refining the input of initial conditions, specifically the parameter representing precedent ponded water height in the system. The improved version will be implemented in a dedicated framework for modeling all infiltration-based SUDS. The INFILTRON-Mod suite will be adopted to incorporate more complex physics that influence water infiltration in real soils, such as air entrapment, water repellency, and preferential flow, even if we offer here the first step towards the implementation of preferential flows.

In addition, there is room for the improvement of the prediction of water fluxes and water height in the filter at the same time. In other words, the optimization of parameters using water fluxes or water height degrades the prediction of the other variable. Following the establishment of the dual permeability platform, specific circumstances led to unfavorable *NSE* (*NSE*-Sutcliffe Efficiency) values for the filtered water height in bioretention modeling. This was primarily attributed to the inclusion of initial water content below field capacity, causing the activation of macropores and resulting in a notable increase in infiltration volume. While the model attempted to capture the overall curve, further refinement is necessary, particularly when considering preexisting water ponds in the system.

Enhancing the simplified model demands further meticulous development and fine-tuning of input parameters to faithfully mimic both water infiltration and water height dynamics within the system. This undertaking acknowledges the intricate nature of real-world phenomena. Subsequent experimentation involving finer time intervals, especially concerning bioretention systems without the presence of an Infiltration Water Storage (IWS) zone at the filter's base, deserves exploration. Furthermore, it is advisable to introduce heightened complexity by considering a greater number of soil layers within the filter structure, despite the potential augmentation of input parameters. This approach would facilitate a more accurate representation of the system's behavior and layering (due to clogging at the surface) and typical feature

Reference

Abbaspour, K.C., Johnson, C.A., van Genuchten, M.Th., 2004. Estimating Uncertain Flow and Transport Parameters Using a Sequential Uncertainty Fitting Procedure. Vadose Zone J. 3, 1340–1352. https://doi.org/10.2136/vzj2004.1340

Abbaspour, K.C., Schulin, R., van Genuchten, M.Th., 2001. Estimating unsaturated soil hydraulic parameters using ant colony optimization. Adv. Water Resour. 24, 827–841. https://doi.org/10.1016/S0309-1708(01)00018-5

Abou Najm, M.R., Stewart, R.D., Di Prima, S., Lassabatere, L., 2021. A Simple Correction Term to Model Infiltration in Water-Repellent Soils. Water Resour. Res. 57, e2020WR028539.

Ahiablame, L.M., Engel, B.A., Chaubey, I., 2012. Effectiveness of Low Impact Development Practices: Literature Review and Suggestions for Future Research. Water. Air. Soil Pollut. 223, 4253–4273. https://doi.org/10.1007/s11270-012-1189-2

Alaoui, A., 2015. Modelling susceptibility of grassland soil to macropore flow. J. Hydrol. 525, 536–546. https://doi.org/10.1016/j.jhydrol.2015.04.016

Alastal, K., Ababou, R., 2019. Moving Multi-Front (MMF): A generalized Green-Ampt approach for vertical unsaturated flows. J. Hydrol. 579, 124184. https://doi.org/10.1016/j.jhydrol.2019.124184

Allaire, S.E., Roulier, S., Cessna, A.J., 2009. Quantifying preferential flow in soils: A review of different techniques. J. Hydrol. 378, 179–204. https://doi.org/10.1016/j.jhydrol.2009.08.013

Althoff, D., Rodrigues, L.N., 2021. Goodness-of-fit criteria for hydrological models: Model calibration and performance assessment. J. Hydrol. 600, 126674. https://doi.org/10.1016/j.jhydrol.2021.126674

Anderson, D., Burnham, K., 2004. Model selection and multi-model inference. Second NY Springer-Verl. 63, 10.

Angulo-Jaramillo, R., Bagarello, V., Iovino, M., Lassabatere, L., 2016. Infiltration Measurements for Soil Hydraulic Characterization. Springer International Publishing, Cham. https://doi.org/10.1007/978-3-319-31788-5

Angulo-jaramillo, R., Bagarello, V., Laurent Lassabatere, asssimo L., 2016. Initration Measurements for Soil Hydraulic Characterization.

Arora, B., Mohanty, B.P., McGuire, J.T., 2011. Inverse estimation of parameters for multidomain flow models in soil columns with different macropore densities. Water Resour. Res. 47, 1–17. https://doi.org/10.1029/2010WR009451

Arya, L.M., Paris, J.F., 1981. A Physicoempirical Model to Predict the Soil Moisture Characteristic from Particle-Size Distribution and Bulk Density Data. Soil Sci. Soc. Am. J. 45, 1023–1030. https://doi.org/10.2136/sssaj1981.03615995004500060004x

Asleson, B.C., Nestingen, R.S., Gulliver, J.S., Hozalski, R.M., Nieber, J.L., 2009. Performance Assessment of Rain Gardens. JAWRA J. Am. Water Resour. Assoc. 45, 1019–1031. https://doi.org/10.1111/j.1752-1688.2009.00344.x

Asry, A., Kouyi, G.L., Fletcher, T.D., Bonneau, J., Tedoldi, D., Lassabatere, L., 2023. Sets of infiltration models for water infiltration in sustainable urban drainage systems. J. Hydrol. 129477. https://doi.org/10.1016/j.jhydrol.2023.129477

Azam, M.-H., Morille, B., Bernard, J., Musy, M., Rodriguez, F., 2018. A new urban soil model for SOLENE-microclimat: Review, sensitivity analysis and validation on a car park. Urban Clim. 24, 728–746.

Bakalowicz, M., 2005. Karst groundwater: a challenge for new resources. Hydrogeol. J. 13, 148–160. https://doi.org/10.1007/s10040-004-0402-9

Balas, G.J., Packard, A.K., Seiler, P.J., 2009. Uncertain Model Set Calculation from Frequency Domain Data, in: Hof, P.M.J., Scherer, C., Heuberger, P.S.C. (Eds.), Model-Based Control: Bridging Rigorous Theory and Advanced Technology. Springer US, Boston, MA, pp. 89–105. https://doi.org/10.1007/978-1-4419-0895-7_6

Barbu, I.A., Ballestero, T.P., 2015. Unsaturated Flow Functions for Filter Media Used in Low-Impact Development—Stormwater Management Systems. J. Irrig. Drain. Eng. 141, 04014041. https://doi.org/10.1061/(ASCE)IR.1943-4774.0000766

Baroni, G., Tarantola, S., 2014. A General Probabilistic Framework for uncertainty and global sensitivity analysis of deterministic models: A hydrological case study. Environ. Model. Softw. 51, 26–34. https://doi.org/10.1016/j.envsoft.2013.09.022

Basche, A.D., DeLonge, M.S., 2019. Comparing infiltration rates in soils managed with conventional and alternative farming methods: A meta-analysis. PLOS ONE 14, e0215702. https://doi.org/10.1371/journal.pone.0215702

Bayes, T., 1763. LII. An essay towards solving a problem in the doctrine of chances. By the late Rev. Mr. Bayes, FRS communicated by Mr. Price, in a letter to John Canton, AMFR S. Philos. Trans. R. Soc. Lond. 370–418.

Beatty, S.M., Smith, J.E., 2013. Dynamic soil water repellency and infiltration in post-wildfire soils. Geoderma 192, 160–172.

Bechet, B., Le Bissonnais, Y., Ruas, A., Aguilera, A., Andrieu, H., Barbe, E., Billet, P., Cavailhes, J., Cohen, M., Cornu, S., 2017. Sols artificialisés et processus d’artificialisation des sols: déterminants, impacts et leviers d’action. Synthèse. Inra.

Ben Slimene, E., Lassabatere, L., Winiarski, T., Gourdon, R., 2015. Modeling Water Infiltration and Solute Transfer in a Heterogeneous Vadose Zone as a Function of Entering Flow Rates. J. Water Resour. Prot. 07, 1017–1028. https://doi.org/10.4236/jwarp.2015.713083

Bertrand-Krajewski, J.-L., 2021. Integrated urban stormwater management: Evolution and multidisciplinary perspective. J. Hydro-Environ. Res., Sustainable Urban Drainage 38, 72–83. https://doi.org/10.1016/j.jher.2020.11.003

Bertrand-Krajewski, J.L., Muste, M., 2008. Understanding and managing uncertainty. Data Requir. Integr. Urban Water Manag. Paris UNESCO Publ. Taylor Francis.

Beven, K., 2006. A manifesto for the equifinality thesis. J. Hydrol. 320, 18–36. https://doi.org/10.1016/j.jhydrol.2005.07.007

Beven, K., Binley, A., 2014. GLUE: 20 years on. Hydrol. Process. 28, 5897–5918. https://doi.org/10.1002/hyp.10082

Beven, K., Germann, P., 1981. WATER FLOW IN SOIL MACROPORES II. A COMBINED FLOW MODEL. J. Soil Sci. 32, 15–29. https://doi.org/10.1111/j.1365-2389.1981.tb01682.x

Bingham, D., 1933. An introduction to Bayesian statistics and model calibration 1–19.

Birkholzer, J., Tsang, C.-F., 1997. Solute channeling in unsaturated heterogeneous porous media. Water Resour. Res. 33, 2221–2238. https://doi.org/10.1029/97WR01209

Blöschl, G., Grayson, R.B., Sivapalan, M., 1995. On the representative elementary area (REA) concept and its utility for distributed rainfall-runoff modelling. Hydrol. Process. 9, 313–330.

BoM, C.P., 2021. Climate in Victoria, Bureau of meteorology reference evapotranspiration calculations.

Bonneau, J., Fletcher, T.D., Costelloe, J.F., Burns, M.J., 2017. Stormwater infiltration and the 'urban karst'–A review. J. Hydrol. 552, 141–150.

Bonneau, J., Fletcher, T.D., Costelloe, J.F., Poelsma, P.J., James, R.B., Burns, M.J., 2018. Where does infiltrated stormwater go? Interactions with vegetation and subsurface anthropogenic features. J. Hydrol. 567, 121–132. https://doi.org/10.1016/j.jhydrol.2018.10.006

Bonneau, J., Lipeme Kouyi, G., Lassabatere, L., Fletcher, T.D., 2021. Field validation of a physically-based model for bioretention systems. J. Clean. Prod. 312. https://doi.org/10.1016/j.jclepro.2021.127636

Bouarafa, S., Lassabatere, L., Lipeme-Kouyi, G., Angulo-Jaramillo, R., 2019. Hydrodynamic characterization of Sustainable urban Drainage Systems (SuDS) by using beerkan infiltration experiments. Water Switz. 11. https://doi.org/10.3390/w11040660

Brady, N.C., Weil, R.R., Weil, R.R., 2008. The nature and properties of soils. Prentice Hall Upper Saddle River, NJ.

Brattebo, B.O., Booth, D.B., 2003. Long-term stormwater quantity and quality performance of permeable pavement systems 37, 4369–4376. https://doi.org/10.1016/S0043-1354(03)00410-X

Braud, I., Breil, P., Thollet, F., Lagouy, M., Branger, F., Jacqueminet, C., Kermadi, S., Michel, K., 2013. Evidence of the impact of urbanization on the hydrological regime of a medium-sized periurban catchment in France. J. Hydrol., Hydrology of peri-urban catchments: processes and modelling 485, 5–23. https://doi.org/10.1016/j.jhydrol.2012.04.049

Brears, R., 2017. Urban Water Sec u rity Challenges in Water Management Series.

Bresinsky, L., Kordilla, J., Engelhardt, I., Livshitz, Y., Sauter, M., 2023. Variably saturated dual-permeability flow modeling to assess distributed infiltration and vadose storage dynamics of a karst aquifer – The Western Mountain Aquifer in Israel and the West Bank. J. Hydrol. X 18, 100143. https://doi.org/10.1016/j.hydroa.2022.100143

Brown, R.A., Hunt, W.F., 2011. Underdrain Configuration to Enhance Bioretention Exfiltration to Reduce Pollutant Loads. J. Environ. Eng. 137, 1082–1091. https://doi.org/10.1061/(ASCE)EE.1943-7870.0000437

Brown, R.A., Hunt, W.F., Skaggs, R.W., Assistant, G.R., 2010. Modeling Bioretention Hydrology with DRAINMOD. Low Impact Dev. 10.

Brown, R.A., Skaggs, R.W., Hunt, W.F., 2013. Calibration and validation of DRAINMOD to model bioretention hydrology. J. Hydrol. 486, 430–442. https://doi.org/10.1016/j.jhydrol.2013.02.017

Brunetti, G., Papagrigoriou, I.-A., Stumpp, C., 2020. Disentangling model complexity in green roof hydrological analysis: A Bayesian perspective. Water Res. 182, 115973.

Brunetti, G., Šimůnek, J., Piro, P., 2016a. A comprehensive numerical analysis of the hydraulic behavior of a permeable pavement. J. Hydrol. 540, 1146–1161. https://doi.org/10.1016/j.jhydrol.2016.07.030

Burns, M.J., Fletcher, T.D., Walsh, C.J., Ladson, A.R., Hatt, B.E., 2012. Hydrologic shortcomings of conventional urban stormwater management and opportunities for reform. Landsc. Urban Plan. 105, 230–240. https://doi.org/10.1016/j.landurbplan.2011.12.012

Campbell, K., McKay, M.D., Williams, B.J., 2006. Sensitivity analysis when model outputs are functions. Reliab. Eng. Syst. Saf. 91, 1468–1472. https://doi.org/10.1016/j.ress.2005.11.049

Carbone, M., Brunetti, G., Piro, P., 2015. Modelling the hydraulic behaviour of growing media with the explicit finite volume solution. Water Switz. 7, 568–591. https://doi.org/10.3390/w7020568

Carsel, R.F., Parrish, R.S., 1988. Developing joint probability descriptions of soil water retention. Water Resour. Res. 24, 755–769.

Chen, C., Wagenet, R.J., 1992. Simulation of water and chemicals in macropore soils Part 1. Representation of the equivalent macropore influence and its effect on soilwater flow. J. Hydrol. 130, 105–126. https://doi.org/10.1016/0022-1694(92)90106-6

Chocat, B., 2013. CANOE: An Urban Hydrology Software Package, in: Tanguy, J.-M. (Ed.), Modeling Software. John Wiley & Sons, Inc., Hoboken, NJ USA, pp. 209–218. https://doi.org/10.1002/9781118557891.ch17

Chocat, B., 1997. Encyclopédie de l'hydrologie urbaine et de l'assainissement. Tech. & Doc.

Chocat, B., Battaglia, P., Blanchard, M., Bouillon, H., Guézo, B., Norotte, O., Thomazeau, R.L., 2003. Ville et son assainissement. Certu Ministère Equipement Transp. Logement Tour. Mer Ed. Certu 503p.

Chocat, B., Cabane, P., 1999. Hydrologie urbaine : modélisation et effet d'échelle. Houille Blanche 85, 106–111. https://doi.org/10.1051/lhb/1999091

Chow, W., Dawson, R., Glavovic, B., Haasnoot, M., Pelling, M., Solecki, W., 2022. IPCC Sixth Assessment Report (AR6): Climate Change 2022-Impacts, Adaptation and Vulnerability: Factsheet Human Settlements.

Clark, S.E., Pitt, R., Field, R., 2010. Groundwater contamination potential from infiltration of urban stormwater runoff. Eff. Urban. Groundw. Eng. Case-Based Approach Sustain. Dev. 119–156.

Concialdi, P., Di Prima, S., Bhanderi, H.M., Stewart, R.D., Abou Najm, M.R., Lal Gaur, M., Angulo-Jaramillo, R., Lassabatere, L., 2020. An open-source instrumentation package for intensive soil hydraulic characterization. J. Hydrol. 582, 124492. https://doi.org/10.1016/j.jhydrol.2019.124492

Connor, T.O., Sullivan, D., Clar, M., Barfield, B.J., 2003. CONSIDERATIONS IN THE DESIGN OF TREATMENT BEST MANAGEMENT PRACTICES (BMPs) TO IMPROVE WATER QUALITY. Proc. Water Environ. Fed. 2003, 1186–1205. https://doi.org/10.2175/193864703784828471

Coutinho, A.P., Lassabatere, L., Winiarski, T., Cabral, J.J. da S.P., Antonino, A.C.D., Angulo-Jaramillo, R., 2015. Vadose Zone Heterogeneity Effect on Unsaturated Water Flow Modeling at Meso-Scale. J. Water Resour. Prot. 07, 353–368. https://doi.org/10.4236/jwarp.2015.74028

Craul, P.J., 1985. A description of urban soils and their desired characteristics. J. Arboric. 11, 330–339.

D. N. Moriasi, J. G. Arnold, M. W. Van Liew, R. L. Bingner, R. D. Harmel, T. L. Veith, 2007. Model Evaluation Guidelines for Systematic Quantification of Accuracy in Watershed Simulations. Trans. ASABE 50, 885–900. https://doi.org/10.13031/2013.23153

Daniel, T.C., Bouma, J., 1974. Column Studies of Soil Clogging in a Slowly Permeable Soil as a Function of Effluent Quality. J. Environ. Qual. 3, 321–326. https://doi.org/10.2134/jeq1974.00472425000300040005x

Davis, A.P., 2008. Field Performance of Bioretention: Hydrology Impacts. J. Hydrol. Eng. 13, 90–95. https://doi.org/10.1061/(asce)1084-0699(2008)13:2(90)

Davis, A.P., Hunt, W.F., Traver, R.G., Clar, M., 2009. Bioretention Technology: Overview of Current Practice and Future Needs. J. Environ. Eng. 135, 109–117. https://doi.org/10.1061/(ASCE)0733-9372(2009)135:3(109)

DeBusk, K.M., Hunt, W.F., Line, D.E., 2011. Bioretention outflow: Does it mimic nonurban watershed shallow interflow? J. Hydrol. Eng. 16, 274–279.

Dekker, L.W., Ritsema, C.J., Wendroth, O., Jarvis, N., Oostindie, K., Pohl, W., Larsson, M., Gaudet, J.P., 1999. Moisture distributions and wetting rates of soils at experimental fields in the Netherlands, France, Sweden and Germany. J. Hydrol. 215, 4–22. https://doi.org/10.1016/S0022-1694(98)00258-3

Delbart, C., n.d. Variabilité spatio-temporelle du fonctionnement d'un aquifère karstique du Dogger: suivis hydrodynamiques et géochimiques multifréquences; traitement du signal des réponses physiques et géochimiques.

Deletic, A., Dotto, C.B.S., McCarthy, D.T., Kleidorfer, M., Freni, G., Mannina, G., Uhl, M., Henrichs, M., Fletcher, T.D., Rauch, W., Bertrand-Krajewski, J.L., Tait, S., 2012. Assessing uncertainties in urban drainage models. Phys. Chem. Earth Parts ABC 42–44, 3–10. https://doi.org/10.1016/j.pce.2011.04.007

Di Prima, S., Stewart, R.D., Castellini, M., Bagarello, V., Abou Najm, M.R., Pirastru, M., Giadrossich, F., Iovino, M., Angulo-Jaramillo, R., Lassabatere, L., 2020. Estimating the macroscopic capillary length from Beerkan infiltration experiments and its impact on saturated soil hydraulic conductivity predictions. J. Hydrol. 589, 125159. https://doi.org/10.1016/j.jhydrol.2020.125159

Dietz, M.E., Clausen, J.C., 2005. A Field Evaluation of Rain Garden Flow and Pollutant Treatment. Water. Air. Soil Pollut. 167, 123–138. https://doi.org/10.1007/s11270-005-8266-8

Ding, B., Rezanezhad, F., Gharedaghloo, B., Van Cappellen, P., Passeport, E., 2019. Bioretention cells under cold climate conditions: Effects of freezing and thawing on water infiltration, soil structure, and nutrient removal. Sci. Total Environ. 649, 749–759.

Doerr, S.H., Shakesby, R.A., Dekker, L.W., Ritsema, C.J., 2006. Occurrence, prediction and hydrological effects of water repellency amongst major soil and land-use types in a humid temperate climate. Eur. J. Soil Sci. 57, 741–754. https://doi.org/10.1111/j.1365-2389.2006.00818.x

Dotto, C.B.S., Deletic, A., McCarthy, D.T., Fletcher, T.D., 2011. Calibration and sensitivity analysis of urban drainage models: MUSIC rainfall/runoff module and a simple stormwater quality model. Australas. J. Water Resour. 15, 85–94.

Draper, N.R., Smith, H., 1998. Applied regression analysis. John Wiley & Sons.

Durner, W., Flühler, H., 2005. Soil Hydraulic Properties. Encycl. Hydrol. Sci. 1–17. https://doi.org/10.1002/0470848944.hsa077c

Durner, W., Lipsius, K., 2005. Determining Soil Hydraulic Properties, in: Anderson, M.G., McDonnell, J.J. (Eds.), Encyclopedia of Hydrological Sciences. John Wiley & Sons, Ltd, Chichester, UK, p. hsa077b. https://doi.org/10.1002/0470848944.hsa077b

Dussaillant, A., Cozzetto, K., Brander, K., Potter, K., 2003. Green-Ampt model of a rain garden and comparison to Richards equation model. WIT Trans. Ecol. Environ. 67.

Dussaillant, A.R., Cuevas, A., Potter, K.W., 2005. Raingardens for stormwater infiltration and focused groundwater recharge: simulations for different world climates. Water Supply 5, 173–179. https://doi.org/10.2166/ws.2005.0097

Eckart, K., McPhee, Z., Bolisetti, T., 2017. Performance and implementation of low impact development – A review. Sci. Total Environ. 607–608, 413–432. https://doi.org/10.1016/j.scitotenv.2017.06.254

Edwards, W.M., Shipitalo, M.J., Owens, L.B., Dick, W.A., 1993. Factors Affecting Preferential Flow of Water and Atrazine through Earthworm Burrows under Continuous No-Till Corn. J. Environ. Qual. 22, 453–457. https://doi.org/10.2134/jeq1993.00472425002200030008x

Elliott, A.H., Trowsdale, S.A., 2007. A Review of Models of Low Impact Urban Stormwater Drainage A review of models for low impact urban stormwater drainage. Environ. Model. Softw. · 22, 394e405. https://doi.org/10.1016/j.envsoft.2005.12.005

Fanelli, R., Prestegaard, K., Palmer, M., 2017. Evaluation of infiltration-based stormwater management to restore hydrological processes in urban headwater streams. Hydrol. Process. 31, 3306–3319. https://doi.org/10.1002/hyp.11266

FAWB., 2009. Adoption Guidelines for Stormwater Biofiltration Systems. Facility for Advancing Water Biofiltration (No. Version 3). Monash University.

Fayer, M.J., Version, U.-H., 2000. 3.0: Unsaturated Soil Water and Heat Flow Model, Theory, User Manual, and Examples. Pac. Northwest Natl. Lab. Rep. PNNL-13249 Richland WA.

Ferguson, B.K., 2017. Stormwater infiltration, Stormwater Infiltration. https://doi.org/10.1201/9780203738238

Ferguson, B.K., 1994. Stormwater Infiltration. CRC Press.

Feuillette, M.A., Frédéric, R., 2016. Mission sur le fonctionnement hydrologique du bassin de la Seine, Rapport au Premier ministre. Agence de l’Eau Seine et Normandie.

Fischer, E.M., Knutti, R., 2016. Observed heavy precipitation increase confirms theory and early models. Nat. Clim. Change 6, 986–991.

Fisher, R.A., 1970. Statistical methods for research workers, in: Breakthroughs in Statistics: Methodology and Distribution. Springer, pp. 66–70.

Flanagan, K., Ah-Leung, S., Bacot, L., Bak, A., Barraud, S., Branchu, P., Castebrunet, H., Cossais, N., de Gouvello, B., Deroubaix, J.-F., 2019. Un guide méthodologique pour l'évaluation des performances des ouvrages de maîtrise à la source des eaux pluviales, in: Novatech 2019. p. 5p.

Fletcher, T.D., Andrieu, H., Hamel, P., 2013. Understanding, management and modelling of urban hydrology and its consequences for receiving waters: A state of the art. Adv. Water Resour., 35th Year Anniversary Issue 51, 261–279. https://doi.org/10.1016/j.advwatres.2012.09.001

Fletcher, T.D., Shuster, W., Hunt, W.F., Ashley, R., Butler, D., Arthur, S., Trowsdale, S., Barraud, S., Semadeni-Davies, A., Bertrand-Krajewski, J.-L., Mikkelsen, P.S., Rivard, G., Uhl, M., Dagenais, D., Viklander, M., 2015a. SUDS, LID, BMPs, WSUD and more – The evolution and application of terminology surrounding urban drainage. Urban Water J. 12, 525–542. https://doi.org/10.1080/1573062X.2014.916314

Fleury, P., Plagnes, V., Bakalowicz, M., 2007. Modelling of the functioning of karst aquifers with a reservoir model: Application to Fontaine de Vaucluse (South of France). J. Hydrol. 345, 38–49. https://doi.org/10.1016/j.jhydrol.2007.07.014

Flury, M., Flühler, H., Jury, W.A., Leuenberger, J., 1994a. Susceptibility of soils to preferential flow of water: A field study. Water Resour. Res. 30, 1945–1954. https://doi.org/10.1029/94WR00871

Flury, M., Flühler, H., Jury, W.A., Leuenberger, J., 1994b. Susceptibility of soils to preferential flow of water: A field study. Water Resour. Res. 30, 1945–1954. https://doi.org/10.1029/94WR00871

Force, W.E.F.D. of U.S.C.T., Federation, W.E., Institute (US), W.R., 2012. Design of Urban Stormwater Controls: MOP 23. McGraw Hill Professional.

Francés, A.P., 2008. Spatio-temporal groundwater recharge assessment: a data-integration and modelling approach. Laboratorio Nacional de Energia e Geologia (Portugal).

Friendly, M., Monette, G., Fox, J., 2013. Elliptical Insights: Understanding Statistical Methods through Elliptical Geometry. Stat. Sci. 28. https://doi.org/10.1214/12-STS402

Gelman, A., Carlin, J.B., Stern, H.S., Dunson, D.B., Vehtari, A., Rubin, D.B., 2013. Bayesian data analysis. CRC press.

Gelman, A., Rubin, D.B., 1992. Inference from Iterative Simulation Using Multiple Sequences. Stat. Sci. 7, 457–472. https://doi.org/10.1214/ss/1177011136

Gerke, H.H., van Genuchten, M.T., 1993b. A dual-porosity model for simulating the preferential movement of water and solutes in structured porous media. Water Resour. Res. 29, 305–319. https://doi.org/10.1029/92WR02339

Germann, P., Beven, K., 1982a. Macropores and water flow in soils. Water Resour. Res. 18, 1311–1325.

Ghanem, R., Higdon, D., Owhadi, H. (Eds.), 2017. Handbook of Uncertainty Quantification. Springer International Publishing, Cham. https://doi.org/10.1007/978-3-319-12385-1

GIEC, 2022. IPCC Sixth Assessment Report (AR6): Climate Change 2022-Impacts, Adaptation and Vulnerability: Factsheet Human Settlements.

Giles, M.B., 2015. Multilevel Monte Carlo methods. Acta Numer. 24, 259–328. https://doi.org/10.1017/S096249291500001X

Gill, M.K., Kaheil, Y.H., Khalil, A., McKee, M., Bastidas, L., 2006. Multiobjective particle swarm optimization for parameter estimation in hydrology. Water Resour. Res. 42.

Głąb, T., Palmowska, J., Zaleski, T., Gondek, K., 2016. Effect of biochar application on soil hydrological properties and physical quality of sandy soil. Geoderma 281, 11–20. https://doi.org/10.1016/j.geoderma.2016.06.028

Göbel, P., Dierkes, C., Coldewey, W.G., 2007. Storm water runoff concentration matrix for urban areas. J. Contam. Hydrol. 91, 26–42. https://doi.org/10.1016/j.jconhyd.2006.08.008

Goutaland, D., Winiarski, T., Lassabatere, L., Dubé, J.S., Angulo-Jaramillo, R., 2013. Sedimentary and hydraulic characterization of a heterogeneous glaciofluvial deposit: Application to the modeling of unsaturated flow. Eng. Geol. 166, 127–139. https://doi.org/10.1016/j.enggeo.2013.09.006

Grayson, R., Blöschl, G. (Eds.), 2001. Spatial patterns in catchment hydrology: observations and modelling. Cambridge University Press, Cambridge, U.K. ; New York.

Greco, R., 2002. Preferential flow in macroporous swelling soil with internal catchment: Model development and applications. J. Hydrol. 269, 150–168. https://doi.org/10.1016/S0022-1694(02)00215-9

Grimm, N.B., Faeth, S.H., Golubiewski, N.E., Redman, C.L., Wu, J., Bai, X., Briggs, J.M., 2008. Global Change and the Ecology of Cities. Science 319, 756–760. https://doi.org/10.1126/science.1150195

Guo, H., Lim, F.Y., Zhang, Y., Lee, L.Y., Hu, J.Y., Ong, S.L., Yau, W.K., Ong, G.S., 2015. Soil column studies on the performance evaluation of engineered soil mixes for bioretention systems. Desalination Water Treat. 54, 3661–3667. https://doi.org/10.1080/19443994.2014.922284

Guo, J.C.Y., Luu, T.M., 2015. Hydrologic Model Developed for Stormwater Infiltration Practices. J. Hydrol. Eng. 20, 06015001. https://doi.org/10.1061/(ASCE)HE.1943-5584.0001161

Gupta, H.V., Kling, H., Yilmaz, K.K., Martinez, G.F., 2009. Decomposition of the mean squared error and NSE performance criteria: Implications for improving hydrological modelling. J. Hydrol. 377, 80–91. https://doi.org/10.1016/j.jhydrol.2009.08.003

Habitat, U.N., 2022. World Cities Report 2022: Envisaging the Future of Cities. Retrieved from. Nairobi: Kenya: United Nations Human Settlements Programme ….

Hallett, P.D., Nunan, N., Douglas, J.T., Young, I.M., 2004. Millimeter-Scale Spatial Variability in Soil Water Sorptivity. Soil Sci. Soc. Am. J. 68, 352–358. https://doi.org/10.2136/sssaj2004.3520

Hamel, P., Daly, E., Fletcher, T.D., 2013. Source-control stormwater management for mitigating the impacts of urbanisation on baseflow: A review. J. Hydrol. 485, 201–211.

Hamel, P., Fletcher, T.D., 2014. Modelling the impact of stormwater source control infiltration techniques on catchment baseflow: MODELLING THE IMPACT OF STORMWATER INFILTRATION ON CATCHMENT BASEFLOW. Hydrol. Process. 28, 5817–5831. https://doi.org/10.1002/hyp.10069

Hatt, B.E., Fletcher, T.D., Deletic, A., 2009. Hydrologic and pollutant removal performance of stormwater biofiltration systems at the field scale. J. Hydrol. 365, 310–321. https://doi.org/10.1016/j.jhydrol.2008.12.001

Haverkamp, R., Parlange, J.-Y., 1986. PREDICTING THE WATER-RETENTION CURVE FROM PARTICLE-SIZE DISTRIBUTION: 1. SANDY SOILS WITHOUT ORGANIC MATTER: 1. Soil Sci. 142, 325.

Heasom, W., Traver, R.G., Welker, A., 2006. Hydrologic modeling of a bioinfiltration best management practice 1. JAWRA J. Am. Water Resour. Assoc. 42, 1329–1347.

Hendrickx, J.M.H., Dekker, L.W., Boersma, O.H., 1993. Unstable Wetting Fronts in Water-Repellent Field Soils. J. Environ. Qual. 22, 109–118. https://doi.org/10.2134/jeq1993.00472425002200010014x

Hendrickx, J.M.H., Flury, M., 2001. Uniform and preferential flow mechanisms in the vadose zone. Concept. Models Flow Transp. Fract. Vadose ZoneNatlAcadPress Wash. DC 149–187.

Herrmann, D.L., Schifman, L.A., Shuster, W.D., 2018. Widespread loss of intermediate soil horizons in urban landscapes. Proc. Natl. Acad. Sci. 115, 6751–6755. https://doi.org/10.1073/pnas.1800305115

Hillel, D., 2003. INTRODUCTION TO ENVIRONMENTAL SOIL PHYSICS. Elsevier.

Hillel, D., 1971. Soil and Water: Physical Principles and Processes, Soil Science Society of America Journal. ACADEMI C PRESS , INC . https://doi.org/10.2136/sssaj1972.03615995003600050003x

Hilten, R.N., Lawrence, T.M., Tollner, E.W., 2008b. Modeling stormwater runoff from green roofs with HYDRUS-1D. J. Hydrol. 358, 288–293. https://doi.org/10.1016/j.jhydrol.2008.06.010

Holden, J., 2005. Piping and woody plants in peatlands: Cause or effect?: PIPING IN PEATLANDS. Water Resour. Res. 41. https://doi.org/10.1029/2004WR003909

Hopmans, J., Simunek, J., Jirka, 1999. Review of inverse estimation of soil hydraulic properties.

Hopmans, J.W., 1999. Review of inverse estimation of soil hydraulic properties, in: Proc. Int. Workshop, Characterization and Measurement of the Hydraulic Properties of Unsaturated Porous Media, Riverside, USA, 1999. Univ. California, pp. 643–658.

Hopmans, J.W., Šimůnek, J., Romano, N., Durner, W., 2002. 3.6. 2. Inverse Methods. Methods Soil Anal. Part 4 Phys. Methods 5, 963–1008. https://doi.org/10.2136/sssabookser5.4.c40

Hsieh, C., Davis, A.P., 2005. Evaluation and Optimization of Bioretention Media for Treatment of Urban Storm Water Runoff. J. Environ. Eng. 131, 1521–1531. https://doi.org/10.1061/(ASCE)0733-9372(2005)131:11(1521)

Huber, W.C., Cannon, L., Stouder, M., 2004. BMP modeling concepts and simulation.

Huber, W.C., Heaney, J.P., Medina, M.A., Peltz, W.A., Sheikh, H., Smith, G.F., 1975. Storm Water Management Model User'S Manuel. Version Ii. Env. Prot Technol Ser EPA.

Hunt, W.F., Jarrett, A.R., Smith, J.T., Sharkey, L.J., 2006. Evaluating Bioretention Hydrology and Nutrient Removal at Three Field Sites in North Carolina. J. Irrig. Drain. Eng. 132, 600–608. https://doi.org/10.1061/(ASCE)0733-9437(2006)132:6(600)

Illgen, M., Harting, K., Schmitt, T.G., Welker, A., 2007. Runoff and infiltration characteristics of pavement structures--review of an extensive monitoring program. Water Sci. Technol. J. Int. Assoc. Water Pollut. Res. 56, 133–140. https://doi.org/10.2166/wst.2007.750

Ines, A.V.M., Droogers, P., 2002. Inverse modelling in estimating soil hydraulic functions: a Genetic Algorithm approach. Hydrol. Earth Syst. Sci. 6, 49–66. https://doi.org/10.5194/hess-6-49-2002

Jacobs, W.R., Dodd, T.J., Anderson, S.R., 2018. Frequency-domain analysis for nonlinear systems with time-domain model parameter uncertainty. IEEE Trans. Autom. Control 64, 1905–1915.

Jain, S.K., Singh, V.P., van Genuchten, M.Th., 2004. Analysis of Soil Water Retention Data Using Artificial Neural Networks. J. Hydrol. Eng. 9, 415–420. https://doi.org/10.1061/(ASCE)1084-0699(2004)9:5(415)

James, W., 1994. Current Practices in Modelling the Management of Stormwater Impacts. CRC Press.

Jarvis, N.J., 2007. A review of non-equilibrium water flow and solute transport in soil macropores: principles, controlling factors and consequences for water quality. Eur. J. Soil Sci. 58, 523–546. https://doi.org/10.1111/j.1365-2389.2007.00915.x

Jarvis, N.J., 1998. Modeling the impact of preferential flow on nonpoint source pollution, Physical nonequilibrium in soils: modeling and application.

Jarvis, N.J., Ga, A., 2003. Review and comparison of models for describing non-equilibrium and preferential flow and transport in the vadose zone ˇ imu 272, 14–35.

Jefferson, A.J., Bhaskar, A.S., Hopkins, K.G., Fanelli, R., Avellaneda, P.M., McMillan, S.K., 2017. Stormwater management network effectiveness and implications for urban watershed function: A critical review. Hydrol. Process. 31, 4056–4080. https://doi.org/10.1002/hyp.11347

Johnson, J.P., Hunt, W.F., 2019. A retrospective comparison of water quality treatment in a bioretention cell 16 years following initial analysis. Sustainability 11, 1945.

Joseph, J.F., Guillaume, J.H., 2013. Using a parallelized MCMC algorithm in R to identify appropriate likelihood functions for SWAT. Environ. Model. Softw. 46, 292–298.

Kale, R.V., Sahoo, B., 2011. Green-Ampt Infiltration Models for Varied Field Conditions: A Revisit. Water Resour. Manag. 25, 3505–3536. https://doi.org/10.1007/s11269-011-9868-0

Kanso, T., Tedoldi, D., Gromaire, M.-C., Ramier, D., Saad, M., Chebbo, G., 2018. Horizontal and Vertical Variability of Soil Hydraulic Properties in Roadside Sustainable Drainage Systems (SuDS)—Nature and Implications for Hydrological Performance Evaluation. Water Switz. 10, 987. https://doi.org/10.3390/w10080987

Khan, U., Valeo, C., Chu, A., He, J., 2013. A Data Driven Approach to Bioretention Cell Performance: Prediction and Design. Water 5, 13–28. https://doi.org/10.3390/w5010013

Köhne, J.M., Mohanty, B.P., Šimůnek, J., 2006. Inverse Dual-Permeability Modeling of Preferential Water Flow in a Soil Column and Implications for Field-Scale Solute Transport. Vadose Zone J. 5, 59–76. https://doi.org/10.2136/vzj2005.0008

Lal, R., Stewart, B.A., 2017. Urban soils, Urban Soils. https://doi.org/10.1201/9781315154251

Lamboni, M., Monod, H., Makowski, D., 2011. Multivariate sensitivity analysis to measure global contribution of input factors in dynamic models. Reliab. Eng. Syst. Saf. 96, 450–459. https://doi.org/10.1016/j.ress.2010.12.002

Lassabatère, L., Angulo-Jaramillo, R., Soria Ugalde, J.M., Cuenca, R., Braud, I., Haverkamp, R., 2006. Beerkan Estimation of Soil Transfer Parameters through Infiltration Experiments-BEST. Soil Sci. Soc. Am. J. 70, 521–532. https://doi.org/10.2136/sssaj2005.0026

Lassabatere, L., Asri, A., 2022. R codes for the study of sets of simplified infiltration models for modeling and management of sustainable urban drainage systems. https://doi.org/10.5281/zenodo.7190966

Lassabatere, L., Di Prima, S., Angulo-Jaramillo, R., Keesstra, S., Salesa, D., 2019. Beerkan multi-runs for characterizing water infiltration and spatial variability of soil hydraulic properties across scales. Hydrol. Sci. J. 64, 165–178. https://doi.org/10.1080/02626667.2018.1560448

Lassabatere, L., Yilmaz, D., Peyrard, X., Peyneau, P.E., Lenoir, T., Šimůnek, J., Angulo-Jaramillo, R., 2014. New Analytical Model for Cumulative Infiltration into Dual-Permeability Soils. Vadose Zone J. 13, vzj2013.10.0181. https://doi.org/10.2136/vzj2013.10.0181

Leij, F.J., 1996. The UNSODA unsaturated soil hydraulic database: user’s manual. National Risk Management Research Laboratory, Office of Research and ….

Lenderink, G., Fowler, H.J., 2017. Understanding rainfall extremes. Nat. Clim. Change 7, 391–393. https://doi.org/10.1038/nclimate3305

Li, C., Fletcher, T.D., Duncan, H.P., Burns, M.J., 2017. Can stormwater control measures restore altered urban flow regimes at the catchment scale? Sci. Total Environ. 549, 631–653. https://doi.org/10.1016/j.scitotenv.2021.147592

Li, H., Davis, A.P., 2008. Urban Particle Capture in Bioretention Media. I: Laboratory and Field Studies. J. Environ. Eng. 134, 409–418. https://doi.org/10.1061/(ASCE)0733-9372(2008)134:6(409)

Li, J., Zhao, R., Li, Y., Chen, L., 2018. Modeling the effects of parameter optimization on three bioretention tanks using the HYDRUS-1D model. J. Environ. Manage. 217, 38–46.

Li, M., Yang, X., Chen, L., Shen, Z., 2017. Modeling of Bioretention Systems’ Hydrologic Performance: A Case Study in Beijing, in: International Low Impact Development Conference China 2016. Presented at the International Low Impact Development Conference China 2016, American Society of Civil Engineers, Beijing, China, pp. 108–117. https://doi.org/10.1061/9780784481042.013

Lisenbee, W.A., Hathaway, J.M., Burns, M.J., Fletcher, T.D., 2021a. Modeling bioretention stormwater systems: Current models and future research needs. Environ. Model. Softw. 144, 105146. https://doi.org/10.1016/j.envsoft.2021.105146

Lisenbee, W.A., Hathaway, J.M., Burns, M.J., Fletcher, T.D., 2021b. Modeling bioretention stormwater systems: Current models and future research needs. Environ. Model. Softw. 144, 105146. https://doi.org/10.1016/j.envsoft.2021.105146

Lisenbee, W.A., Hathaway, J.M., Burns, M.J., Fletcher, T.D., 2021c. Modeling bioretention stormwater systems: Current models and future research needs. Environ. Model. Softw. 144, 105146. https://doi.org/10.1016/j.envsoft.2021.105146

Liu, J.S., 2001. Monte Carlo strategies in scientific computing. Springer.

Liu, R., Fassman-Beck, E., 2017. Hydrologic response of engineered media in living roofs and bioretention to large rainfalls: experiments and modeling: Hydrologic response of engineered media in living roofs and bioretention to large rainfalls: experiments and modeling. Hydrol. Process. 31, 556–572. https://doi.org/10.1002/hyp.11044

Liu, W., Chen, W., Peng, C., 2014. Assessing the effectiveness of green infrastructures on urban flooding reduction : A community scale study. Ecol. Model. 291, 6–14. https://doi.org/10.1016/j.ecolmodel.2014.07.012

Liu, Y., Gupta, H.V., 2007. Uncertainty in hydrologic modeling: Toward an integrated data assimilation framework: HYDROLOGIC DATA ASSIMILATION. Water Resour. Res. 43. https://doi.org/10.1029/2006WR005756

Lu, Z., Zhang, D., 2003. On importance sampling Monte Carlo approach to uncertainty analysis for flow and transport in porous media. Adv. Water Resour. 26, 1177–1188. https://doi.org/10.1016/S0309-1708(03)00106-4

Mair, A., Dupuy, L.X., Ptashnyk, M., 2022. Model for water infiltration in vegetated soil with preferential flow oriented by plant roots. Plant Soil 478, 709–729. https://doi.org/10.1007/s11104-022-05501-6

Majdalani, S., Angulo-Jaramillo, R., Di Pietro, L., 2008. Estimating preferential water flow parameters using a binary genetic algorithm inverse method. Environ. Model. Softw. 23, 950–956. https://doi.org/10.1016/j.envsoft.2007.12.002

Makler-Pick, V., Gal, G., Gorfine, M., Hipsey, M.R., Carmel, Y., 2011. Sensitivity analysis for complex ecological models – A new approach. Environ. Model. Softw. 26, 124–134. https://doi.org/10.1016/j.envsoft.2010.06.010

Marino, S., Hogue, I.B., Ray, C.J., Kirschner, D.E., 2008. A methodology for performing global uncertainty and sensitivity analysis in systems biology. J. Theor. Biol. 254, 178–196. https://doi.org/10.1016/j.jtbi.2008.04.011

Marsalek, J., Jiménez-Cisneros, B., Karamouz, M., Malmquist, P.A., Goldenfum, J., Chocat, B., 2006. Urban water cycle processes and interactions: Urban water series - UNESCO-IHP. Urban Water Cycle Process. Interact. Urban Water Ser. - UNESCO-IHP 1–131.

Masson, V., Lemonsu, A., Hidalgo, J., Voogt, J., 2020. Urban Climates and Climate Change. Annu. Rev. Environ. Resour. 45, 411–444. https://doi.org/10.1146/annurev-environ-012320-083623

Massoudieh, A., Maghrebi, M., Kamrani, B., Nietch, C., Tryby, M., Aflaki, S., Panguluri, S., 2017. A flexible modeling framework for hydraulic and water quality performance assessment of stormwater green infrastructure. Environ. Model. Softw. 92, 57–73. https://doi.org/10.1016/j.envsoft.2017.02.013

McPherson, M.B., Schneider, W.J., 1974. Problems in modeling urban watersheds. Water Resour. Res. 10, 434–440. https://doi.org/10.1029/WR010i003p00434

Melbourne Water, 2020. Guideline of Biofiltration systems in Development Services Schemes. Melbourne Water,Manager Catchment & Water Quality.

Meng, Y., Wang, H., Chen, J., Zhang, S., 2014. Modelling hydrology of a single bioretention system with HYDRUS-1D. Sci. World J. 2014.

Milelli, M., 2016. Urban heat island effects over Torino.

Millward, A.A., Paudel, K., Briggs, S.E., 2011. Naturalization as a strategy for improving soil physical characteristics in a forested urban park. Urban Ecosyst. 14, 261–278. https://doi.org/10.1007/s11252-010-0153-4

Min, S.-K., Zhang, X., Zwiers, F.W., Hegerl, G.C., 2011. Human contribution to more-intense precipitation extremes. Nature 470, 378–381. https://doi.org/10.1038/nature09763

Mishra, S., 2009. Uncertainty and sensitivity analysis techniques for hydrologic modeling. J. Hydroinformatics 11, 282–296. https://doi.org/10.2166/hydro.2009.048

Mitchell Ayers, E., Kangas, P., 2018. Soil layer development and biota in bioretention. Water 10, 1587.

Mitchell, V.G., Mein, R.G., McMahon, T.A., 2001. Modelling the urban water cycle. Environ. Model. Softw. 16, 615–629. https://doi.org/10.1016/S1364-8152(01)00029-9

Miyazaki, T., 2006. Water flow in soils, Developments in Agricultural Engineering. Taylor & Francis Group. https://doi.org/10.1016/B978-0-444-88080-2.50009-0

Moreira de Melo, T., Pedrollo, O.C., 2015. Artificial Neural Networks for Estimating Soil Water Retention Curve Using Fitted and Measured Data. Appl. Environ. Soil Sci. 2015, e535216. https://doi.org/10.1155/2015/535216

Moriasi, D., Gitau, M., Pai, N., Daggupati, P., 2015. Hydrologic and Water Quality Models: Performance Measures and Evaluation Criteria. Trans. ASABE Am. Soc. Agric. Biol. Eng. 58, 1763–1785. https://doi.org/10.13031/trans.58.10715

Moriasi, D.N., Gitau, M.W., Pai, N., Daggupati, P., 2015. Hydrologic and water quality models: Performance measures and evaluation criteria. Trans. ASABE 58, 1763–1785.

Morvannou, A., Forquet, N., Vanclooster, M., Molle, P., 2013. Which hydraulic model to use for vertical flow constructed wetlands?, in: 4th International Conference HYDRUS Software Applications to Subsurface Flow and Contaminant Transport Problems. Simunek, J., pp. 245–255.

Mualem, Y., 1986. Hydraulic Conductivity of Unsaturated Soils: Prediction and Formulas. Methods Soil Anal. Part 1 9, 799–823.

Muerdter, C.P., Wong, C.K., LeFevre, G.H., 2018. Emerging investigator series: the role of vegetation in bioretention for stormwater treatment in the built environment: pollutant removal, hydrologic function, and ancillary benefits. Environ. Sci. Water Res. Technol. 4, 592–612.

Mullaly, J., 2019. WSUD Asset Management Operation and Maintenance, in: Approaches to Water Sensitive Urban Design. Elsevier, pp. 455–474.

Muth, C., Oravecz, Z., Gabry, J., 2018. User-friendly Bayesian regression modeling: A tutorial with rstanarm and shinystan. Quant. Methods Psychol. 14, 99–119.

Nash, J.E., Sutcliffe, J.V., 1970. River flow forecasting through conceptual models part I—A discussion of principles. J. Hydrol. 10, 282–290.

Nemes, A., Schaap, M.G., Leij, F.J., Wösten, J.H.M., 2001. Description of the unsaturated soil hydraulic database UNSODA version 2.0. J. Hydrol. 251, 151–162. https://doi.org/10.1016/S0022-1694(01)00465-6

Niazi, M., Nietch, C., Maghrebi, M., Jackson, N., Bennett, B.R., Tryby, M., Massoudieh, A., 2017. Storm Water Management Model: Performance Review and Gap Analysis. J. Sustain. Water Built Environ. 3, 04017002. https://doi.org/10.1061/JSWBAY.0000817

Niehoff, D., Fritsch, U., Bronstert, A., 2002. Land-use impacts on storm-runoff generation: scenarios of land-use change and simulation of hydrological response in a meso-scale catchment in SW-Germany. J. Hydrol. 267, 80–93. https://doi.org/10.1016/S0022-1694(02)00142-7

Nimmer, M., Thompson, A., Misra, D., 2010. Modeling water table mounding and contaminant transport beneath storm-water infiltration basins. J. Hydrol. Eng. 15, 963–973.

Noguchi, S., Nik, A.R., Kasran, B., Tani, M., Sammori, T., Morisada, K., 1997. Soil Physical Properties and Preferential Flow Pathways in Tropical Rain Forest, Bukit Tarek, Peninsular Malaysia. J. For. Res. 2, 115–120. https://doi.org/10.1007/BF02348479

Noguchi, S., Tsuboyama, Y., Sidle, R.C., Hosoda, I., 1999. Morphological characteristics of macropores and the distribution of preferential flow pathways in a forested slope segment. Soil Sci. Soc. Am. J. 63, 1413–1423.

Ogden, F.L., Saghafian, B., 1997. Green and Ampt Infiltration with Redistribution. J. Irrig. Drain. Eng. 123, 386–393. https://doi.org/10.1061/(ASCE)0733-9437(1997)123:5(386)

O'Gorman, P.A., 2015. Precipitation Extremes Under Climate Change. Curr. Clim. Change Rep. 1, 49–59. https://doi.org/10.1007/s40641-015-0009-3

Pagliai, M., Vignozzi, N., Pellegrini, S., 2004. Soil structure and the effect of management practices. Soil Tillage Res. 79, 131–143.

Palla, A., Gnecco, I., Lanza, L.G., 2009. Unsaturated 2D modelling of subsurface water flow in the coarse-grained porous matrix of a green roof. J. Hydrol. 379, 193–204. https://doi.org/10.1016/j.jhydrol.2009.10.008

Parsopoulos, K.E., Vrahatis, M.N., 2002. Recent approaches to global optimization problems through Particle Swarm Optimization. Nat. Comput. 1, 235–306. https://doi.org/10.1023/A:1016568309421

Payne, E.G.I., Hatt, B.E., Deletic, A., Dobbie, M.F., McCarthy, D.T., Chandrasena, G.I., 2015. Adoption guidelines for stormwater biofiltration systems—Summary report. Coop. Res. Cent. Water Sensitive Cities Melb.

Philip, J., 1968. The theory of absorption in aggregated media. Soil Res. 6, 1. https://doi.org/10.1071/SR9680001

Philip, J.R., 1969. Theory of Infiltration, in: Advances in Hydroscience. Elsevier, pp. 215–296. https://doi.org/10.1016/B978-1-4831-9936-8.50010-6

Pörtner, H.-O., Roberts, D.C., Adams, H., Adler, C., Aldunce, P., Ali, E., Begum, R.A., Betts, R., Kerr, R.B., Biesbroek, R., 2022. Climate change 2022: Impacts, adaptation and vulnerability. IPCC Geneva, Switzerland:

Pouyat, R.V., Yesilonis, I.D., Russell-Anelli, J., Neerchal, N.K., 2007. Soil Chemical and Physical Properties That Differentiate Urban Land-Use and Cover Types. Soil Sci. Soc. Am. J. 71, 1010–1019. https://doi.org/10.2136/sssaj2006.0164

Price, K., 2011. Effects of watershed topography, soils, land use, and climate on baseflow hydrology in humid regions: A review. Prog. Phys. Geogr. Earth Environ. 35, 465–492. https://doi.org/10.1177/0309133311402714

Prince George's County, M., 2007. Bioretention manual. Dep. Environ. Resour.

Rasse, D.P., Smucker, A.J.M., Santos, D., 2000. Alfalfa Root and Shoot Mulching Effects on Soil Hydraulic Properties and Aggregation. Soil Sci. Soc. Am. J. 64, 725–731. https://doi.org/10.2136/sssaj2000.642725x

Rawls, W., Pachepsky, Y.A., Ritchie, J., Sobecki, T., Bloodworth, H., 2003. Effect of soil organic carbon on soil water retention. Geoderma 116, 61–76.

Rawls, W.J., Gish, T.J., Brakensiek, D.L., 1991. Estimating Soil Water Retention from Soil Physical Properties and Characteristics, in: Stewart, B.A. (Ed.), Advances in Soil Science: Volume 16, Advances in Soil Science. Springer, New York, NY, pp. 213–234. https://doi.org/10.1007/978-1-4612-3144-8_5

Rezaei, M., Seuntjens, P., Joris, I., Boënne, W., Van Hoey, S., Campling, P., Cornelis, W.M., 2016. Sensitivity of water stress in a two-layered sandy grassland soil to variations in groundwater depth and soil hydraulic parameters. Hydrol. Earth Syst. Sci. 20, 487–503. https://doi.org/10.5194/hess-20-487-2016

Richards, L.A., 1931. Capillary conduction of liquids through porous mediums, 5th ed. Physics.

Ritter, A., Hupet, F., MunÄoz-Carpena, R., Lambot, S., Vanclooster, M., 2003. Using inverse methods for estimating soil hydraulic properties from ®eld data as an alternative to direct methods. Agric. Water Manag.

Robineau, T., Tognelli, A., Goblet, P., Renard, F., Schaper, L., 2018. A double medium approach to simulate groundwater level variations in a fissured karst aquifer. J. Hydrol. 565, 861–875. https://doi.org/10.1016/j.jhydrol.2018.09.002

Rodriguez, F., Andrieu, H., Morena, F., 2008. A distributed hydrological model for urbanized areas – Model development and application to case studies. J. Hydrol. 351, 268–287. https://doi.org/10.1016/j.jhydrol.2007.12.007

Roesner, L.A., Rossman, L.A., Davis, J., Girona, J., 2010a. Environmental Modelling & Software A new applications manual for the Storm Water Management Model (SWMM) 25, 813–814. https://doi.org/10.1016/j.envsoft.2009.11.009

Roesner, L.A., Rossman, L.A., Davis, J., Girona, J., 2010b. Environmental Modelling & Software A new applications manual for the Storm Water Management Model (SWMM) 25, 813–814. https://doi.org/10.1016/j.envsoft.2009.11.009

Rose, C.W., 2004. An introduction to the environmental physics of soil, water and watersheds. Cambridge University Press.

Rossman, L.A., 2010. Modeling Low Impact Development Alternatives with SWMM. J. Water Manag. Model. 6062. https://doi.org/10.14796/jwmm.r236-11

Roulier, S., Robinson, B., Kuster, E., Schulin, R., 2008. Analysing the preferential transport of lead in a vegetated roadside soil using lysimeter experiments and a dual-porosity model. Eur. J. Soil Sci. 59, 61–70.

Roulier, S., Robinson, B., Kuster, E., Schulin, R., 2007. Analysing the preferential transport of lead in a vegetated roadside soil using lysimeter experiments and a dual-porosity model. Eur. J. Soil Sci. 0, 070822040136006-??? https://doi.org/10.1111/j.1365-2389.2007.00954.x

Roy-Poirier, A., Champagne, P., Filion, Y., 2010. Review of Bioretention System Research and Design: Past, Present, and Future. J. Environ. Eng. 136, 878–889. https://doi.org/10.1061/(ASCE)EE.1943-7870.0000227

Sage, J., Berthier, E., Gromaire, M.-C., 2020. Modeling Soil Moisture Redistribution and Infiltration Dynamics in Urban Drainage Systems. J. Hydrol. Eng. 25, 04020041. https://doi.org/10.1061/(asce)he.1943-5584.0001978

Saltelli, A. (Ed.), 2004. Sensitivity analysis in practice: a guide to assessing scientific models. Wiley, Hoboken, NJ.

Saltelli, A., Annoni, P., 2010. How to avoid a perfunctory sensitivity analysis. Environ. Model. Softw. 25, 1508–1517. https://doi.org/10.1016/j.envsoft.2010.04.012

Sambridge, M., Mosegaard, K., 2002. Monte Carlo methods in geophysical inverse problems. Rev. Geophys. 40, 3-1-3–29.

Sanzana, P., Gironás, J., Braud, I., Muñoz, J., Vicuña, S., Reyes-Paecke, S., de la Barrera, F., Branger, F., Rodríguez, F., Vargas, X., 2019. Impact of urban growth and high residential irrigation on streamflow and groundwater levels in a peri-urban semiarid catchment. JAWRA J. Am. Water Resour. Assoc. 55, 720–739.

Schaap, M.G., Leij, F.J., van Genuchten, M.Th., 2001. rosetta : a computer program for estimating soil hydraulic parameters with hierarchical pedotransfer functions. J. Hydrol. 251, 163–176. https://doi.org/10.1016/S0022-1694(01)00466-8

Schifman, L.A., Shuster, W.D., 2019. Comparison of Measured and Simulated Urban Soil Hydrologic Properties. J. Hydrol. Eng. 24, 10.1061/(ASCE)HE.1943-5584.0001684. https://doi.org/10.1061/(ASCE)HE.1943-5584.0001684

Schübl, M., Stumpp, C., Brunetti, G., 2022. A Bayesian perspective on the information content of soil water measurements for the hydrological characterization of the vadose zone. J. Hydrol. 613, 128429. https://doi.org/10.1016/j.jhydrol.2022.128429

Schueler, T.R., Fraley-McNeal, L., Cappiella, K., 2009. Is Impervious Cover Still Important? Review of Recent Research. J. Hydrol. Eng. 14, 309–315. https://doi.org/10.1061/(ASCE)1084-0699(2009)14:4(309)

Shuster, W.D., Bonta, J., Thurston, H., Warnemuende, E., Smith, D., 2005. Impacts of impervious surface on watershed hydrology: A review. Urban Water J. 2, 263–275.

SILO, 2020. SILO climate database,data.qld.gov.au [WWW Document]. Res. Data Aust. URL https://researchdata.edu.au/silo-climate-database/969133 (accessed 12.21.23).

Silverman, B.W., 1981. Using kernel density estimates to investigate multimodality. J. R. Stat. Soc. Ser. B Methodol. 43, 97–99.

Simunek, J., 2008. Simulating Nonequilibrium Movement of Water , Solutes and Particles Using HYDRUS : A Review of Recent Applications. https://doi.org/10.17221/1200-SWR

Simůnek, J., 2005. 78 : Models of Water Flow and Solute Transport. Encycl. Hydrol. Sci.

Šimůnek, J., Hopmans, J.W., 2002. 1.7 parameter optimization and nonlinear fitting. Methods Soil Anal. Part 4 Phys. Methods 5, 139–157.

Šimůnek, J., Jarvis, N.J., van Genuchten, M.Th., Gärdenäs, A., 2003. Review and comparison of models for describing non-equilibrium and preferential flow and transport in the vadose zone. J. Hydrol. 272, 14–35. https://doi.org/10.1016/S0022-1694(02)00252-4

Simůnek, J., Sejna, M., Saito, H., van Genuchten, M.Th., 2009. The HYDRUS-1D Software Package for Simulating the One-Dimensional Movement of Water, Heat, and Multiple Solutes in Variably-Saturated Media, Environmental Sciences.

Šimůnek, J., van Genuchten, M.Th., 2008. Modeling Nonequilibrium Flow and Transport Processes Using HYDRUS. Vadose Zone J. 7, 782–797. https://doi.org/10.2136/vzj2007.0074

Simunek, J., Van Genuchten, M.Th., Sejna, M., 2011. The HYDRUS Software Package for Simulating the Two- and Three-Dimensions Movement of Water, Heat, and Multiple Solutes in Variably-Saturated Media. Tech. Man. 230.

Six, J., Bossuyt, H., Degryze, S., Denef, K., 2004. A history of research on the link between (micro)aggregates, soil biota, and soil organic matter dynamics. Soil Tillage Res., Advances in Soil Structure Research 79, 7–31. https://doi.org/10.1016/j.still.2004.03.008

Song, X., Zhang, J., Zhan, C., Xuan, Y., Ye, M., Xu, C., 2015. Global sensitivity analysis in hydrological modeling: Review of concepts, methods, theoretical framework, and applications. J. Hydrol. 523, 739–757. https://doi.org/10.1016/j.jhydrol.2015.02.013

Spraakman, S., Van Seters, T., Drake, J., Passeport, E., 2020. How has it changed? A comparative field evaluation of bioretention infiltration and treatment performance post-construction and at maturity. Ecol. Eng. 158, 106036. https://doi.org/10.1016/j.ecoleng.2020.106036

Swartzendruber, D., Hillel, D., 1973. The Physics of Infiltration, in: Hadas, A., Swartzendruber, D., Rijtema, P.E., Fuchs, M., Yaron, B. (Eds.), Physical Aspects of Soil Water and Salts in Ecosystems, Ecological Studies. Springer Berlin Heidelberg, Berlin, Heidelberg, pp. 3–15. https://doi.org/10.1007/978-3-642-65523-4_1

Tedoldi, D., Chebbo, G., Pierlot, D., Kovacs, Y., Gromaire, M.-C., 2016. Impact of runoff infiltration on contaminant accumulation and transport in the soil/filter media of Sustainable Urban Drainage Systems: A literature review. Sci. Total Environ. 569–570, 904–926. https://doi.org/10.1016/j.scitotenv.2016.04.215

Tennøe, S., Halnes, G., Einevoll, G.T., 2018. Uncertainpy: A Python Toolbox for Uncertainty Quantification and Sensitivity Analysis in Computational Neuroscience. Front. Neuroinformatics 12.

Thom, J.K., Szota, C., Coutts, A.M., Fletcher, T.D., Livesley, S.J., 2020. Transpiration by established trees could increase the efficiency of stormwater control measures. Water Res. 173, 115597. https://doi.org/10.1016/j.watres.2020.115597

Thomas, Z., Bloux, A., Hamon, Y., Rouault, F., 2011. How do morphological characteristics of hillslope control water movement in the saturated and unsaturated zone?, in: AGU Fall Meeting Abstracts. pp. H33F-1372.

Thomas, Z., Mérot, P., 2009. Interactions between hedgerow, soil and hydrology., in: 2nd International. Conference BioHydrology 2009.

Tian, W., 2013. A review of sensitivity analysis methods in building energy analysis. Renew. Sustain. Energy Rev. 20, 411–419. https://doi.org/10.1016/j.rser.2012.12.014

Tseng, P.-H., Jury, W.A., 1993. Simulation of field measurement of hydraulic conductivity in unsaturated heterogeneous soil. Water Resour. Res. 29, 2087–2099.

University of Tennessee, D. of E. and C.D. of W.R., 2014. Permanent Stormwater Management and Design Guidance Manual.

Upson, R., Read, D.J., Newsham, K.K., 2009. Nitrogen form influences the response of Deschampsia antarctica to dark septate root endophytes. Mycorrhiza 20, 1–11. https://doi.org/10.1007/s00572-009-0260-3

US Environmental Protection Agency (USEPA), 1993. Guidance specifying management measures for sources of nonpoint pollution in coastal waters.

US Environmental Protection Agency (USEPA), 1975. Storm Water Management Model User'S Manuel. Version Ii. Env. Prot Technol Ser EPA.

USEPA, 2000. Environmental Protection Agency. Low Impact Development (LID): A Literature Review. n.

Van Dam, J.C.V., Stricker, J.N.M., Droogers, P., 1994. Inverse Method to Determine Soil Hydraulic Functions - DIVISION S-l-SOIL PHYSICS. Soil Sci. Soc. Am. J. 58, 647–652.

van de Schoot, R., Depaoli, S., King, R., Kramer, B., Märtens, K., Tadesse, M.G., Vannucci, M., Gelman, A., Veen, D., Willemsen, J., 2021. Bayesian statistics and modelling. Nat. Rev. Methods Primer 1, 1.

Van der Lee, J., Gehrels, J.C., 1990. Modelling aquifer recharge–introduction to the lumped parameter model EARTH. Free Univ. Amst. Neth. 30.

Van Genuchten, M., 1999. General model for the hydraulic conductivity of unsaturated soils. Book Chapter.

Van Genuchten, M. Th., Nielsen, D.R., 1985. On describing and predicting the hydraulic properties. Ann. Geophys. 3, 615–628. https://doi.org/10.1016/0148-9062(86)91047-8

Van Genuchten, M.T., Dalton, F.N., 1986. Models for simulating salt movement in aggregated field soils. Geoderma 38, 165–183.

Vereecken, H., Weihermüller, L., Assouline, S., Šimůnek, J., Verhoef, A., Herbst, M., Archer, N., Mohanty, B., Montzka, C., Vanderborght, J., Balsamo, G., Bechtold, M., Boone, A., Chadburn, S., Cuntz, M., Decharme, B., Ducharne, A., Ek, M., Garrigues, S., Goergen, K., Ingwersen, J., Kollet, S., Lawrence, D.M., Li, Q., Or, D., Swenson, S., Vrese, P., Walko, R., Wu, Y., Xue, Y., 2019. Infiltration from the Pedon to Global Grid Scales: An Overview and Outlook for Land Surface Modeling. Vadose Zone J. 18, 1–53. https://doi.org/10.2136/vzj2018.10.0191

Voter, C.B., Loheide II, S.P., 2020. Where and When Soil Amendment is Most Effective as a Low Impact Development Practice in Residential Areas. JAWRA J. Am. Water Resour. Assoc. 56, 776–789. https://doi.org/10.1111/1752-1688.12870

Vrugt, J.A., 2016. Markov chain Monte Carlo simulation using the DREAM software package: Theory, concepts, and MATLAB implementation. Environ. Model. Softw. 75, 273–316. https://doi.org/10.1016/j.envsoft.2015.08.013

Vrugt, J.A., Diks, C.G.H., Gupta, H.V., Bouten, W., Verstraten, J.M., 2005. Improved treatment of uncertainty in hydrologic modeling: Combining the strengths of global optimization and data assimilation: TREATMENT OF UNCERTAINTY IN HYDROLOGIC MODELING. Water Resour. Res. 41. https://doi.org/10.1029/2004WR003059

Vrugt, J.A., Gupta, H.V., Bastidas, L.A., Bouten, W., Sorooshian, S., 2003. Effective and efficient algorithm for multiobjective optimization of hydrologic models. Water Resour. Res. 39.

Vrugt, J.A., Sadegh, M., 2013. Toward diagnostic model calibration and evaluation: Approximate Bayesian computation. Water Resour. Res. 49, 4335–4345.

Vrugt, J.A., Schoups, G., Hopmans, J.W., Young, C., Wallender, W.W., Harter, T., Bouten, W., 2004. Inverse modeling of large-scale spatially distributed vadose zone properties using global optimization. Water Resour. Res. 40. https://doi.org/10.1029/2003WR002706

Vrugt, J.A., Stauffer, P.H., Wöhling, Th., Robinson, B.A., Vesselinov, V.V., 2008. Inverse Modeling of Subsurface Flow and Transport Properties: A Review with New Developments. Vadose Zone J. 7, 843–864. https://doi.org/10.2136/vzj2007.0078

Vrugt, J.A., Ter Braak, C.J., Gupta, H.V., Robinson, B.A., 2009. Equifinality of formal (DREAM) and informal (GLUE) Bayesian approaches in hydrologic modeling? Stoch. Environ. Res. Risk Assess. 23, 1011–1026.

Wadzuk, B.M., Hickman Jr, J.M., Traver, R.G., 2015. Understanding the role of evapotranspiration in bioretention: Mesocosm study. J. Sustain. Water Built Environ. 1, 04014002.

Wang, J., 2017. Water quality and hydrological assessment and modeling of bioretention basins in tropical cities (Thesis). Massachusetts Institute of Technology.

Wang, R., Dong, Z., Zhou, Z., Wang, N., Xue, Z., Cao, L., 2020. Effect of vegetation patchiness on the subsurface water distribution in abandoned farmland of the Loess Plateau, China. Sci. Total Environ. 746, 141416. https://doi.org/10.1016/j.scitotenv.2020.141416

Wang, Z., Feyen, J., Ritsema, C.J., 1998. Susceptibility and predictability of conditions for preferential flow. Water Resour. Res. 34, 2169–2182. https://doi.org/10.1029/98WR01761

Webber, J.L., Fletcher, T.D., Cunningham, L., Fu, G., Butler, D., Burns, M.J., 2020. Is green infrastructure a viable strategy for managing urban surface water flooding? Urban Water J. 17, 598–608. https://doi.org/10.1080/1573062X.2019.1700286

Wesseling, J., Kroes, J., Campos Oliveira, T., Damiano, F., 2020. The impact of sensitivity and uncertainty of soil physical parameters on the terms of the water balance: Some case studies with default R packages. Part I: Theory, methods and case descriptions. Comput. Electron. Agric. 170, 105054. https://doi.org/10.1016/j.compag.2019.105054

Wessolek, G., 2008. Sealing of soils, in: Urban Ecology. Springer, pp. 161–179.

White, R., 1985. The influence of macropores on the transport of dissolved and suspended matter through soil, in: Advances in Soil Science. Springer, pp. 95–120.

Willard, L., Wynn-Thompson, T., Krometis, L., Neher, T., Badgley, B., 2017. Does it pay to be mature? Evaluation of bioretention cell performance seven years postconstruction. J. Environ. Eng. 143, 04017041.

Wilson, C.E., Hunt, W.F., Winston, R.J., Smith, P., 2015. Comparison of runoff quality and quantity from a commercial low-impact and conventional development in Raleigh, North Carolina. J. Environ. Eng. 141, 05014005.

Winiarski, T., Lassabatere, L., Angulo-Jaramillo, R., Goutaland, D., 2013. Characterization of the Heterogeneous Flow and Pollutant Transfer in the Unsaturated Zone in the Fluvio-glacial Deposit. Procedia Environ. Sci. 19, 955–964. https://doi.org/10.1016/j.proenv.2013.06.105

Wöhling, T., Samaniego, L., Kumar, R., 2013. Evaluating multiple performance criteria to calibrate the distributed hydrological model of the upper Neckar catchment. Environ. Earth Sci. 69, 453–468. https://doi.org/10.1007/s12665-013-2306-2

Yilmaz, D., Sabre, M., Lassabatère, L., Dal, M., Rodriguez, F., 2016. Storm water retention and actual evapotranspiration performances of experimental green roofs in French oceanic climate. Eur. J. Environ. Civ. Eng. 20, 344–362. https://doi.org/10.1080/19648189.2015.1036128

Zégre, N., Skaugset, A.E., Som, N.A., McDonnell, J.J., Ganio, L.M., 2010. In lieu of the paired catchment approach: Hydrologic model change detection at the catchment scale: IN LIEU OF THE PAIRED CATCHMENT APPROACH. Water Resour. Res. 46. https://doi.org/10.1029/2009WR008601

Zhang, K., Chui, T.F.M., 2019. A review on implementing infiltration-based green infrastructure in shallow groundwater environments: Challenges, approaches, and progress. J. Hydrol. 579, 124089. https://doi.org/10.1016/j.jhydrol.2019.124089

Zi, Z., 2011. Sensitivity analysis approaches applied to systems biology models. IET Syst. Biol. 5, 336–346. https://doi.org/10.1049/iet-syb.2011.0015

Zou, Qi, Hou, Li, Yu, Zhai, 2019. Integrating Multiple-Try DREAM(ZS) to Model-Based Bayesian Geoacoustic Inversion Applied to Seabed Backscattering Strength Measurements. J. Mar. Sci. Eng. 7, 372. https://doi.org/10.3390/jmse7100372

Publication

This study is a paper-based thesis consisting of 5 chapter. Chapter 1 is the Introduction of the work. Chapter 2 is the literature review used in this study. Chapter 3 and 4 are published (under revision) or are under review in scientific journals. Chapter 5 is the article under submission.

Journal papers:

- (Chapter 3): Asry, A., Kouyi, G.L., Fletcher, T.D., Bonneau, J., Tedoldi, D., Lassabatere, L., 2023a. Sets of infiltration models for water infiltration in sustainable urban drainage systems. Journal of Hydrology 623, 129477. https://doi.org/10.1016/j.jhydrol.2023.129477.
- (Chapter 4): Asry, A., Kouyi, G.L., Fletcher, T.D., Tedoldi, D., Lassabatere, L., 2023. Physically-based dual-permeability models infiltration model for modeling and management the SUDS. Journal of Water Research, under submission.
- (Chapter 5): Asry, A., Kouyi, G.L., Fletcher, T.D., Tedoldi, D., Lassabatere, L., 2023. Model uncertainty and sensitivity analysis of infiltration in SUDS. Journal of Hydrologie X, under submission.

Conference papers:

- Asry, A., Lipeme Kouyi, G., Bonneau, J., Fletcher, T.D., Lassabatere, L., 2023b. INFILTRON-Mod, a simplified preferential infiltration model for modeling bioretention systems (other). display. https://doi.org/10.5194/egusphere-egu23-5608.
- Asry, A., Lipeme Kouyi, G., Bonneau, J., Fletcher, T.D., Lassabatere, L., 2022. Modeling bioretention systems using different sets of simplified preferential infiltration models EGU22-9245. https://doi.org/10.5194/egusphere-egu22-9245.
- Asry, A., Bonneau, J., Fernandes, G., Lipeme Kouyi, G., Chocat, B., Fletcher, T.D., Lassabatere, L., 2021. Modelling uniform and preferential flow in bioretention systems EGU21-10576. https://doi.org/10.5194/egusphere-egu21-10576.

Appendix

1. Appendix 1

Inversion and model calibration

Inverse modeling is a mathematical methodology employed to identify unknown causes by analyzing their effects. It is commonly utilized to ascertain soil model parameters for system characterization (Arora et al., 2011; Hopmans et al., 2002; Ines and Droogers, 2002; Majdalani et al., 2008; Sambridge and Mosegaard, 2002; Vrugt et al., 2008).

In a common inverse problem, considering a model $\emptyset$ in which the discrete time evolution of the state vector $\varphi_t$is described by.

$$\varphi_t = \emptyset\left(\varphi_{t-1}, \theta^*, \breve{U}\right) \tag{0-1}$$

Where $\breve{U}$ represents the observed forcing (initial or boundary condition), $\theta^*$is the vector of the parameters value and t denotes the time step. In the current context, $\emptyset$ is the physical infiltration-based model presented in the following article. Assume that realistic upper and lower bounds of each parameter set of models $\theta^* = \{\theta_1^*, \ldots\ldots, \theta_i^*\}$ can be specified as a priory, thereby defining the feasible space of solutions:

$$\theta^* \in \theta \subseteq R^p \tag{0-2}$$

If the $\hat{Y}(\theta) = \left\{\hat{Y}_1(\theta), \ldots\ldots, \hat{Y}_n(\theta)\right\}$ is the vector of model simulation output performed by model $\emptyset$, and n is the total number of observations (Vrugt et al., 2008). These output predictions are directly related to the model state according to:

$$\hat{Y} = \Omega(\varphi_t) \tag{0-3}$$

The measurement operator $\Omega(\varphi_t)$ maps the state space into measurement or model output space. Finally, the error vector can be defined by:

$$E = f(\hat{Y}(\theta^*), Y) = \{E_1, \ldots\ldots, E_n\} \tag{0-4}$$

here Y is the measurement vector of data on the field, the aim of parameters estimation or model calibration now becomes finding the best value of θ^* such that, and we forced f as RMSE is the statistics of the measure E, is in some sense forced to be as close to 0 as possible.

Bayes' theorem

Bayesian statistics is founded upon the mathematical principle known as Bayes' theorem:

$$f(\theta|y) = \frac{f(y|\theta) * f(\theta)}{f(y)} \propto f(y|\theta) * f(\theta) \qquad \text{(0-5)}$$

$f(\theta|y)$, is the "posterior" PDF incorporating both the subjective judgment and observed data (the posterior probability) describing the plausibility of all models, given our observations, is proportional to both the likelihood of these data, given those models, and the probability of the models themselves.

$f(y|\theta) = L(\theta|y)$, is the "likelihood" function, which is the conditional probability of observing the additionally available data, y, given specific values of θ

$f(y)$, is the probability of observation.

$f(\theta)$, is the "prior" probability density function (PDF) (the prior probability distribution), which is related to the initial knowledge about θ.

In this study, the proposed models (*CH1*, *CH2*, *CH3*) are stand to likelihood function, and our objective is to fit the model to the observed data to estimate the unknown parameters of these models. Although these models are a simplification of physical processes in the soil found in infiltration systems, they aim to capture the primary factors of the underlying soil physics system that we wish to improve our understanding of, which leads to cumulative infiltration that we observe on the field. Models may differ substantially in their complexity, taking into account the many possible factors or mechanisms that act on the underlying system and sources of stochasticity and variability resulting in the given data we observe. Fitting the models to the observed data permits the estimation of the model parameters or functions of these, leading to an improved understanding of the system and associated underlying factors.

Within the Bayesian model-fitting framework, probabilities are assigned to the model parameters, describing the associated uncertainties. In Bayesian statistics, the focus is on estimating the entire posterior distribution of the model parameters. Unfortunately, the expression for the posterior distribution is typically only known up to a constant of proportionality, a constant term in the posterior distribution that is not a function of the parameters and, in general, cannot be explicitly calculated. We note that this intractability of the posterior distribution was the primary practical reason why many scientists in favour of frequentist statistics discarded Bayesian statistics.

MCI or monte Carlo filtering provides a uniform distribution of input parameters space (section 0) for exploring optimum solutions; which may be the source of uncertainty of parameters, thus referred to as over-parameterization models (Brunetti et al., 2016c; Draper and Smith, 1998). Instead of a grid search used in MCI, we must obtain samples from the posterior probability density function (PDF). Sampling from a PDF requires a different approach, requiring samples distributed proportionally to the posterior PDF density. This implies that we require more samples in high-probability regions and fewer samples in low-probability regions. Algorithms can generate random samples from certain simple probability density functions (PDFs) directly. However, in most cases, the process of generating random samples involves Markov Chain Monte Carlo simulation, which entails generating random samples from a known distribution (i.e., the proposal PDF), adjusting the weights of those samples based on their probability in the target distribution, and then determining whether to accept the proposed sample based on a probabilistic decision rule. Although this process eventually produces samples that follow the target PDF, it can be computationally intensive and inefficient (van de Schoot et al., 2021).

2. **Appendix 2.** Uncertainties on optimized parameter $\boldsymbol{K_s}$ curves

ENTPE 1_1

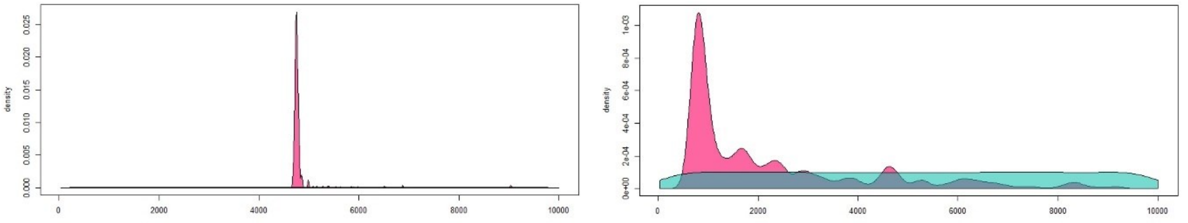

CH1 : Ks = 4744 mm/h

CH2 : Ks = 750 mm/h

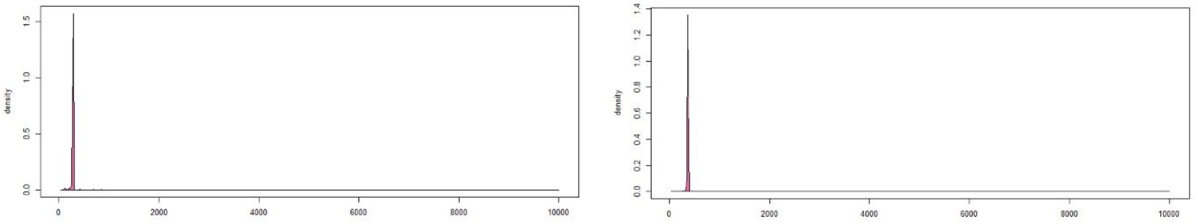

CH3 : Ks = 279 mm/h

GA : Ks = 366 mm/h

ENTPE 1_2

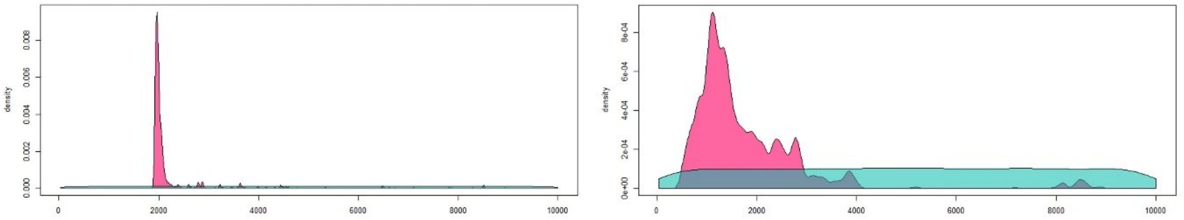

CH1 : Ks = 1928 mm/h

CH2 : Ks = 546 mm/h

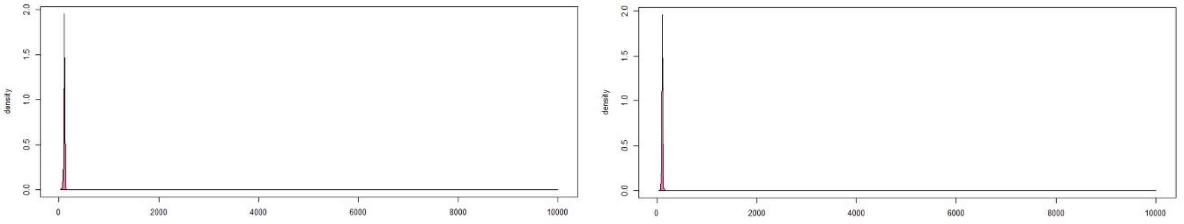

CH3 : Ks = 107 mm/h

GA : Ks = 107 mm/h

ENTPE 1_3

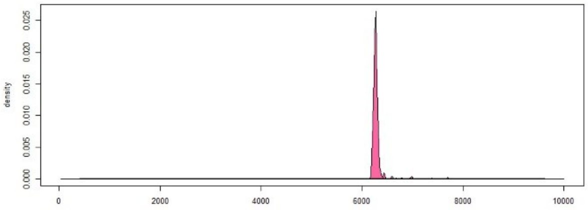

CH1 : Ks = 6260 mm/h

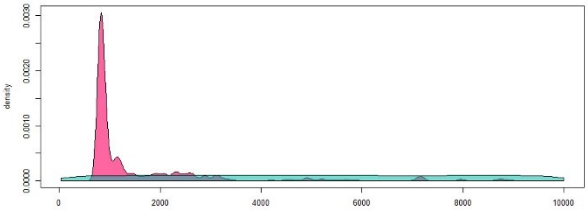

CH2 : Ks = 804 mm/h

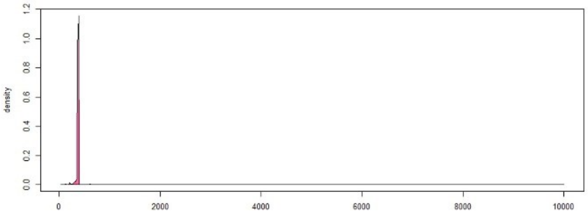

CH3 : Ks = 373 mm/h

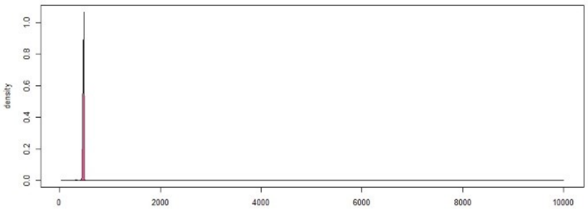

GA : Ks = 474 mm/h

ENTPE 2_1

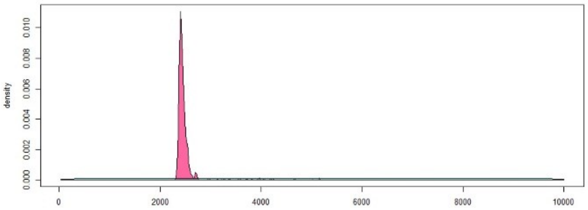

CH1 : Ks = 2378 mm/h

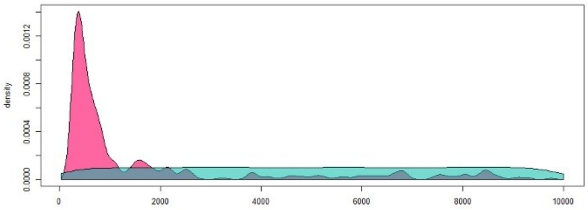

CH2 : Ks = 295 mm/h

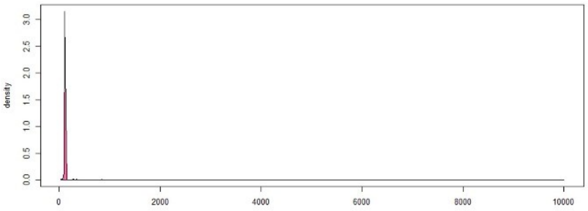

CH3 : Ks = 114 mm/h

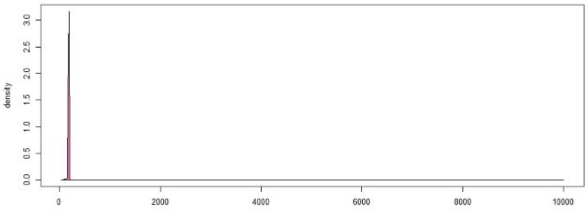

GA : Ks = 183 mm/h

ENTPE 2_3

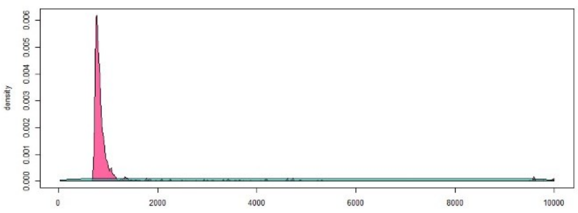

CH1 : Ks = 736 mm/h

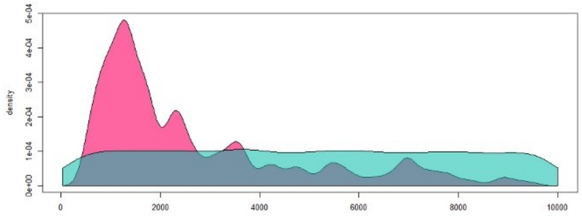

CH2 : Ks = 488 mm/h

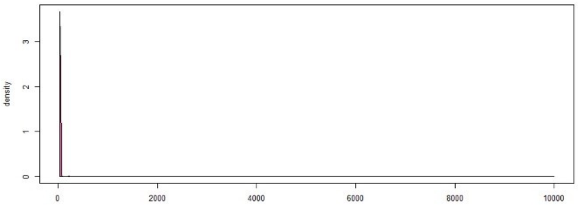

CH3 : Ks = 40 mm/h

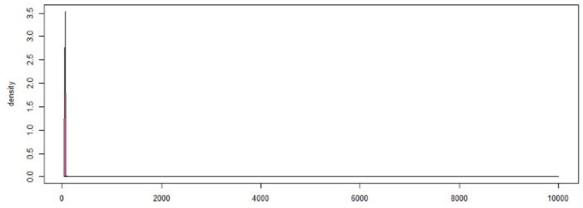

GA : Ks = 48 mm/h

Appendix 1. Uncertainties on the rest of the optimized parameters

ENTPE 1_1

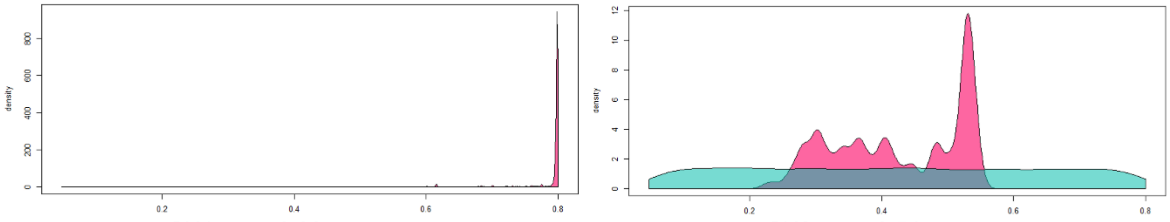

CH1 : m = 0,80

CH2 : m = 0,54

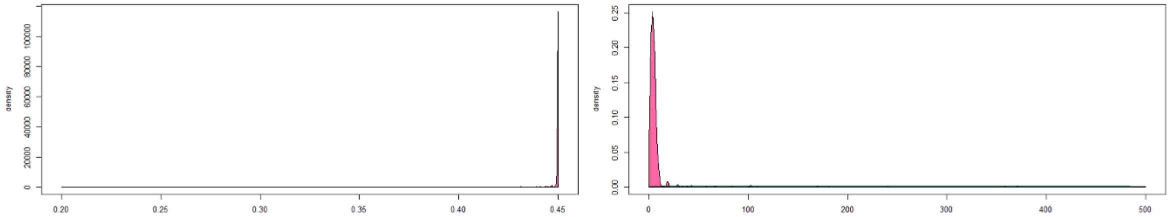

CH3 : θi = 0,45

GA : hg = 3,12 mm

ENTPE 1_2

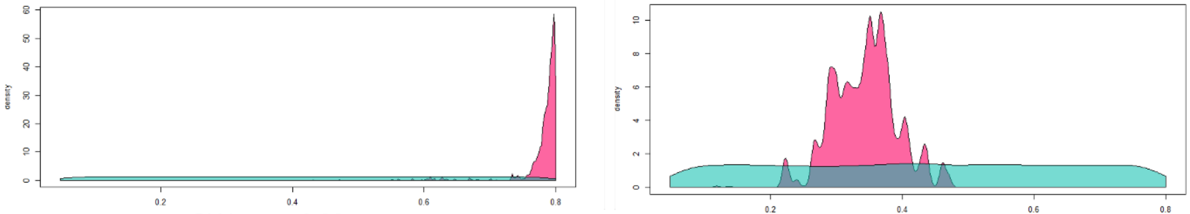

CH1 : m = 0,80

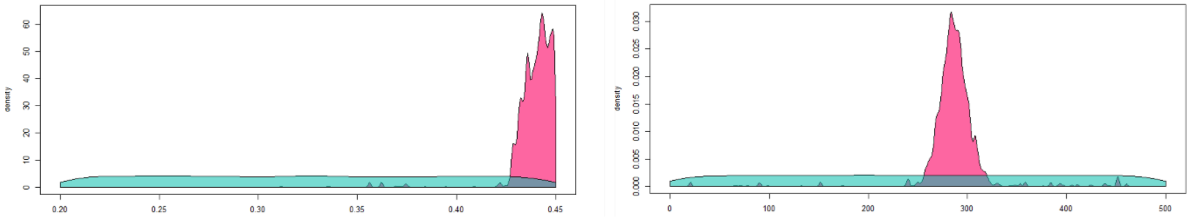

CH3 : θi = 0,44

GA : hg = 286 mm

ENTPE 1_3

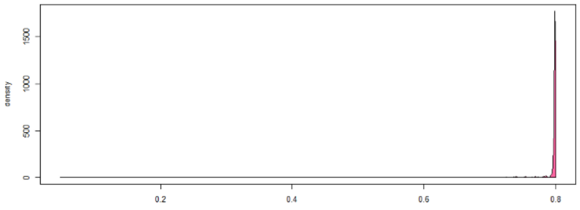

CH1 : m = 0,80

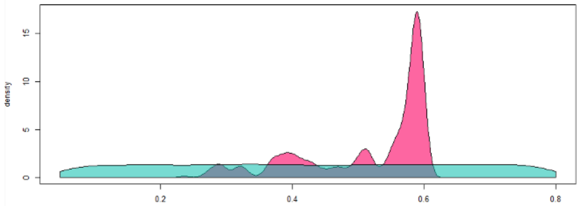

■ posterior ■ prior

CH2 : m = 0,59

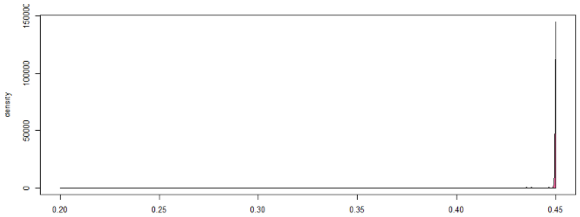

CH3 : θi = 0,45

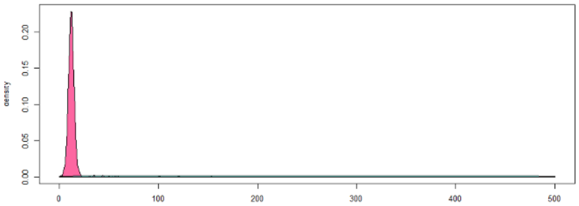

GA : hg = 12 mm

ENTPE 2_1

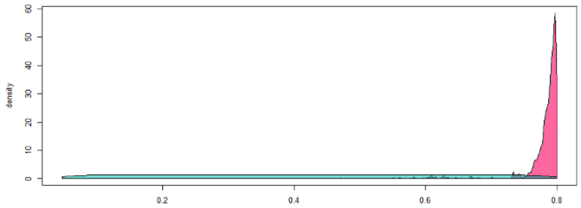

CH1 : m = 0,80

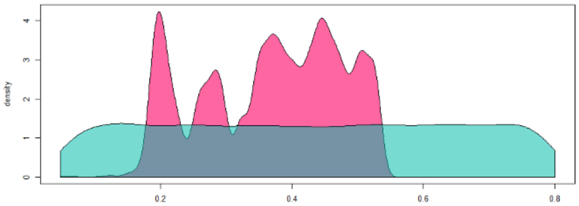

■ posterior ■ prior

CH2 : m = 0,51

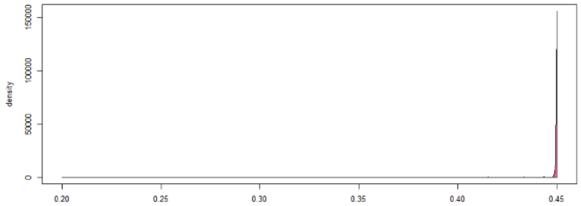

CH3 : θi = 0,45

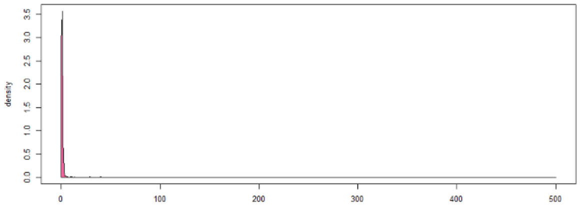

GA : hg = 0,003 mm

ENTPE 2_2

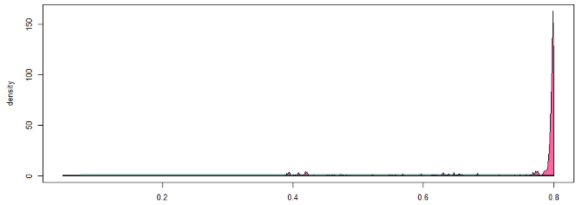

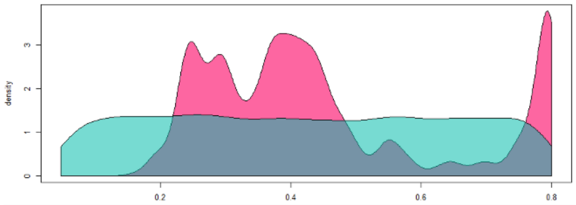

■ posterior ■ prior

CH2 : m = 0,80

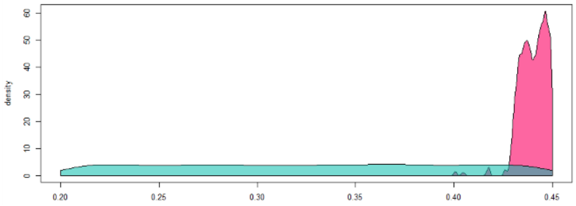

CH3 : θi = 0,45

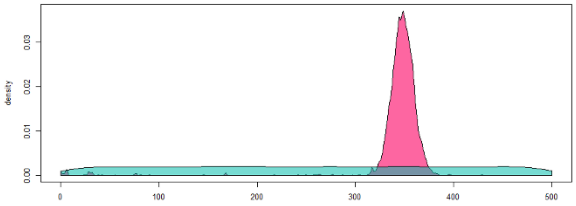

GA : hg = 348 mm

ENTPE 2_3

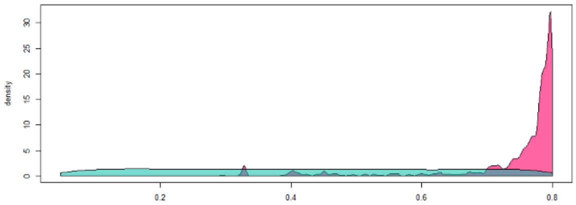

CH1 : m = 0,80

posterior prior

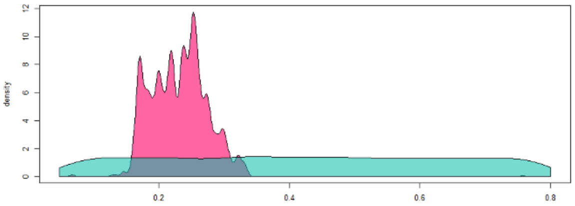

CH2 : m = 0,33

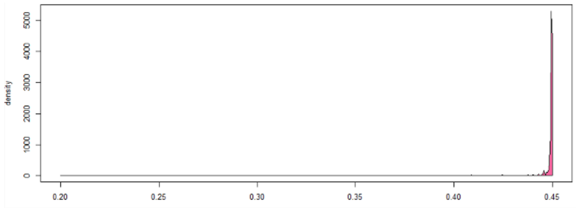

CH3 : θi = 0,45

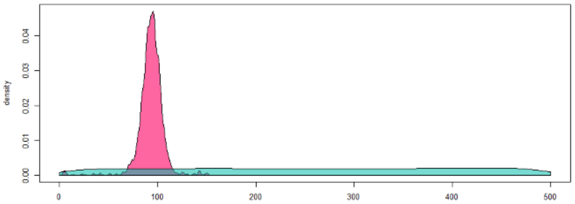

GA : hg = 94 mm

ENTPE 1_1

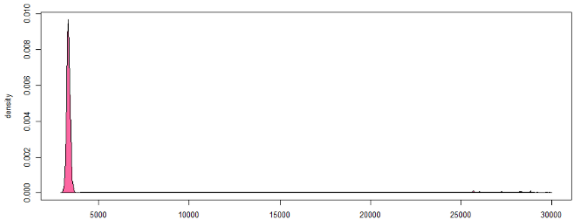

CH1 : zsoil = 3317 mm

posterior prior

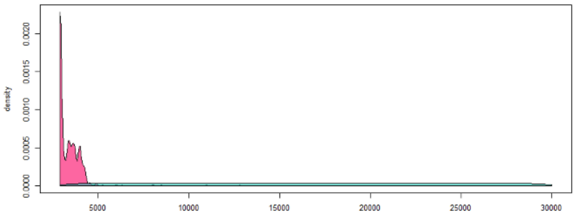

CH2 : zsoil = 2901 mm

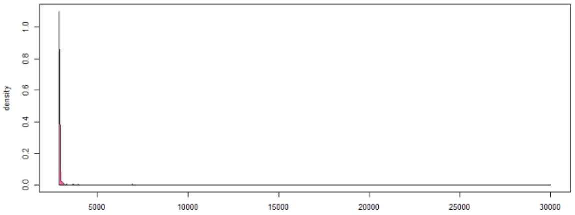

CH3 : zsoil = 2900 mm

ENTPE 1_2

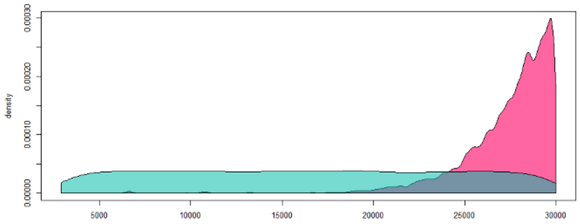

CH1 : zsoil = 29512 mm

posterior prior

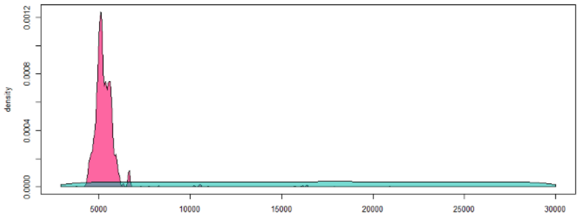

CH2 : zsoil = 4414 mm

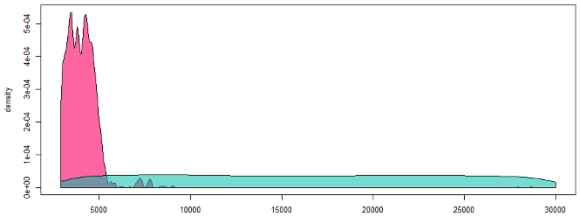

CH3 : zsoil = 4381 mm

ENTPE 1_3

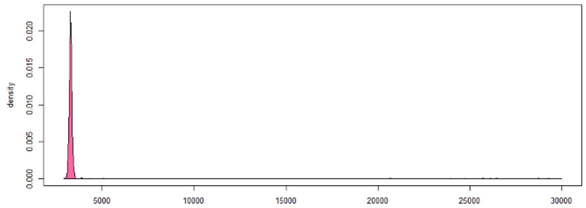

CH1 : zsoil = 3261 mm

🟥 posterior 🟦 prior

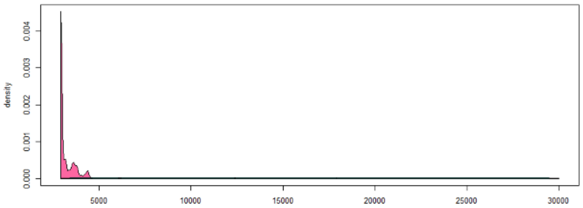

CH2 : zsoil = 2900 mm

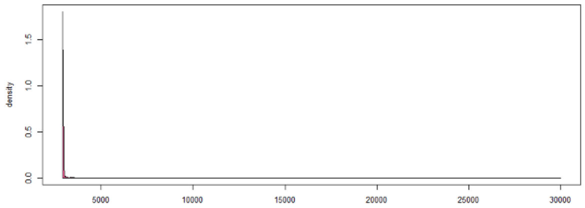

CH3 : zsoil = 2900 mm

ENTPE 2_1

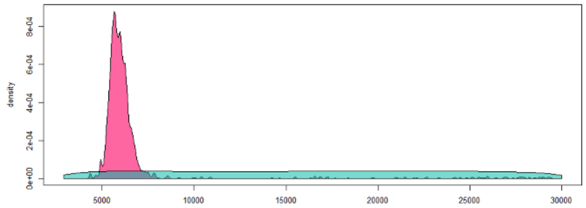

CH1 : zsoil = 5939 mm

🟥 posterior 🟦 prior

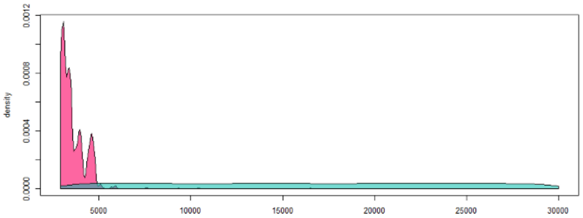

CH2 : zsoil = 2901 mm

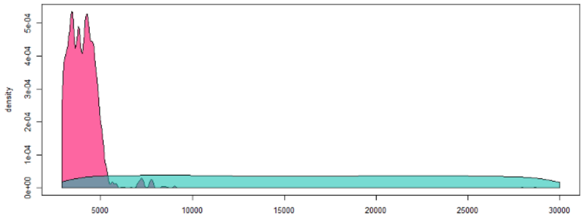

CH3 : zsoil = 2900 mm

ENTPE 2_2

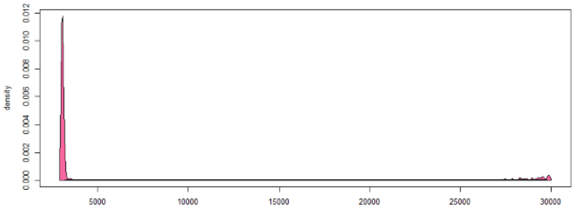

CH1 : zsoil = 3044 mm

■ posterior ■ prior

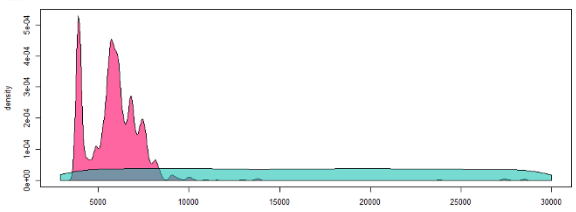

CH2 : zsoil = 3922 mm

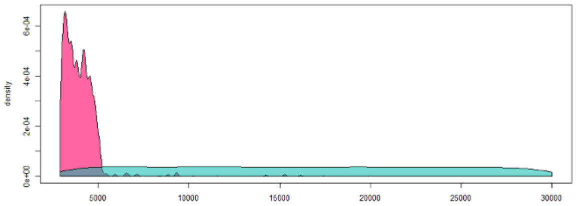

CH3 : zsoil = 4508 mm

ENTPE 2_3

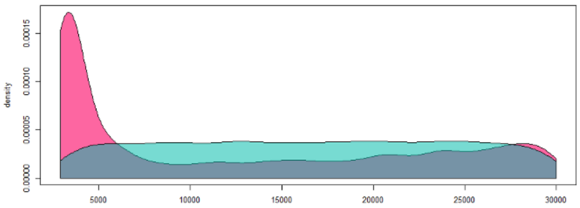

CH1 : zsoil = 2945 mm

■ posterior ■ prior

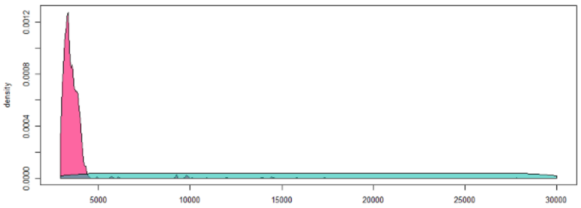

CH2 : zsoil = 2927 mm

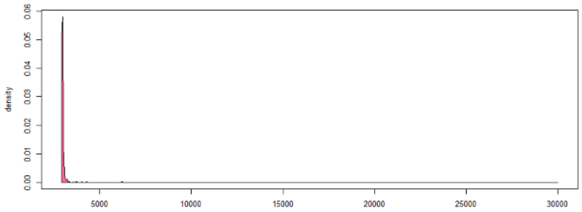

CH3 : zsoil = 2901 mm

FOLIO ADMINISTRATIF

THESE DE L'INSA LYON, MEMBRE DE L'UNIVERSITE DE LYON

NOM : ASRY DATE de SOUTENANCE : 30/11/2023
(avec précision du nom de jeune fille, le cas échéant)

Prénoms : Asra

TITRE : Modélisation hydrologique de l'infiltration des eaux pluviales dans les sols urbains en prenant en compte les chemins préférentiels

NATURE : Doctorat Numéro d'ordre : 2023ISAL0095

Ecole doctorale : Ecole Doctorale MEGA

Spécialité : Mécanique, énergétique, génie civil, acoustique

RESUME : L'infiltration joue un rôle crucial dans le cycle urbain de l'eau en servant comme limite entre le ruissellement et l'écoulement et le stockage dans le sol. Cette étude vise à relever le défi de modéliser de manière pragmatique et fiable l'infiltration pour les Systèmes de Gestion Durable des Eaux Pluviales (SUDS), en mettant l'accent sur une approche basée sur des principes physiques, cherchant un équilibre entre complexité et parcimonie.
Cela nécessite de réduire au maximum le nombre de paramètres, l'utilisation de paramètres physiques mesurables sur le terrain et l'examen de l'impact des macropores sur les taux d'infiltration à travers les SUDS. Diverses méthodes ont été introduites et évaluées pour répondre à ces questions. Dans un premier temps, cette thèse propose le développement d'un nouveau module appelé INFILTRON-mod, un modèle d'infiltration basé sur des principes physiques et pouvant être calibré facilement, démontrant ainsi son potentiel d'intégration dans des modèles hydrologiques. Un ensemble important de données expérimentales ainsi que des résultats synthétiques (Hydrus) sont utilisés pour la validation. Ensuite, la thèse étend le modèle proposé en incorporant un concept de perméabilité duale pour prendre en compte les écoulements préférentiels dans les SUDS. Finalement, cette étude conduit à une analyse de l'incertitude et de la sensibilité des modèles proposés.
Pour conclure, cette thèse a produit des informations cruciales pour l'optimisation de la modélisation des ouvrages de gestion des eaux urbaines en couplant un volet « physique des sols » et un volet « modélisation hydrologique des SUDS ». Il est recommandé de poursuivre les recherches pour améliorer et élargir la portée des modèles proposés, contribuant ainsi à une meilleure prise en compte des phénomènes hydrologiques et leur complexité au sein des SUDS.

MOTS-CLÉS : SUDS, infiltration, hydrologie, modélisation, sols

Laboratoire (s) de recherche : DEEP

Directeurs de thèse : Prof. Gislain, Lipeme Kouyi et Prof. Laurent Lassabatère

Président de jury :

Composition du jury : Dr. Fabrice Rodriguez, Prof. Zahra Thomas, Dr. Pascal Molle, Dr. David Ramier, Prof. Gislain Lipeme Kouyi, Prof. Laurent, Lassabatère, Prof. Tim D, Fletcher